A SPECTROSCOPIC AND PHOTOMETRIC INVESTIGATION OF SOME EXTREMELY HYDROGEN-DEFICIENT STARS

Keith Morrison

A Thesis Submitted for the Degree of PhD
at the
University of St Andrews

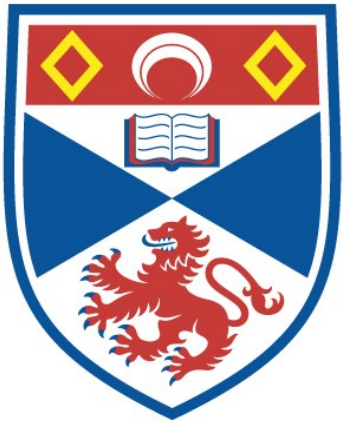

1988

A Spectroscopic and Photometric Investigation of some Extremely Hydrogen-Deficient Stars

by

Keith Morrison

A dissertation submitted for the degree of Doctor of Philosophy at the University of St Andrews

St Andrews September 1987

To my Parents

CERTIFICATE

I certify that Keith Morrison has spent nine terms in research work at the University Observatory, St Andrews, that he has fulfilled the conditions of Ordinance General No. 12 and Senate Regulations under Resolution of the University Court, 1967, No. 1, and that he is qualified to submit the accompanying dissertation in application for the degree of Ph.D.

DECLARATION

Except where reference is made to the work of others, the research described in this thesis is my own work. No part of this work has been submitted for another degree at this or any other University. Under Ordinance General No. 12, I was admitted to the Faculty of Science on 1st October 1983, to carry out an investigation into extremely hydrogen-deficient stars. I was accepted as a candidate for the degree of Ph.D. on 1st October 1984, under Resolution of the University Court, 1967, No. 1.

K. Morrison

ABSTRACT

A photometric study of the extreme helium stars has detected three new variables (BD+1°4381, BD-1°3438, LSIV-1°2) and confirmed the suspected variability of two others (LSII+33°5, BD-9°4395). The timescale of the variations in BD+1°4381 ($\sim$21 days), BD-1°3438 (5-8 days), LSIV-1°2 ($\sim$11 days) and LSII+33°5 (3-4 days), and the presence of colour changes concomitant with the luminosity variations, indicates that they are radial pulsators. In contrast, BD-9°4395 is believed to be pulsating non-radially.

Photometric investigations of the extremely hydrogen-deficient binaries Upsilon Sagittarii, CPD-58°2721 and KS Persei are presented. KS Persei is suspected of having a $\sim$5-day periodicity in addition to the $\sim$30 day previously reported. A frequency analysis of the complex light curve of CPD-58°2721 shows it may be reconstructed from two sine-waves with periods of 9.3 and 14.1 days. For Upsilon Sagittarii, the results indicate that the variability previously ascribed to eclipses can instead be understood in terms of radial pulsation of the visible component, with a period of $\sim$20 days. Additional rapid, $\sim$0.02 mag luminosity variations with a period of 239 seconds are reported. Their origin is uncertain, and they are the shortest form of variability reported for this type of object. Theoretical modelling of the light curve indicates an early B-type main-sequence secondary with a mass of $\sim 11 M_{\odot}$, much higher than previously thought. A possible future merging of the binary components would result in a Type I supernova. There is no evidence of eclipses in any of the stars.

A fine abundance analysis of CPD-58°2721 yielded T_{eff}=14,000K, log g=1.25, $n_H:n_{He}$=0.005, $n_N:n_C$=40 and suggests an overabundance of heavy metals when compared to related objects. Its spectrum shows marked changes in the strengths of low excitation metallic lines which are evidence of temperature changes during pulsation. Spectroscopy of the surrounding nebulosity shows it to have an emission spectrum typical of an HII region. Radial-velocity measurements indicate it is probably part of the surrounding Eta Carina nebula, whilst the star is more distant.

ACKNOWLEDGMENTS

I am indebted to my supervisor Dr P.W.Hill for his support and assistance on academic and other matters during the period of my studies at St Andrews. I am very grateful to Professor D.W.N. Stibbs for making available to me the facilities of the University Observatory and for his helpful advice. My thanks to the Directors and staff of the South African Astronomical Observatory, the Anglo-Australian Telescope, the Instituto de Astrofisica de Andalucia, and the European Space Agency Villafranca satellite tracking station for their assistance during my observing trips. I would also like to thank Dr G.Malcolm for his tireless observing at the Boyden Observatory.

My sincerest thanks to Dr U.Heber for his hospitality during my trips to Kiel and for all his hard work, and also to Professor K.Hunger, Dr D.Schönberner and other staff of the Institut fur Theoretische Physik, Kiel and Dr J.S.Drilling of Louisiana State University.

I am also grateful to past and present research fellows and students of the University Observatory St Andrews. In particular I would like to thank Dr S.A.Bell for making his photometry reduction packages available to me, Dr W.J.Skillen for the invaluable use of his Fourier-analysis package and many useful discussions on the interpretation of its results, and to Dr A.J.Adamson for the use of his plotting routines.

I acknowledge the Science and Engineering Research Council for their financial support in the form of a postgraduate studentship award without which none of this work would have been possible.

In submitting this thesis to the University of St. Andrews I understand that I am giving permission for it to be made available for use in accordance with the regulations of the University Library for the time being in force, subject to any copyright vested in the work not being affected thereby. I also understand that the title and abstract will be published, and that a copy of the work may be made and supplied to any bona fide library or research worker.

CONTENTS

Chapter 1 Introduction

1.1 Hydrogen-Deficiency in Stars.....1

1.2 The Extreme Helium Stars.....5

1.3 The Extremely Hydrogen-Deficient Binaries.....7

1.4 Photometry: Observations and Reductions

a. SAAO Photometry.....9

b. OSN Photometry.....11

1.5 Spectroscopy: Observations and Reductions.....13

Chapter 2 Photometry of some Extremely Hydrogen-Deficient Stars

2.1 BD+1°4381

a. Observations.....17

b. Discussion.....20

2.2 BD-1°3438

a. Observations.....22

b. Discussion.....23

2.3 LSIV-1°2

a. Observations.....24

b. Discussion.....26

2.4 LSII+33°5

a. Observations.....27

b. Discussion.....28

2.5 BD-9°4395

a. Observations.....30
b. Discussion.....31
2.6 KS Persei
a. Observations.....32
b. Discussion.....33

Chapter 3 Photometric Observations and Interpretation of Upsilon Sagittarii

3.1 Introduction.....35
3.2 Observations
a. Observational Details.....37
b. Photometry.....38
3.3 Frequency Analysis
a. Long-term Variability.....39
b. Short-Timescale Variability.....40
3.4 Discussion
a. The Origin of the 20-Day Variability.....42
b. The Origin of the 239-Second Variation.....45
3.5 Modelling the Light Curve.....47
3.6 Evolutionary Status.....51

Chapter 4 Light and Colour Variations in the Extremely Hydrogen-Deficient Binary CPD-58°2721

4.1 Introduction.....59
4.2 Observations
a. Photometry.....60
b. CPD-58°2721B and CPD-58°2721C.....61

c. Mean Properties.....63

4.3 Frequency Analysis.....64

4.4 Origin of the Variations.....68

Chapter 5 A Spectroscopic Investigation and Fine Analysis of CPD-58°2721

5.1 The Surrounding Nebula

a. Description.....73

b. The Relation of the Nebula to CPD-58°2721.....76

5.2 The Spectrum Variability of CPD-58°2721

a. The Absorption Spectrum.....80

b. The Emission Spectrum.....83

5.3 A Fine Analysis of CPD-58°2721

a. Determination of Atmospheric Parameters.....84

b. Abundance Determinations.....88

Summary of Work.....93

Suggestions for Future Work.....97

References.....100

Tables

1.1 List of extreme helium stars.....6

1.2 List of extremely hydrogen-deficient binaries.....6

2.1 Positions and mean uvby photometry of BD+1°4381.....17

2.2 The 1984 uvby photometry of BD+1°4381.....17

2.3 The 1985/86 uvby photometry of BD+1°4381.....17

2.4 Positions and mean uvby photometry of BD-1°3438.....21

2.5 The uvby photometry of BD-1°3438.....22

2.6 The uvby photometry of LSIV-1°2.....24

2.7 Magnitudes and colours for LSII+33°5.....27

2.8 The uvby photometry of LSII+33°5.....28

2.9 The uvby photometry of BD-9°4395.....30

2.10 Positions and mean uvby photometry of BD-9°4395.....31

2.11 Adopted frequencies in the solution of the V curve of BD-9°4395.....31

2.12 Magnitudes and colours for KS Persei.....32

2.13 The uvby photometry of KS Persei.....32

3.1 Positions and photometric means of Ups Sgr.....37

3.2 The uvby photometry 38

3.3 The UBV photometry.....38

3.4 High-speed V-band photometry.....38

3.5 Parameters of the theoretical light curves.....48

4.1 The uvby photometry of CPD-58°2721.....61

4.2 The UBVRI photometry.....61

4.3 Photometric uvby means.....63

4.4 Photometric UBVRI means.....63

4.5 Fourier decomposition of the light and colour curves.....63

4.5 Temperatures and periods for nine EHdBs and EHe stars.....71

5.1 Lines used in the abundance analysis of CPD-58°2721.....88

5.2 Atmospheric parameters and normalised abundances.....89

Figures

1.1 Log g-log T_{eff} diagram for some hydrogen-deficient stars.....2

1.2 Format for the 1982/84 spectroscopy observations.....14

1.3 Format for the 1985 spectroscopy observations.....14

2.1 The 1984 uvby photometry of BD+1°4381.....18

2.2 Sine fits to the 1984 V and (b-y) curves of BD+1°4381.....18

2.3 The 1985/86 uvby photometry of BD+1°4381.....19

2.4 Sine fits to the 1985 V photometry of BD+1°4381.....21

2.5 The uvby photometry of BD-1°3438.....23

2.6 The uvby photometry of LSIV-1°2.....25

2.7 Sine fits to the V and (b-y) curves of LSIV-1°2.....25

2.8 The uvby photometry of LSII+33°5.....27

2.9 The uvby photometry of BD-9°4395.....30

2.10 The uvby photometry of KS Persei.....32

3.1 The UBV photometry of Ups Sgr.....37

3.2 The uvby photometry.....37

3.3 High-speed V-band photometry.....39

3.4 The power spectrum of the high-speed V-band photometry.....40

3.5 Expanded plot of the power spectrum of Figure 3.4.....40

3.6 O-C times of maxima in the high-speed photometry.....41

3.7 The high-speed V-band photometry after filtering.....41

3.8 Theoretical binary-star light curves for Ups Sgr.....47

3.9 Fit-by-Eye of the theoretical and observed V curves.....48

3.10 Theoretical luminosity-mass relations for Ups Sgr at 1600A.....49

3.11 Theoretical luminosity-mass relations for Ups Sgr at 5500A.....49

4.1 The 1985 uvby photometry of CPD-58°2721.....62
4.2 The UBVRI photometry 62
4.3 The 1986 uvby photometry 63
4.4 Classical power spectrum of the differential V curve.....63
4.5 The pre-whitened differential V curve.....66
4.6 Multiple frequency fit to the differential V curve.....66
4.7 The $[c_1]$ and V variability.....71

5.1 Plate of the Eta Carina Nebula.....72
5.2 Plate of CPD-58°2721 and the surrounding region.....72
5.3 The CaII H and K lines of CPD-58°2721 and CPD-58°2721B.....74
5.4 [SII] nebular emission lines.....74
5.5 Variation of v_{HEL} along the slit length.....76
5.6 The Hα and [NII] nebular emission lines.....79
5.7 Spectra of CPD-58°2721 and HD168476.....79
5.8 Changes in lines strengths.....80
5.9 The behaviour of the FeII lines.....80
5.10 v_{HEL} for all lines.....82
5.11 v_{HEL} for the TiII, CrII and FeII lines.....82
5.12 Line-profile changes of Hβ 83
5.13 Line-profile changes of Hα 83
5.14 Observed flux distributions for CPD-58°2721 and related objects.....84
5.15 Model flux distributions.....84
5.16 Model fitting to the SiII and SiIII lines.....86
5.17 Model fitting to the HeI line profiles.....86
5.18 Calculation of the microturbulence velocity v_t.....87
5.19 The effect of v_t on the NII 4643A line.....87
5.20 Theoretical curves of growth for FeII.....88
5.21 Theoretical curve of growth for SII.....88
5.22 Model fitting to the Hδ line.....89
5.23 Chemical composition pattern of CPD-58°2721 and related objects.....90

1. Introduction

1.1 Hydrogen-Deficiency in Stars

The extreme helium stars and the extremely hydrogen-deficient binaries represent a small group of stars which exhibit an astonishing lack of hydrogen in their atmospheres, having typically $n_H:n_{He} \lesssim 10^{-3}$. They are part of the larger group of stars found in many spectral ranges which exhibit hydrogen deficiency in their outer layers to varying degrees.

Classification into different groups can be fairly arbitrary depending on which properties of the star are taken into account. They differ not only in the amount by which they are hydrogen deficient but in position on the HR diagram, population type, mass, and CNO and iron-group abundances. Investigators have tried to classify them meaningfully by grouping stars with similar properties. From this it is fair to say that five well-defined groups have emerged. Although a few objects display properties of more than one group, most objects can be classified according to the following scheme:

a) Hot blue subdwarfs (sdOs)

b) Moderate or intermediate-helium (IHe) stars

c) Extreme helium (EHe) stars

d) Extremely hydrogen-deficient binaries (EHdBs)

e) R Corona Borealis (RCB) stars

Also to be included are the helium-rich (DO, DB, C_2) white dwarfs and the nuclei of some planetary nebulae (CPN). The Wolf-Rayet

stars are also believed to be hydrogen-deficient. It is usual to convert the log L-log T_{eff} diagram to the log g-log T_{eff} diagram as this eliminates errors due to badly determined luminosities, g (surface gravity) being determined directly from the spectrum of the star. The positions of the various object types in the log g-log T_{eff} diagram are shown in Fig. 1.1.

The question must be asked whether the helium enrichment might be attributed to superficial processes like the action of radiation pressure on the helium lines. It is understood that although this may be true in a few instances the observed abundances are real. The hydrogen-deficient stars show population I and II characteristics and must represent a wide range of evolutionary stages. They are found in the disk and halo populations of our Galaxy; different groups appear to favour different heights above the galactic plane. The sdOs ($T_{eff} \gtrsim 35{,}000K$) are found at high galactic latitudes. They fall several magnitudes ($M_v \sim +4$) below the hydrogen main-sequence and appear to be intermediate between the helium main-sequence and the white-dwarf region. They are regarded as helium core-burning objects on or near the helium main-sequence with only a thin outer helium envelope (Heber et al. 1984).

Whilst with the other hydrogen-deficient objects we are almost certainly dealing with highly-evolved objects, the evolutionary status of the IHe stars is uncertain. Their surface gravities and temperatures ($T_{eff} > 20{,}000K$) are typical of zero-age main-sequence stars (Hunger 1975) which suggests we are dealing with young

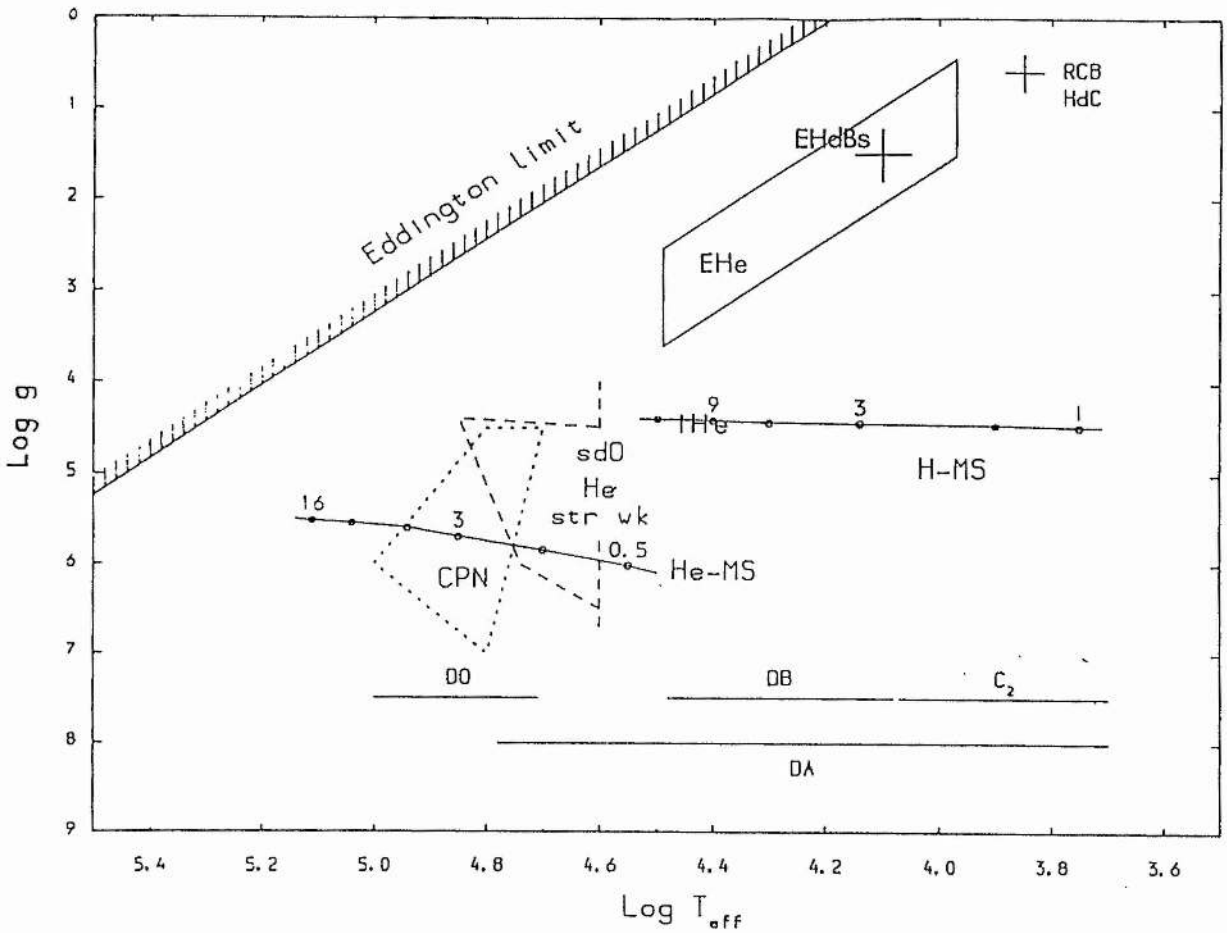

Figure 1.1 The log g-log T_{eff} diagram for some hydrogen-deficient stars (adapted from Hill 1986). The objects and regions are indicative rather than definitive. Also shown is the position of the hydrogen-rich (DA) white dwarfs. The numbers along the hydrogen and helium main-sequences are in solar masses.

stars. Their confinement to the galactic plane strengthens this idea. However, there is some evidence (Hunger 1986) to suggest that they do not form a uniform class but can be divided into old, low mass ($M \lesssim 2M_{\odot}$) stars and young, high mass stars ($M \gtrsim 2M_{\odot}$). Osmer & Peterson (1974) show that the latter group probably represent an extension to higher temperatures of the helium-weak peculiar A stars, just as the sdOs as can be considered a continuation of the helium-weak sdBs to higher temperatures. This dichotomy of helium enrichment with temperature has been interpreted as diffusion effects.

The RCB stars, EHe stars and EHdBs all lie above the hydrogen main-sequence and have temperatures in the range 2,500-34,000K. The RCB stars, a group of about 30 giant variable stars, are the coolest of the three groups but intrinsically the most luminous with $M_V \sim -6$ (Drilling 1986). They stay near maximum light for much of the time, but undergo drops in light of 0.5 to 9 magnitudes at irregular intervals (Feast 1986). They are similar in mass and chemical composition to the larger group of non-variable hydrogen-carbon (HdC) stars (Warner 1967). The EHe stars and EHdBs ($T_{eff} \gtrsim 8,500K$) show a similar deficiency of hydrogen at their surfaces as the RCB stars but do not show the large irregular drops in light characteristic of the RCB stars.

An important question to ask is whether these groups might be linked, representing perhaps a series of evolutionary phases. Whilst the positions of some of the objects in the HR diagram suggest evolutionary sequences, there are serious

objections to such an interpretation. No two groups have been connected satisfactorily; inhomogeneities in heights above the galactic plane, birth/death-rates or abundances are not reconcilable with an evolutionary connection. What is obvious is that at some earlier stage, either mass-loss of the hydrogen-rich envelope or mixing with the inner layers occurred, or a combination of both. The EHdBs are the only helium-rich stars for which there is any evidence of a close companion and the possibility of mass-exchange to explain the loss of the outer hydrogen-rich layer. The idea of the hydrogen deficiency arising from the collapse of a helium-rich gas-cloud is ruled out by observations showing them to be in close association with stars of apparently 'normal' composition. If hydrogen deficiency represents an evolutionary stage(s) through which most 'normal' stars can be expected to pass, it must be very short lived to account for the small numbers observed. Alternatively it may really represent a peculiar group of objects which have arrived at that stage by some particular, unusual factors and events.

In subsequent chapters, the properties of two groups of hydrogen-deficient stars are investigated, the EHe stars and the EHdBs.

1.2 The Extreme Helium Stars

The EHe stars are a group of about twenty hot, highly luminous stars whose atmospheres are extremely hydrogen-deficient ($n_H:n_{He} \lesssim 10^{-3}$), and which form an almost continuous temperature sequence between 8,500K and 34,000K (Schönberner et al. 1982). They show no evidence for binarity (Jeffery et al. 1987a). Table 1.1 is a list of all EHe stars known at the present time (taken from Drilling & Hill 1986).

The spectra of the EHe stars show strong lines of helium and very sharp lines of neutral, singly or doubly ionised metals. All the permitted lines of HeI are present and many of the profiles show the presence of forbidden components. Hydrogen lines are weak or absent, and Balmer line emission is not seen. All the elements normally detected in early B-stars are present, with the metallic lines greatly enhanced due to the lower opacity of the helium atmosphere. C, N and Ne show large overabundances, while O is often greatly diminished or absent. They are metal-rich, with Z=0.05. Even with carbon omitted they are still as metal-rich as the Sun. Only five EHe stars BD+10°2179, HD 168476, HD 124448, BD-9°4395 and BD-1°3438 have been examined by fine analysis to determine their abundances.

For models based on single-star evolution, there are two conceivable ways to produce the extreme hydrogen-deficiency observed in the EHe stars - either by ejection of the hydrogen-rich envelope at a certain phase of evolution, or by burning the hydrogen-rich atmosphere into helium by mixing of the star. Paczynski (1971) considered the loss of the hydrogen-rich atmosphere during evolution and found that this could happen for models with $\geqslant 5M_{\odot}$ just after the exhaustion of helium in the core. However, the EHe stars are believed to have masses of only about $1M_{\odot}$ so that the ejection scenario does not seem likely on account of their low masses. Instead he chose mixing as the most plausible explanation, regarding the observed surface enrichment of helium and carbon as direct evidence for mixing of the deep interior and stellar surface. He suggested that such mixing could perhaps be identified with thermal pulses of the helium shell in a double-shell burning phase (Schwarzschild and Härm 1967).

Schönberner (1977) suggested that the EHe stars are remnants of post-asymptotic giant-branch stars contracting to become white dwarfs which had somehow lost their hydrogen-rich envelopes. This scheme postulated that the EHe stars and RCB stars are in successive stages of evolution. However, Schönberner (1979) was unable to account for the EHe stars by the ejection of the hydrogen-rich envelopes of post-AGB stars by stellar winds. Hamann et al. (1982) investigated the mass-loss rates of EHe stars using ultra-violet spectra and found rates to be about the same order of magnitude as 'normal' stars with similar luminosities. More

Table 1.1 Extreme Helium Stars

NAME	RA (2000)	DEC	V	(B-V)
LSS 99	06 54 46	-10 48 41	12.29	0.70
BD+10°2179	10 38 55	+10 03 48	9.95	-0.19
LSS 3184	14 01 37	-66 10 02	12.60	0.03
HD124448	14 14 59	-46 17 19	9.98	-0.10
LSS 3378	15 38 59	-48 35 57	11.48	0.44
BD-9°4395	16 28 35	-09 19 34	10.54	0.06
HD160641	17 41 50	-17 54 08	9.83	0.14
LSE 78	17 42 34	-46 58 46	11.22	0.06
LSS 4357	17 44 25	-19 38 03	12.62	0.41
LSIV-1°2	17 51 27	-01 43 15	11.01	0.38
BD-1°3438	18 03 55	-01 00 13	10.33	0.46
LSIV+6°2	18 06 55	+06 21 46	12.17	-0.07
HD168476	18 23 15	-56 37 43	9.27	-0.01
LSS 5121	18 43 16	-18 31 47	13.25	0.32
LSIV-14°109	18 59 39	-14 26 11	11.15	0.33
LSII+33°5	19 45 17	+33 58 25	10.31	0.16
BD+1°4381	20 51 21	+02 18 47	9.56	0.19

Table 1.2 Extremely Hydrogen-Deficient Binaries

NAME	RA (2000)	DEC	V	(B-V)
KS Persei	04 48 54	+43 16 32	7.85	0.49
CPD-58°2721	10 47 57	-59 08 37	10.50	0.72
LSS 4300	17 37 59	-35 23 05	9.78	0.84
Ups Sgr	19 21 44	-15 57 18	4.61	0.10

recently, Webbink (1984) and Iben & Tutukov (1984) have investigated the merging of degenerate CO and He white dwarfs in close binaries to produce an EHe star. However, at this stage the origin of the hydrogen deficiency of the EHe stars must remain uncertain.

1.3 The Extremely Hydrogen-Deficient Binaries

The two single-lined spectroscopic binaries Upsilon Sagittarii (Ups Sgr) and KS Persei (HD30353), with orbital periods of 138 and 360 days respectively, exhibit extreme hydrogen-deficiency ($n_H:n_{He} \lesssim 10^{-3}$) and for some time have been considered to form a unique class of object (Plavec 1986). Drilling et al.(1985) showed that CPD-58°2721 (=LSS 1922, Drilling 1980) should be included as the third member of this group. A provisional orbital period of 43 days has been determined by Jeffery et al.(1987b). Using IUE and ground-based observations, Schönberner et al.(1982) and Drilling et al.(1984a) derive effective temperatures of 11,100K (CPD-58°2721), 10,500K (Ups Sgr), and 9,000K (KS Persei). Although the binary period is not known, radial-velocity measurements have also shown LSS 4300 (=HD320156) to be a single-lined spectroscopic binary (Jeffery et al. 1987a). With an effective temperature of T_{eff}=14,400K (Schönberner & Drilling 1984) it appears to represent an extension of the group to higher temperatures. From visual spectra, a higher effective temperature of 14,000K is indicated for CPD-58°2721 (Sect. 5.3), similar to that for LSS 4300. Although the presence of a companion has not been detected at visible wavelengths in any of the EHdBs, hot companions have been detected

in Ups Sgr and KS Persei from ultra-violet observations (Duvignau et al. 1979, Hack et al. 1980, Drilling & Schönberner 1982, Parthasarathy et al. 1986). Hot companions are less likely to be observable in CPD-58^{o}2721 and LSS 4300 due to the higher temperature of the primary.

These binaries are the only highly-luminous extreme helium-rich stars for which there is any evidence of a companion star (Drilling et al. 1984b, Jeffery et al. 1987a), and for these stars the hydrogen deficiency has found a natural explanation in binary evolution involving mass transfer (Plavec 1971, Schönberner & Drilling 1983). It is supposed that the system currently comprises a helium supergiant of $\sim 1M_{\odot}$ (primary) and a star of larger mass close to the main sequence (secondary). The supergiant primary is filling its Roche lobe for the second time and transferring mass towards the secondary. The presence of Hα and Hβ in emission in the spectrum supports the idea of mass-transfer. Whereas the EHe stars are carbon and nitrogen-rich relative to the Sun, the EHdBs are carbon-poor but nitrogen-rich. This overabundance of nitrogen has been interpreted as the exposure of CNO-processed material at the surface of the star following mass-transfer/loss. This is an evolution quite distinct from that of the EHe stars. Details of the four known EHdBs are given in Table 1.2 (taken from Drilling and Hill 1986).

1.4 Photometry: Observations and Reductions

1.4a SAAO PHOTOMETRY

Photometric observations of 3 EHe stars and 2 EHdBs were made at the South African Astronomical Observatory (SAAO) in 1984 May-July, 1985 April-June, and 1986 April-May. The 0.5-m telescope and Modular Photometer, and 1.0-m telescope and St Andrews Photometer, were used to obtain observations in the uvby system (SAAO Facilities Manual 1982). Telescope operation and recording of data were computer controlled

Two criteria were used in the selection of the comparison and check stars, that they should be in close proximity to the target star, and that they should be of approximately the same spectral type. Additionally, one or both should be within one magnitude of the target star. Each observational sequence normally consisted of a series of measurements of the target (Vr), comparison (C) and check (K) stars in the order C,Vr,C,Vr,K,Vr,C. The total sequence occupied about 45 minutes. Sky measurements were made at least once during each sequence, and more frequently when the sky background was high or when the sky background was changing quickly, such as at moon-rise and moon-set. Integration times were chosen to obtain approximately equal counts through each filter in the sequence yvbuubvy. This observing style more easily allows for the detection of erroneous integrations counts. Usually 20 standard star observations or more were made each night.

The observations were reduced on a computer at SAAO by Mrs J.E.Westerhuys to the standard Strömgren system (Crawford & Barnes 1970, Grønbech et al. 1976). The reductions utilised the most recently derived set of colour equations, using average estimates of the scale factors, colour terms, and extinctions derived over several observing seasons. Zero points were determined for each night from the standard star observations in order to obtain actual magnitudes and colours from the colour equations.

The data sets of the different observers in the 1985 observing season were not all reduced with the same set of colour equations in the original reductions at SAAO. It was necessary to re-reduce all the observations to the same set of colour equations at St Andrews using a copy of the program supplied by SAAO. A problem was encountered with the program procedure for handling the sky subtraction. In this procedure, only the most recent sky observation is considered, in strict chronological order, rather than a mean or interpolated value. This produced problems when the sky background was not negligible. It was necessary to edit the data files to ensure that an incorrect sky observation would not be picked up in the reductions.

1.4b OSN PHOTOMETRY

Strömgren observations of 4 EHe stars and 2 EHdBs were made over a 13-day period in 1985 August with the 0.75-m Steavenson telescope at the Observatorio del Sierra Nevada (OSN) of the Instituto de Astrofisica de Andalucia. Observations were made simultaneously in the four colours with the Danish six-channel uvby-Hß photometer (Florentin-Neilsen 1983). Telescope operation and recording of data were computer controlled. Each integration actually consisted of a series of one-second integrations. A calculation of the standard deviation of the one-second counts in each filter allowed an estimate of the quality of each integration.

Each of the target stars and their associated comparison and check stars were typically observed for 1-2 hours each night in the sequence C, Vr, K, C, Vr, K, ..., although the exact observing sequence varied for each object. Fewer check star observations were made for those comparison stars known not to vary from previous observations. Integration times were chosen so that the counts were above the theoretical one-percent noise level in each filter. For each observation, 3 consecutive integrations were usually obtained, averaged to improve the photon statistics. Poor seeing prompted the use of a large diaphragm (46" diameter). As many of the stars lie in crowded star fields, care had to be exercised in selecting a region free from background stars for sky measurements.

Typically, 20-30 observations of standard stars were made during the night taken from the list of uvby standard stars in the Astronomical Almanac for 1985. The procedure was to observe some 5 standards at the very beginning and end of the night, and at regular intervals in between. Each target star had an associated standard star nearby, which was observed at the beginning and end of every observing sequence. Due to mishandling of the computer disc files by the Instituto de Astrofisica de Andalucia, the files were lost, the only record of the observations being a hard-copy obtained simultaneously with the disc files at the time of the observations. This necessitated the laborious typing in by hand of the data (some ~150,000 characters) into computer files at St Andrews.

From the standard star observations, nightly estimates of the extinctions, scale factors and colour terms were obtained using Dr S.A.Bell's reduction package STANCOL (Bell 1987). As the determination of these parameters was not always satisfactory for a given night, average values from all the nights were used in the reductions. This is justified as these may be expected to change only slightly during the period of the observations. The target, comparison and check stars were in such close proximity that differential extinction between the programme stars was usually negligible. Zero-points were determined on 9 nights, which allowed actual magnitudes and colours to be estimated for these nights.

The programme star data was reduced using a modified version of Dr S.A.Bell's photometry reduction package SIMPHOT, a detailed description of which is given elsewhere (Bell 1987). This provides instrumental differential magnitudes in each of the four colours. The instrumental magnitudes and colours of the programme stars were corrected to the standard Strömgren colour system and Johnson V magnitudes using the transformation equations given below derived from the standard star observations :

$$V_{std} = \text{zero point} + y_{inst} - 0.015(\pm 0.017).(b-y)_{std}$$

$$(b-y)_{std} = \text{zero point} + 1.005(\pm 0.003).(b-y)_{inst}$$

$$(v-b)_{std} = \text{zero point} + 1.002(\pm 0.007).(v-b)_{inst} + 0.007(\pm 0.009).(b-y)_{std}$$

$$(u-b)_{std} = \text{zero point} + 1.051(\pm 0.006).(u-b)_{inst} + 0.085(\pm 0.022).(b-y)_{std}$$

where $(b-y)_{inst}$ and $(b-y)_{std}$ refer to the extinction-corrected instrumental (b-y) and standard (b-y) respectively. Differences between the instrumental and standard system in y, (b-y) and (v-b) are negligible, but amount to several hundredths of a magnitude in (u-b).

1.5 Spectroscopy: Observations and Reductions

Spectroscopic observations of CPD-58°2721 and the surrounding nebula were obtained with the 3.9-m Anglo-Australian Telescope (AAT) in 1982 February by Dr P.W.Hill, 1984 April by the writer, and 1985 March by the writer and Dr C.S.Jeffery. The Boksensberg Image Photon Counting System on the Royal Greenwich Observatory

Cassegrain Spectrograph (Robinson 1985) was used with the 82-cm camera to obtain two-dimensional spectra at a dispersion of 10Amm^{-1}. For the 1982/84 observations a 'short' slit-length of 19 pixels (each 1.4" on the sky) aligned W-E and approximately S-N was used to obtain observations in the spectral ranges 3240-4190A and 5750-6790A. In 1985 March a 'long' slit-length of 245 pixels (each 0.72" on the sky) aligned W-E was used to obtain a spectroscopic mapping across the nebula in the wavelength interval 6540-6780A, which includes the important Hα, [NII] 6548,6583A and [SII] 6719, 6734A nebular emission lines (Chap. 5).

Reductions were carried out with the help of Dr C.S.Jeffery using the STARLINK spectral reduction package SPICA on VAX computers of STARLINK and the University of St Andrews. Any characteristic small-scale sensitivity patterns across the detector were first removed by division of a normalised, rectified spectrum of a tungsten lamp (the flatfield) obtained at the beginning and end of each night. Fig. 1.2 shows the contributions in the short-slit spectroscopy to the different pixels along the slit aligned along an axis (approximately S-N) passing through CPD-58°2721 and a close 'companion' star 11" south of CPD-58°2721. To improve the signal-to-noise in the long-slit spectroscopy the pixels were summed in blocks of 10 (pixels 241-245 were excised from the data) during the data-reduction phase. Fig. 1.3 shows the data re-formatted into 24 pixels (each 7.2" on the sky).

Figure 1.2 The various contributions to the signal along the slit length in the 1982/84 short-slit spectroscopy, in this case for the slit aligned along an axis (19 degrees off S-N) passing through CPD-58°2721 and the close 'companion'. The 19 pixels provide a total coverage of 26.6 arcsec on the sky.

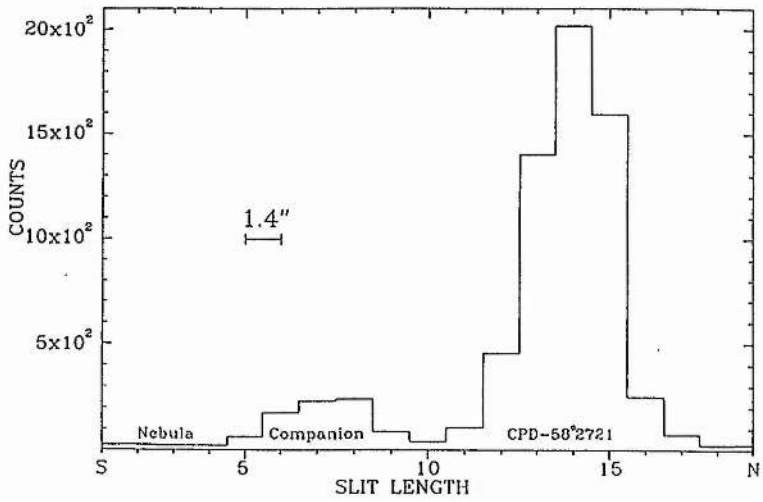

Figure 1.3 The various contributions to the signal along the slit length in the 1985 long-slit spectroscopy. The slit was aligned W-E, so that the close 'companion' makes no contribution. The original 245 pixels have been co-added in blocks of 10 to improve signal-to-noise (pixels 241-245 excluded). The 12th pixel corresponds to the star. The total coverage is 172.8 arcsec on the sky.

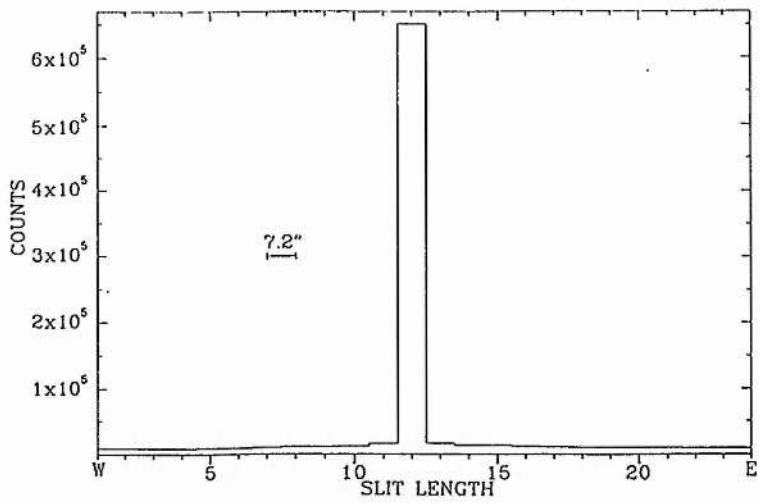

The arc spectrum of a copper-argon hollow-cathode lamp was recorded before and after each stellar exposure. A mean comparison spectrum from the two arc exposures compensated for the small shifts generally found between each pair and provided a comparison spectrum to define the wavelength scale of each stellar spectrum. The wavelength identifications given by Schinckel et al. (1982) were used to identify the arc lines. Wavelength calibration was by a least-squares polynomial fit, usually of 5th order, to the centroids of the lines of the comparison spectrum. The larger residuals for some calibrated spectra may be due to random measurement errors in the measured positions of the comparison spectra. Calibrations of red spectra are generally less certain than those in the blue region due to the paucity of lines in the comparison spectra at red wavelengths. Pixels corresponding to star or nebula were summed separately and extracted as one-dimensional spectra from the short-slit spectroscopy. Those pixels judged to be free of stellar contamination were used in the 'sky' subtraction. A polynomial fit to the wavelength-calibrated stellar data removed the slow variations present in the spectrum due to sensitivity variations across the detector and the shape of the stellar continuum. The scan-distortion along the slit in the short-slit observations was removed before wavelength calibration. However, the scan-distortion is more severe in the long-slit spectroscopy, and because of the need to obtain accurate radial-velocity measurements, it was necessary to calibrate the spectrum from each cross-section separately.

Two Cassegrain Echelle Spectrograms (CASPEC) of CPD-58°2721 obtained in 1985 April at the European Southern Observatory were kindly supplied by Dr U. Heber of Kiel University for use in a fine analysis. The observations were made with a 3.6-m telescope and CCD detector over the range 3900-4800A. Exposure times were 30 min. Details of the observations and reduction methods have been described by Heber et al. (1986). As the spectrum of CPD-58°2721 shows significant changes in the strengths of lines (Sect. 5.2) on a timescale of days the various AAT spectra obtained over several observing seasons are unsuited to use in the fine analysis.

A low dispersion spectrum of CPD-58°2721 covering the range 1150-2000A was obtained by the writer on the night of 1985 July 13/14th with the International Ultraviolet Explorer (IUE) satellite from the Villafranca satellite tracking station of the European Space Agency. A detailed description of the satellite and its operation has been given by Bogess et al. (1978a, 1978b). The short wavelength prime (SWP) camera was used to obtain a 7-hour exposure, but because of the large reddening of CPD-58°2721 it is not possible to obtain a well-exposed spectrum. The supplied image on the IUE Guest Observer Tape had been corrected for geometric distortion and calibrated in wavelength and flux. The image was extracted at Kiel and re-calibrated using the recommendations of Bohlin & Holm (1980). An additional IUE spectrum of CPD-58°2721 made with the long wavelength redundant (LWR) camera covering 1825-3300A, and SWP and LWR spectra of BD+1°4381, LSIV-1°2 and LSS 4300, were obtained from the World Data Centre.

2. Photometry of some Extremely Hydrogen-Deficient Stars

2.1 BD+1°4381

2.1a OBSERVATIONS

Photometric uvby observations of BD+1°4381 and its comparison (BD+2°4257) and check (BD+0°4598) stars were made at SAAO with the 0.5-m telescope on 15 nights during a 35-day period in 1984 May-June by the writer, Dr C.S.Jeffery and Mr R.A.Malaney, and on 26 nights during a 41-day period in 1985 April-June by the writer and Drs P.W.Hill and C.S.Jeffery. Observations were also made with the 1.0-m telescope during a 10-day period in 1986 April-May by Dr P.W.Hill. Additional observations of BD+1°4381 were obtained at OSN with a 0.75-m telescope in 1985 August on 10 nights during a 13-day period by the writer and Mr G.P.H.Willingale. Integration times for the OSN observations were chosen so that counts through the y filter were approximately 65(Vr), 80(C), and 40(K) thousand. Only differential magnitudes and colours in the standard system are given from the OSN observations. Details of the programme stars are given in Table 2.1. The observations are tabulated in Tables 2.2 & 2.3; the mean uvby magnitudes and colours of Table 2.1 are derived from the 1985 SAAO observations in Table 2.3. Parentheses indicate standard deviation about the mean in millimagnitudes, and n is the number of observations.

Table 2.1 Positions and mean uvby photometry of the programme stars from the 1984/85/86 SAAO observations of BD+1°4381.

	RA(1950)	Dec	Sp	<V>	<b-y>	<v-b>	<u-b>	<c_1>	<m_1>	n
BD+1°4381	20^h49^m	+02°07'	A	9.524 (023)	0.182 (007)	0.212 (005)	0.590 (011)	0.166 (011)	0.030 (007)	119
BD+2°4257 Comparison	20^h48^m	+03°05'	A2	9.251 (007)	0.130 (005)	0.279 (004)	1.576 (007)	1.019 (007)	0.148 (006)	119
BD+0°4598 Check	20^h49^m	+01°20'	A2	10.066 (011)	0.165 (009)	0.399 (010)	1.679 (020)	0.881 (022)	0.234 (015)	80

Table 2.2 The 1984 SAAO uvby photometry of BD+1°4381.

H.J.D.	Comparison				Variable - Comparison				Check - Comparison			
-2445000	V	(b-y)	(v-b)	(u-b)	V	(b-y)	(v-b)	(u-b)	V	(b-y)	(v-b)	(u-b)
844.651	9.254	0.128	0.288	1.598	0.266	0.028	-0.067	-0.996				
849.612	9.239	0.132	0.280	1.577	0.303	0.054	-0.072	-0.987	0.813	0.045	0.120	0.098
849.649	9.239	0.136	0.277	1.579	0.300	0.044	-0.064	-0.982	0.793	0.056	0.119	0.089
857.617	9.245	0.131	0.280	1.580	0.261	0.057	-0.074	-0.987				
858.605	9.257	0.121	0.280	1.582	0.255	0.060	-0.079	-0.999	0.829	0.023	0.120	0.119
858.658	9.258	0.122	0.275	1.577	0.252	0.052	-0.074	-0.993	0.802	0.034	0.140	0.100
859.594	9.249	0.133	0.283	1.586	0.256	0.052	-0.065	-0.990	0.813	0.034	0.118	0.111
859.639	9.255	0.133	0.286	1.592	0.256	0.053	-0.073	-1.003	0.820	0.027	0.130	0.094
860.577	9.247	0.127	0.283	1.582	0.257	0.058	-0.079	-1.002	0.810	0.045	0.121	0.083
860.613	9.253	0.127	0.283	1.575	0.254	0.054	-0.073	-0.993	0.820	0.034	0.120	0.087
860.659	9.245	0.131	0.274	1.573	0.260	0.049	-0.058	-0.986	0.820	0.032	0.136	0.095
861.441	9.262	0.142	0.287	1.580	0.253	0.056	-0.062	-0.988	0.851	0.046	0.125	0.217
861.530	9.255	0.136	0.286	1.588	0.252	0.046	-0.067	-1.001	0.826	0.030	0.124	0.122
861.583	9.247	0.131	0.282	1.577	0.253	0.046	-0.069	-0.995	0.798	0.046	0.117	0.101
861.649	9.248	0.126	0.277	1.572	0.250	0.057	-0.070	-0.998	0.814	0.036	0.126	0.111
862.533	9.253	0.134	0.282	1.581	0.272	0.054	-0.066	-0.996	0.835	0.041	0.122	0.132
862.567	9.251	0.128	0.284	1.588	0.275	0.055	-0.071	-1.004	0.823	0.038	0.134	0.118
862.630	9.252	0.131	0.284	1.579	0.279	0.053	-0.068	-1.002	0.811	0.035	0.126	0.095
866.564	9.241	0.136	0.282	1.581	0.289	0.043	-0.065	-0.995	0.827	0.019	0.125	0.111
866.604	9.254	0.129	0.279	1.581	0.281	0.054	-0.073	-1.008	0.825	0.028	0.120	0.100
866.645	9.260	0.122	0.280	1.573	0.281	0.047	-0.068	-0.991	0.816	0.017	0.154	0.132
873.571	9.248	0.121	0.282	1.577	0.298	0.056	-0.070	-0.998				
873.610	9.244	0.128	0.276	1.559	0.288	0.053	-0.067	-0.981				
873.637	9.245	0.131	0.271	1.564	0.292	0.052	-0.069	-0.990				
873.662	9.244	0.130	0.280	1.572	0.293	0.050	-0.067	-0.993				
873.678	9.238	0.133	0.285	1.575	0.301	0.051	-0.069	-1.002				
874.556	9.249	0.118	0.286	1.578	0.286	0.062	-0.070	-0.988	0.817	0.028	0.126	0.107
874.698	9.241	0.124	0.287	1.577	0.288	0.061	-0.073	-0.991				
874.625	9.237	0.136	0.267	1.571	0.293	0.052	-0.059	-0.988	0.808	0.032	0.125	0.084
874.651	9.242	0.126	0.280	1.578	0.290	0.051	-0.062	-0.989				
874.672	9.240	0.127	0.286	1.572	0.293	0.057	-0.076	-0.993				
875.576	9.264	0.123	0.287	1.588	0.291	0.057	-0.068	-0.988				
875.600	9.249	0.136	0.275	1.565	0.282	0.047	-0.060	-0.975				
875.632	9.252	0.127	0.284	1.578	0.285	0.053	-0.070	-0.990				
875.655	9.254	0.136	0.284	1.577	0.283	0.053	-0.068	-0.983				
875.670	9.259	0.138	0.289	1.581	0.278	0.049	-0.070	-0.979				
876.560	9.268	0.137	0.283	1.580	0.275	0.052	-0.069	-0.990				
876.654	9.266	0.133	0.277	1.568	0.273	0.054	-0.066	-0.984				
877.552	9.254	0.132	0.280	1.576	0.273	0.054	-0.066	-0.981				
877.582	9.258	0.130	0.283	1.581	0.259	0.065	-0.066	-0.981				
877.600	9.261	0.132	0.284	1.574	0.269	0.054	-0.071	-0.986				
877.629	9.257	0.132	0.280	1.571	0.273	0.059	-0.063	-0.978				
877.650	9.270	0.128	0.286	1.581	0.266	0.056	-0.070	-0.981				
877.666	9.275	0.132	0.284	1.581	0.277	0.046	-0.074	-0.982				
878.546	9.249	0.132	0.283	1.580	0.271	0.055	-0.065	-0.983				
878.629	9.244	0.131	0.282	1.574	0.275	0.058	-0.067	-0.980				
878.651	9.249	0.133	0.279	1.579	0.279	0.053	-0.064	-0.982				

Table 2.3 The 1985/86 SAAO and 1985 OSN uvby photometry of BD+1°4381.

H.J.D.	Comparison				Variable - Comparison				Check - Comparison			
-2446000	V	(b-y)	(v-b)	(u-b)	V	(b-y)	(v-b)	(u-b)	V	(b-y)	(v-b)	(u-b)
181.593	9.257	0.131	0.283	1.578	0.245	0.044	-0.074	-0.999	0.804	0.045	0.105	0.094
181.654	9.252	0.127	0.279	1.577	0.245	0.047	-0.062	-0.997	0.821	0.043	0.128	0.117
182.608	9.256	0.141	0.278	1.572	0.226	0.040	-0.074	-1.006				
185.612	9.256	0.128	0.277	1.582	0.227	0.047	-0.067	-1.011	0.820	0.028	0.129	0.108
186.561	9.258	0.132	0.278	1.562	0.234	0.050	-0.075	-1.001				
186.636	9.244	0.132	0.279	1.569	0.244	0.041	-0.074	-1.002				
187.626	9.246	0.132	0.276	1.576	0.254	0.042	-0.067	-1.004				
190.606	9.253	0.130	0.278	1.598	0.267	0.045	-0.070	-1.007				
191.593	9.260	0.138	0.276	1.572	0.279	0.041	-0.058	-0.982				
193.628	9.252	0.127	0.276	1.577	0.295	0.056	-0.072	-0.989	0.825	0.028	0.124	0.130
193.659	9.258	0.133	0.275	1.571	0.294	0.047	-0.069	-0.989				
194.590	9.246	0.124	0.276	1.569	0.298	0.047	-0.064	-0.983	0.826	0.029	0.121	0.106
194.615	9.247	0.128	0.274	1.579	0.298	0.048	-0.065	-0.989	0.812	0.043	0.117	0.095
194.643	9.244	0.130	0.275	1.579	0.295	0.056	-0.065	-0.991	0.814	0.042	0.119	0.085
197.576	9.251	0.125	0.281	1.570	0.268	0.051	-0.067	-0.979	0.817	0.039	0.110	0.098
197.600	9.253	0.125	0.277	1.571	0.264	0.052	-0.063	-0.981	0.816	0.037	0.121	0.093
197.624	9.252	0.128	0.277	1.572	0.267	0.050	-0.063	-0.981	0.822	0.030	0.114	0.101
197.647	9.255	0.126	0.277	1.573	0.261	0.057	-0.066	-0.980	0.810	0.034	0.124	0.116
198.537	9.250	0.133	0.274	1.570	0.264	0.046	-0.065	-0.980	0.820	0.031	0.124	0.098
198.569	9.245	0.129	0.275	1.577	0.266	0.055	-0.063	-0.980	0.826	0.031	0.119	0.104
198.597	9.248	0.131	0.273	1.572	0.263	0.050	-0.059	-0.976	0.814	0.029	0.127	0.104
198.625	9.244	0.131	0.275	1.571	0.262	0.052	-0.059	-0.975	0.818	0.033	0.130	0.090
198.649	9.238	0.131	0.276	1.577	0.270	0.049	-0.058	-0.979				
200.527	9.254	0.127	0.279	1.573	0.257	0.046	-0.071	-0.985	0.806	0.045	0.106	0.093
200.556	9.252	0.133	0.275	1.572	0.257	0.041	-0.064	-0.977	0.814	0.029	0.132	0.099
200.585	9.253	0.127	0.279	1.576	0.260	0.046	-0.071	-0.985	0.811	0.045	0.112	0.075
200.614	9.251	0.128	0.279	1.575	0.259	0.051	-0.070	-0.982	0.819	0.042	0.113	0.082
200.647	9.259	0.126	0.275	1.574	0.252	0.053	-0.071	-0.981	0.817	0.031	0.120	0.100
201.534	9.250	0.131	0.276	1.575	0.244	0.052	-0.069	-0.988	0.818	0.029	0.134	0.089
201.565	9.245	0.131	0.270	1.577	0.247	0.047	-0.062	-0.989	0.816	0.028	0.134	0.098
201.593	9.246	0.130	0.273	1.577	0.242	0.044	-0.061	-0.987	0.804	0.035	0.129	0.093
201.622	9.241	0.125	0.277	1.573	0.250	0.048	-0.072	-0.987	0.821	0.034	0.113	0.103
201.650	9.243	0.124	0.277	1.574	0.245	0.051	-0.070	-0.985	0.810	0.041	0.121	0.108
202.540	9.248	0.134	0.276	1.575	0.242	0.049	-0.072	-0.989	0.824	0.027	0.123	0.098
202.568	9.253	0.122	0.278	1.578	0.239	0.054	-0.074	-0.989	0.821	0.037	0.120	0.094
202.596	9.254	0.125	0.275	1.573	0.239	0.046	-0.065	-0.983	0.816	0.031	0.119	0.113
202.624	9.247	0.125	0.272	1.573	0.245	0.052	-0.068	-0.990	0.813	0.043	0.117	0.102
202.651	9.250	0.127	0.275	1.574	0.242	0.048	-0.067	-0.992	0.822	0.038	0.111	0.081
203.603	9.248	0.127	0.269	1.560	0.246	0.045	-0.067	-0.988	0.825	0.026	0.117	0.108
203.631	9.244	0.129	0.269	1.563	0.250	0.044	-0.063	-0.988	0.815	0.030	0.136	0.107
203.653	9.251	0.126	0.274	1.572	0.240	0.051	-0.070	-1.000	0.816	0.035	0.120	0.091
209.544	9.247	0.133	0.272	1.569	0.275	0.048	-0.062	-0.967	0.814	0.030	0.120	0.112
209.573	9.243	0.134	0.275	1.578	0.277	0.054	-0.066	-0.981	0.818	0.038	0.123	0.085
209.614	9.243	0.133	0.277	1.577	0.279	0.045	-0.067	-0.976	0.817	0.033	0.120	0.094
209.642	9.242	0.132	0.279	1.575	0.273	0.056	-0.070	-0.977	0.816	0.025	0.122	0.112
210.526	9.248	0.128	0.275	1.577	0.278	0.053	-0.062	-0.980	0.813	0.040	0.108	0.076
210.641	9.252	0.130	0.276	1.575	0.277	0.053	-0.067	-0.976	0.822	0.021	0.129	0.096
211.541	9.259	0.131	0.279	1.572	0.279	0.057	-0.062	-0.967	0.813	0.035	0.119	0.100
211.568	9.252	0.132	0.281	1.578	0.294	0.050	-0.063	-0.971	0.823	0.033	0.114	0.094
211.658	9.260	0.123	0.278	1.583	0.285	0.061	-0.062	-0.976	0.815	0.038	0.123	0.093
214.532	9.246	0.130	0.279	1.572	0.318	0.058	-0.063	-0.963	0.811	0.037	0.108	0.099
214.551	9.246	0.130	0.279	1.575	0.316	0.063	-0.063	-0.967	0.809	0.036	0.118	0.101
215.522	9.257	0.135	0.274	1.563	0.313	0.065	-0.063	-0.952	0.822	0.040	0.129	0.137
215.547	9.248	0.130	0.279	1.572	0.319	0.069	-0.058	-0.955	0.808	0.042	0.124	0.098
216.529	9.248	0.133	0.275	1.572	0.325	0.063	-0.065	-0.962	0.826	0.033	0.120	0.113

216.551	9.249	0.135	0.275	1.581	0.323	0.058	-0.057	-0.968	0.820	0.030	0.130	0.104
216.661	9.256	0.139	0.272	1.569	0.317	0.054	-0.059	-0.956				
217.526	9.256	0.132	0.276	1.573	0.323	0.058	-0.055	-0.948	0.811	0.049	0.141	0.162
217.658	9.248	0.132	0.274	1.575	0.330	0.056	-0.057	-0.960				
218.530	9.245	0.132	0.281	1.565	0.315	0.064	-0.065	-0.963	0.812	0.035	0.122	0.086
218.651	9.252	0.130	0.280	1.576	0.315	0.059	-0.064	-0.971	0.812	0.042	0.115	0.087
219.537	9.250	0.130	0.275	1.584	0.306	0.061	-0.063	-0.984	0.820	0.030	0.117	0.081
219.641	9.257	0.133	0.275	1.573	0.292	0.061	-0.059	-0.966	0.817	0.031	0.125	0.135
220.548	9.248	0.132	0.277	1.574	0.289	0.057	-0.067	-0.979	0.813	0.044	0.106	0.099
220.648	9.246	0.124	0.273	1.569	0.285	0.056	-0.067	-0.981	0.814	0.043	0.093	0.099
221.548	9.253	0.134	0.280	1.583	0.288	0.056	-0.066	-0.979	0.812	0.044	0.106	0.098
221.648	9.248	0.125	0.274	1.571	0.285	0.056	-0.067	-0.981	0.814	0.043	0.093	0.098
295.531					0.267	0.053	-0.055	-1.004				
295.559					0.252	0.065	-0.064	-0.992				
296.383					0.254	0.063	-0.060	-0.989	0.826	0.026	0.118	0.101
296.393					0.258	0.063	-0.064	-0.985				
296.403					0.254	0.064	-0.059	-0.993	0.814	0.043	0.119	0.105
296.580					0.254	0.061	-0.060	-0.989				
297.552					0.245	0.062	-0.059	-0.987				
297.559					0.246	0.064	-0.069	-0.981	0.816	0.025	0.114	0.099
297.567					0.250	0.066	-0.068	-0.987				
298.570					0.246	0.063	-0.072	-0.991				
298.575					0.235	0.058	-0.071	-0.994	0.805	0.041	0.127	0.111
298.583					0.246	0.056	-0.062	-0.988				
299.512					0.254	0.066	-0.067	-0.994	0.826	0.033	0.129	0.104
299.522					0.245	0.051	-0.065	-0.996				
299.529					0.233	0.057	-0.081	-0.991	0.811	0.035	0.115	0.110
300.514					0.245	0.057	-0.061	-0.997	0.819	0.035	0.116	0.098
300.523					0.243	0.058	-0.076	-0.992				
300.532					0.247	0.051	-0.069	-0.997	0.829	0.027	0.116	0.097
300.543					0.242	0.056	-0.076	-1.007	0.827	0.029	0.129	0.099
301.579					0.232	0.052	-0.074	-0.979				
301.587					0.222	0.067	-0.074	-0.986	0.804	0.039	0.118	0.119
301.593					0.241	0.061	-0.071	-0.999				
301.601					0.244	0.060	-0.070	-0.999	0.822	0.026	0.124	0.091
304.509					0.245	0.057	-0.067	-0.997				
304.515					0.248	0.057	-0.060	-0.996				
304.525					0.259	0.051	-0.064	-0.980	0.820	0.026	0.134	0.113
304.531					0.273	0.054	-0.064	-0.997				
304.542					0.268	0.052	-0.065	-1.001	0.825	0.036	0.115	0.100
306.546					0.258	0.054	-0.060	-0.993				
306.559					0.264	0.050	-0.066	-0.986	0.802	0.021	0.128	0.084
306.564					0.270	0.053	-0.060	-1.004	0.820	0.024	0.134	0.107
306.573					0.278	0.048	-0.056	-0.999	0.818	0.025	0.132	0.086
307.498					0.253	0.070	-0.068	-1.019				
307.506					0.259	0.060	-0.057	-1.013				
307.520					0.254	0.054	-0.062	-0.985	0.825	0.034	0.111	0.108
307.527					0.261	0.064	-0.066	-1.039				
307.536					0.249	0.063	-0.059	-1.045				
547.661	9.246	0.145	0.279	1.581	0.249	0.033	-0.063	-0.998				
551.653	9.247	0.134	0.280	1.578	0.263	0.048	-0.067	-1.001				
552.640	9.254	0.131	0.281	1.583	0.261	0.049	-0.063	-0.996				
555.630	9.245	0.131	0.286	1.589	0.255	0.050	-0.065	-0.990	0.825	0.027	0.122	0.107
556.637	9.250	0.134	0.281	1.582	0.252	0.051	-0.060	-0.987	0.811	0.035	0.131	0.106

From inspection of the 1984 observations presented in Fig. 2.1 (taken from Jeffery and Malaney 1985), BD+1°4381 shows a variation in V of 0.04 mag. Smaller amplitude variations are apparent in (u-b), whilst variations in (b-y) and (v-b) are comparable to the scatter in the data. Although the timebase of the observations is of the same order as the timescale of the variation, useful information can still be obtained from a frequency analysis. On the assumption that the light curve is singly periodic the method of least squares was used to fit a sine-wave function (Skillen 1985) to the V observations (Fig. 2.2, taken from Jeffery & Malaney 1985). frequency was swept over a small range close to the estimated frequency in order to obtain the best solution which was found to correspond to a period of 21.2 days. The 10 per cent error is only estimated but is consistent with the formal error expected had the data been equally spaced. A similar technique was applied to the (b-y) colour curve, but since the amplitude of the colour variation is small compared to the scatter in the data, the frequency obtained from the light curve is to be preferred. Whilst the fit to the light curve was encouraging, further accurate photometry over an extended period was required to determine whether BD+1°4381 is singly periodic, and to improve the period determination.

The light and colour curves for the 1985 SAAO observations are shown in Fig. 2.3 along with the 1985 OSN and 1986 SAAO observations. The light variability of BD+1°4381 appears to be due to a periodic variation of about 23 days (noting successive light minima at JD 2446194 and 217) and amplitude 0.07 mag in V. The

Figure 2.1 Differential light and colour plots for the 1984 SAAO observations of BD+1°4381. All but the V curve have been offset by arbitrary constants.

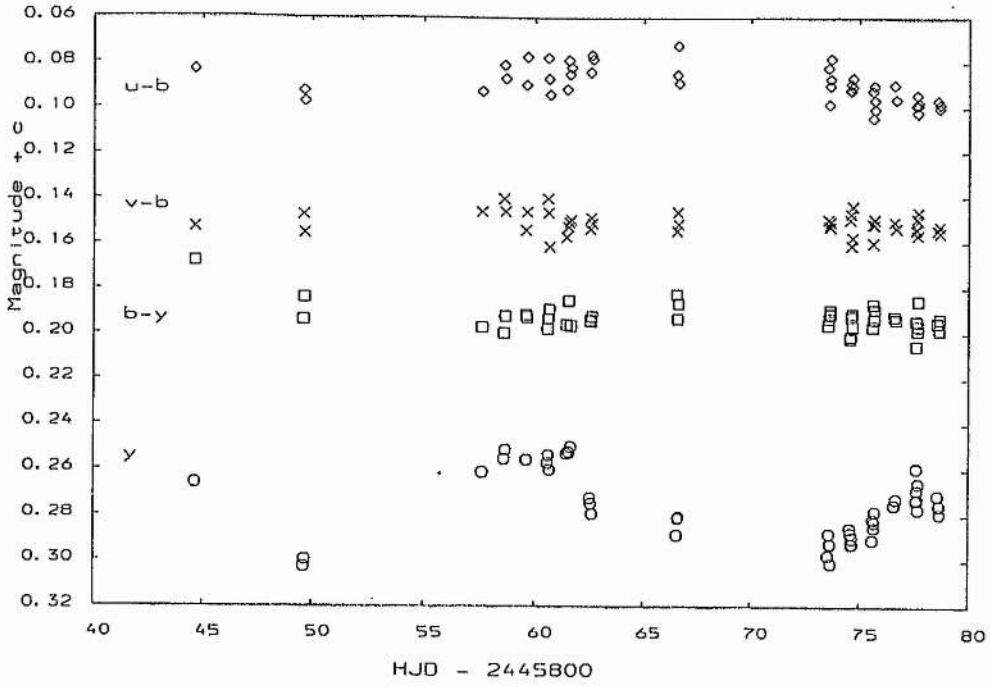

Figure 2.2 Differential V and (b-y) data of Figure 2.1 phased with a period of 21.1 days. The curves have been offset by arbitrary constants.

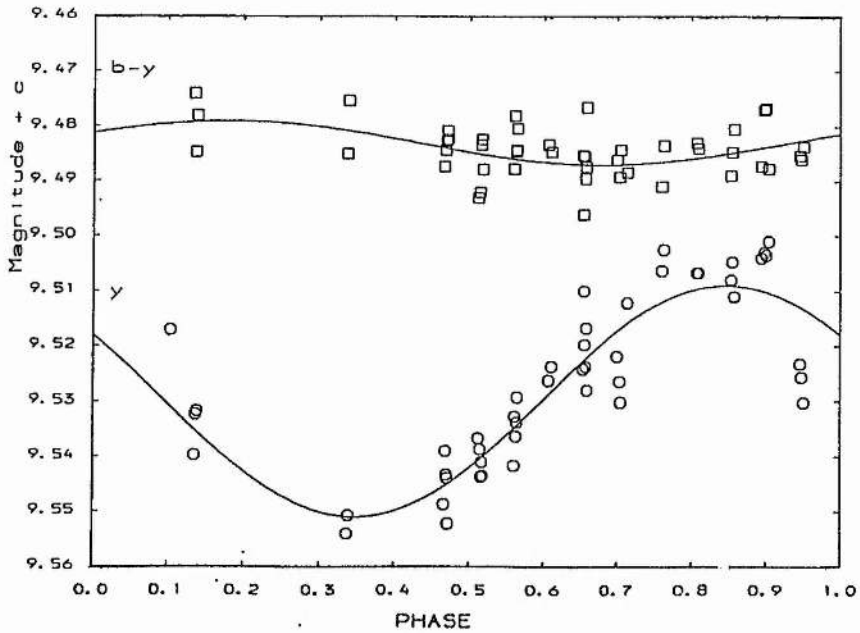

shape of the light curve appears variable, the fundamental variation appearing superimposed on a secular or longer-term dimming of BD+1°4381, a feature also present in the light curves of the RCB stars (Alexander et al. 1972, Fernie 1982). This introduces a difficulty when attempting to determine the period of the star. Assuming the slow variation to be independent of the fundamental period, it was removed by applying a high-pass filter to the data. A best fit with the 1985 SAAO observations using a sine-wave function was obtained with a period of 22.1 days. The data from the 1984 and 1985 SAAO observations were combined and a single sine-wave function swept over a range of periods between 15-30 days in order to obtain the best fit to the combined data sets. The goodness of fit was determined from a number of statistical parameters, including the multiple correlation coefficient. The data are still insufficient to determine the period unambiguously, an uncertainty of 1 cycle per year remaining in the frequency. The two best values for the period are 21.5 and 23.0 days. It is now possible to determine the amplitude of the colour variations more precisely from the 1985 SAAO observations than was possible with the 1984 SAAO observations. The amplitude of the light curve is 0.057 ± 0.003 mag and in (u-b) the variation is 0.015 ± 0.002 mag. The variations in (b-y) and (v-b) are somewhat smaller and at 0.005 ± 0.002 are comparable with the scatter in the data. Maximum changes of 0.2 in surface gravity and 200K in T_{eff} are estimated from model atmospheres of EHe stars (Heber & Schönberner 1981) for the observed colour changes.

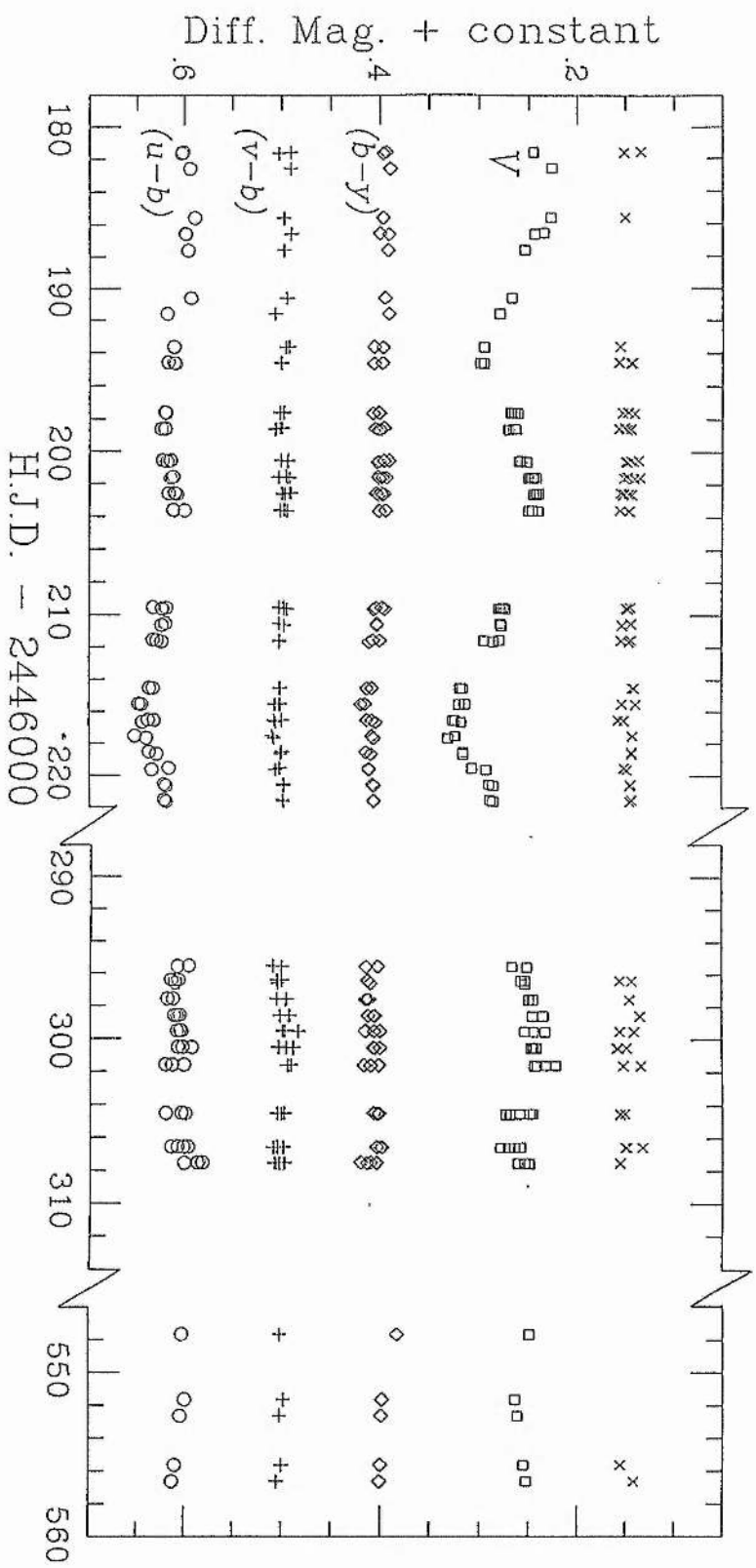

Figure 2.3 Differential 1985/86 uvby photometry of BD+1°4381. All but the V curve have been offset by arbitrary constants. The crosses show the V curve for the K-C observations.

In an attempt to resolve the period ambiguity Fig. 2.4 shows sine-waves covering the time of the OSN observations generated from least-squares fits with 21.5 and 23.0-day periods to the 1985 SAAO data. The time difference of 100 days between the mid-dates of the two sets of data represents 4.65 and 4.34 cycles, a phase lag of 0.31 in the 23.0-day period (full line) to the 21.5-day period (dashed line). Clearly the 21.5-day period provides a very poor fit, and whilst the 23.0-day period is to be preferred the fit is not very satisfactory. The dotted line in Fig. 2.4 represents the best fit from sweeping a sine-wave through the 1985 SAAO and OSN data. This gave a period of 24.2 days. Any analysis of the light curve of BD+1^{o}4381 for periodic behaviour is complicated in that the shape of the light curve appears to be variable. It is not possible to say whether any similar trend is present in the 1984 SAAO or 1985 OSN observations.

2.1b DISCUSSION

BD+1^{o}4381 was found to be extremely hydrogen-deficient by Drilling (1979). He noted that the spectrum of BD+1^{o}4381 (Drilling 1979) resembles those of the EHdBs Ups Sgr and KS Persei. Using satellite and ground-based observations, Drilling et al. (1984a) derived an effective temperature of 9,500$\pm$400K for BD+1^{o}4381, similar to those for Ups Sgr and KS Persei, both of which also show small-amplitude light and colour variations.

The presence of colour changes concomitant with the light variations is indicative of temperature changes and suggests strongly that the star is pulsating radially. By contrast, colour changes have not been detected in the two hot EHe variables, BD-9°4395 and HD160641. The variations observed in these stars have consequently been attributed to non-radial pulsations (Jeffery et al. 1985, Lynas-Gray et al. 1987), where geometrical distortions of the stellar disk at constant temperature lead to apparent brightness changes. BD+1°4381 appears to represent a straightforward extension of radial pulsation in RCB stars (Alexander et al. 1972) to higher temperatures. Variability studies on the two coolest EHe stars, LSS 3378 (Drilling 1973) and LSIV-14°109 (Drilling 1979), would help greatly in determining the reality of a $P\text{-}T_{eff}$ sequence and the relation of the cooler EHe stars to the RCB stars.

Attempts to reconcile the various period determinations have failed to yield a singly-periodic light curve which matches the 1984 SAAO, 1985 SAAO and 1985 OSN observations (the 1986 SAAO data are too few to be usable in this context). Some coherence is demonstrable in that independent analyses of both the 1984 and 1985 SAAO samples give a period of 21-22 days. However, both of these studies share the difficulty that the data strings are either too undersampled in combination or too short in isolation for a period to be determined unambiguously. The formal uncertainty given by the bandwidth of the truncated signal sequence is approximately ± 7 days. The failure to find a singly-periodic model for the light

Figure 2.4 Differential V curve for BD+1°4381. P=23.0 days (full line), P=21.5 days (dashed line), P=24.2 days (dotted line). See text for an explanation.

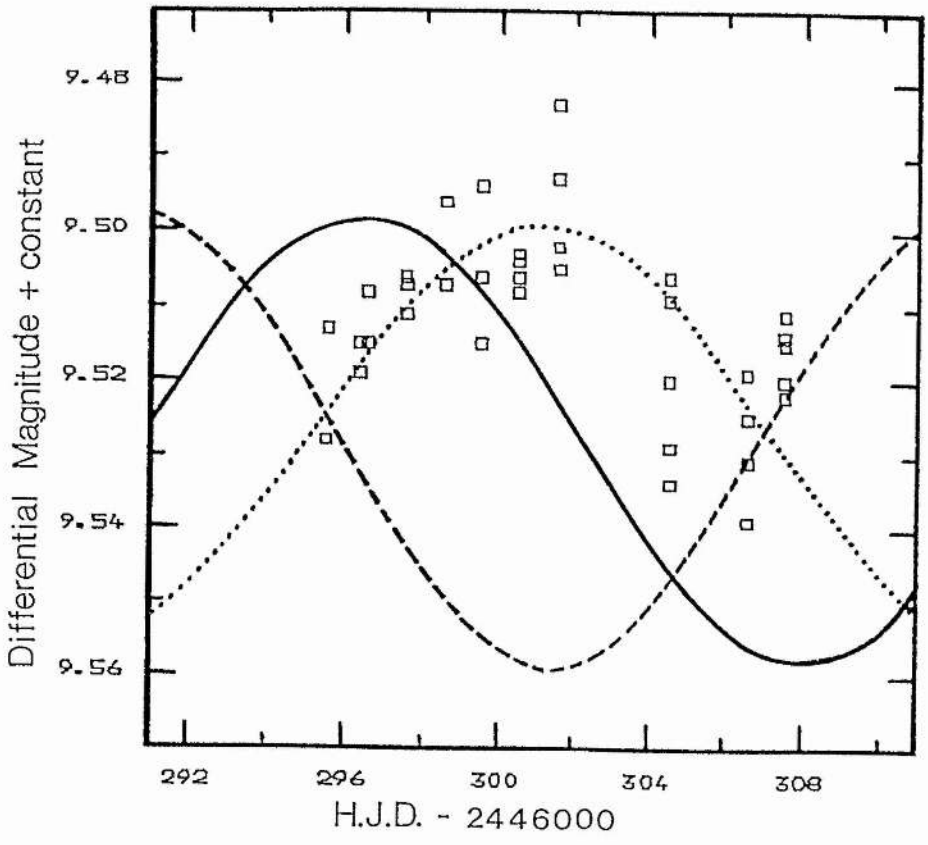

Table 2.4 Positions and mean uvby photometry of BD-1°3438.

	RA(1950)	Dec	Sp	<V>	<b-y>	<v-b>	<u-b>	$<c_1>$	$<m_1>$	n
BD-1°3438	18^h01^m	-00°58'	B	10.304 (018)	0.381 (007)	0.410 (007)	1.068 (016)	0.248 (016)	0.029 (010)	138
BD-1°3435 Comparison	18^h00^m	-01°20'	B9	7.965 (006)	0.152 (003)	0.216 (003)	1.372 (006)	0.940 (006)	0.064 (005)	138
BD-0°3406 Check	18^h02^m	-00°47'	A0	10.517 (010)	0.282 (011)	0.352 (010)	1.767 (015)	1.063 (022)	0.070 (017)	124

curve and the longer-term trend in the 1985 SAAO data noted above leads to the conclusion that the light curve may not be completely regular, the inconsistencies in the estimates of the period owing themselves to real irregularities in the period. There is no difficulty with such a conclusion since strictly regular oscillations are anticipated by neither previous observations of highly luminous helium stars (e.g. Ups Sgr: Chap. 3; RY Sgr: Alexander et al. 1972) nor by theory ("pulsations in high luminosity stars are extremely non-adiabatic": Saio 1986). Such an interpretation may also be useful in explaining the light curve of BD-1°3438 presented in Sect. 2.2.

2.2 BD-1°3438

2.2a OBSERVATIONS

Photometric uvby observations of BD-1°3438 and its comparison (BD-1°3435) and check (BD-0°3406) stars were made at SAAO with the 0.5-m telescope on 26 nights during a 41-day period in 1985 April-June by the writer and Drs P.W.Hill and C.S.Jeffery. Additional observations of BD-1°3438 were obtained at OSN with a 0.75-m telescope in 1985 August on 6 nights during a 9-day period by the writer and Mr G.P.H.Willingale. Only differential magnitudes and colours in the standard system are given from the OSN observations.

Table 2.5 The uvby photometry of BD-1°3438.

H.J.D.	Comparison				Variable - Comparison				Check - Comparison			
-2446000	V	(b-y)	(v-b)	(u-b)	V	(b-y)	(v-b)	(u-b)	V	(b-y)	(v-b)	(u-b)
181.497	7.963	0.152	0.220	1.374	2.321	0.244	0.197	-0.291	2.553	0.137	0.137	0.413
181.635	7.963	0.154	0.216	1.370	2.324	0.236	0.191	-0.302	2.557	0.134	0.123	0.371
182.460	7.966	0.157	0.217	1.366	2.354	0.226	0.195	-0.291	2.540	0.132	0.138	0.395
182.544	7.963	0.148	0.220	1.370	2.350	0.243	0.198	-0.292				
182.562	7.965	0.149	0.220	1.372	2.352	0.238	0.198	-0.287	2.559	0.131	0.144	0.415
182.640	7.962	0.151	0.216	1.366	2.345	0.231	0.196	-0.296	2.554	0.135	0.131	0.419
185.429	7.972	0.148	0.217	1.354	2.327	0.221	0.184	-0.320	2.532	0.108	0.115	0.385
185.657	7.968	0.152	0.219	1.373	2.343	0.228	0.197	-0.304	2.561	0.144	0.136	0.391
186.602	7.964	0.153	0.216	1.367	2.357	0.227	0.195	-0.312	2.546	0.126	0.139	0.394
187.598	7.964	0.154	0.217	1.370	2.342	0.245	0.194	-0.315	2.544	0.138	0.131	0.374
187.650	7.973	0.151	0.217	1.374	2.361	0.225	0.191	-0.304	2.547	0.128	0.136	0.409
191.561	7.972	0.155	0.221	1.377	2.346	0.224	0.212	-0.275				
191.631	7.975	0.154	0.214	1.369	2.353	0.240	0.204	-0.247				
193.483	7.961	0.153	0.215	1.366	2.386	0.253	0.208	-0.256				
193.534	7.963	0.151	0.214	1.372	2.377	0.232	0.201	-0.247	2.543	0.151	0.121	0.412
194.411	7.951	0.152	0.207	1.342	2.352	0.243	0.190	-0.299				
194.506	7.965	0.150	0.215	1.369	2.350	0.234	0.193	-0.289	2.546	0.147	0.120	0.391
194.537	7.965	0.150	0.215	1.367	2.354	0.235	0.203	-0.283	2.553	0.129	0.120	0.390
195.461	7.959	0.155	0.215	1.380	2.375	0.231	0.203	-0.290	2.555	0.135	0.122	0.374
195.489	7.972	0.155	0.213	1.377	2.353	0.233	0.200	-0.290	2.543	0.136	0.135	0.390
197.433	7.967	0.155	0.216	1.373	2.373	0.224	0.199	-0.297	2.559	0.112	0.147	0.391
197.457	7.971	0.151	0.221	1.373	2.377	0.221	0.193	-0.294	2.564	0.112	0.127	0.376
197.483	7.964	0.152	0.217	1.368	2.377	0.225	0.193	-0.290	2.544	0.129	0.142	0.384
197.508	7.963	0.150	0.217	1.369	2.370	0.236	0.197	-0.293	2.545	0.128	0.143	0.394
197.530	7.965	0.148	0.216	1.369	2.377	0.230	0.197	-0.288	2.550	0.121	0.137	0.399
198.411	7.958	0.150	0.217	1.371	2.379	0.225	0.204	-0.271	2.564	0.116	0.126	0.400
198.434	7.959	0.151	0.216	1.373	2.376	0.227	0.199	-0.281	2.562	0.115	0.139	0.402
198.457	7.961	0.148	0.220	1.376	2.379	0.233	0.197	-0.294	2.562	0.122	0.140	0.394
198.482	7.960	0.149	0.219	1.372	2.370	0.238	0.194	-0.280	2.544	0.129	0.139	0.396
199.486	7.961	0.154	0.216	1.372	2.344	0.222	0.206	-0.281	2.570	0.110	0.140	0.383
199.509	7.964	0.152	0.218	1.369	2.344	0.232	0.190	-0.293	2.552	0.132	0.132	0.385
199.535	7.970	0.150	0.215	1.369	2.340	0.233	0.194	-0.285	2.548	0.130	0.138	0.381
200.404	7.959	0.154	0.213	1.369	2.339	0.226	0.202	-0.295	2.554	0.137	0.137	0.380
200.426	7.961	0.153	0.215	1.369	2.337	0.228	0.197	-0.300	2.555	0.126	0.129	0.389
200.449	7.964	0.150	0.217	1.371	2.331	0.238	0.197	-0.298	2.543	0.137	0.133	0.385
200.471	7.965	0.150	0.217	1.372	2.337	0.236	0.190	-0.295	2.557	0.116	0.143	0.405
200.488	7.962	0.153	0.218	1.374	2.337	0.234	0.193	-0.304				
201.400	7.964	0.149	0.214	1.370	2.357	0.234	0.195	-0.298	2.538	0.133	0.143	0.388
201.423	7.963	0.150	0.213	1.371	2.364	0.233	0.196	-0.292	2.557	0.118	0.141	0.390
201.445	7.961	0.152	0.215	1.368	2.356	0.234	0.201	-0.288	2.546	0.138	0.138	0.389
201.468	7.961	0.148	0.216	1.372	2.364	0.229	0.202	-0.283	2.554	0.125	0.141	0.399
201.490	7.959	0.148	0.217	1.376	2.361	0.232	0.189	-0.287	2.546	0.127	0.144	0.401
202.407	7.968	0.150	0.217	1.375	2.346	0.239	0.192	-0.304	2.539	0.152	0.121	0.370
202.430	7.960	0.153	0.217	1.373	2.346	0.237	0.190	-0.303	2.552	0.128	0.135	0.381
202.452	7.960	0.150	0.218	1.374	2.344	0.235	0.198	-0.296	2.550	0.131	0.140	0.375
202.474	7.961	0.151	0.216	1.373	2.341	0.237	0.192	-0.300	2.541	0.136	0.134	0.386
202.497	7.960	0.150	0.213	1.372	2.342	0.233	0.198	-0.294	2.539	0.135	0.142	0.406
203.428	7.960	0.151	0.216	1.369	2.333	0.228	0.197	-0.295	2.556	0.123	0.136	0.389
203.451	7.960	0.151	0.216	1.369	2.327	0.225	0.200	-0.290	2.545	0.127	0.144	0.386
203.474	7.958	0.151	0.215	1.368	2.328	0.233	0.205	-0.297	2.559	0.115	0.136	0.407
203.497	7.958	0.151	0.216	1.366	2.323	0.235	0.194	-0.298	2.549	0.125	0.131	0.397
203.520	7.958	0.152	0.211	1.362	2.327	0.228	0.202	-0.287	2.544	0.130	0.138	0.399
203.544	7.960	0.148	0.210	1.364	2.318	0.245	0.199	-0.301	2.548	0.126	0.141	0.404
205.379	7.954	0.154	0.213	1.365	2.325	0.231	0.186	-0.330	2.546	0.134	0.140	0.380
205.402	7.964	0.150	0.221	1.375	2.330	0.221	0.190	-0.317	2.551	0.133	0.127	0.385

205.425	7.965	0.153	0.218	1.375	2.318	0.238	0.185	-0.325	2.549	0.120	0.139	0.394
205.448	7.969	0.154	0.220	1.380	2.323	0.230	0.190	-0.316	2.544	0.138	0.142	0.388
205.471	7.971	0.158	0.221	1.381	2.328	0.226	0.190	-0.315	2.543	0.134	0.131	0.388
205.494	7.973	0.158	0.219	1.380	2.324	0.229	0.192	-0.317	2.551	0.130	0.128	0.381
205.516	7.977	0.157	0.219	1.380	2.324	0.226	0.196	-0.308	2.547	0.129	0.136	0.399
205.539	7.982	0.156	0.220	1.381	2.324	0.229	0.193	-0.310	2.562	0.125	0.129	0.392
205.562	7.981	0.157	0.219	1.383	2.321	0.233	0.192	-0.312	2.543	0.135	0.131	0.411
209.405	7.974	0.148	0.219	1.372	2.354	0.232	0.188	-0.304	2.548	0.130	0.145	0.401
209.432	7.974	0.152	0.214	1.371	2.351	0.230	0.194	-0.304	2.551	0.123	0.139	0.411
209.474	7.968	0.151	0.216	1.369	2.357	0.230	0.185	-0.314	2.559	0.122	0.130	0.397
209.497	7.967	0.148	0.217	1.369	2.346	0.233	0.197	-0.298	2.542	0.138	0.133	0.384
210.394	7.963	0.155	0.219	1.375	2.345	0.232	0.192	-0.324	2.554	0.123	0.134	0.411
210.416	7.956	0.155	0.222	1.375	2.350	0.232	0.182	-0.323	2.558	0.124	0.139	0.391
210.437	7.961	0.151	0.217	1.373	2.356	0.227	0.185	-0.321	2.560	0.135	0.127	0.400
210.466	7.963	0.154	0.215	1.374	2.347	0.227	0.200	-0.318	2.547	0.131	0.138	0.376
210.486	7.962	0.154	0.215	1.373	2.351	0.225	0.196	-0.308	2.547	0.129	0.139	0.391
210.566	7.964	0.149	0.214	1.364	2.340	0.245	0.187	-0.311	2.535	0.148	0.132	0.393
210.587	7.963	0.153	0.208	1.364	2.339	0.243	0.193	-0.323	2.542	0.135	0.138	0.386
210.609	7.967	0.151	0.208	1.366	2.352	0.226	0.193	-0.314	2.549	0.134	0.128	0.391
211.392	7.965	0.156	0.210	1.364	2.317	0.228	0.194	-0.320				
211.415	7.965	0.150	0.213	1.364	2.310	0.237	0.198	-0.319	2.532	0.141	0.151	0.394
211.436	7.961	0.149	0.215	1.369	2.312	0.233	0.194	-0.323	2.538	0.127	0.146	0.397
211.463	7.958	0.152	0.213	1.369	2.321	0.226	0.194	-0.317	2.555	0.115	0.148	0.408
211.487	7.958	0.151	0.215	1.375	2.321	0.228	0.194	-0.324	2.542	0.131	0.139	0.397
211.508	7.965	0.148	0.219	1.366	2.314	0.235	0.191	-0.314	2.540	0.143	0.126	0.394
211.609	7.970	0.155	0.217	1.366	2.317	0.231	0.188	-0.320	2.544	0.137	0.133	0.390
211.632	7.970	0.155	0.218	1.372	2.325	0.225	0.195	-0.318	2.567	0.113	0.142	0.412
212.448	7.985	0.153	0.216	1.385	2.307	0.237	0.190	-0.330	2.575	0.125	0.141	0.375
212.470	7.981	0.162	0.219	1.382	2.301	0.222	0.194	-0.316	2.550	0.122	0.139	0.394
212.491	7.983	0.160	0.221	1.377	2.311	0.220	0.186	-0.313	2.550	0.118	0.134	0.376
214.449	7.959	0.153	0.217	1.368	2.358	0.219	0.186	-0.302	2.559	0.131	0.128	0.417
214.471	7.963	0.150	0.218	1.368	2.359	0.225	0.192	-0.301	2.557	0.137	0.145	0.430
214.493	7.962	0.150	0.217	1.372	2.346	0.228	0.184	-0.314	2.554	0.137	0.127	0.385
214.615	7.956	0.158	0.215	1.372	2.351	0.224	0.189	-0.311	2.560	0.130	0.125	0.400
214.633	7.962	0.154	0.213	1.369	2.357	0.215	0.193	-0.311				
215.368	7.962	0.149	0.218	1.384	2.346	0.229	0.184	-0.292	2.561	0.135	0.133	0.432
215.390	7.964	0.150	0.218	1.378	2.345	0.227	0.194	-0.295	2.557	0.140	0.133	0.416
215.412	7.963	0.154	0.214	1.376	2.348	0.224	0.188	-0.301	2.563	0.124	0.142	0.411
215.440	7.961	0.156	0.215	1.374	2.345	0.220	0.200	-0.295	2.548	0.140	0.406	0.392
215.461	7.966	0.151	0.215	1.375	2.338	0.230	0.193	-0.309	2.547	0.139	0.135	0.366
215.486	7.967	0.147	0.220	1.374	2.338	0.230	0.184	-0.306	2.542	0.144	0.146	0.402
215.587	7.969	0.149	0.217	1.371	2.339	0.223	0.190	-0.296	2.550	0.122	0.148	0.410
215.608	7.966	0.151	0.214	1.370	2.344	0.224	0.193	-0.300	2.554	0.126	0.137	0.406
215.629	7.969	0.152	0.214	1.368	2.333	0.228	0.191	-0.298	2.550	0.123	0.141	0.393
216.447	7.962	0.156	0.213	1.370	2.331	0.223	0.197	-0.299	2.560	0.115	0.150	0.401
216.468	7.963	0.156	0.214	1.372	2.326	0.229	0.193	-0.308	2.554	0.124	0.132	0.383
216.489	7.961	0.158	0.215	1.373	2.329	0.219	0.206	-0.291	2.548	0.131	0.149	0.426
216.592	7.966	0.148	0.218	1.373	2.321	0.228	0.189	-0.304	2.554	0.133	0.124	0.385
216.620	7.971	0.143	0.220	1.370	2.327	0.233	0.187	-0.301	2.550	0.130	0.129	0.408
216.637	7.973	0.146	0.210	1.367	2.323	0.229	0.200	-0.309				
217.358	7.965	0.157	0.203	1.357	2.330	0.230	0.202	-0.307	2.550	0.119	0.156	0.397
217.379	7.977	0.147	0.213	1.373	2.327	0.225	0.189	-0.320	2.539	0.116	0.135	0.386
217.399	7.971	0.152	0.211	1.375	2.337	0.221	0.193	-0.324	2.567	0.127	0.130	0.405
217.427	7.970	0.147	0.216	1.373	2.337	0.225	0.179	-0.305	2.557	0.145	0.126	0.412
217.448	7.975	0.150	0.208	1.375	2.326	0.231	0.205	-0.319	2.550	0.141	0.155	0.418
217.469	7.973	0.148	0.214	1.371	2.326	0.224	0.200	-0.302	2.542	0.157	0.148	0.389
217.561	7.975	0.150	0.215	1.373	2.327	0.218	0.191	-0.305	2.552	0.124	0.142	0.379
217.584	7.978	0.152	0.211	1.368	2.320	0.226	0.181	-0.298	2.548	0.141	0.144	0.401
217.606	7.979	0.152	0.213	1.369	2.329	0.220	0.198	-0.313				
217.623	7.972	0.154	0.220	1.375	2.312	0.215	0.188	-0.323	2.534	0.109	0.146	0.379

218.358	7.958	0.162	0.219	1.372	2.316	0.223	0.173	-0.326	2.563	0.134	0.128	0.419
218.384	7.962	0.157	0.215	1.373	2.323	0.218	0.188	-0.314	2.564	0.124	0.117	0.405
218.406	7.966	0.149	0.222	1.377	2.311	0.236	0.190	-0.294	2.552	0.128	0.119	0.400
218.439	7.963	0.153	0.222	1.372	2.313	0.238	0.183	-0.311	2.561	0.115	0.153	0.415
218.463	7.963	0.154	0.221	1.371	2.322	0.222	0.197	-0.315				
218.487	7.963	0.152	0.221	1.378	2.322	0.224	0.181	-0.305	2.554	0.140	0.135	0.395
218.567	7.964	0.153	0.220	1.373	2.317	0.228	0.186	-0.329	2.540	0.133	0.131	0.414
218.593	7.960	0.156	0.214	1.371	2.316	0.221	0.196	-0.331	2.556	0.109	0.151	0.410
218.619	7.961	0.154	0.216	1.369	2.314	0.241	0.192	-0.327	2.551	0.113	0.107	0.390
219.407	7.968	0.155	0.215	1.368	2.315	0.224	0.200	-0.296	2.548	0.156	0.136	0.399
219.433	7.969	0.153	0.214	1.367	2.328	0.234	0.181	-0.295	2.559	0.119	0.144	0.400
219.460	7.964	0.156	0.216	1.372	2.322	0.221	0.194	-0.303	2.576	0.103	0.150	0.367
219.493	7.964	0.154	0.215	1.376	2.330	0.227	0.182	-0.317	2.548	0.150	0.135	0.360
219.580	7.965	0.149	0.218	1.377	2.315	0.214	0.216	-0.307				
219.607	7.969	0.152	0.219	1.379	2.317	0.224	0.181	-0.296	2.567	0.130	0.123	0.362
220.468	7.962	0.156	0.220	1.383	2.340	0.224	0.199	-0.320	2.554	0.138	0.105	0.384
220.493	7.966	0.150	0.219	1.378	2.331	0.223	0.206	-0.311	2.565	0.110	0.159	0.403
220.584	7.959	0.154	0.215	1.379	2.336	0.231	0.185	-0.300	2.561	0.147	0.113	0.381
220.610	7.967	0.151	0.215	1.379	2.344	0.218	0.209	-0.326				
221.468	7.966	0.158	0.222	1.388	2.341	0.224	0.199	-0.320	2.553	0.137	0.105	0.384
221.493	7.968	0.151	0.221	1.382	2.332	0.223	0.206	-0.311	2.566	0.111	0.159	0.403
221.584	7.959	0.155	0.214	1.378	2.336	0.232	0.186	-0.301	2.561	0.147	0.147	0.380
221.610	7.966	0.151	0.214	1.374	2.344	0.218	0.209	-0.326				
298.414					2.326	0.226	0.196	-0.295				
298.424					2.342	0.225	0.185	-0.303	2.549	0.128	0.143	0.413
298.442					2.344	0.226	0.192	-0.312				
298.448					2.336	0.213	0.192	-0.318				
299.468					2.319	0.230	0.184	-0.312	2.546	0.125	0.131	0.387
299.478					2.308	0.226	0.194	-0.317	2.532	0.139	0.133	0.398
299.487					2.312	0.216	0.203	-0.295	2.547	0.124	0.141	0.410
299.494					2.326	0.210	0.200	-0.293				
300.438					2.342	0.229	0.190	-0.291				
300.449					2.349	0.219	0.182	-0.294	2.534	0.128	0.138	0.404
300.459					2.335	0.215	0.196	-0.285	2.550	0.116	0.125	0.403
301.437					2.353	0.220	0.199	-0.297	2.558	0.116	0.135	0.402
301.446					2.340	0.235	0.190	-0.286	2.542	0.134	0.129	0.407
301.456					2.368	0.219	0.199	-0.298	2.555	0.132	0.128	0.391
304.475					2.320	0.222	0.186	-0.308				
304.489					2.341	0.240	0.163	-0.326				
306.437					2.330	0.234	0.187	-0.313	2.552	0.124	0.132	0.397
306.446					2.340	0.221	0.197	-0.297	2.539	0.133	0.140	0.409
306.455					2.351	0.221	0.180	-0.320	2.546	0.136	0.129	0.383
306.464					2.360	0.225	0.197	-0.319	2.549	0.132	0.144	0.403

Details of the programme stars are given in Table 2.4. The observations are tabulated in Table 2.5, from which the mean uvby magnitudes and colours of Table 2.4 are derived. The mean (b-y) and c_1 colours for the check star BD-0°3406 were incorrectly given by Jeffery et al.(1986). BD-1°3438 showed a variation in V of 0.08 mag during the period of the observations. Smaller-amplitude variations are apparent in (u-b), whilst any variations in (b-y) and (v-b) are comparable to the scatter in the data. Although the differential photometry of BD-1°3438 (Fig. 2.5) appears irregular and displays much scatter, particularly when the moon was bright, a visual inspection of the best-defined part of the light curve (JD 2446190-221) indicates maximum changes in brightness on a timescale of about 5-8 days.

2.2b DISCUSSION

BD-1°3438 was identified as a member of the EHe stars from blue objective prism plates obtained with the Curtis Schmidt telescope at Cerro Tololo by MacConnell et al. (1972), who noted the similarity of its spectrum to those of the EHe stars HD124448 and HD168476. Schönberner (1978) later estimated $n_H:n_{He} \lesssim 10^{-4}$ from a spectroscopic fine analysis of the star. Drilling et al. (1984a) derived an effective temperature of $10{,}900^{+}_{-}400$K. Landolt (1986a; Walker & Kilkenny 1981) first reported that BD-1°3438 might be variable from observations discrepant with the discovery magnitudes and colours quoted by MacConnell et al.(1972).

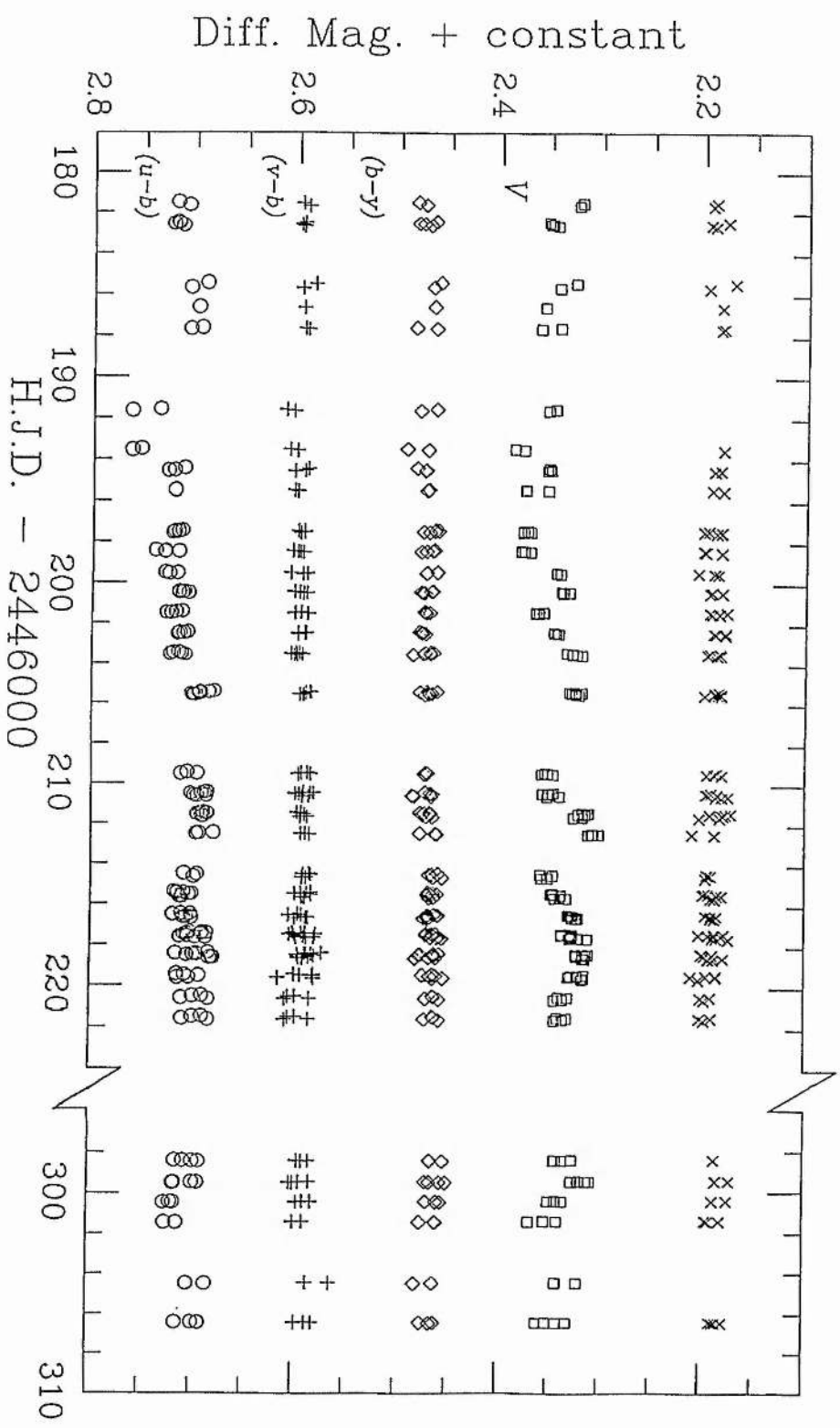

Figure 2.5 Differential uvby photometry of BD-1°3438. All but the V curve have been offset by arbitrary constants. The crosses show the V curve for the K-C observations.

The presence of colour changes in Fig. 2.5 suggests strongly that the star is pulsating radially rather than non-radially. Although BD+1°4381 and BD-1°3438 have similar effective temperatures, the former star has a much longer pulsation period of about 21 days. The period observed for BD+1°4381 can be understood as radial pulsation of the star in the fundamental mode (Saio 1986). However, Saio finds that BD-1°3438 lies outside the instability region for pulsation in the fundamental mode, and that its period is consistent with radial pulsation of the star in the first-overtone mode.

2.3 LSIV-1°2

2.3a OBSERVATIONS

Strömgren observations of LSIV-1°2 were obtained on 10 nights at the OSN with a 0.75-m telescope during a 12-day period in 1985 August by the writer and Mr G.P.H.Willingale. Integration times were chosen so that counts through the y-filter were approximately 20(Vr), 50(C) and 300(K) thousand. Only differential magnitudes and colours in the standard system are presented. Comparison and check star details for LSIV-1°2 are given below.

Table 2.6 Differential uvby photometry of LSIV-1°2.

H.J.D.	Variable - Comparison				Check - Comparison			
-2446000	V	(b-y)	(v-b)	(u-b)	V	(b-y)	(v-b)	(u-b)
296.471	0.995	0.117	-0.101	-1.095	-2.266	-0.016	-0.026	0.004
296.488	0.993	0.105	-0.088	-1.106	-2.235	-0.028	-0.019	-0.004
297.409	0.992	0.097	-0.098	-1.096	-2.255	-0.002	-0.035	-0.023
297.417	0.985	0.116	-0.107	-1.103	-2.252	-0.034	-0.016	-0.010
298.465	0.964	0.114	-0.101	-1.117	-2.243	-0.030	-0.012	-0.018
298.475	0.971	0.105	-0.090	-1.119				
298.482	0.944	0.116	-0.112	-1.128	-2.251	-0.025	-0.022	0.009
298.492	0.969	0.103	-0.128	-1.140				
299.429	0.956	0.106	-0.106	-1.079	-2.260	-0.018	-0.025	0.009
299.438	0.950	0.108	-0.106	-1.134	-2.266	-0.021	-0.028	0.000
299.447	0.959	0.096	-0.106	-1.117	-2.270	-0.035	-0.017	-0.012
300.410	0.957	0.106	-0.109	-1.114	-2.265	-0.030	-0.018	-0.009
300.420	0.966	0.108	-0.105	-1.134	-2.255	-0.031	-0.017	-0.015
300.469	0.948	0.114	-0.114	-1.113				
300.478	0.959	0.103	-0.102	-1.093	-2.270	-0.028	-0.027	0.001
300.486	0.961	0.120	-0.118	-1.115	-2.263	-0.028	-0.028	0.008
301.492	1.005	0.098	-0.105	-1.109				
301.500	1.003	0.129	-0.118	-1.091				
304.425	1.034	0.124	-0.102	-1.104	-2.254	-0.035	-0.026	-0.010
304.439	1.040	0.098	-0.101	-1.131	-2.266	-0.027	-0.026	-0.014
304.452	0.000	0.000	-0.083	-1.114	-2.271	-0.024	-0.022	-0.031
305.387	1.037	0.097	-0.110	-1.113	-2.287	-0.021	-0.015	0.014
305.395	1.032	0.108	-0.116	-1.102	-2.267	-0.027	-0.023	-0.020
305.401	1.004	0.133	-0.106	-1.109				
306.358	1.008	0.103	-0.091	-1.073	-2.255	-0.029	-0.024	-0.012
306.366	0.999	0.124	-0.085	-1.104	-2.244	-0.031	-0.021	-0.024
306.374	1.007	0.114	-0.110	-1.077	-2.257	-0.030	-0.013	-0.010
306.383	0.995	0.123	-0.092	-1.093	-2.256	-0.030	-0.016	-0.016
306.391	1.001	0.129	-0.112	-1.104	-2.262	-0.033	-0.027	-0.030
307.433	1.003	0.106	-0.089	-1.074	-2.274	-0.027	-0.042	-0.008
307.440	0.996	0.136	-0.110	-1.101	-2.226	-0.035	-0.027	-0.031
307.448	0.990	0.127	-0.107	-1.103	-2.272	-0.025	-0.022	-0.006
307.456	1.022	0.076	-0.082	-1.070	-2.280	-0.028	-0.019	0.009

	R.A.(1950.0)	Dec.(1950.0)	m_v	Sp.
LSIV-1°2 (Vr)	$17^h\ 48^m\ 51^s$	-01° 42' 32"	11.0	B
HD162472 (C)	$17^h\ 48^m\ 41^s$	-01° 28' 52"	10.2	A0
HD162692 (K)	$17^h\ 49^m\ 47^s$	-01° 25' 09"	7.7	A2

The results are presented in Table 2.6. K-C shows a lot of scatter, though this may just be the result of high air-mass observations and an increasingly bright moon. One V and (b-y) measurement has been omitted as the y observation showed a large r.m.s error. Fig. 2.6 clearly shows the light variability of LSIV-1°2 but the amplitudes of any colour changes are comparable with the scatter in the data, although some variation does seem to be present. Differential mean magnitudes and colours for LSIV-1°2 are as follows :

	dV	d(b-y)	d(v-b)	d(u-b)
Vr-C (n=33)	0.991 ± 0.027	0.111 ± 0.013	-0.104 ± 0.011	-1.060 ± 0.017
K-C (n=27)	-2.260 ± 0.013	-0.027 ± 0.007	-0.023 ± 0.007	-0.007 ± 0.012

A visual inspection of the light curve suggests one dominant variation with a period of ~10 days. On the simplifying assumption that the light curve is singly periodic, a sine wave was fitted to the data using the method of least squares. The u,v,b,V curves gave best fits for P ≈ 11-12 days and indicate an amplitude of 0.07-0.08 mag in the light curve, the semi-amplitudes in each filter being 0.041, 0.040, 0.037 and 0.036 mag respectively. Fits to the V and (b-y) observations are shown in Fig. 2.7. Further observations are needed to confirm the periodic nature of the light

Figure 2.6 Differential light and colour curves for LSIV-1°2. Each has been offset by an arbitrary constant.

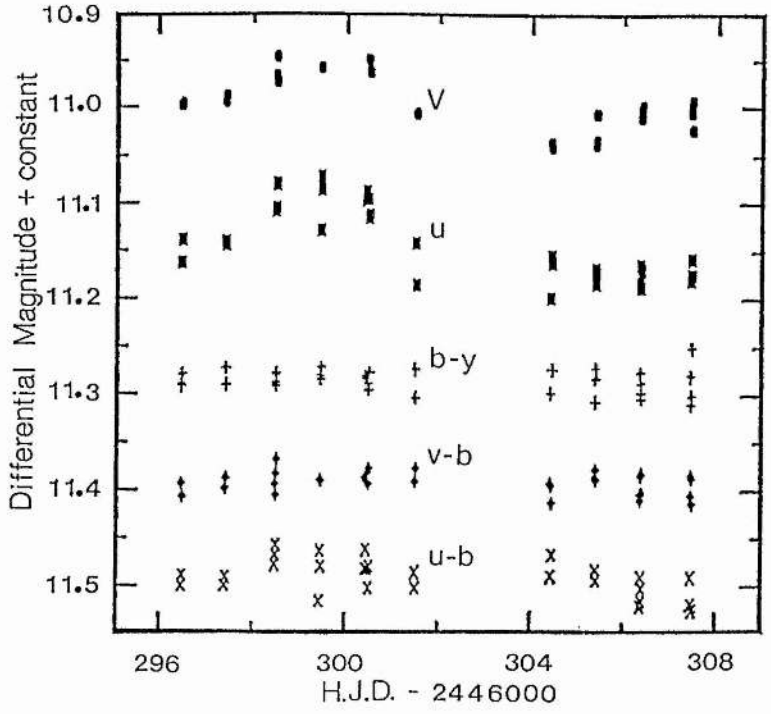

Figure 2.7 Sine-wave fits to the V and (b-y) curves of Figure 2.6 assuming curve to be singly periodic with P=11 days.

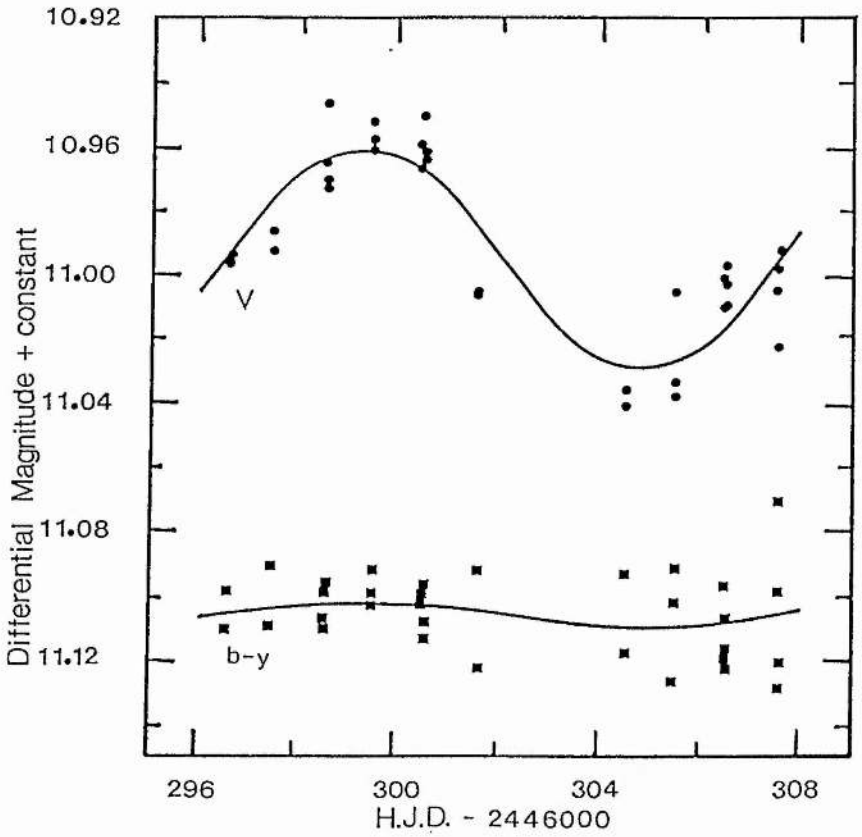

curve.

2.3b DISCUSSION

LSIV-1°2 was identified as a member of the EHe stars by Drilling (1980). Drilling et al.(1984a) later estimated an effective temperature of 11,900±400K. LSIV-1°2 has a spectrum similar to that of another EHe star, HD168476 (Lynas-Gray et al. 1981), but with weak hydrogen lines present. Of the six cooler EHe stars (8,000-13,000K), those for which variability studies have been conducted have all proven to be variable. The coolest of these, BD+1°4381, is periodic and appears to represent a straightforward extension of radial pulsation in RCB stars (Alexander et al. 1972), whilst the hotter star BD-1°3438 appears irregular. The photometry presented here suggests that the variation of LSIV-1°2 is more akin to the variability of BD+1°4381 but on a shorter timescale, and should be associated with radial pulsation of the star. It is important to improve the period determination for LSIV-1°2 in order to see how it fits into the context of pulsation in EHe stars.

2.4 LSII+33°5

2.4a OBSERVATIONS

Strömgren observations of LSII+33°5 were obtained with a 0.75-m telescope at the OSN on 9 nights during a 12-day period in 1985 August by the writer and Mr G.P.H.Willingale. The programme stars (Table 2.7) were typically observed for 1-1½ hours each night, although on some nights two sets of observations of LSII+33°5 were made 1-2 hours apart. Differential magnitudes and colours are presented in Table 2.8, corrected to the standard system. Zero-points were determined on 9 nights from which the mean magnitudes and colours in Table 2.7 are derived. The writer is unaware of any published Strömgren colours for LSII+33°5.

The differential mean magnitudes and colours of LSII+33°5 from Table 2.8 were as follows :

	dV	d(b-y)	d(v-b)	d(u-b)
Vr-C (n=46)	$2.418^{+}_{-}0.017$	$0.163^{+}_{-}0.009$	$0.025^{+}_{-}0.006$	$-1.175^{+}_{-}0.017$
K-C (n=41)	$1.801^{+}_{-}0.008$	$0.101^{+}_{-}0.007$	$0.038^{+}_{-}0.006$	$-0.537^{+}_{-}0.009$

The photometric variability of LSII+33°5 (Fig. 2.8) appears irregular, with maximum brightness changes over 3-4 days (identifying light minima at JD 2446297, 301 and 304). It showed an 0.07 mag variation in V and a colour variation of 0.03 mag in (u-b). Any variations in (v-b) and (b-y) are comparable with the scatter in the data. Integration times were chosen so that

Table 2.7 Target, comparison and check star details for LSII+33°5. The magnitudes and colours are the average of the 9 nightly means.

	RA (1950.0)	Dec	Sp	V	(b-y)	(v-b)	(u-b)
LSII+33°5(Vr)	$19^h43^m24^s$	+33°51'04"	B	10.36 ± 0.04	0.22 ± 0.01	0.19 ± 0.02	0.29 ± 0.06
HD186439 (C)	$19^h42^m15^s$	+33°48'56"	B8	7.94 ± 0.05	0.06 ± 0.01	0.17 ± 0.02	1.47 ± 0.06
HD225565 (K)	$19^h41^m08^s$	+34°18'07"	A0	9.74 ± 0.05	0.15 ± 0.01	0.21 ± 0.02	0.94 ± 0.06

Figure 2.8 Differential light and colour curves for LSII+33°5. Each has been offset by an arbitrary constant. The V curve for K-C is also shown.

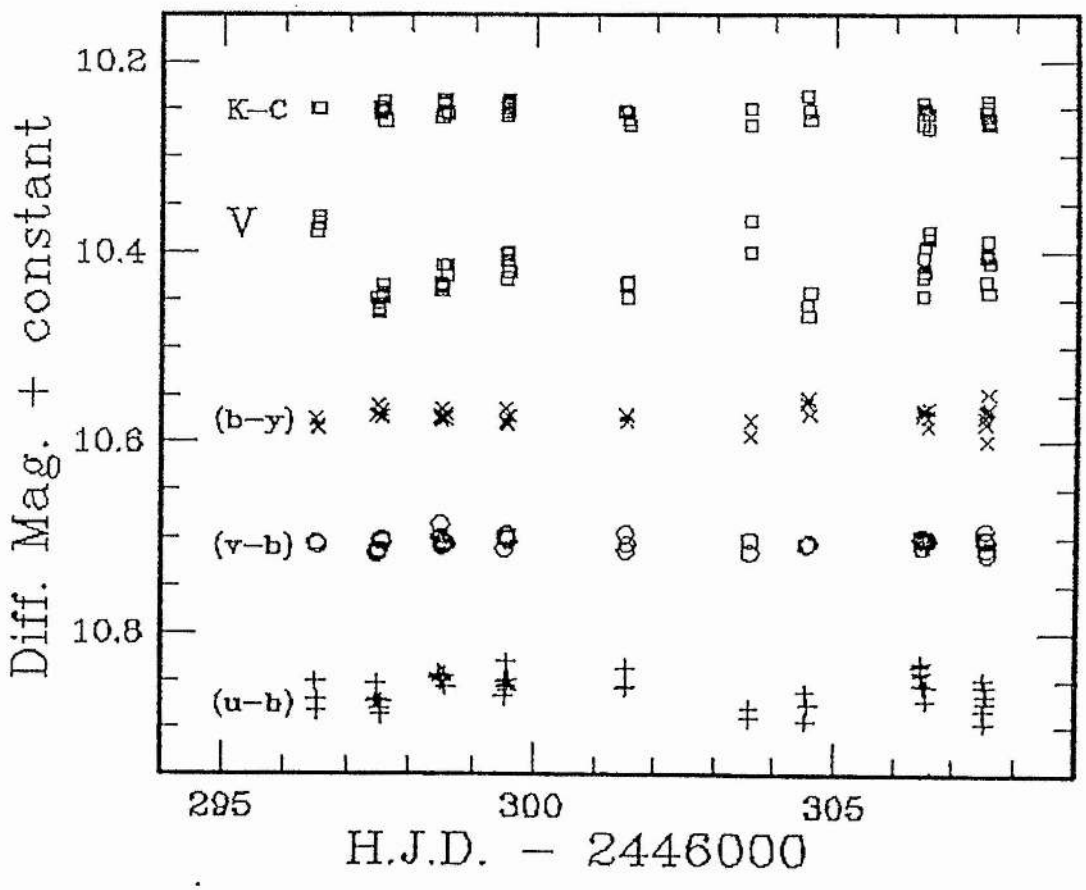

approximately equal photon counts were obtained for each Vr and K measurement (3 integrations of $5x10^4$ counts in V). The standard deviation of the Vr-C observations on JD 2446306 and 307 was roughly 2-3 times that to be expected from the observational error indicated by the K-C observations if LSII+33°5 is stable over a timescale of about an hour. However, other nights are not consistent with the idea of short timescale variability, and as LSII+33°5 lies in a very crowded star field (l=69°, b=5°) this result needs careful checking to exclude the possibility of effects introduced by background stars through telescope instabilities.

2.4b DISCUSSION

LSII+33°5 (HD225642) was identified as a member of the EHe stars by Drilling (1978). Drilling et al. (1984a) derived T_{eff}=15,000K for LSII+33°5 from a study of its ultra-violet flux. However, LSII+33°5 is anomalous in that its spectrum displays numerous strong lines of OII, which are either weak or absent in other EHe stars of similar temperature. Landolt (1986a) suggested that LSII+33°5 might be photometrically variable from discrepant V magnitudes obtained by himself and by Drilling (1975), and from small differences noted by Drilling et al.(1984a) in two IUE observations. Similar to BD-1°3438, LSII+33°5 displays irregular changes in light and colour, but on a shorter timescale of about 3-4 days (Sect. 2.4). HD168476 (T_{eff}=12,400K) is also an irregular photometric variable, observations so far suggesting a possible timescale of about a week (Hill 1986, private communication). However, further observations and improved theoretical models of

Table 2.8 Differential uvby photometry of LSII+33°5.

H.J.D.	Variable - Comparison				Check - Comparison			
-2446000	V	(b-y)	(v-b)	(u-b)	V	(b-y)	(v-b)	(u-b)
296.502	2.376	0.166	0.025	-1.183	1.798	0.096	0.038	-0.525
296.517	2.367	0.174	0.025	-1.161				
296.529	2.360	0.177	0.028	-1.149	1.798	0.105	0.032	-0.542
297.463	2.446	0.163	0.036	-1.161				
297.475	2.461	0.162	0.038	-1.181	1.797	0.095	0.048	-0.535
297.483	2.457	0.152	0.033	-1.164	1.802	0.093	0.042	-0.538
297.491	2.452	0.162	0.032	-1.162	1.802	0.104	0.044	-0.538
297.534	2.447	0.158	0.023	-1.154	1.789	0.104	0.034	-0.535
297.543	2.433	0.164	0.022	-1.146	1.800	0.097	0.035	-0.539
297.555	2.440	0.163	0.025	-1.161	1.811	0.091	0.038	-0.543
298.471	2.431	0.166	0.006	-1.192	1.807	0.099	0.032	-0.530
298.481	2.438	0.164	0.019	-1.188	1.793	0.106	0.028	-0.540
298.489	2.432	0.169	0.022	-1.190	1.801	0.101	0.038	-0.534
298.499	2.434	0.155	0.030	-1.184	1.792	0.099	0.046	-0.535
298.507	2.411	0.163	0.026	-1.189	1.788	0.104	0.038	-0.542
298.559	2.423	0.166	0.025	-1.190	1.803	0.099	0.035	-0.555
298.568	2.411	0.161	0.027	-1.178				
299.504	2.400	0.169	0.032	-1.166	1.804	0.101	0.047	-0.545
299.512	2.426	0.155	0.021	-1.185	1.791	0.103	0.031	-0.536
299.523	2.406	0.171	0.016	-1.176	1.802	0.093	0.043	-0.531
299.531	2.419	0.163	0.021	-1.205	1.794	0.104	0.046	-0.539
299.544	2.405	0.173	0.017	-1.178	1.798	0.096	0.042	-0.547
299.551	2.397	0.171	0.024	-1.173	1.788	0.103	0.039	-0.527
299.559	2.419	0.163	0.024	-1.186				
301.496	2.432	0.161	0.034	-1.176	1.801	0.099	0.045	-0.540
301.505	2.446	0.163	0.016	-1.198	1.802	0.102	0.045	-0.526
301.514	2.429	0.169	0.027	-1.177	1.809	0.108	0.036	-0.533
303.570	2.364	0.184	0.023	-1.152	1.798	0.114	0.038	-0.519
303.574	2.397	0.168	0.035	-1.142	1.814	0.108	0.036	-0.546
304.523	2.454	0.149	0.028	-1.172	1.784	0.129	0.045	-0.528
304.538	2.466	0.145	0.027	-1.141	1.800	0.101	0.034	-0.551
304.570	2.441	0.161	0.026	-1.157	1.809	0.101	0.040	-0.524
306.451	2.425	0.157	0.022	-1.201	1.816	0.094	0.041	-0.544
306.459	2.444	0.159	0.019	-1.190	1.791	0.109	0.033	-0.524
306.466	2.404	0.159	0.020	-1.194	1.802	0.102	0.029	-0.545
306.473	2.420	0.163	0.030	-1.203	1.798	0.097	0.043	-0.535
306.480	2.393	0.158	0.031	-1.179	1.799	0.092	0.042	-0.539
306.544	2.377	0.175	0.021	-1.160	1.803	0.104	0.035	-0.541
306.551	2.385	0.164	0.026	-1.177	1.804	0.092	0.037	-0.541
307.508	2.430	0.165	0.021	-1.185	1.802	0.096	0.040	-0.534
307.517	2.404	0.160	0.023	-1.151	1.808	0.091	0.034	-0.551
307.525	2.401	0.172	0.013	-1.176	1.795	0.104	0.030	-0.530
307.533	2.386	0.190	0.021	-1.135	1.790	0.106	0.040	-0.526
307.544	2.402	0.157	0.038	-1.161	1.815	0.098	0.045	-0.549
307.553	2.441	0.140	0.032	-1.179	1.811	0.098	0.034	-0.559
307.563	2.410	0.156	0.024	-1.167				

pulsations in extremely hydrogen-deficient stars are a necessity before it will be possible to say whether LSII+33^{o}5 represents a blueward extension, in the period-temperature plane, of the instability region to radial pulsation.

LSII+33^{o}5 is a crucial addition to the EHe stars confirmed to be variable as it falls within the temperature range 13,000-23,000K previously devoid of any confirmed variability (there is contradictory evidence on the variability of HD124448 (T_{eff}=15,500K) and BD+10^{o}2179 (T_{eff}=17,500K) - see Jeffery et al. 1986 and references therein). Those variables with higher temperatures than this interval are believed to be pulsating non-radially (Jeffery et al. 1985, Lynas-Gray et al. 1987) whilst those of lower temperature appear to be pulsating radially (Jeffery & Malaney 1985). This dichotomy has been interpreted as a change from radial to non-radial pulsation with increasing surface gravity. With an effective temperature intermediate between these two groups, it is important to understand the nature of the variability of LSII+33^{o}5. This star deserves a detailed photometric study.

2.5 BD-9°4395

2.5a OBSERVATIONS

Photometric observations of BD-9°4395 in the uvby system were obtained on 28 nights during a 52-day period in 1984 May-July at the SAAO with the 0.5-m telescope by the writer, Drs P.W.Hill and C.S.Jeffery, and Mr R.A.Malaney. Integration times were chosen so that approximately 100,000 counts were obtained for the comparison and check stars, and 30,000 counts for BD-9°4395. Details of the programme stars are given in Table 2.9; their mean magnitudes and colours are derived from the journal of the observations given in Table 2.10.

It is obvious that the differential light curve of BD-9°4395 in Fig. 2.9 exhibits a complex behaviour, and that if the variability is periodic it must be multi-periodic. The standard deviations of $\sim$0.008 mag of the differential colours of the comparison stars (in the sense K-C) is not significantly exceeded by that observed for BD-9°4395 (in the sense Vr-C), so that there is no evidence for colour variations of BD-9°4395. Jeffery et al. (1985) subjected the data to a detailed frequency analysis, and although not conclusive, it demonstrates the multiperiodic nature of the photometric variations. The adopted frequency solution for the differential V-light curve contains 7 terms and is given in Table 2.11. The 3.5 and 11.2 day periods are claimed to be unambiguous, whilst the remaining five terms are provisional.

Table 2.9 The uvby photometry of BD-9°4395.

H.J.D.	Comparison				Variable - Comparison				Check - Comparison			
-2445000	V	(b-y)	(v-b)	(u-b)	V	(b-y)	(v-b)	(u-b)	V	(b-y)	(v-b)	(u-b)
839.498	8.130	0.089	0.150	0.899	2.398	0.066	-0.022	-0.743	0.886	0.225	0.292	0.710
839.535	8.129	0.086	0.153	0.895	2.393	0.068	-0.034	-0.731	0.879	0.232	0.285	0.693
841.361	8.139	0.080	0.159	0.902	2.384	0.060	-0.039	-0.733				
841.443	8.146	0.078	0.152	0.901	2.392	0.058	-0.049	-0.752	0.875	0.227	0.292	0.715
841.577	8.122	0.085	0.148	0.904	2.404	0.052	-0.034	-0.745	0.875	0.223	0.291	0.711
842.309	8.112	0.066	0.167	0.913	2.425	0.058	-0.043	-0.735	0.885	0.230	0.286	0.707
844.451	8.101	0.065	0.159	0.903	2.413	0.059	-0.041	-0.747	0.872	0.219	0.288	0.710
844.507	8.120	0.070	0.168	0.914	2.427	0.054	-0.044	-0.735				
844.536	8.119	0.065	0.166	0.915	2.425	0.059	-0.041	-0.735	0.876	0.228	0.288	0.710
844.562	8.127	0.071	0.165	0.915	2.422	0.066	-0.047	-0.741	0.867	0.224	0.290	0.713
846.329	8.123	0.065	0.171	0.921	2.358	0.072	-0.044	-0.748	0.880	0.234	0.286	0.711
846.406	8.107	0.061	0.160	0.901	2.374	0.061	-0.037	-0.741				
846.462	8.100	0.062	0.152	0.885	2.392	0.051	-0.024	-0.735				
848.305	8.111	0.066	0.160	0.905	2.366	0.063	-0.022	-0.731	0.877	0.224	0.298	0.724
848.370	8.119	0.067	0.159	0.918	2.358	0.055	-0.029	-0.692	0.874	0.223	0.291	0.712
848.450	8.126	0.064	0.163	0.910	2.352	0.064	-0.038	-0.742	0.883	0.224	0.292	0.708
848.517	8.124	0.066	0.159	0.905	2.356	0.060	-0.044	-0.745	0.885	0.217	0.296	0.718
849.298	8.105	0.073	0.165	0.915	2.355	0.069	-0.052	-0.749	0.890	0.231	0.280	0.701
849.328	8.114	0.069	0.164	0.913	2.369	0.059	-0.051	-0.745	0.888	0.223	0.291	0.717
849.437	8.120	0.070	0.162	0.909	2.383	0.059	-0.046	-0.747	0.886	0.226	0.281	0.706
849.476	8.116	0.074	0.158	0.909	2.389	0.055	-0.037	-0.740	0.881	0.226	0.290	0.709
849.519	8.114	0.072	0.163	0.908	2.384	0.072	-0.046	-0.748				
849.554	8.111	0.077	0.161	0.904	2.386	0.070	-0.040	-0.741				
857.378	8.122	0.068	0.160	0.910	2.370	0.062	-0.051	-0.763	0.887	0.225	0.297	0.726
857.426	8.121	0.067	0.164	0.916	2.365	0.060	-0.047	-0.760	0.889	0.220	0.288	0.710
857.522	8.123	0.068	0.162	0.911	2.361	0.061	-0.050	-0.753	0.883	0.224	0.292	0.718
858.292	8.112	0.068	0.162	0.921	2.359	0.059	-0.046	-0.755	0.891	0.225	0.293	0.721
858.373	8.116	0.070	0.162	0.915	2.345	0.069	-0.046	-0.750	0.884	0.225	0.299	0.710
858.525	8.118	0.067	0.160	0.916	2.337	0.070	-0.047	-0.757	0.880	0.233	0.284	0.703
859.304	8.106	0.065	0.164	0.911	2.303	0.066	-0.045	-0.753	0.888	0.228	0.286	0.716
859.384	8.112	0.069	0.162	0.909	2.302	0.061	-0.039	-0.749	0.887	0.227	0.288	0.712
859.482	8.117	0.070	0.161	0.907	2.292	0.059	-0.034	-0.747	0.888	0.224	0.301	0.717
859.515	8.119	0.072	0.164	0.914	2.302	0.059	-0.046	-0.757	0.886	0.226	0.279	0.710
860.301	8.119	0.070	0.166	0.925	2.395	0.057	-0.049	-0.748	0.891	0.222	0.293	0.725
860.381	8.120	0.069	0.163	0.912	2.398	0.054	-0.036	-0.728	0.881	0.227	0.299	0.707
860.472	8.123	0.073	0.163	0.907	2.415	0.049	-0.043	-0.731	0.884	0.229	0.294	0.721
860.499	8.126	0.069	0.162	0.910	2.403	0.060	-0.039	-0.735	0.884	0.223	0.297	0.706
861.268	8.130	0.073	0.172	0.932	2.437	0.055	-0.030	-0.723	0.897	0.231	0.301	0.734
861.360	8.135	0.075	0.162	0.915	2.433	0.060	-0.027	-0.720	0.878	0.226	0.297	0.729
861.486	8.131	0.068	0.168	0.916	2.438	0.057	-0.046	-0.729	0.879	0.233	0.289	0.718
862.280	8.117	0.077	0.159	0.927	2.426	0.041	-0.045	-0.751	0.888	0.223	0.305	0.734
862.305	8.113	0.078	0.161	0.925	2.394	0.062	-0.048	-0.756	0.873	0.221	0.300	0.714
862.351	8.111	0.072	0.167	0.918	2.410	0.052	-0.051	-0.761	0.894	0.219	0.287	0.735
862.425	8.106	0.071	0.168	0.912	2.370	0.066	-0.053	-0.746	0.873	0.221	0.292	0.713
862.485	8.119	0.068	0.163	0.912	2.363	0.066	-0.044	-0.739	0.862	0.226	0.286	0.723
863.265	8.104	0.078	0.162	0.918	2.405	0.076	-0.026	-0.726	0.893	0.216	0.319	0.729

865.268	8.113	0.065	0.162	0.910	2.366	0.067	-0.031	-0.709	0.879	0.234	0.285	0.709
865.303	8.121	0.063	0.161	0.910	2.393	0.060	-0.038	-0.736	0.877	0.227	0.302	0.714
865.332	8.123	0.065	0.166	0.908	2.386	0.063	-0.045	-0.720	0.895	0.237	0.274	0.714
865.361	8.132	0.064	0.165	0.910	2.384	0.074	-0.030	-0.721	0.900	0.217	0.316	0.721
866.259	8.124	0.069	0.169	0.923	2.382	0.054	-0.063	-0.750	0.901	0.221	0.286	0.681
866.298	8.121	0.070	0.165	0.918	2.367	0.068	-0.036	-0.754	0.888	0.222	0.295	0.704
866.354	8.125	0.065	0.169	0.911	2.373	0.061	-0.051	-0.754	0.884	0.228	0.287	0.710
866.390	8.124	0.064	0.170	0.913	2.376	0.055	-0.040	-0.756	0.879	0.230	0.294	0.704
866.414	8.122	0.071	0.161	0.906	2.379	0.051	-0.055	-0.749	0.893	0.214	0.295	0.714
866.441	8.122	0.073	0.162	0.906	2.369	0.057	-0.037	-0.747	0.881	0.223	0.290	0.716
866.490	8.124	0.066	0.162	0.911	2.356	0.052	-0.028	-0.733	0.873	0.220	0.298	0.725
866.510	8.122	0.065	0.169	0.913	2.367	0.075	-0.059	-0.748	0.883	0.223	0.279	0.707
873.251	8.122	0.074	0.164	0.922	2.405	0.063	-0.038	-0.740	0.879	0.217	0.295	0.716
873.366	8.123	0.070	0.164	0.906	2.387	0.066	-0.041	-0.737	0.875	0.225	0.292	0.726
873.500	8.128	0.067	0.163	0.911	2.381	0.051	-0.033	-0.737	0.872	0.234	0.282	0.702
874.233	8.120	0.081	0.168	0.923	2.354	0.056	-0.051	-0.750	0.882	0.217	0.299	0.723
874.351	8.120	0.071	0.166	0.907	2.361	0.058	-0.043	-0.745	0.883	0.227	0.290	0.720
874.491	8.121	0.069	0.163	0.905	2.371	0.068	-0.044	-0.746	0.882	0.229	0.298	0.722
875.226	8.112	0.068	0.171	0.928	2.475	0.059	-0.048	-0.742	0.885	0.229	0.285	0.706
875.334	8.114	0.065	0.166	0.919	2.475	0.060	-0.044	-0.733	0.882	0.229	0.291	0.706
876.234	8.104	0.070	0.178	0.931	2.417	0.069	-0.050	-0.755	0.883	0.228	0.280	0.706
876.285	8.107	0.069	0.164	0.915	2.414	0.057	-0.037	-0.740	0.878	0.235	0.293	0.699
876.334	8.103	0.068	0.166	0.913	2.418	0.054	-0.039	-0.741	0.883	0.224	0.292	0.718
876.386	8.106	0.070	0.167	0.906	2.407	0.066	-0.047	-0.754	0.880	0.227	0.287	0.712
876.477	8.122	0.067	0.164	0.911	2.399	0.071	-0.042	-0.746	0.870	0.224	0.292	0.718
877.224	8.106	0.069	0.163	0.926	2.373	0.061	-0.025	-0.739	0.877	0.225	0.299	0.713
877.271	8.110	0.071	0.170	0.917	2.382	0.056	-0.049	-0.744	0.889	0.216	0.293	0.714
877.483	8.129	0.071	0.165	0.914	2.385	0.065	-0.046	-0.742	0.884	0.225	0.282	0.718
878.230	8.129	0.068	0.173	0.935	2.442	0.068	-0.041	-0.750	0.874	0.237	0.283	0.707
878.485	8.130	0.069	0.170	0.918	2.407	0.062	-0.050	-0.742	0.882	0.228	0.287	0.711
879.224	8.131	0.069	0.168	0.930	2.381	0.074	-0.039	-0.743	0.890	0.224	0.294	0.709
879.274	8.119	0.069	0.161	0.913	2.376	0.071	-0.041	-0.737	0.885	0.228	0.294	0.721
879.293	8.116	0.063	0.159	0.912	2.387	0.062	-0.040	-0.748	0.889	0.232	0.298	0.704
879.323	8.127	0.064	0.161	0.914	2.376	0.064	-0.035	-0.747	0.885	0.236	0.296	0.716
879.341	8.141	0.069	0.166	0.917	2.376	0.070	-0.038	-0.740	0.894	0.229	0.290	0.716
879.387	8.123	0.061	0.162	0.898	2.365	0.072	-0.047	-0.745	0.888	0.229	0.283	0.710
879.406	8.147	0.065	0.173	0.915	2.367	0.080	-0.047	-0.738	0.892	0.239	0.281	0.722
879.430	8.158	0.075	0.169	0.922	2.368	0.058	-0.037	-0.741	0.884	0.219	0.297	0.721
879.448	8.156	0.075	0.171	0.917	2.365	0.048	-0.047	-0.749	0.864	0.224	0.291	0.723
879.472	8.157	0.078	0.153	0.916	2.380	0.048	-0.032	-0.749				
884.293	8.120	0.070	0.165	0.913	2.382	0.058	-0.050	-0.754	0.878	0.227	0.291	0.715
884.401	8.116	0.072	0.162	0.905	2.378	0.051	-0.034	-0.739	0.889	0.208	0.309	0.717
885.421	8.125	0.071	0.160	0.918	2.433	0.065	-0.037	-0.729				
886.422	8.132	0.070	0.162	0.916	2.427	0.064	-0.045	-0.743				
887.431	8.124	0.173	0.163	0.913	2.372	0.069	-0.043	-0.741				
889.424	8.123	0.068	0.163	0.915	2.424	0.061	-0.044	-0.739				
891.359	8.113	0.074	0.160	0.912	2.366	0.066	-0.048	-0.757				

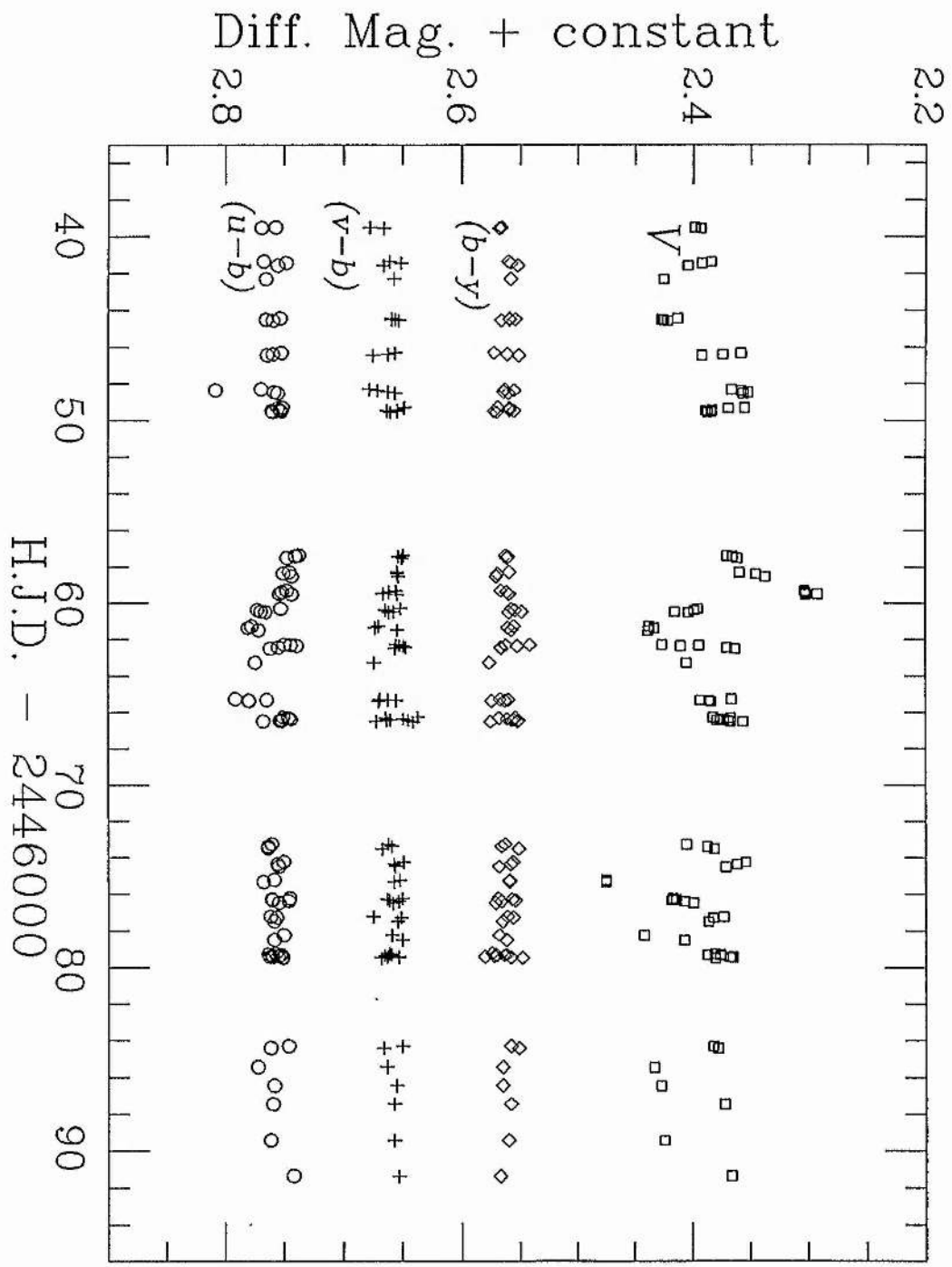

Figure 2.9 Differential light and colour plots for BD-9°4395. All but the V curve have been offset by arbitrary constants.

2.5b DISCUSSION

BD-9°4395 was identified as an EHe star by MacConnell et al. (1972). A quantitative analysis by Kaufmann & Schönberner (1977) gave log g=2.6 and $n_H/n_{He}=1.5\times10^{-3}$. Drilling et al. (1984a) estimated $T_{eff}=23{,}000\pm700$K. The values for log g and T_{eff} indicate that it lies in a region of the log g versus T_{eff} diagram which is traversed by the evolutionary tracks of stars with condensed C/O cores and pure helium envelopes, and with masses of $\sim1M_\odot$ (Schönberner 1977). Photometric observations of this star by Landolt (1979, private communication) and Kilkenny (1985, private communication) indicated its variability, the latter observations appearing to rule out any short period variations on a timescale less than a day.

The observations confirm that the star is not pulsating in a single-radial mode as seems likely in the case of BD+1°4381 and the RCB star RY Sgr (Alexander et al. 1972). Jeffery et al. (1985) concluded that the timescale of the variations observed in BD-9°4395, together with the absence of detectable colour changes accompanying the pulsation, suggests that the variability arises from non-radial oscillations of the star.

Table 2.10 Positions and mean uvby photometry of the programme stars for BD-9°4395.

	RA(1950)	Dec	Sp	<V>	<b-y>	<v-b>	<u-b>	$<c_1>$	$<m_1>$	n
BD-9°4395	16^h26^m	+02°07'	A	10.506 (035)	0.133 (014)	0.122 (007)	0.171 (013)	-0.073 (013)	-0.011 (016)	93
BD-9°4385 Comparison	16^h23^m	+03°05'	F0	8.121 (011)	0.071 (012)	0.163 (005)	0.913 (008)	0.586 (008)	0.092 (014)	93
BD-9°4389 Check	16^h24^m	+01°20'	A0	9.004 (013)	0.295 (006)	0.456 (008)	1.623 (012)	0.716 (014)	0.160 (012)	81

Table 2.11 The adopted frequency solution for the differential V light-curve of BD-9°4395. The uncertainties quoted for the amplitudes are standard errors, and the error associated with the frequencies is equal to the frequency resolution of the data sample, 0.029 cycles day^{-1}.

Frequency (cycles day^{-1})	Amplitude (mag)	Period (day)
0.28445	0.033 ± 0.002	3.516
0.08917	0.028 ± 0.002	11.215
0.42222	0.023 ± 0.002	2.368
0.13772	0.019 ± 0.002	7.261
0.31530	0.016 ± 0.002	3.172
0.50462	0.011 ± 0.003	1.982
0.54870	0.010 ± 0.002	1.822

2.6 KS Persei

2.6a OBSERVATIONS

Strömgren observations of KS Persei were obtained at the OSN with a 0.75-m telescope on 12 nights during a 13-day period in 1985 August by the writer and Mr G.P.H.Willingale. Each of the target stars (Vr) and their associated comparison (C) and check (K) stars (Table 2.12) were typically observed for 1-1$\frac{1}{2}$ hours towards the end of each night. After the first night a brighter star, HD30410, was used in place of the original check star (HD30308). The comparison star (HD30196) is the same as 'Comparison 1' used by Osawa et al.(1963) in their observations of KS Persei. Differential magnitudes and colours are presented in Table 2.13 corrected to the standard system. Zero-points were determined on 9 nights from which the mean magnitudes and colours in Table 2.12 are derived. The results compare well with the observations of Cameron (1966).

The mean differential magnitudes and colours of KS Persei from Table 2.13 were as follows :

	dV	d(b-y)	d(v-b)	d(u-b)
Vr-C (n=72)	-0.686 ± 0.019	0.036 ± 0.005	0.049 ± 0.013	-0.415 ± 0.034
K-C (n=63)	-0.931 ± 0.004	0.307 ± 0.003	0.496 ± 0.004	0.664 ± 0.007

Table 2.13 Differential uvby photometry of KS Persei.

H.J.D.	Variable - Comparison				Check - Comparison			
-2446000	V	(b-y)	(v-b)	(u-b)	V	(b-y)	(v-b)	(u-b)
295.623	-0.741	0.034	0.038	-0.487				
295.638	-0.740	0.035	0.028	-0.476				
295.646	-0.743	0.033	0.029	-0.469				
295.667	-0.738	0.033	0.023	-0.474				
296.601	-0.724	0.041	0.030	-0.458	-0.942	0.311	0.493	0.674
296.610	-0.714	0.028	0.030	-0.446	-0.940	0.311	0.495	0.673
296.618	-0.720	0.037	0.033	-0.454	-0.938	0.310	0.490	0.672
296.640	-0.711	0.033	0.032	-0.449	-0.942	0.311	0.498	0.674
296.656	-0.711	0.029	0.035	-0.448	-0.946	0.311	0.493	0.676
297.618	-0.690	0.036	0.035	-0.419	-0.934	0.307	0.499	0.666
297.627	-0.689	0.035	0.040	-0.427	-0.941	0.312	0.491	0.672
297.634	-0.691	0.033	0.036	-0.421	-0.936	0.309	0.499	0.657
297.644	-0.688	0.035	0.039	-0.442	-0.935	0.306	0.499	0.647
297.651	-0.692	0.030	0.036	-0.439	-0.940	0.305	0.497	0.648
297.660	-0.685	0.029	0.045	-0.432	-0.934	0.306	0.502	0.663
298.631	-0.692	0.036	0.040	-0.436	-0.935	0.308	0.497	0.661
298.638	-0.686	0.038	0.043	-0.447	-0.937	0.306	0.501	0.661
298.646	-0.688	0.029	0.044	-0.435	-0.939	0.304	0.501	0.657
298.652	-0.686	0.028	0.046	-0.448	-0.927	0.306	0.504	0.657
298.660	-0.690	0.035	0.033	-0.445	-0.936	0.308	0.494	0.658
299.612	-0.698	0.038	0.030	-0.427	-0.938	0.309	0.493	0.669
299.620	-0.693	0.037	0.034	-0.435	-0.939	0.313	0.494	0.662
299.627	-0.682	0.036	0.039	-0.445	-0.934	0.309	0.496	0.663
299.639	-0.695	0.036	0.032	-0.434				
299.647	-0.694	0.039	0.035	-0.441	-0.929	0.309	0.502	0.655
299.654	-0.686	0.039	0.041	-0.448	-0.930	0.307	0.500	0.663
299.661	-0.687	0.033	0.039	-0.443	-0.930	0.305	0.501	0.662
299.669	-0.689	0.033	0.034	-0.432				
300.615	-0.688	0.033	0.040	-0.438	-0.934	0.306	0.501	0.663
300.627	-0.680	0.032	0.043	-0.436	-0.938	0.312	0.489	0.671
300.634	-0.692	0.040	0.035	-0.434	-0.931	0.306	0.502	0.659
300.641	-0.684	0.034	0.043	-0.448	-0.936	0.307	0.489	0.667
300.648	-0.689	0.039	0.037	-0.439	-0.934	0.308	0.502	0.664
300.655	-0.675	0.034	0.051	-0.449	-0.929	0.305	0.498	0.664
300.664	-0.672	0.031	0.044	-0.445	-0.935	0.306	0.491	0.669
301.612	-0.673	0.040	0.044	-0.432	-0.938	0.312	0.491	0.657
301.621	-0.664	0.034	0.045	-0.431				
303.631	-0.673	0.032	0.063	-0.412				
303.641	-0.680	0.040	0.055	-0.411	-0.932	0.308	0.501	0.657
303.652	-0.682	0.044	0.052	-0.406	-0.937	0.307	0.496	0.666
303.660	-0.676	0.040	0.051	-0.403	-0.936	0.307	0.497	0.661
303.669	-0.686	0.040	0.050	-0.399	-0.936	0.306	0.495	0.669
304.624	-0.688	0.046	0.061	-0.414	-0.940	0.308	0.494	0.665
304.633	-0.691	0.043	0.059	-0.410	-0.941	0.306	0.495	0.663
304.639	-0.692	0.043	0.060	-0.419	-0.936	0.304	0.502	0.660
304.648	-0.688	0.043	0.059	-0.411	-0.934	0.305	0.497	0.668
304.658	-0.694	0.046	0.055	-0.407	-0.941	0.307	0.488	0.673
304.666	-0.693	0.043	0.053	-0.400				
305.644	-0.670	0.042	0.058	-0.384	-0.930	0.311	0.492	0.666
305.651	-0.668	0.043	0.065	-0.397	-0.927	0.298	0.502	0.661
305.658	-0.682	0.040	0.057	-0.383	-0.940	0.306	0.489	0.675
305.665	-0.674	0.040	0.065	-0.390	-0.934	0.304	0.500	0.661
305.673	-0.678	0.043	0.063	-0.394	-0.938	0.308	0.499	0.661
306.615	-0.663	0.042	0.053	-0.372	-0.943	0.311	0.493	0.668
306.621	-0.672	0.036	0.064	-0.356	-0.935	0.309	0.492	0.667

306.629	-0.668	0.037	0.057	-0.376	-0.941	0.311	0.492	0.664
306.635	-0.662	0.031	0.070	-0.379	-0.934	0.304	0.499	0.664
306.643	-0.661	0.032	0.061	-0.366	-0.930	0.307	0.493	0.673
306.650	-0.671	0.031	0.067	-0.378	-0.940	0.303	0.498	0.658
306.658	-0.659	0.029	0.072	-0.379	-0.933	0.300	0.499	0.656
306.665	-0.663	0.032	0.062	-0.374	-0.931	0.308	0.489	0.674
306.674	-0.663	0.036	0.056	-0.366	-0.932	0.309	0.487	0.675
306.682	-0.662	0.035	0.054	-0.367	-0.936	0.314	0.492	0.666
307.614	-0.668	0.032	0.065	-0.363	-0.934	0.308	0.492	0.651
307.622	-0.677	0.039	0.074	-0.367	-0.937	0.307	0.495	0.666
307.629	-0.669	0.032	0.072	-0.369	-0.939	0.309	0.492	0.662
307.638	-0.678	0.034	0.066	-0.365	-0.938	0.311	0.487	0.665
307.645	-0.676	0.037	0.063	-0.376	-0.942	0.308	0.493	0.662
307.652	-0.689	0.040	0.064	-0.363	-0.938	0.309	0.494	0.668
307.660	-0.680	0.036	0.067	-0.364	-0.934	0.307	0.496	0.667
307.667	-0.681	0.034	0.067	-0.368	-0.940	0.309	0.492	0.676
307.674	-0.688	0.036	0.059	-0.355	-0.938	0.303	0.494	0.663

Table 2.12 Target, comparison and check star details for KS Persei. The magnitudes and colours are the average of the 9 nightly means.

		RA (1950.0)	Dec	Sp	V	(b-y)	(v-b)	(u-b)
KS Persei	(Vr)	$04^h45^m20^s$	$+43^\circ11'19''$	A5	7.74 ± 0.04	0.35 ± 0.01	0.49 ± 0.02	1.14 ± 0.07
HD30196	(C)	$04^h43^m56^s$	$+43^\circ18'45''$	F0	8.43 ± 0.04	0.31 ± 0.01	0.44 ± 0.02	1.56 ± 0.05
HD30410	(K)	$04^h45^m52^s$	$+43^\circ27'20''$	G8	7.49 ± 0.04	0.62 ± 0.02	0.94 ± 0.02	2.22 ± 0.05

Figure 2.10 Differential light and colour curves for KS Persei.

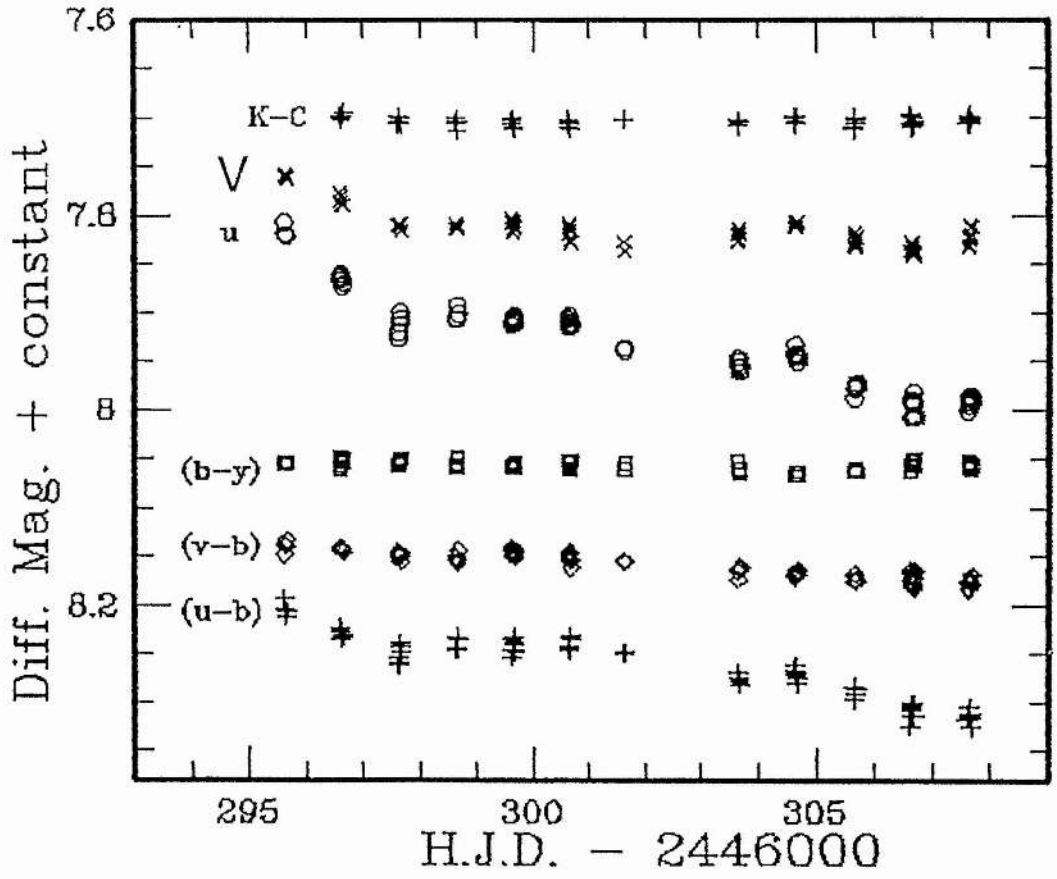

Fig. 2.10 shows that the amplitude of the photometric variations is largest at the shorter wavelengths with a 0.17 mag and 0.07 mag range in u and V respectively, and colour variations of 0.10 mag and 0.04 mag in (u-b) and (v-b) respectively. The V observations showed a dimming of 0.05 mag over the first three nights, followed by a periodic variation of 0.02 mag with a period of about 5 days (identifying light maxima at JD 2446299 and JD 2446304). The 5-day variation is present in the u,v and b light-curves but appears to be superimposed on a secular, or longer-term dimming of KS Persei which is most severe in u. Further observations are needed to confirm the reality of the 5-day periodicity.

2.6b DISCUSSION

With an effective temperature of 9,000K, KS Persei (HD30353) is the coolest of the EHdBs. It also has the longest binary period of 360 days (Heard 1962). Like all the EHdBs, the spectrum of KS Persei shows strong lines of nitrogen whilst those of carbon are weak. Wallerstein et al.(1967) estimated an extreme $n_N:n_C$ ratio for KS Persei of 10^3. Drilling & Schönberner (1982) reported the detection of a hot companion from a study of low resolution IUE spectra.

Photometric variations had previously been noted in KS Persei by Bakos (reported by Heard 1962). Although Osawa et al. (1963), using Johnson UBV photometry, failed to detect the presence of eclipses they reported semi-regular light variations of ~30 days of up to 0.14 mag in V, which may account for the longer-term dimming superimposed on the 5-day periodicity reported here. From the orbital elements given by Heard (1962), it is noted that if KS Persei is an eclipsing binary then the visible component would have been eclipsing the invisible component at about the time of our observations. If the primary (the visible star) is a helium supergiant in or near its Roche-lobe some 3-5 magnitudes brighter in the visible region than the companion as Drilling & Schönberner (1982) suggest, then eclipses would be shallow (< 0.1 mag) and of long duration (~ 30 days). However, previous photometric and spectroscopic monitoring has failed to detect any evidence of eclipses. The 30-day semi-regular variation reported by Osawa et al.(1963) and Heard (1962) was observed at times when the system could not have been eclipsing. The photometric behaviour of KS Persei is similar to that observed in Ups Sgr for which a semi-regular pulsation period of 20 days with an amplitude of 0.15 mag in V has been observed (Chap. 3).

3. Photometric Observations and Interpretation of Upsilon Sagittarii

3.1 Introduction

The EHdB Ups Sgr is a single-lined spectroscopic binary which has an orbital period of 138 days (Wilson 1914) and shows hydrogen greatly reduced in its atmosphere ($n_H/n_{He} \lesssim 10^{-4}$; Schönberner & Drilling 1983). An effective temperature of 10,500K has been estimated from IUE and ground-based observations (Drilling et al. 1984a). Although the presence of a companion has not been detected at visible wavelengths in any of the EHdBs, hot companions have been detected in Ups Sgr and KS Persei from ultra-violet observations (Drilling & Schönberner 1982, Parthasarathy et al. 1986). Schönberner & Drilling (1983) have proposed that Ups Sgr currently consists of a highly luminous supergiant primary of $\sim 1M_\odot$ which is filling its Roche lobe for the second time and transferring mass towards the hotter secondary. The idea of mass-loss from the primary is supported by the presence of approximately stationary lines of Balmer emission in the spectrum (Hack 1960). Adopting a primary mass of $1M_\odot$, the mass function $f(M)=1.677$ (Seydel 1929) gives a minimum mass for the secondary of $3M_\odot$.

Gaposchkin (1945) reported the detection of eclipses in Ups Sgr from photographic photometry. Eggen et al. (1950) later reported the detection of eclipses photoelectrically but of only one-half the amplitude reported by Gaposchkin. In both cases the light curve was poorly determined and the existence of eclipses

remained questionable. However, the correlation between the light minima and the expected times of eclipses from the radial-velocity curve lead to the belief that Ups Sgr was an eclipsing binary system of the β-Lyrae type. Greenstein (1950), and later Hack (1960), attempted to correlate spectral variations with the binary phase. Hack examined spectrograms obtained over 163 cycles and concluded that the B-type characteristics of its spectrum are strengthened relative to the F-type characteristics at the phases between 0-65 days while the inverse is true at phases between 80 and 120 days, although she found exceptions in some cycles.

Detection of eclipses in the ultra-violet region was claimed by Duvignau et al.(1979) in Copernicus and S2/68 satellite data. Their results, however, are based on poorly spaced observations at 9 different phases. More importantly, their results suggested the presence of non-eclipse related light variations. Rao and Venugopal (1985) obtained ultra-violet observations with the ANS satellite at the estimated time of eclipse of the secondary (phase 0.0), as well as at phases 0.7 and 0.3 (obtained 1.3 cycles before and after respectively). They identified the presence of a partial eclipse of the secondary from the fact that the observations at phase 0.0 are 0.17 mag and 0.11 mag fainter than at phases 0.7 and 0.3.

3.2 Observations

3.2a OBSERVATIONAL DETAILS

Photometry in the uvby and UBV systems of Ups Sgr and two comparison stars, HD182645 and HD182678, was obtained in the interval 1985 April-September. Observations in the uvby system were made on 10 nights over a 21-day period with the 0.5-m telescope at SAAO during April-May by the writer. Further uvby observations were obtained with the 0.75-m telescope at OSN on 7 nights over a 10-day period in July by Mr S.A.Bell, and on 9 nights over a 13-day period in August by the writer and Mr G.P.H.Willingale. UBV observations made with a 0.41-m telescope on 55 nights over 125 days during May-September at the Boyden Observatory, South Africa were kindly supplied by Mr G.J.Malcolm and Mr S.A.Bell. Instrumentation, observational methods and reduction techniques to the standard systems for the SAAO and OSN observations are described in Sect. 1.4, while the Boyden observations have been described by Malcolm & Bell (1986a, 1986b). Only differential magnitudes were obtained, except at SAAO from which the mean uvby magnitudes and colours in Table 3.1 are derived; n represents the number of observations. The UBV data for the comparison star HD182645 is taken from Nicolet (1978), from which (B-V) and (U-B) have been estimated for Ups Sgr and HD182678 using means of the differential data in Table 3.3. The estimates for Ups Sgr are in good agreement with those obtained by Drilling et al. (1984b). The uvby and UBV observations are tabulated in

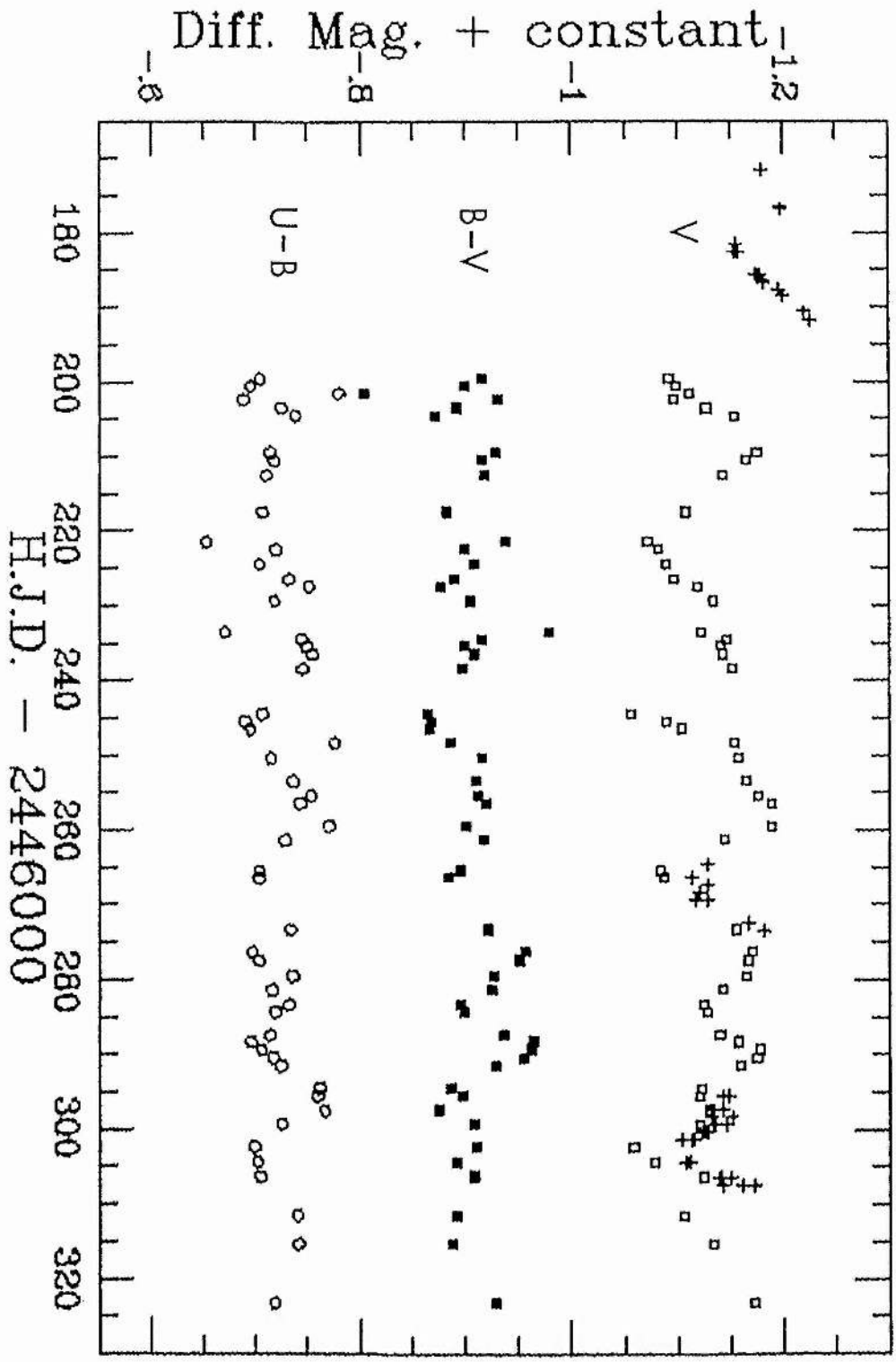

Figure 3.1 Differential UBV photometry of Ups Sgr. The plus signs are V magnitudes from the Stromgren 'y' observations. The (B-V) and (U-B) curves have been offset by arbitrary constants.

Figure 3.2 Differential uvby photometry of Ups Sgr. The curves have been offset by arbitrary constants.

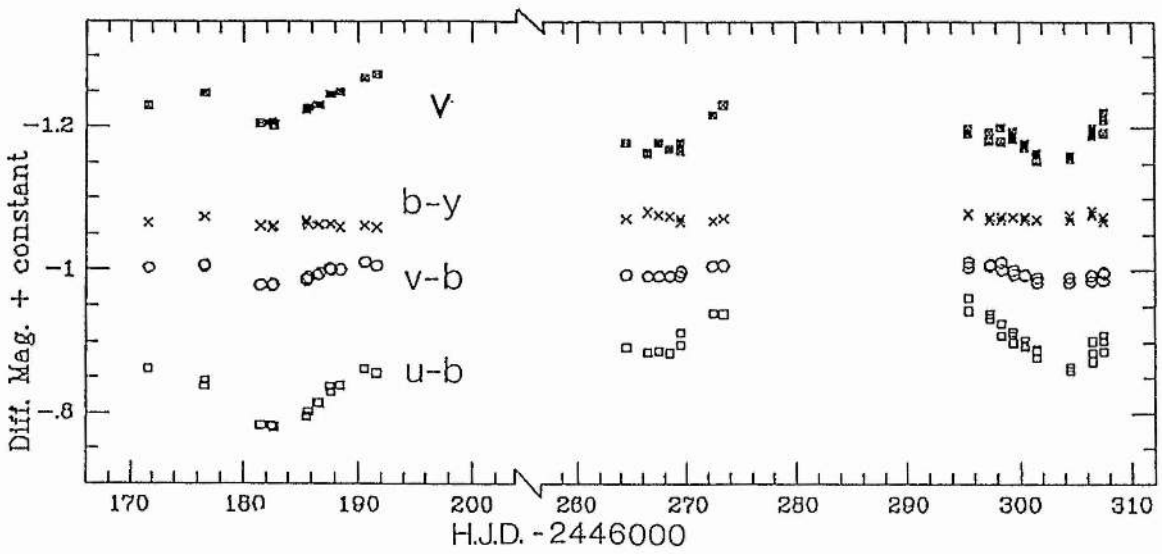

Table 3.1 Positions and mean uvby photometry of the programme stars.

	n	RA(1950)	Dec	Sp	<V>	<b-y>	<v-b>	<u-b>	<B-V>	<U-B>
Ups Sgr	17	$19^h18^m52^s$	$-16^\circ03'02''$		4.529 (023)	0.107 (004)	0.203 (014)	0.596 (033)	0.01	-0.56
HD182645 Comparison	17	$19^h23^m20^s$	$-15^\circ09'14''$	B8V	5.715 (011)	0.067 (004)	0.119 (005)	0.938 (007)	0.02*	-0.34*
HD182678 Check	13	$19^h23^m34^s$	$-14^\circ39'07''$	A1V	6.713 (008)	0.032 (003)	0.170 (004)	1.288 (004)	0.06	-0.07

*Nicolet (1978).

Tables 3.2 and 3.3 respectively.

Additional high-speed photometry with a V filter was carried out by Mr G.J.Malcolm at Boyden on 1 night in 1986 August over a 4-hour period to search for short-timescale variations. The observations consisted of a total of 434 20-second integrations of Ups Sgr in four ~1-hour sets, with a comparison star observation before and after each set. Only extinction-corrected differential magnitudes in the instrumental system are presented (Table 3.4).

3.2b PHOTOMETRY

Fig. 3.1 shows the differential UBV data obtained at Boyden, with additional V magnitudes from the y observations obtained at the SAAO and the OSN. The total brightness variation over the 153 days of monitoring was 0.17 mag. The corresponding colour variations in (B-V) and (U-B) (from the Boyden observations only) were 0.18 mag and 0.13 mag respectively. The OSN observations were made at high air-masses, whilst the Boyden observations were made when Ups Sgr was situated close to the zenith. Comparison of the differential V magnitudes for 7 nights on which observations were obtained at both Boyden and at the OSN show small differences of a few hundredths of a magnitude. These discrepancies are accountable in terms of the 'scatter' introduced by the short-timescale variations discussed in Sect. 3.3b, and from observing at high air-masses. The light curve shows no evidence for the presence of eclipses. From the ephemeris given by Plavec (1979) primary eclipse (eclipse of the secondary by the primary) should have

Table 3.2 Differential uvby photometry of Ups Sgr.

H.J.D.	Variable - Comparison				Check - Comparison			
-2446000	V	(b-y)	(v-b)	(u-b)	V	(b-y)	(v-b)	(u-b)
171.633	-1.180	0.039	0.077	-0.382				
176.619	-1.198	0.031	0.075	-0.359	0.998	-0.032	0.047	0.350
176.647	-1.198	0.030	0.072	-0.365	0.996	-0.038	0.052	0.354
181.550	-1.156	0.043	0.101	-0.303	0.996	-0.034	0.050	0.346
182.513	-1.157	0.046	0.102	-0.302	0.991	-0.027	0.048	0.343
182.664	-1.153	0.043	0.100	-0.300	0.999	-0.035	0.051	0.349
185.527	-1.176	0.039	0.093	-0.316	0.991	-0.039	0.049	0.349
185.554	-1.174	0.036	0.095	-0.315	1.004	-0.047	0.042	0.342
185.677	-1.177	0.042	0.090	-0.321				
186.483	-1.181	0.042	0.088	-0.335	0.996	-0.038	0.055	0.351
186.663	-1.181	0.040	0.085	-0.334	0.997	-0.036	0.053	0.348
187.542	-1.196	0.041	0.078	-0.357	0.997	-0.037	0.049	0.343
187.668	-1.196	0.041	0.080	-0.350	0.996	-0.037	0.052	0.344
188.465	-1.200	0.045	0.080	-0.358	1.001	-0.036	0.055	0.350
190.582	-1.220	0.042	0.069	-0.382				
191.637	-1.225	0.045	0.074	-0.376				
264.460	-1.128	0.032	0.086	-0.412	0.994	-0.030	0.053	0.354
266.427	-1.114	0.023	0.080	-0.406	1.000	-0.031	0.053	0.354
267.449	-1.128	0.027	0.088	-0.407	1.000	-0.030	0.054	0.355
268.450	-1.120	0.029	0.088	-0.405	0.993	-0.031	0.054	0.357
269.417	-1.117	0.032	0.088	-0.416	0.995	-0.032	0.054	0.358
269.473	-1.128	0.037	0.082	-0.433	1.003	-0.031	0.054	0.359
272.434	-1.167	0.036	0.074	-0.460	0.997	-0.033	0.054	0.356
273.435	-1.182	0.032	0.073	-0.459	0.997	-0.030	0.054	0.355
295.446	-1.148	0.026	0.068	-0.464				
295.456	-1.142	0.024	0.075	-0.482	1.002	-0.031	0.051	0.343
297.361	-1.143	0.035	0.073	-0.460				
297.369	-1.132	0.029	0.071	-0.454	1.008	-0.037	0.061	0.349
298.369	-1.151	0.034	0.068	-0.430	0.985	-0.031	0.043	0.366
298.374	-1.131	0.029	0.078	-0.447				
299.399	-1.146	0.030	0.079	-0.435				
299.407	-1.136	0.029	0.084	-0.429	0.998	-0.033	0.051	0.350
299.412	-1.134	0.030	0.085	-0.420				
300.364	-1.128	0.033	0.084	-0.414				
300.374	-1.127	0.029	0.087	-0.422	0.985	-0.030	0.051	0.350
300.384	-1.122	0.033	0.087	-0.417	0.995	-0.031	0.054	0.348
301.406	-1.115	0.032	0.095	-0.410	0.987	-0.035	0.045	0.346
301.415	-1.113	0.032	0.096	-0.407	0.992	-0.033	0.056	0.346
301.424	-1.104	0.033	0.089	-0.399	0.993	-0.028	0.042	0.369
304.383	-1.112	0.034	0.089	-0.380	0.992	-0.033	0.051	0.353
304.395	-1.107	0.028	0.096	-0.385	1.004	-0.036	0.057	0.344
306.407	-1.141	0.021	0.087	-0.393				
306.415	-1.150	0.026	0.086	-0.406	1.006	-0.037	0.057	0.354
306.423	-1.139	0.025	0.094	-0.422	0.984	-0.031	0.050	0.350
307.470	-1.173	0.035	0.082	-0.408				
307.477	-1.161	0.031	0.084	-0.423	0.982	-0.033	0.042	0.358
307.484	-1.143	0.029	0.093	-0.429				

Table 3.3 Differential UBV photometry of Ups Sgr.

H.J.D.	Variable - Comparison			Check - Comparison		
-2446000	V	(B-V)	(U-B)	V	(B-V)	(U-B)
199.636	-1.092	-0.016	-0.204	0.997	0.033	0.268
200.632	-1.099	0.000	-0.195	0.989	0.034	0.273
201.620	-1.111	0.095	-0.281	0.981	0.041	0.265
202.473	-1.097	-0.032	-0.188	0.991	0.035	0.275
203.517	-1.127	0.007	-0.225	0.984	0.037	0.266
204.607	-1.153	0.028	-0.239	0.991	0.026	0.275
209.529	-1.175	-0.029	-0.214	0.998	0.034	0.275
210.577	-1.164	-0.017	-0.218	0.991	0.039	0.271
212.528	-1.142	-0.018	-0.211	0.980	0.044	0.272
217.480	-1.107	0.016	-0.207	0.981	0.045	0.281
221.481	-1.072	-0.039	-0.153	0.994	0.035	0.280
222.511	-1.082	0.000	-0.220	0.999	0.034	0.271
224.433	-1.089	-0.009	-0.204	0.989	0.027	0.293
226.471	-1.096	0.009	-0.233	0.986	0.032	0.274
227.434	-1.119	0.022	-0.251	0.987	0.033	0.274
229.387	-1.133	-0.005	-0.219	0.995	0.033	0.261
233.589	-1.122	-0.080	-0.171	0.983	0.038	0.282
234.512	-1.146	-0.016	-0.245	0.993	0.024	0.282
235.446	-1.141	-0.001	-0.249	0.988	0.038	0.279
236.504	-1.143	-0.009	-0.255	1.003	0.033	0.270
238.406	-1.152	0.001	-0.246	0.995	0.037	0.255
244.472	-1.056	0.035	-0.206	0.987	0.034	0.266
245.451	-1.089	0.032	-0.190	0.986	0.040	0.272
246.430	-1.104	0.033	-0.196	0.992	0.032	0.280
248.353	-1.154	0.012	-0.276	0.991	0.040	0.260
250.407	-1.158	-0.016	-0.215	0.993	0.034	0.277
253.430	-1.164	-0.011	-0.236	0.991	0.040	0.272
255.347	-1.176	-0.013	-0.255	0.987	0.038	0.269
256.368	-1.188	-0.021	-0.244	0.991	0.034	0.273
259.382	-1.189	-0.002	-0.271	0.988	0.037	0.273
261.340	-1.145	-0.019	-0.229	0.991	0.032	0.269
265.436	-1.084	0.004	-0.204	0.986	0.034	0.277
266.394	-1.088	0.015	-0.203	0.985	0.045	0.275
273.316	-1.155	-0.023	-0.234	0.990	0.029	0.265
276.320	-1.171	-0.057	-0.198	0.991	0.043	0.267
277.356	-1.167	-0.051	-0.202	0.998	0.038	0.267
279.432	-1.164	-0.028	-0.236	0.984	0.041	0.265
281.373	-1.143	-0.026	-0.216	0.992	0.030	0.282
283.338	-1.125	0.004	-0.233	0.987	0.040	0.265
284.313	-1.128	0.000	-0.220	0.982	0.038	0.273
287.372	-1.140	-0.037	-0.215	0.990	0.044	0.267
288.284	-1.157	-0.065	-0.196	0.988	0.035	0.274
289.284	-1.177	-0.063	-0.206	0.986	0.043	0.258
290.333	-1.175	-0.056	-0.219	0.987	0.037	0.266
291.396	-1.159	-0.030	-0.224	0.988	0.035	0.278
294.442	-1.123	0.012	-0.261	0.996	0.021	0.271
295.428	-1.121	0.002	-0.260	0.989	0.024	0.268
297.425	-1.130	0.023	-0.267	0.994	0.027	0.272
299.282	-1.121	-0.010	-0.226	0.982	0.038	0.264
302.293	-1.059	-0.012	-0.199	0.983	0.037	0.272
304.296	-1.078	0.007	-0.202	0.981	0.044	0.269
306.291	-1.125	-0.009	-0.205	0.984	0.039	0.264
311.406	-1.106	0.007	-0.241	0.988	0.032	0.269
315.292	-1.133	0.011	-0.243	0.987	0.033	0.276
323.262	-1.172	-0.029	-0.218	0.986	0.032	0.274

Table 3.4 High-speed differential V-band photometry of Ups Sgr on JD 2446648.

H.J.D.	dV	H.J.D.	dV	H.J.D.	dV	H.J.D.	dV
0.24712	-1.131	0.29771	-1.132	0.33764	-1.143	0.38491	-1.126
0.24825	-1.128	0.29797	-1.131	0.33791	-1.141	0.38518	-1.129
0.25181	-1.121	0.29823	-1.131	0.33816	-1.135	0.38544	-1.123
0.25208	-1.122	0.29850	-1.140	0.33892	-1.142	0.38572	-1.122
0.25435	-1.126	0.29877	-1.127	0.33918	-1.146	0.38598	-1.123
0.25461	-1.123	0.29902	-1.125	0.33945	-1.148	0.38624	-1.126
0.25488	-1.121	0.29929	-1.116	0.33973	-1.149	0.38651	-1.129
0.25514	-1.123	0.29956	-1.123	0.33998	-1.152	0.38678	-1.127
0.25542	-1.123	0.29983	-1.122	0.34025	-1.151	0.38703	-1.129
0.25600	-1.124	0.30009	-1.128	0.34051	-1.146	0.38731	-1.126
0.25625	-1.130	0.30035	-1.134	0.34115	-1.135	0.38757	-1.123
0.25652	-1.135	0.30062	-1.128	0.34141	-1.133	0.38784	-1.121
0.25679	-1.139	0.30088	-1.147	0.34167	-1.135	0.38850	-1.120
0.25735	-1.121	0.30114	-1.135	0.34195	-1.133	0.38877	-1.120
0.25763	-1.118	0.30142	-1.137	0.34222	-1.140	0.38903	-1.124
0.25790	-1.118	0.30168	-1.127	0.34247	-1.140	0.38929	-1.122
0.25815	-1.112	0.30195	-1.124	0.34274	-1.143	0.38956	-1.124
0.25842	-1.121	0.30220	-1.129	0.34300	-1.142	0.38983	-1.129
0.25869	-1.122	0.30247	-1.121	0.34327	-1.131	0.39010	-1.128
0.25894	-1.126	0.30274	-1.128	0.34353	-1.125	0.39035	-1.122
0.25921	-1.122	0.30301	-1.133	0.34430	-1.139	0.39062	-1.111
0.25948	-1.128	0.30327	-1.135	0.34456	-1.144	0.39135	-1.124
0.25975	-1.139	0.30353	-1.136	0.34482	-1.142	0.39161	-1.125
0.26000	-1.127	0.30380	-1.130	0.34509	-1.144	0.39190	-1.123
0.26027	-1.122	0.30407	-1.137	0.34535	-1.146	0.39216	-1.128
0.26054	-1.125	0.30432	-1.130	0.34562	-1.144	0.39242	-1.131
0.26124	-1.141	0.30459	-1.125	0.34588	-1.147	0.39269	-1.132
0.26151	-1.142	0.30536	-1.128	0.34615	-1.135	0.39296	-1.129
0.26178	-1.143	0.30563	-1.139	0.34642	-1.132	0.39321	-1.124
0.26204	-1.142	0.30590	-1.138	0.34668	-1.134	0.39349	-1.123
0.26231	-1.146	0.30615	-1.137	0.34694	-1.128	0.39375	-1.120
0.26257	-1.148	0.30642	-1.141	0.34880	-1.121	0.39402	-1.120
0.26283	-1.143	0.30668	-1.139	0.34908	-1.116	0.39428	-1.122
0.26310	-1.132	0.30696	-1.144	0.34933	-1.116	0.39454	-1.123
0.26385	-1.134	0.30722	-1.139	0.35084	-1.134	0.39481	-1.122
0.26410	-1.140	0.30748	-1.130	0.35110	-1.145	0.39507	-1.127
0.26437	-1.140	0.30775	-1.135	0.35137	-1.137	0.39534	-1.129
0.26463	-1.135	0.30801	-1.129	0.35163	-1.129	0.39561	-1.127
0.26489	-1.142	0.30827	-1.134	0.35189	-1.122	0.39587	-1.124
0.26516	-1.153	0.30853	-1.139	0.35263	-1.130	0.39614	-1.122
0.26542	-1.137	0.30881	-1.140	0.35290	-1.142	0.39709	-1.127
0.26570	-1.137	0.30908	-1.142	0.35316	-1.134	0.39735	-1.128
0.26597	-1.135	0.30988	-1.127	0.35343	-1.142	0.39763	-1.134
0.26622	-1.139	0.31014	-1.123	0.35369	-1.141	0.39789	-1.128
0.26649	-1.129	0.31041	-1.115	0.35395	-1.145	0.39815	-1.132
0.26675	-1.135	0.31066	-1.120	0.35422	-1.140	0.39842	-1.129
0.26701	-1.135	0.31094	-1.113	0.35450	-1.140	0.39869	-1.129
0.26728	-1.136	0.31121	-1.115	0.35475	-1.135	0.39894	-1.120
0.26755	-1.131	0.31147	-1.117	0.35502	-1.128	0.39921	-1.119
0.26782	-1.138	0.31173	-1.121	0.35528	-1.127	0.39948	-1.120
0.26808	-1.146	0.31200	-1.122	0.35555	-1.126	0.40012	-1.125
0.26834	-1.132	0.31226	-1.130	0.35610	-1.133	0.40039	-1.128
0.26903	-1.126	0.31253	-1.129	0.35638	-1.139	0.40064	-1.130
0.26930	-1.125	0.31279	-1.123	0.35665	-1.137	0.40091	-1.136
0.26958	-1.130	0.31306	-1.114	0.35690	-1.135	0.40117	-1.131

0.26984 -1.133
0.27010 -1.141
0.27036 -1.135
0.27063 -1.140
0.27090 -1.134
0.27116 -1.127
0.27143 -1.132
0.27169 -1.130
0.27196 -1.120
0.27222 -1.128
0.27248 -1.129
0.27275 -1.138
0.27303 -1.130
0.27328 -1.137
0.27355 -1.139
0.27428 -1.116
0.27453 -1.115
0.27480 -1.112
0.27536 -1.126
0.27564 -1.117
0.27591 -1.126
0.27616 -1.132
0.27643 -1.129
0.27669 -1.125
0.27695 -1.119
0.27723 -1.121
0.27749 -1.119
0.27812 -1.140
0.27944 -1.123
0.28822 -1.123
0.28871 -1.122
0.28899 -1.126
0.29132 -1.124
0.29159 -1.122
0.29186 -1.125
0.29213 -1.131
0.29240 -1.127
0.29267 -1.133
0.29292 -1.136
0.29319 -1.133
0.29345 -1.128
0.29373 -1.128
0.29399 -1.119
0.29425 -1.119
0.29452 -1.123
0.29477 -1.127
0.29504 -1.132
0.29531 -1.138
0.29558 -1.138
0.29585 -1.135
0.29610 -1.129
0.29637 -1.130
0.29664 -1.123
0.29689 -1.122
0.31387 -1.135
0.31413 -1.129
0.31439 -1.135
0.31466 -1.133
0.31492 -1.143
0.31520 -1.140
0.31547 -1.139
0.31573 -1.134
0.31600 -1.125
0.31625 -1.127
0.31652 -1.127
0.31680 -1.131
0.31706 -1.129
0.31732 -1.136
0.31759 -1.135
0.31785 -1.142
0.31812 -1.139
0.31837 -1.130
0.31865 -1.124
0.31923 -1.126
0.31950 -1.133
0.31975 -1.125
0.32002 -1.139
0.32028 -1.135
0.32056 -1.140
0.32081 -1.139
0.32108 -1.132
0.32135 -1.128
0.32161 -1.122
0.32187 -1.125
0.32213 -1.126
0.32241 -1.125
0.32292 -1.137
0.32319 -1.141
0.32344 -1.141
0.32371 -1.136
0.32397 -1.130
0.32425 -1.127
0.32452 -1.121
0.32477 -1.122
0.32504 -1.122
0.32531 -1.134
0.32557 -1.130
0.32590 -1.133
0.32693 -1.125
0.33483 -1.136
0.33510 -1.127
0.33538 -1.124
0.33564 -1.117
0.33590 -1.125
0.33616 -1.126
0.33685 -1.147
0.33711 -1.149
0.33737 -1.146
0.35717 -1.122
0.35744 -1.125
0.35770 -1.124
0.35796 -1.126
0.35823 -1.129
0.35850 -1.131
0.35877 -1.137
0.35902 -1.142
0.35929 -1.141
0.35955 -1.141
0.35983 -1.137
0.36009 -1.135
0.36035 -1.137
0.36062 -1.131
0.36088 -1.134
0.36114 -1.136
0.36141 -1.136
0.36168 -1.139
0.36194 -1.140
0.36220 -1.148
0.36279 -1.125
0.36305 -1.119
0.36381 -1.136
0.36409 -1.138
0.36436 -1.141
0.36461 -1.142
0.36488 -1.144
0.36514 -1.141
0.36541 -1.141
0.36566 -1.135
0.36594 -1.140
0.36621 -1.133
0.36647 -1.137
0.36673 -1.137
0.36700 -1.140
0.37695 -1.118
0.37789 -1.137
0.38006 -1.126
0.38033 -1.126
0.38058 -1.128
0.38085 -1.128
0.38112 -1.131
0.38137 -1.136
0.38164 -1.132
0.38191 -1.132
0.38218 -1.125
0.38245 -1.123
0.38306 -1.129
0.38333 -1.131
0.38359 -1.132
0.38386 -1.131
0.38413 -1.134
0.38439 -1.136
0.38466 -1.136
0.40145 -1.126
0.40171 -1.122
0.40197 -1.124
0.40224 -1.119
0.40250 -1.119
0.40276 -1.119
0.40303 -1.126
0.40330 -1.125
0.40357 -1.130
0.40382 -1.132
0.40409 -1.122
0.40436 -1.118
0.40462 -1.114
0.40488 -1.113
0.40570 -1.127
0.40595 -1.126
0.40622 -1.133
0.40649 -1.132
0.40675 -1.124
0.40701 -1.122
0.40728 -1.122
0.40755 -1.118
0.40782 -1.119
0.40808 -1.116
0.40870 -1.129
0.40895 -1.128
0.40922 -1.131
0.40950 -1.134
0.40976 -1.129
0.41002 -1.125
0.41028 -1.127
0.41055 -1.126
0.41081 -1.122
0.41108 -1.125
0.41135 -1.131
0.41161 -1.135
0.41188 -1.134
0.41247 -1.126
0.41274 -1.120
0.41299 -1.127
0.41327 -1.116
0.41353 -1.119
0.41380 -1.120
0.41406 -1.126
0.41432 -1.125
0.41459 -1.126
0.41487 -1.126
0.41512 -1.127
0.41539 -1.123
0.41565 -1.120
0.41624 -1.114
0.41732 -1.136

occurred on JD 2446238, and secondary eclipses around JD 2446170 and JD 2446308. Whilst light minima do occur close to these eclipse times their depths are not significant and they correlate with the 20-day pulsation period described below. The uvby observations are shown in Fig. 3.2. The colour changes in (u-b) and (v-b) appear to be in phase with the V observations. Any changes in (b-y) are comparable to the scatter in the data.

3.3 Frequency analysis

3.3a LONG-TERM VARIABILITY

The light variability of Ups Sgr appears quasi-periodic. Identifying successive minima in the light curve (Fig. 3.1) at JD 2446181, 199, 221, 244, 265, 283 and 302, a characteristic period for Ups Sgr of 20.2 ± 2.0 days is estimated. Fernie (1982) used a similar technique to determine a pulsation period of 46 ± 5 days for RCrB. A Fourier analysis of the data indicated periodicities of 20.9, 20.8 and 20.7 days present in the individual U, B and V light curves of Ups Sgr respectively. Many of the variations in hydrogen-deficient stars may be quasi-periodic as the pulsations appear to be extremely non-adiabatic (Trimble 1972, Saio et al. 1984). In this case a Fourier-type analysis is inappropriate since it searches for strictly-periodic variations. Phasing the data from each passband on its dominant frequency found from the Fourier analysis shows a substantial scatter about the fit, indicating the inadequacy of the solution. An inspection of the power spectrum of the (U-B) observations shows a significant

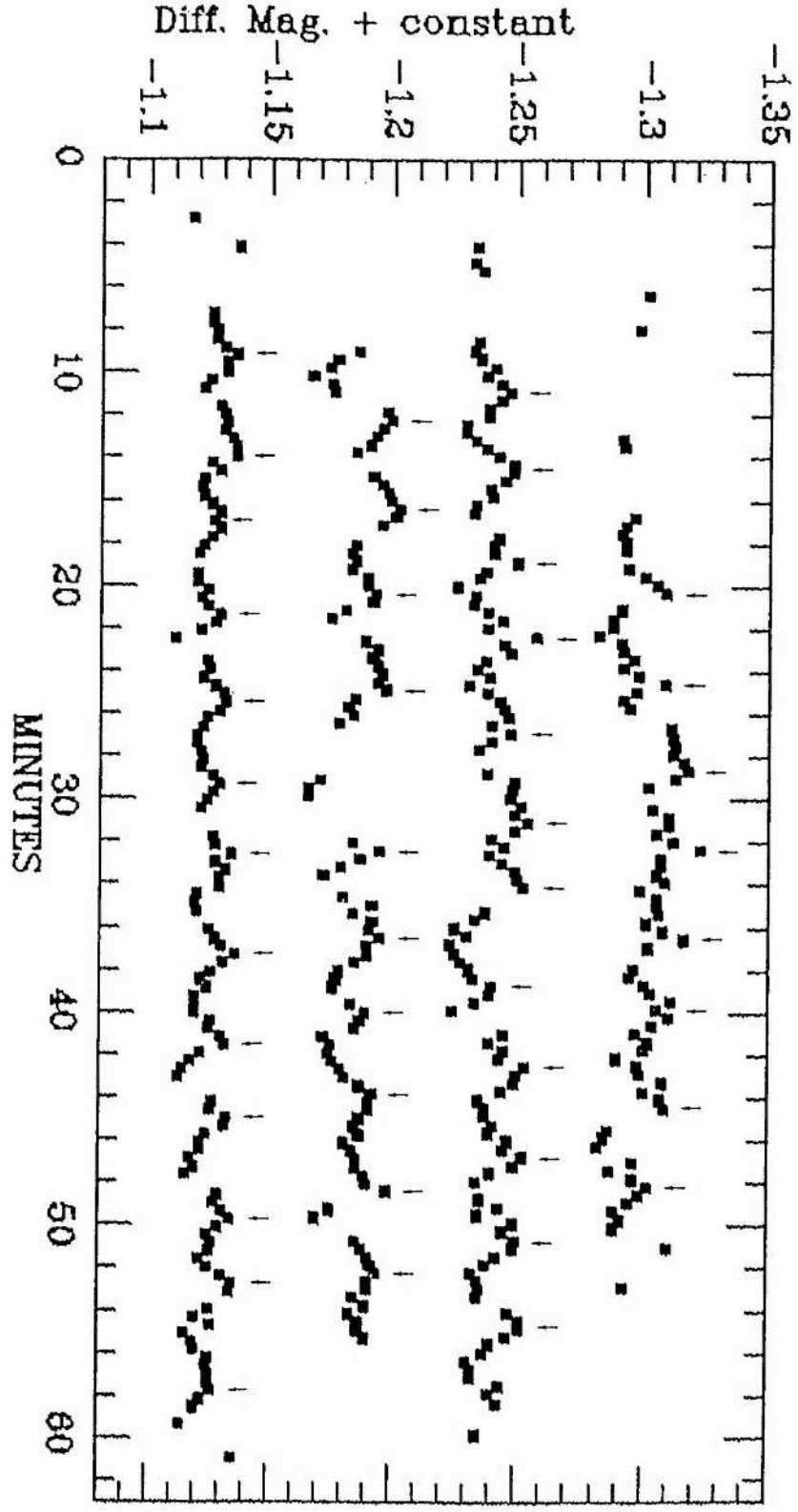

Figure 3.3 Differential V observations of Ups Sgr on JD 2446648. This is an almost continuous light curve 4.1 hr long and should be read left-to-right, top to bottom. The arrows indicate light maxima of the 239-sec period.

peak corresponding to a period of 20.7 days, in agreement with that found from the individual U,B and V light curves.

3.3b SHORT-TIMESCALE VARIABILITY

A visual inspection of the data for 1986 August 5/6 (Fig. 3.3) indicates small luminosity variations with a period of about 4 minutes. Their amplitude is variable, but with a typical peak-to-peak range of $\sim$0.02 mag. These variations are reminiscent of a non-radially pulsating white dwarf (eg. ZZ Ceti, Robinson 1979). A mean period can be estimated by measuring the time between consecutive light maxima, which are marked by arrows in Fig. 3.3. From 35 measurements a mean period of 0.00278 ± 0.00031 days (240 sec) is estimated. The error is consistent with random measurement errors.

The data was searched for strictly-periodic content in the frequency range 1-5000 cycles day^{-1} with the Fourier-analysis package PULSAR (Skillen 1985). The power spectrum of the data showed the presence of a strong peak at $\sim$360 cycles day^{-1} (Figs. 3.4 & 3.5). The solution was optimised to 361 cycles day^{-1} (0.00277 days = 239 sec) by sweeping the data with a sine-wave over a small frequency range. Observed minus calculated times of light maxima are shown in Fig. 3.6 using periods of 239 sec and 240 sec (found from the Fourier analysis and from the mean duration between light maxima respectively) phased with respect to the first light maximum at HJD 2446648.25679. It is obvious that the 239-sec period represents a better fit to the data. Tests were made using

Figure 3.4 The power spectrum of the data for the night of JD 2446648.

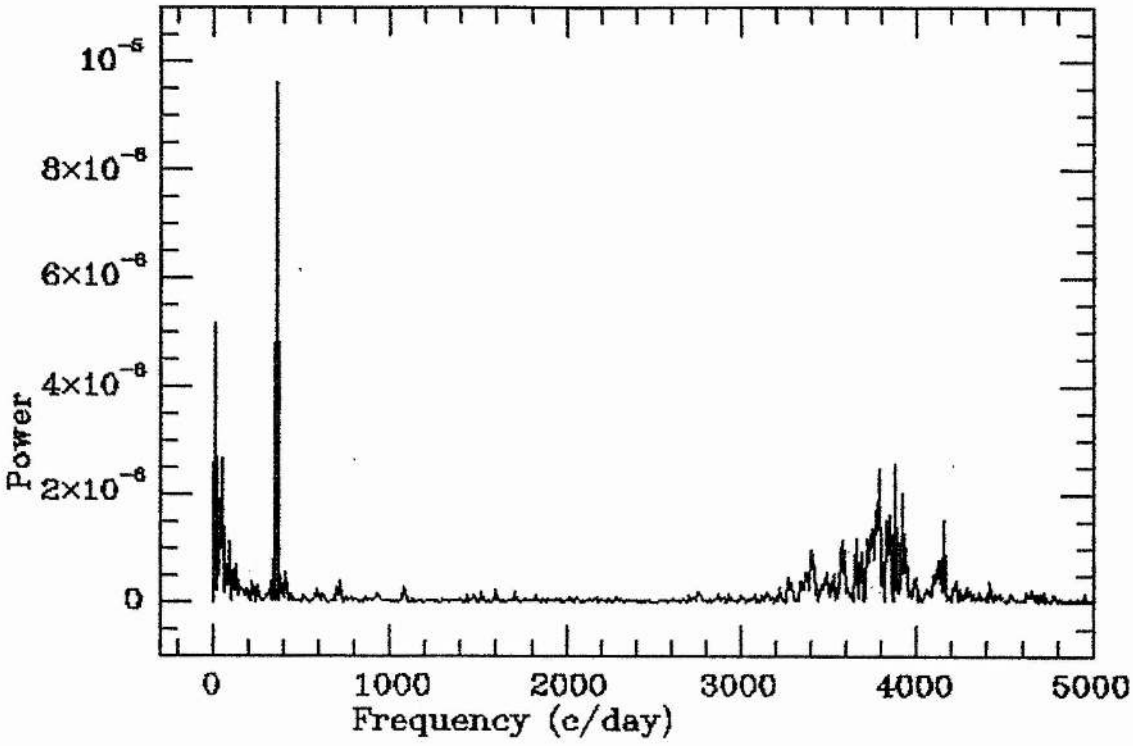

Figure 3.5 An expanded plot of the power spectrum of Figure 3.4.

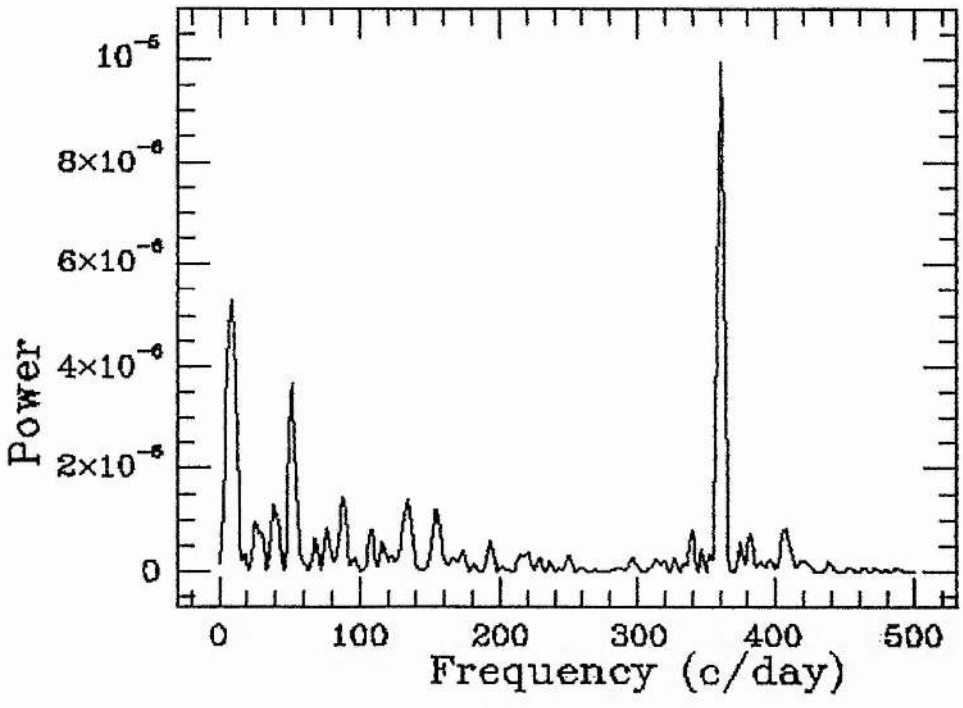

different spectral windows (the transform of the data window) to identify any aliases that might be introduced into the power spectrum from regularities in the data sampling. The broad region of enhanced power centred around 3800 cycles day^{-1} is aliasing from the sampling intervals. The power spectra of the data subsets using only the first quarter, and the middle half of the data, similarly showed peaks at 361 cycles day^{-1}. An independent confirmation of the significance of the 239-sec period was made using a string-length or phase-dispersion minimisation technique (Dworetsky 1983). The 239-sec periodicity was removed by the regression of a sine-wave on the data, and the power spectrum of the pre-whitened data examined for evidence of any remaining periodic content. Significant peaks are present at 8 (2.7 hr) and 52 (28 min) cycles day^{-1}, which are also present in the power spectrum of the unwhitened data (Fig. 3.5). The peak at 2.7 hr is an alias introduced by small-magnitude shifts between the 4 component data sets, which are artifacts of the observational and reduction techniques. The peak at 28 min appears to be related to an apparently secular brightening of Ups Sgr which occurred over the first part of the observations and can be seen most clearly in the pre-whitened data of Fig. 3.7.

The frequency resolution is estimated from $1.5/T \approx 9$ cycles day^{-1}, where T is the timespan in days of the observations (Loumos & Deeming 1978). The width of the peak at 361 cycles day^{-1} in the power spectrum is due entirely to the resolution of the data set showing that the oscillation is periodic with constant frequency over the timespan of the observations. The power spectrum of a

Figure 3.6 O-C fits to the light maxima indicated in the data of Figure 3.3 using a 239-sec (filled squares) and a 240-sec period, both phased to the first light maximum at HJD 2446648.25679. The residuals from the fit with the 240-sec period have been shifted in ordinate by -0.35 cycles.

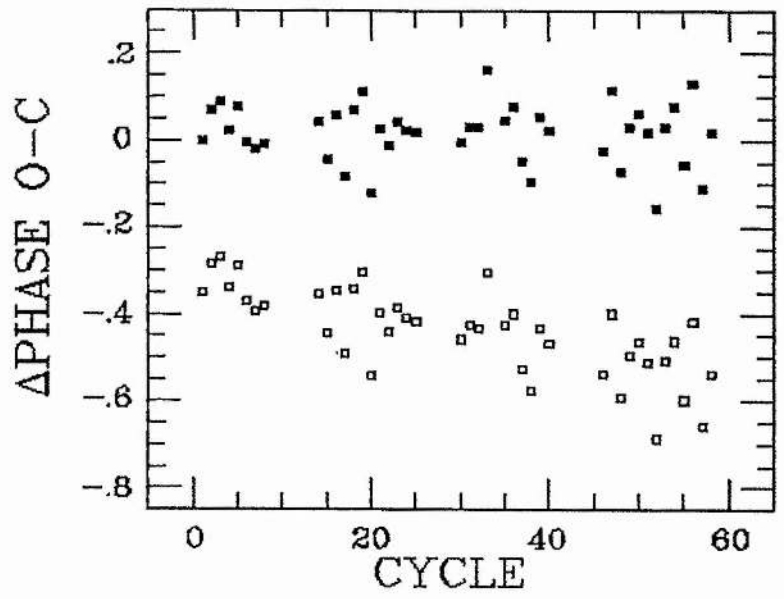

Figure 3.7 The data of Figure 3.3 with the 239-sec period filtered out by regression of a sine-wave on the data. Zero magnitude is arbitrarily defined, and time is HJD-2446648.0.

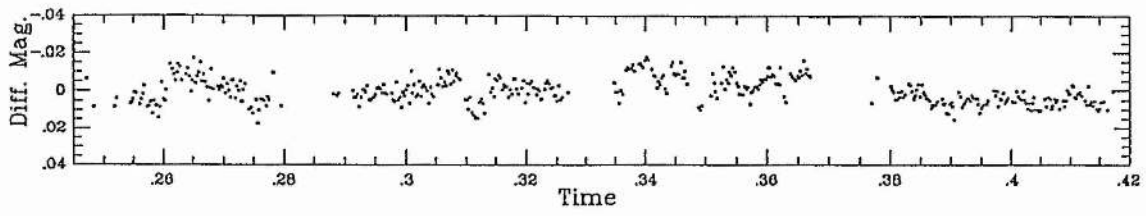

quasi-periodic variation would be expected to show a broad region of enhanced power centred on the mean period of the oscillation. That the data displays irregular variations that remain after pre-whitening shows the inadequacy of a description of the light curve in terms of a single sine-wave. The variations are sufficiently transient that no periodicities are evident. It is noted that mass-exchanging binary systems often show rapid flickering on timescales of minutes which appear as random and unpredictable variations in brightness (Robinson et al. 1987).

3.4 Discussion

3.4a THE ORIGIN OF THE 20-DAY VARIABILITY

The four known EHdBs all show photometric variability. KS Persei shows irregular light (0.15 mag in V) and colour variations on a timescale of ~30 days (Heard 1962, Osawa et al. 1963). The presence of additional periodic, smaller-amplitude variations (0.02 mag) over about 5 days is suggested in Sect. 2.6. CPD-58°2721 shows quasi-periodic light (0.17 mag in V) and colour variations with a characteristic period of 9.4 ± 1.5 days (Chap. 4). The writer is not aware of any detailed photometric studies of LSS 4300, but Landolt (1986b) reports a range in brightness of 0.15 mag over 3 years and the possibility that LSS 4300 may show maximum changes in brightness over a time interval as short as a day.

The RCB star RY Sgr (T_{eff}=7,100K) and the EHe star BD+1°4381 (T_{eff}=9,500K) have pulsation periods of about 38 (Feast 1979) and 21 days (Sect. 2.1) respectively, and are consistent with radial pulsation of the star in the fundamental mode (Saio 1986). The pulsation period P of a star is related to its mean stellar density ρ by the relationship $Q=P\rho^{1/2}$, where Q is the pulsation constant. This can be rewritten as $Q=Pg^{3/4}M^{-1/4}$, where g and M are the surface gravity and mass respectively. Adopting $M=1M_{\odot}$ and log g=0.65 for RY Sgr (Schönberner 1975) gives 0.055 for the value of Q. For Ups Sgr we have $M=1M_{\odot}$ and log g=1.0 (Hack & Pasinetti 1963, Schönberner & Drilling 1983) which leads to Q=0.054. The consistency of the Q-estimates suggests that the pulsational characteristics are similar in these stars and is evidence that Ups Sgr may also be pulsating in the fundamental mode. A Period-T_{eff} relation for radial pulsation in the extremely hydrogen-deficient stars appears to be emerging and the 20-day period of Ups Sgr fits well into this sequence. There is no evidence for the presence of eclipses. That the observations of Gaposchkin (1945) and Eggen et al. (1950) were misinterpreted would seem to be due to the sparseness and incomplete nature of the observations, and the fortuitous agreement of light minima with the expected times of eclipses. In view of this the writer is sceptical of the reports of eclipses in the ultra-violet region. The presence of eclipses in Ups Sgr has yet to be confirmed, and if eclipses do occur they must be of such small amplitude ($\lesssim$ 0.1 mag) in the visible region that they are masked by the light variations due to pulsation of the primary.

Using synthetic colours calculated from model stellar atmospheres Heber & Schönberner (1981) related UBV colours and effective temperatures for the EHe stars by a reddening-free parameter q which they defined as :

$$q = (U-B)-C(B-V)-b(B-V)^2$$

where $C=a-2b(B-V)_o$, and a and b represent the slopes of the reddening lines in the UBV system. As the last two terms on the right-hand side of the expression are small for Ups Sgr, we find $q \approx (U-B)$. Similarly, uvby colours and effective temperatures for the EHe stars are related by a reddening-free index $[c_1]$ given by :

$$[c_1] = c_1-0.1(b-y)$$

For Ups Sgr, $[c_1] \approx (u-b)$ as (b-y) and (v-b) are small, so that changes in (U-B) and (u-b) are both indicative of temperature changes. As the individual U, B, V and u, v, b, y light curves are in phase with the (U-B) and (u-b) variations respectively, it indicates the temperature and luminosity variations are in phase.

Greenstein (1950) and Hack (1960) reported that the spectrum of Ups Sgr shows changes in the strengths and profiles of lines. The changes in absorption line strengths exhibit a strong dependence on excitation potential, with changes most marked in lines of low excitation. This behaviour of Ups Sgr is very similar to that observed in the spectrum of CPD-58°2721 (Sect. 5.2a) which shows marked changes in the strengths of low-excitation lines on a timescale of days. As in the case of CPD-58°2721, the changes of

line strengths in Ups Sgr are interpreted as confirmation of temperature changes of the primary star during pulsation. The phase dependence reported by Hack (1960) between the spectral changes in the absorption lines and the binary period was probably not real, but due to the data sample being distributed in such a way as to imply that the dependence was real.

3.4b THE ORIGIN OF THE 239-SECOND VARIATION

Such a short periodicity has not previously been reported in the EHdBs. Might the 239-sec periodicity be identified with the secondary? For a secondary at least 10 times fainter than the primary in the visible region (so as not to be detected in the spectrum), the observed change of ~ 0.02 mag (2%) in V in the system requires the secondary to be changing by more than 0.2 mag (20%) over 4 minutes. Such short-period oscillations are known to occur in single white dwarfs and those in close binary systems where the variations have usually been associated with non-radial oscillations (Nather 1978, Robinson 1979). However, the amplitudes of the oscillations are typically only about 1%. With a mass $\gtrsim 3M_{\odot}$, the secondary cannot be such a highly evolved object as a white dwarf. Apart from the Sun, the only main-sequence stars that show light variability on a timescale less than about 20 min are the rapidly rotating Ap stars (Kurtz 1985), but again the amplitude of the variation is only about 1%. The sound speed in the outer layers of the primary, v_s, is given approximately by the relation $v_s \sim (kT/\mu m_H)^{1/2}$ where k is the Boltzmann constant, T the temperature, μ the mean molecular weight of the particles, and m_H

the mass of the hydrogen atom. For an envelope predominantly of helium, and substituting $T=T_{eff}$, the sound speed is ~ 6 km s^{-1}, so that in 4 minutes a perturbation will have propagated only $\sim 10^3$km.

It seems, therefore, that the 239-sec oscillation is a surface effect involving only the outermost layers of the atmosphere of the star. It is now recognised that most, if not all supergiants display photometric variability on timescales of hours to years (de Jager 1980). The lower limit arises because of the large size of the objects and the correspondingly longer travel time compared to more compact stars. The 239-sec variation appears therefore to be incongruous with an explanation involving pulsation of the supergiant primary (or the fainter main-sequence secondary) because of the small-timescale of the variations which implies a more compact object. However, Landolt (1986a) reports that photometry of the supergiant EHe star LSS 3378 (T_{eff}=9,400K) suggests that it may be quasi-periodic on the order of several minutes, and that this appears to be superimposed on a longer-term variation of perhaps 0.243 days, with total amplitudes of 0.06 mag and 0.1 mag respectively in V.

There is no evidence to suggest that the 239-sec variation is an instrumental effect, such as might arise from a periodic error in the telescope drive. Observations of other variable stars with a similar observing style showed no similar effects. Drifting a star across the photometer aperture did not produce any measurable variations in count-rate until the star approached the aperture

edge, so 'worm-error' variations should have little or no effect. The possibility of a faint star on the edge of the aperture drifting in and out of view can be discounted. Such a star would have to be 9th magnitude and about 30" from Ups Sgr, but none is visible on Palomar charts or listed in any star catalogue. The pseudo-random observing style would seem to make it impossible for an instrumental variation to retain its phase in each subsequent hour of observations after each comparison star observation.

3.5 Modelling the light curve

Synthetic binary-star light curves for Ups Sgr were generated using the light-curve synthesis code LIGHT (Hill 1979). Adopting the spectroscopically determined mass function of f(M)=1.677 (Seydel 1929), models were computed at 5 orbital inclinations (i), corresponding to secondary masses (M_2) of 3, 5, 8, 12 and 15$M_\odot$. At each inclination, light curves were generated at wavelengths of 5500A and 1600A for primary radii $R_1=R_L$, $\frac{3}{4}R_L$, and $\frac{1}{2}R_L$, where R_L represents the Roche radius. The primary is assumed to be a 1$M_\odot$ supergiant with T_{eff}=10,500K and log g=1.0. As a consequence of its decreasing share of the total mass of the system for decreasing i, R_L remains nearly constant at about 50$R_\odot$ in all the models. This is comparable to the radius expected for a helium supergiant at these temperatures. The secondary is assumed to be on the main sequence. Effective temperatures and radii for the secondary appropriate to its main-sequence masses were adopted (Allen 1973, Meyer-Hofmeister 1982), with log g=4.0 in all cases. The size of the semi-major axis of the system, A, is calculated from

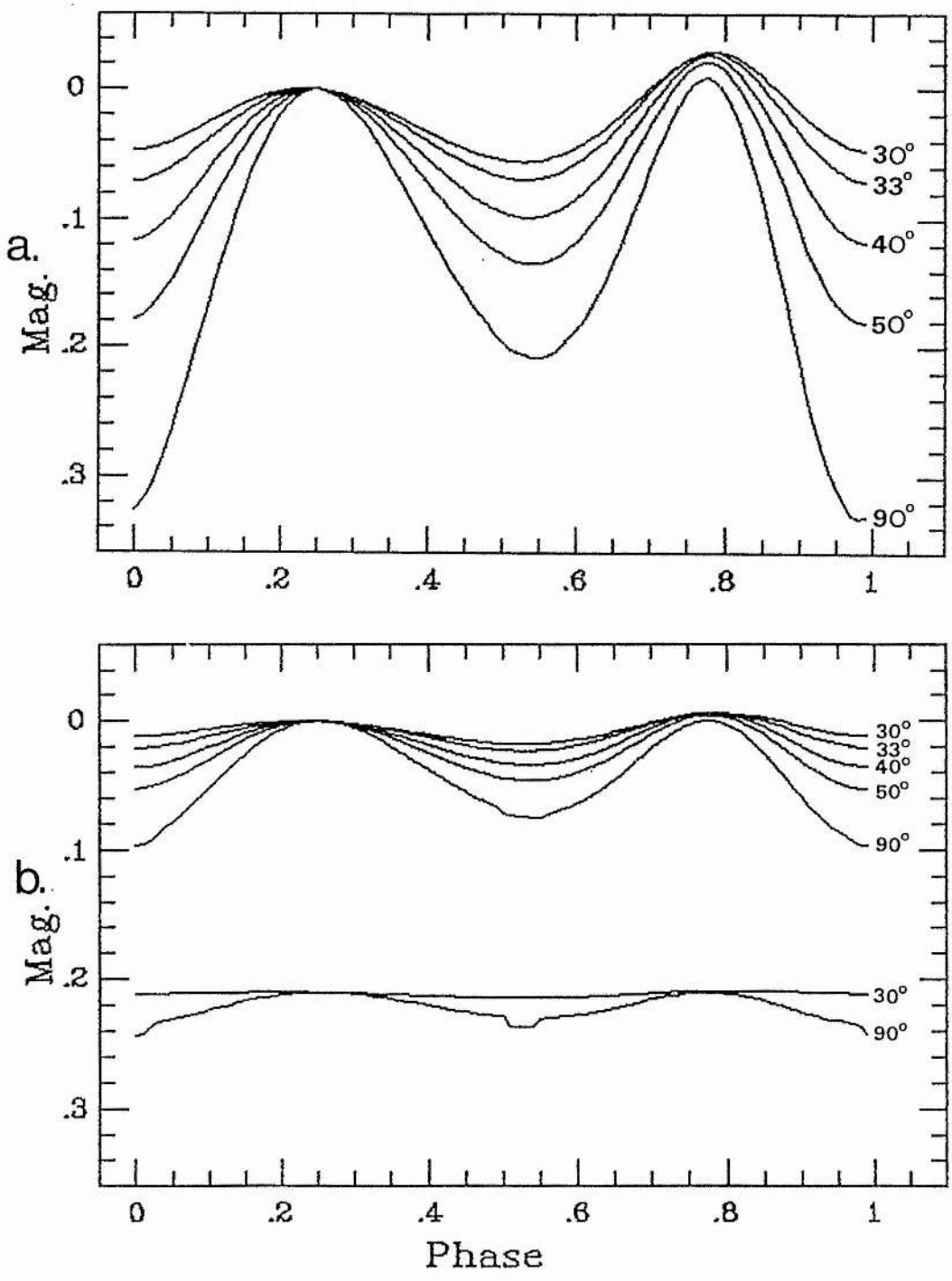

Figure 3.8 Theoretical light curves generated at 5500A for Ups Sgr scaled so that phase 0.25 is defined to have zero magnitude. a) $R_1=R_L$. b) $R_1=\frac{3}{4}R_L$ (top) and $R_1=\frac{1}{2}R_L$ (shifted by 0.21 mag). 0 Phase corresponds to when the secondary is closer to us than the primary.

$A\sin i = A_1 \sin i(1+q)$, where $A_1 \sin i$ is the size of the primary's orbit, and q is the mass-ratio M_1/M_2. From Hack et al. (1980) $A_1 \sin i = 93 \times 10^6$ km, $\omega = 29^\circ$, and an eccentricity of 0.05 so that the orbits are almost circular. The longitude of periastron, ω, is poorly determined. Radiative and black-body atmospheres are assumed throughout. The parameters of the models are tabulated in Table 3.5.

Only the $i=90^\circ$ ($M_2=3M_\odot$) model displays eclipses, and the depths of the eclipses are small (~ 0.01 mag). For large values of i, distortion of the Roche-lobe filling primary gives rise to significant ellipsoidal light variations of up to 0.4 mag (Fig. 3.8a). At $i=50^\circ$ and 40° ($M_2=5M_\odot$ and $8M_\odot$) these variations are still larger than any present in the observed light curve. The ellipsoidal light variations have become sufficiently small (< 0.1 mag) in the $i=33^\circ$ and 30° models ($M_2=12M_\odot$ and $15M_\odot$) so as to make their detection unlikely due to the presence of the larger pulsation-related light variations. Reducing the primary to three-quarters of its Roche radius greatly reduces the amplitude of the ellipsoidal light variations so that their detection would be difficult for $i \lesssim 50^\circ$ (Fig. 3.8b). Models with the primary radius set at half its Roche radius indicate that their detection would be unlikely even at $i=90^\circ$ (Fig. 3.8b). Spectroscopic observations of Ups Sgr suggest that the primary is filling its Roche lobe. The models are therefore only reconcilable with observations if the system is being viewed at a sufficiently small inclination ($i \lesssim 30^\circ$) that the ellipsoidal light variations are not detectable. The small inclination implies a secondary

Table 3.5 The parameters of the model light curves. A, M_2 and R_2 are in solar units.

						5500A			L_1/L_2	1600A	
i^o	A	M_2	R_2	$T_{eff,2}$	Sp	R_L	$\frac{3}{4}R_L$	$\frac{1}{2}R_L$	R_L	$\frac{3}{4}R_L$	$\frac{1}{2}R_L$
90	178	3	2	10,000K	A0	612	345	154	668	433	207
50	207	5	3	13,500K	B7	113	62	27	25	15	7
40	234	8	4	17,000K	B4	43	24	10	4	2	1
33	266	12	6	23,000K	B2	12	6	3	0.46	0.28	0.13
30	284	15	7	30,000K	B0	5	3	1	0.12	0.07	0.03

Figure 3.9 Best fit-by-eye to the observed light curve with the theoretical light curve generated at 5500A for the case $i=30^o$ ($M_2=15M_\odot$) and $R_1=R_L$. Phase is arbitrarily defined to be zero to coincide with the first datum. It was necessary to shift the theoretical curve by 0.4 cycles relative to the ephemeris given for Ups Sgr by Plavec (1979).

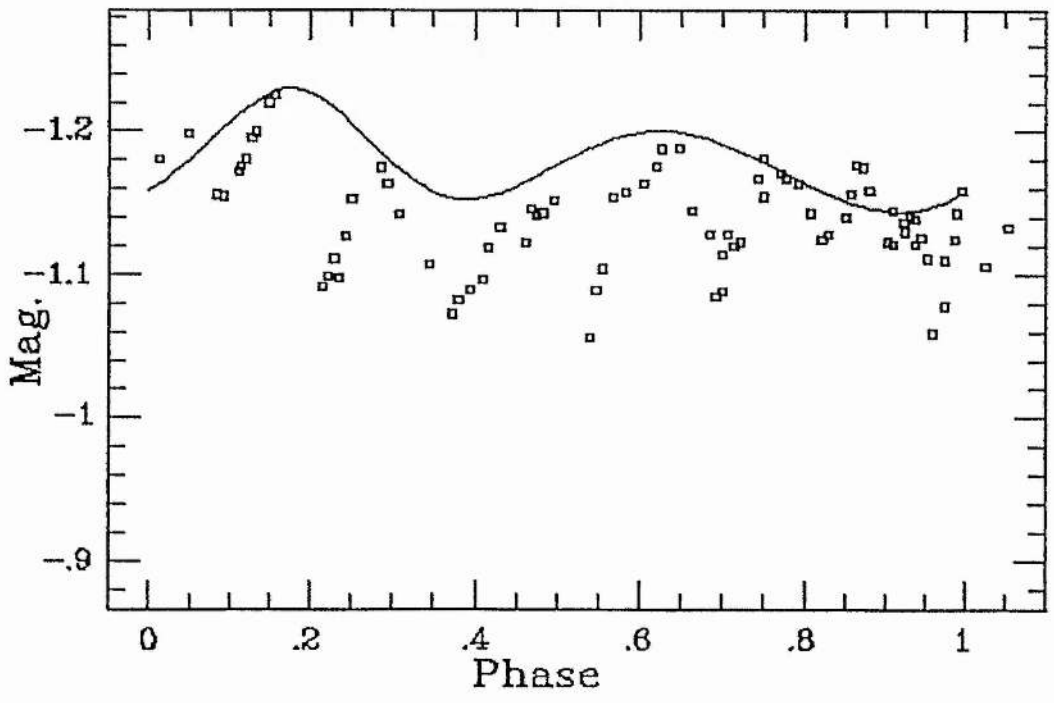

mass $\gtrsim 12M_{\odot}$. Fig. 3.9 is a best fit-by-eye of the theoretical light curve for $i=30^{\circ}$ and $R_1=R_L$ to the observed light curve, and gives an idea of the size of any ellipsoidal variations superimposed upon the 20-day pulsation.

Direct observation of the secondary is only possible in the ultra-violet region. Parthasarathy et al. (1986) examined high-resolution IUE spectra of Ups Sgr. They found that the near ultra-violet (1600A-3200A) is dominated by absorption lines of singly ionised metals which show the same radial velocity shifts as lines in the visible region and must therefore arise in the photosphere of the primary. However, the far ultra-violet ($\lesssim$ 1600A) is characterised by absorption lines of multiply-ionised atoms (NV, CIV, SiIV) which do not show detectable velocity shifts and are associated with the hot, more massive secondary. The fluxes of the primary and secondary must therefore be comparable near 1600A. Fig. 3.10 shows the luminosity ratio of the primary (L_1) to the secondary (L_2) from the 1600A models plotted against M_2. The dashed line corresponding to $L_1=L_2$ represents a best fit to the observations. For $R_1=R_L$ it indicates $M_2 \simeq 11M_{\odot}$. Fig. 3.11 shows the results for the models at 5500A. The smallest flux ratio permitted if the secondary is not to be detected in the visible spectrum is marked with a dashed line corresponding to a secondary 10 times fainter than the primary. For $R_1=R_L$ it indicates that $M_2 \lesssim 13M_{\odot}$, falling to $M_2 \lesssim 8M_{\odot}$ in the models with $R_1=\frac{1}{2}R_L$.

Figure 3.10 Theoretical luminosity ratios from the 1600A models plotted against secondary mass and spectral type. □ $R_1=R_L$, △ $R_1=\frac{3}{4}R_L$, ■ $R_1=\frac{1}{2}R_L$. Effective temperatures are marked in units of $T_{eff}/10^3$.

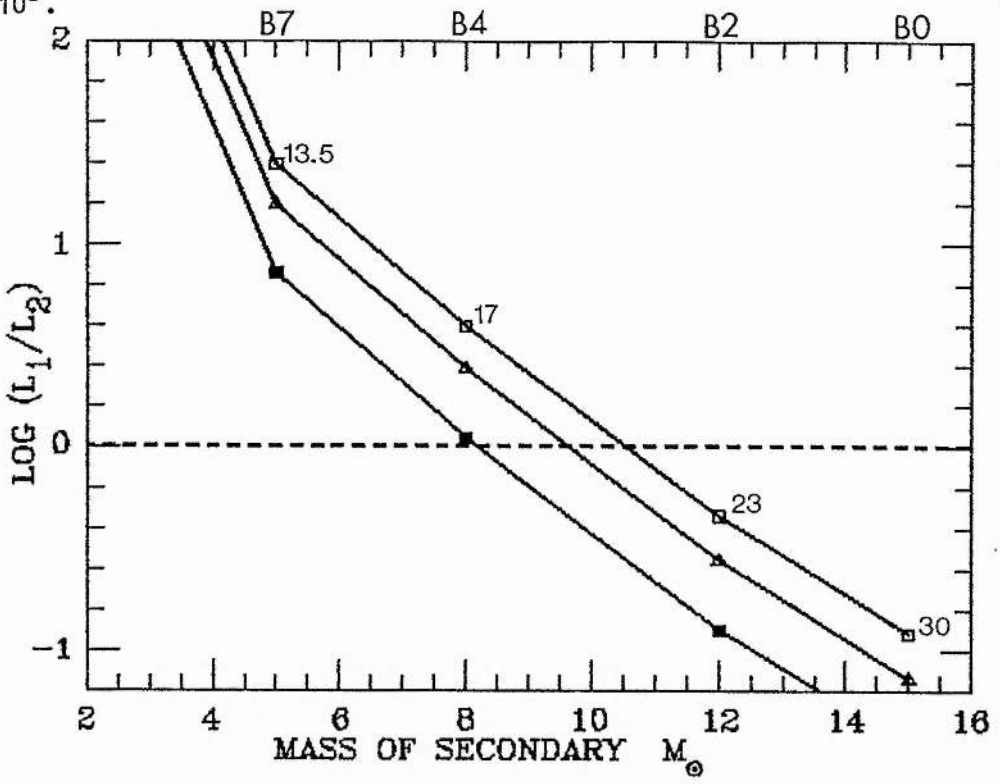

Figure 3.11 Theoretical luminosity ratios from the 5500A models plotted against secondary mass and spectral type. The notation is the same as for Figure 3.10.

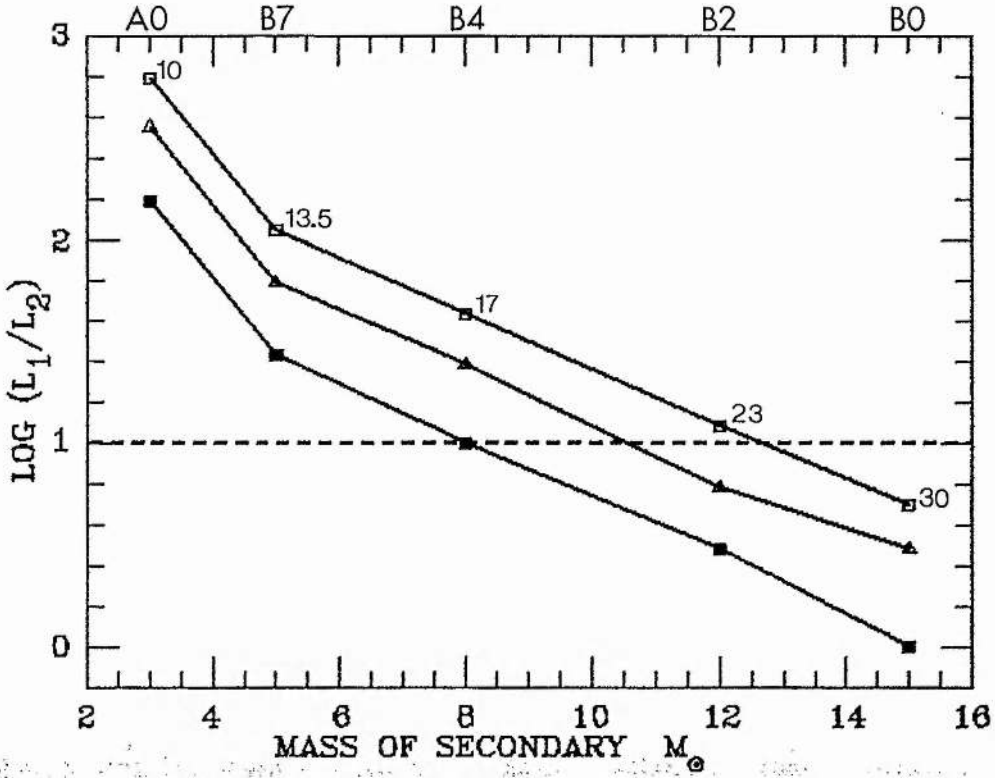

The lines of multiply-ionised atoms identified with the secondary are typical of a late O or early B-star, and the degree of excitation shown by the non-resonance lines indicates that the secondary cannot be earlier than O9 (Parthasarathy et al. 1986). Hack et al. (1980) suggested a spectral type for the secondary of O9.5V from ultra-violet observations. Drilling & Schönberner (1982), however, obtained a best match to the continuum and line spectrum of Ups Sgr with the combination of an A-type supergiant primary and a B2Ib secondary, 3-5 magnitudes fainter in the visible region. They propose a secondary with a mass $\lesssim 4M_{\odot}$ (so that the plane of the system lies close to the line of sight), which is out of thermal equilibrium as it is accreting mass. They explain that such a star can have a similar L/M ratio, and hence a similar spectrum as an early B-type supergiant. However, there is no evidence to suggest that the secondary is significantly disturbed from its thermal-equilibrium state. Indeed the mass-transfer/loss rate required to significantly disturb the secondary from its thermal-equilibrium state would most likely lead to the formation of an accretion disc. This could become the dominant flux source in the system so that a distinctly non-stellar spectrum would be observed. From radio observations, Rao & Venugopal (1985) have determined an upper mass-loss rate from the system of $5\times10^{-7}M_{\odot}yr^{-1}$. Our mass estimate of about $11M_{\odot}$ for the secondary corresponds to an early B-type star, in excellent agreement with the T_{eff} estimates of Schönberner & Drilling (1983) and Parthasarathy et al. (1986). Such a main-sequence star has a luminosity of $\sim 10^{4}L_{\odot}$. However, Parthasarathy et al. have

estimated a much smaller mass of $3M_{\odot}$ for the secondary using Abbot's (1978) relation between the edge velocity and escape velocity of the line profiles presented in the stellar wind, and a luminosity of $200L_{\odot}$ from the Wilson & Dopita (1985) expression. The applicability of both these methods is uncertain in the case of Ups Sgr where the primary and secondary appear to be interacting through mass-transfer/loss, so that these mass and luminosity estimates should be treated with caution.

3.6 Evolutionary Status

From the analysis of Sect. 3.5 a description of the secondary as an early B-type main-sequence star with a mass of about $11M_{\odot}$ has been derived. In this section theoretical and observational considerations are used in order to gain an insight into the likely evolutionary history of Ups Sgr. It is believed that Ups Sgr consists of a highly luminous primary of $\sim 1M_{\odot}$ in which the energy comes from a helium-burning envelope overlying an inert CO core (Paczynski 1971, Schönberner & Drilling 1983), and a more massive secondary which is not seen in the visible spectrum. The peculiar compositions seen at the surface of Ups Sgr and the other EHdBs can be understood in terms of close binary evolution involving mass-transfer/loss. It appears that only those stars which can experience two episodes of Roche-lobe overflow are able to reduce hydrogen to the abundances ($n_H:n_{He} \lesssim 10^{-3}$) that are presently observed in Ups Sgr and the other EHdBs. For stars with initial

masses less than about $5M_{\odot}$, the models of Iben & Tutukov 1985 (hereinafter IT85) indicate that they are unable to expand and fill their Roche lobes again after the exhaustion of central helium and allow a second phase of mass-transfer/loss. For a $4M_{\odot}$ star IT85 found that although the $0.5M_{\odot}$ remnant still has hydrogen relatively abundant at its surface, only a moderate stellar wind is required to remove the remaining hydrogen. The surface abundances ($n_N/n_C \sim 100$) would be similar to those observed in the EHdBs (Hack & Pasinetti 1963, Wallerstein et al. 1967, Schönberner & Drilling 1984). However, at all times during the evolution of the $4M_{\odot}$ model $L < 10^3 L_{\odot}$, which is clearly incompatible with observations of EHdBs which indicate $L \gtrsim 10^4 L_{\odot}$. For those stars with initial masses $\gtrsim 10M_{\odot}$ IT85 find that their models are unable to avoid core collapse and a supernova explosion with a resultant neutron star remnant. Hence the primordial mass of the primary is constrained to the range $\sim 5\text{-}10M_{\odot}$, and consequently the total mass of the primordial system to less than $20M_{\odot}$. In the following discussion all masses and radii are in solar units.

The first episode of mass-transfer/loss in Ups Sgr began when the primary expanded and filled its Roche lobe after the end of hydrogen-core burning (Case B). After the exhaustion of central hydrogen, a star can expand to a radius given approximately by (Iben & Tutukov 1987) :

$$R_{RG} \approx 10^{0.24} M^{2.25}$$

For Ups Sgr to have been able to undergo mass-transfer/loss at this stage it is a necessary condition that $R_L < R_{RG}$. The semi-major axis of the system and the Roche radius of the primary are related

by (Tutukov & Yungelson 1979) :

$$A \approx 1.9 R_L (M_{tot}/M_1)^{0.44}$$

As $M_1 \lesssim 10 M_\odot$, and as the total mass of the system, M_{tot}, must necessarily have been less than $2M_1$, it follows that the primordial system could not have had a semi-major axis greater than $\sim 800 R_\odot$. From Kepler's law a maximum primordial period for the system of $\sim$600 days is obtained.

Yungelson (1982) estimates that for massive binaries undergoing case B transfer the duration of mass-exchange is given approximately by :

$$t \approx 10^{6.3}/M_{MS}^2 \text{ yr}$$

where M_{MS} represents the main-sequence mass of the primary. The mass of the remnant is given by (IT85) :

$$M_r \approx 0.08 M_{MS}^{1.4}$$

It follows that for an initial mass 5-10$M_\odot$, a remnant mass of 0.8-2.0$M_\odot$ will have been produced. The duration of mass-loss is 10^4-10^5 years from which an average mass-loss rate $< 10^{-3}$ $M_\odot yr^{-1}$ follows, although in a real system the rate of mass loss may change dramatically during this interval. How much mass the secondary could have accreted depends sensitively upon the primordial orbital parameters A and q. If the accretion timescale exceeded the thermal adjustment timescale of the secondary then the secondary will have been able to accrete the mass lost by the primary and continue its main-sequence evolution on a new timescale appropriate to its larger mass. If, however, the thermal timescale exceeded the accretion timescale, then the accreting star will have swelled and filled its Roche lobe. A common envelope may have ensued with

loss of mass from the system. The accretion rate is likely to be greatest near the start of the mass-transfer/loss phase, and this is the most likely time for the formation of a common envelope. Conservation of mass was more likely if the initial components were comparable, than was the case where the secondary's mass was significantly less. As the present mass of the secondary appears to be at least as large as that of the primordial primary, it indicates that the secondary must have accreted at least part of the mass lost by the primary during Roche-lobe overflow.

The first mass-transfer/loss phase terminated when the primary shrank at the onset of core-helium burning. The abundance of hydrogen at the surface would then have been ~ 0.2 by mass (De Greve & De Loore 1976, IT85). Ups Sgr is believed to be experiencing its second phase of mass-transfer/loss after the exhaustion of helium at its centre (case BB). IT85 show that the amount of mass lost by the primary during this second mass-loss episode is strongly dependent upon the original main-sequence mass. For a $2.0M_{\odot}$ remnant ($M_{MS}=10M_{\odot}$) about $1M_{\odot}$ of the remaining mass is lost, whilst the $0.8M_{\odot}$ remnant ($M_{MS}=5M_{\odot}$) loses only a very small additional amount of mass. The calculations of Delgado & Thomas (1981) show that the $2M_{\odot}$ remnant loses about half of its mass in a rapid phase of mass-transfer/loss lasting only about 10^4 years. This is followed by a slower mass-transfer/loss phase in which the mass is further reduced only slightly. Schönberner & Drilling (1983) suggest that it is this slower phase that we are currently observing in Ups Sgr. In all cases the final remnant is about $1M_{\odot}$, with hydrogen reduced at the surface to the small

amounts that we observe in Ups Sgr and the other EHdBs.

The secondary cannot be the more evolved object because of its large mass. How likely is it that the secondary is still on the main sequence after the primary has completed helium-core burning? If the secondary accreted a negligible amount of mass during the first mass-transfer/loss episode then for any primordial primary mass it is possible to estimate the mass of the secondary that just allows the primary to complete core-helium burning and undergo a second mass-loss episode whilst the secondary is still on the main sequence. The approximate lifetimes of the hydrogen and helium core-burning phases are given respectively by (Iben & Tutukov 1987) :

$$t_{MS} = 10^{9.38} M_{MS}^{-2.16} \text{ yr} \quad \& \quad t_{He} = 10^{10.7} M_{MS}^{-4.34} \text{ yr}$$

For primary main-sequence masses of $10M_{\odot}$ and $5M_{\odot}$, the corresponding maximum secondary masses are $9.4M_{\odot}$ and $4.0M_{\odot}$ respectively. Therefore, unless the primordial masses were comparable, or the secondary accreted sufficient mass during the first mass-transfer/loss phase, it is reasonable to expect that the secondary is still on the main sequence. Adopting $M_2=11M_{\odot}$, the primordial primary mass is constrained to a mass in excess of $6.6M_{\odot}$ in order to meet the condition, primary$[t_{MS}+t_{He}]$ < secondary$[t_{MS}]$. In contrast to the single RCBs and EHe stars, the EHdBs must be young objects aged between 20 and 120 million years. This is supported by the observation that the EHdBs lie close to the galactic plane and have nearly circular orbits about the galactic centre, whereas the RCBs and the EHe stars appear to be members of the galactic bulge population (Drilling 1986).

As the secondary appears to have become considerably more massive than the primary, and as the present rate of mass-transfer appears to be small, the present phase of Roche-lobe overflow is likely to be conservative of the total mass of the system. Models of accretion onto main-sequence stars show that for small accretion rates the radius stays close to its main-sequence value (Kippenhahn & Meyer-Hofmeister 1977). Evolutionary effects may be detectable from an increasing binary period which is a response to the changing mass-ratio. Wilson (1914) determined a spectroscopic binary period of 137.939 days for Ups Sgr. Seydel (1929) later determined a period of 137.957 days. The discrepancy between the two estimates is accountable within random measurement errors so that the binary period did not change significantly during 10 years. However, as the latter observations were made over 60 years ago, a redetermination of the period with contemporary observations could reveal a slowly increasing binary period. On the assumption that the total mass and angular momentum of the system are conserved, we can formally estimate period changes using the relation $P \propto M_1^{-3} M_2^{-3}$ from Kepler's law. Mass-transfer rates of 10^{-5} and $10^{-4} M_\odot yr^{-1}$ will have produced period increases during 60 years of 0.2 and 2 days respectively.

What of the future evolution of Ups Sgr? As central temperatures are too low to ignite carbon in the primary it will shrink to evolve as a cooling degenerate CO dwarf. With a mass of $\sim 11 M_\odot$, the secondary lies close the $10.6 M_\odot$ limit calculated by IT85 above which a binary component is unable to avoid a supernova

event. If the mass of the secondary lies below this limit, then the direction of evolution taken by the secondary is likely to be similar to that of the primary. Following two episodes of Roche-lobe overflow a $\sim 1M_{\odot}$ degenerate CO or ONe white dwarf secondary will result. Which variety is ultimately produced is sensitively dependent upon the primordial binary characteristics (IT85). If the secondary's mass lies closer to $11M_{\odot}$, then the secondary will be ultimately unable to avoid a Type I supernova explosion with a neutron star remnant and the possible disruption of the system.

On evolving off the main sequence, the secondary will fill its Roche lobe and attempt to transfer mass back towards the primary. The CO dwarf primary will almost certainly be unable to accept this mass, with the result that most of the mass will be lost from the system either in a common-envelope phase or in nova-type ejections. Orbital shrinkage may be severe during this phase. Tutukov & Yungelson (1979) have attempted to estimate orbital shrinkage during a common-envelope phase by way of the expression :

$$A_f = A_i \alpha M_r M_1 / M_2^2$$

where A_i and A_f are the initial and final semi-major axes of the system, and M_2 and M_r are the initial and remnant masses of the secondary respectively. M_1 is the mass of the primary, and α is a parameter close to unity which measures the efficiency with which mass is driven from the system. The mass of the remnant is, to a good approximation, a function of the mass-losing star alone and is given by $0.08M_2 \approx 2M_{\odot}$. This leads to an estimate for the decrease in the semi-major axis from $\sim 250R_{\odot}$ to $\sim 5R_{\odot}$ during the

common-envelope phase, and a corresponding reduction in the binary period to ~1 day. A second common-envelope phase after exhaustion of central helium in the secondary could draw the components closer and reduce the binary period to only a few hours. The penultimate system would be comprised of a pair of degenerate dwarfs, CO/CO or CO/ONe, each of about $1M_{\odot}$. The components might then be close enough that gravitational wave radiation could drive the components together to allow merging in a Hubble time. The total mass of the components ($\sim 2M_{\odot}$) would be above the Chandrasekhar limit ($1.4M_{\odot}$) so that merging must lead to a Type I supernova event, unless some mechanism exists whereby the components are able to throw off sufficient mass during the merging process to reduce the mass of the final product to below $1.4M_{\odot}$. It is noted that the evolutionary scheme proposed by Webbink (1984), whereby the RCBs and the EHe stars may be the resultant merging of degenerate He and CO dwarfs in close binary systems with total masses in the range $\sim 0.75\text{-}1.45M_{\odot}$, is not plausible for Ups Sgr due to the massive secondary.

4. Light and Colour Variations in the Extremely Hydrogen-Deficient Binary CPD-58°2721

4.1 Introduction

Drilling et al.(1985) showed that CPD-58°2721 (=LSS 1922, Drilling 1980) should be included as the third member of the EHdBs. There is no evidence for a companion in the visible spectrum, unlike Ups Sgr and KS Persei for which hot companions have been discovered from ultra-violet observations (Duvignau et al. 1979, Hack et al. 1980, Drilling & Schönberner 1982). A provisional orbital period of 43.25 days has been determined by Jeffery et al.(1987b). Using IUE and ground-based observations, Schönberner et al.(1982) and Drilling et al.(1984a) derived an effective temperature of 11,100K for CPD-58°2721. However, from visual spectra, a higher T_{eff} of 14,000K for CPD-58°2721 has been derived (Sect. 5.3) similar to that for LSS 4300.

Photometric variations have previously been reported in Ups Sgr (Eggen et al. 1950), KS Persei (Osawa et al. 1963) and LSS 4300 (Landolt 1986b). Eggen et al. (1950) ascribed these to eclipses in Ups Sgr, although new observations of its light variations presented in Chap. 3 clearly show the presence of non-eclipse related variations which are attributed to pulsation. In this chapter the photometric variations of CPD-58°2721 are examined, for which the 1985 observations presented here span almost one orbital period. Possible interpretations of the light-curve are discussed.

4.2 Observations

4.2a PHOTOMETRY

CPD-58°2721 was observed with the 0.5-m and 1.0-m telescopes at SAAO during 1985 and 1986. Strömgren observations were made with the 0.5-m telescope on 31 nights during a 40-day period in 1985 April-June by the writer and Drs P.W.Hill and C.S.Jeffery, and on 9 nights during a 10-day period in 1986 April-May with the 1.0-m telescope by Dr P.W.Hill. UBVRI observations made over the period 1985 December to 1986 July with both telescopes were kindly supplied by Dr D.Kilkenny, Mr F.Marang and Mr J.Spencer Jones. Details of observational methods and reduction techniques to the standard UBVRI and uvby systems are described respectively by Menzies et al. (1980) and in Sect. 1.4a. For the uvby observations integration times were chosen for each filter so that counts for the target, comparison and check stars were approximately 30, 50 and 100 thousand respectively. Although the original check star (m_v=11.6, RA(1950)=$10^h45^m55^s$ Dec=-58°51'10") used on the first three nights of the 1985 observations did not appear to vary, a brighter check star HD93712 was used for the remaining observations. The programme stars are identified below :

Table 4.1 Differential uvby photometry of CPD-58°2721 (1985/86).

HJD	Comparison				Variable - Comparison				Check - Comparison			
-2446000	V	(b-y)	(v-b)	(u-b)	V	(b-y)	(v-b)	(u-b)	V	(b-y)	(v-b)	(u-b)
181.267	9.989	0.338	0.309	0.592	0.515	0.253	0.207	0.587				
181.322	9.991	0.344	0.315	0.593	0.513	0.248	0.183	0.590				
181.370	9.988	0.341	0.311	0.591	0.507	0.255	0.193	0.592				
181.430	9.978	0.347	0.309	0.580	0.526	0.236	0.209	0.605				
182.384	9.982	0.336	0.308	0.585	0.489	0.250	0.194	0.587				
182.417	9.987	0.338	0.313	0.583	0.484	0.253	0.200	0.597				
184.253	9.979	0.340	0.307	0.588	0.469	0.251	0.196	0.581				
184.282	9.987	0.337	0.312	0.590	0.467	0.258	0.184	0.582				
184.332	9.990	0.343	0.313	0.593	0.454	0.260	0.190	0.583				
184.361	9.987	0.348	0.310	0.584	0.469	0.236	0.209	0.576				
185.283	9.993	0.338	0.316	0.599	0.472	0.244	0.216	0.588	-1.028	-0.330	-0.149	0.727
185.339	9.992	0.346	0.311	0.599	0.478	0.246	0.211	0.594	-1.032	-0.331	-0.146	0.728
185.396	10.005	0.326	0.313	0.592	0.484	0.251	0.210	0.600	-1.035	-0.314	-0.149	0.721
186.252	9.981	0.349	0.315	0.611	0.507	0.250	0.181	0.589	-1.021	-0.337	-0.157	0.706
186.309	9.985	0.330	0.312	0.598	0.504	0.263	0.197	0.594	-1.026	-0.317	-0.146	0.714
186.366	9.983	0.341	0.314	0.592	0.509	0.255	0.210	0.610	-1.021	-0.330	-0.157	0.720
187.297	9.984	0.345	0.308	0.585	0.524	0.257	0.197	0.591	-1.027	-0.330	-0.147	0.728
187.341	9.991	0.333	0.307	0.596	0.505	0.253	0.211	0.603	-1.027	-0.325	-0.149	0.718
187.384	9.991	0.338	0.310	0.597	0.514	0.239	0.205	0.596	-1.028	-0.330	-0.148	0.712
188.247	9.964	0.330	0.309	0.591	0.527	0.260	0.192	0.591	-1.027	-0.324	-0.149	0.711
188.277	9.973	0.331	0.312	0.590	0.527	0.250	0.196	0.582	-1.030	-0.324	-0.157	0.714
188.321	9.982	0.335	0.309	0.588	0.528	0.242	0.212	0.594	-1.027	-0.329	-0.151	0.715
188.369	9.977	0.342	0.317	0.586	0.526	0.255	0.186	0.574	-1.016	-0.333	-0.162	0.715
193.285	9.986	0.351	0.310	0.582	0.498	0.248	0.206	0.628	-1.029	-0.339	-0.150	0.723
193.330	9.985	0.342	0.309	0.586	0.491	0.248	0.188	0.601	-1.028	-0.332	-0.148	0.719
193.355	9.986	0.337	0.311	0.598	0.493	0.246	0.208	0.622	-1.032	-0.325	-0.154	0.710
194.241	9.985	0.336	0.310	0.597	0.507	0.257	0.224	0.658	-1.024	-0.324	-0.153	0.720
194.268	9.985	0.336	0.311	0.597	0.510	0.246	0.230	0.654	-1.028	-0.326	-0.144	0.727
194.294	9.990	0.339	0.314	0.595	0.511	0.247	0.205	0.643	-1.031	-0.322	-0.159	0.717
194.322	9.997	0.339	0.313	0.592	0.501	0.262	0.206	0.635	-1.037	-0.332	-0.153	0.733
194.351	9.998	0.344	0.314	0.595	0.494	0.251	0.206	0.650	-1.035	-0.339	-0.152	0.724
195.370	9.990	0.336	0.315	0.597	0.525	0.251	0.208	0.657	-1.026	-0.328	-0.162	0.716
195.409	9.984	0.334	0.316	0.601	0.516	0.262	0.199	0.650	-1.028	-0.320	-0.159	0.712
197.248	9.981	0.334	0.321	0.601	0.522	0.256	0.199	0.626	-1.020	-0.326	-0.155	0.715
197.273	9.985	0.335	0.312	0.593	0.525	0.253	0.204	0.638	-1.020	-0.329	-0.152	0.728
197.290	9.991	0.336	0.310	0.593	0.518	0.260	0.218	0.631	-1.021	-0.320	-0.153	0.713
197.327	9.997	0.340	0.313	0.598	0.518	0.255	0.200	0.626	-1.023	-0.325	-0.151	0.701
197.351	10.001	0.342	0.310	0.600	0.508	0.256	0.203	0.610	-1.040	-0.327	-0.154	0.709
197.376	10.003	0.335	0.312	0.597	0.500	0.261	0.206	0.624	-1.042	-0.324	-0.146	0.721
198.243	9.994	0.332	0.312	0.597	0.502	0.259	0.205	0.588	-1.036	-0.320	-0.152	0.711
198.269	9.994	0.335	0.314	0.600	0.498	0.248	0.217	0.624	-1.043	-0.323	-0.151	0.724
198.294	9.997	0.335	0.312	0.603	0.492	0.258	0.200	0.605	-1.033	-0.326	-0.153	0.706
198.320	9.993	0.346	0.314	0.597	0.502	0.243	0.200	0.599	-1.030	-0.337	-0.151	0.713
198.349	9.994	0.339	0.315	0.589	0.498	0.254	0.197	0.602	-1.032	-0.326	-0.157	0.718
199.234	9.992	0.341	0.313	0.604	0.482	0.255	0.200	0.586	-1.037	-0.329	-0.153	0.712
199.259	9.992	0.337	0.315	0.607	0.481	0.253	0.217	0.594	-1.037	-0.326	-0.154	0.710
199.283	9.988	0.336	0.311	0.601	0.488	0.258	0.205	0.594	-1.027	-0.331	-0.148	0.717
199.317	9.982	0.336	0.314	0.602	0.498	0.250	0.198	0.585	-1.022	-0.329	-0.152	0.716
199.351	9.980	0.336	0.312	0.598	0.501	0.252	0.200	0.597	-1.023	-0.323	-0.155	0.717
199.373	9.984	0.333	0.310	0.592	0.494	0.265	0.197	0.592	-1.023	-0.327	-0.147	0.720
199.399	9.986	0.341	0.301	0.588	0.493	0.250	0.209	0.596	-1.030	-0.328	-0.141	0.725
199.432	9.996	0.332	0.311	0.596	0.482	0.256	0.201	0.584	-1.032	-0.331	-0.146	0.716
200.235	9.985	0.337	0.316	0.607	0.469	0.256	0.194	0.563	-1.020	-0.332	-0.154	0.711
200.259	9.983	0.334	0.317	0.602	0.476	0.260	0.190	0.578	-1.019	-0.328	-0.156	0.714
200.283	9.986	0.336	0.307	0.593	0.475	0.253	0.207	0.582	-1.022	-0.324	-0.150	0.719
200.312	9.990	0.333	0.310	0.593	0.466	0.259	0.200	0.596	-1.030	-0.321	-0.151	0.720
200.332	9.988	0.336	0.309	0.596	0.470	0.254	0.200	0.588	-1.023	-0.329	-0.148	0.721
200.356	9.992	0.338	0.312	0.595	0.458	0.267	0.189	0.581	-1.028	-0.331	-0.143	0.716
201.233	9.986	0.337	0.310	0.597	0.462	0.252	0.202	0.583	-1.023	-0.334	-0.140	0.724
201.260	9.983	0.337	0.312	0.596	0.461	0.254	0.198	0.574	-1.018	-0.332	-0.151	0.721
201.284	9.988	0.338	0.310	0.590	0.457	0.255	0.184	0.575	-1.027	-0.333	-0.152	0.721
201.304	9.988	0.341	0.308	0.590	0.455	0.249	0.196	0.570	-1.030	-0.337	-0.149	0.727
201.332	9.991	0.336	0.309	0.591	0.452	0.243	0.212	0.584	-1.033	-0.329	-0.155	0.719
201.352	9.989	0.336	0.307	0.587	0.449	0.255	0.196	0.577	-1.034	-0.330	-0.150	0.725

202.238	9.991	0.338	0.309	0.595	0.451	0.244	0.199	0.594	-1.035	-0.326	-0.148	0.716
202.262	9.995	0.334	0.313	0.593	0.454	0.255	0.196	0.580	-1.040	-0.324	-0.154	0.717
202.286	9.993	0.336	0.306	0.589	0.457	0.250	0.202	0.595	-1.038	-0.328	-0.144	0.725
202.311	9.986	0.337	0.309	0.596	0.462	0.252	0.209	0.587	-1.025	-0.328	-0.149	0.716
202.335	9.983	0.339	0.308	0.594	0.467	0.253	0.197	0.594	-1.028	-0.321	-0.151	0.718
202.359	9.983	0.336	0.313	0.594	0.470	0.255	0.194	0.592	-1.025	-0.322	-0.159	0.723
203.237	9.999	0.341	0.315	0.595	0.471	0.259	0.192	0.599	-1.035	-0.333	-0.150	0.729
203.261	9.989	0.341	0.312	0.597	0.480	0.249	0.200	0.599	-1.025	-0.331	-0.151	0.719
203.285	9.990	0.335	0.306	0.600	0.477	0.260	0.201	0.587	-1.028	-0.322	-0.148	0.713
203.319	9.988	0.339	0.310	0.598	0.478	0.257	0.202	0.640	-1.024	-0.328	-0.149	0.723
203.348	9.988	0.338	0.315	0.594	0.480	0.247	0.196	0.592	-1.026	-0.324	-0.167	0.708
203.376	9.996	0.331	0.310	0.596	0.470	0.256	0.201	0.598	-1.035	-0.323	-0.151	0.710
204.240	9.976	0.332	0.310	0.593	0.513	0.259	0.206	0.621	-1.019	-0.325	-0.156	0.712
205.236	9.987	0.342	0.310	0.594	0.521	0.248	0.214	0.645	-1.030	-0.335	-0.151	0.723
205.265	9.993	0.333	0.317	0.601	0.526	0.242	0.209	0.653	-1.036	-0.323	-0.162	0.713
205.288	9.995	0.332	0.311	0.600	0.530	0.242	0.222	0.637	-1.038	-0.320	-0.158	0.705
205.325	9.989	0.336	0.308	0.590	0.529	0.247	0.219	0.651	-1.034	-0.330	-0.147	0.716
206.233	9.999	0.332	0.309	0.598	0.534	0.254	0.218	0.661	-1.033	-0.330	-0.145	0.722
206.258	10.003	0.331	0.312	0.602	0.538	0.263	0.219	0.654	-1.035	-0.315	-0.151	0.722
209.262	10.022	0.343	0.311	0.594	0.515	0.244	0.206	0.609	-1.029	-0.330	-0.153	0.713
209.289	10.021	0.343	0.311	0.596	0.530	0.240	0.210	0.615	-1.030	-0.327	-0.155	0.715
209.316	10.021	0.344	0.317	0.601	0.533	0.253	0.192	0.594	-1.021	-0.337	-0.159	0.706
209.342	10.018	0.340	0.327	0.615	0.524	0.259	0.188	0.592	-1.035	-0.327	-0.169	0.698
210.253	9.987	0.334	0.323	0.600	0.514	0.245	0.198	0.622	-1.031	-0.319	-0.159	0.721
210.278	9.988	0.335	0.310	0.593	0.505	0.256	0.210	0.612	-1.027	-0.327	-0.151	0.723
210.348	9.988	0.339	0.316	0.598	0.488	0.262	0.199	0.610	-1.025	-0.328	-0.151	0.721
211.239	9.977	0.334	0.311	0.590	0.503	0.249	0.207	0.610	-1.021	-0.325	-0.155	0.718
211.264	9.982	0.332	0.311	0.593	0.497	0.256	0.205	0.609	-1.028	-0.321	-0.151	0.717
211.290	9.991	0.331	0.315	0.592	0.490	0.253	0.209	0.619	-1.040	-0.322	-0.149	0.723
211.315	9.992	0.336	0.320	0.592	0.488	0.251	0.199	0.613	-1.038	-0.328	-0.162	0.718
212.227	9.986	0.326	0.309	0.585	0.471	0.255	0.198	0.637	-1.041	-0.317	-0.155	0.717
212.251	9.995	0.333	0.309	0.594	0.472	0.256	0.188	0.617	-1.047	-0.317	-0.157	0.718
212.276	9.999	0.342	0.312	0.598	0.489	0.250	0.197	0.606	-1.037	-0.323	-0.154	0.715
214.351	10.001	0.333	0.317	0.598	0.480	0.259	0.206	0.622	-1.042	-0.323	-0.158	0.714
214.377	9.994	0.341	0.311	0.593	0.486	0.263	0.201	0.608	-1.036	-0.325	-0.154	0.727
215.236	9.991	0.335	0.321	0.601	0.509	0.256	0.202	0.622	-1.026	-0.324	-0.162	0.714
215.262	9.997	0.332	0.316	0.604	0.499	0.258	0.209	0.623	-1.040	-0.324	-0.154	0.711
215.289	10.001	0.335	0.311	0.601	0.500	0.254	0.220	0.631	-1.043	-0.324	-0.151	0.721
216.222	9.988	0.349	0.325	0.596	0.515	0.231	0.213	0.628	-1.030	-0.340	-0.163	0.716
217.233	9.979	0.344	0.316	0.601	0.517	0.239	0.216	0.605	-1.023	-0.329	-0.155	0.710
217.262	9.978	0.343	0.312	0.593	0.528	0.243	0.190	0.575	-1.017	-0.331	-0.152	0.717
217.289	9.981	0.339	0.318	0.597	0.529	0.235	0.216	0.620	-1.022	-0.332	-0.156	0.719
218.229	9.982	0.338	0.321	0.611	0.494	0.259	0.201	0.597	-1.027	-0.325	-0.155	0.714
218.256	9.998	0.342	0.303	0.596	0.486	0.259	0.199	0.591	-1.036	-0.327	-0.144	0.711
218.284	9.995	0.343	0.308	0.591	0.491	0.243	0.203	0.582	-1.038	-0.330	-0.145	0.719
219.247	9.991	0.349	0.316	0.605	0.517	0.234	0.221	0.574	-1.025	-0.336	-0.157	0.708
219.283	9.996	0.343	0.305	0.593	0.503	0.247	0.203	0.616	-1.032	-0.333	-0.141	0.726
219.313	9.991	0.342	0.306	0.594	0.503	0.268	0.211	0.598	-1.029	-0.330	-0.141	0.714
220.232	9.986	0.348	0.316	0.610	0.542	0.250	0.183	0.606	-1.021	-0.331	-0.160	0.709
220.263	9.992	0.340	0.312	0.604	0.541	0.248	0.199	0.616	-1.017	-0.330	-0.161	0.705
547.374	10.001	0.344	0.317	0.605	0.536	0.247	0.230	0.608	-1.026	-0.325	-0.151	0.709
548.310	9.979	0.344	0.312	0.599	0.564	0.245	0.238	0.607	-1.025	-0.326	-0.155	0.699
548.471	10.005	0.347	0.308	0.595	0.568	0.234	0.235	0.606	-1.033	-0.335	-0.149	0.697
551.362	9.983	0.340	0.309	0.601	0.480	0.254	0.230	0.582	-1.018	-0.326	-0.148	0.708
552.291	9.962	0.351	0.314	0.600	0.449	0.246	0.225	0.584	-1.017	-0.331	-0.148	0.706
553.246	9.968	0.346	0.309	0.595	0.434	0.249	0.234	0.589	-1.020	-0.332	-0.142	0.712
554.251	9.984	0.344	0.313	0.598	0.443	0.246	0.240	0.606	-1.025	-0.334	-0.149	0.707
555.246	9.983	0.344	0.312	0.593	0.446	0.251	0.237	0.612	-1.029	-0.328	-0.144	0.709
556.272	9.970	0.342	0.317	0.599	0.500	0.256	0.223	0.605	-1.022	-0.326	-0.155	0.708

Table 4.2 UBVRI photometry of CPD-58°2721 (1985/86).

	CPD-58°2721					LSS1915			
HJD -2446000	V	(B-V)	(U-B)	(V-R)	(V-I)	V	(B-V)	(U-B)	(V-R)
410.557	10.428	0.752	-0.170	0.557	1.173	9.979	0.386	-0.546	0.272
411.554	10.423	0.761	-0.165	0.559	1.178	9.975	0.387	-0.535	0.278
425.575	10.514	0.754	-0.167	0.558	1.167	9.973	0.378	-0.546	0.271
426.547	10.496	0.742	-0.168	0.553	1.157	9.958	0.391	-0.542	0.268
428.593	10.463	0.787	-0.164	0.554	1.164	9.967	0.389	-0.547	0.287
454.581	10.502	0.757			1.133	9.980	0.392		
455.533	10.489	0.744			1.145	9.961	0.385		
458.577	10.488	0.762			1.134	9.973	0.386		
459.577	10.461	0.756	-0.204			9.962	0.379	-0.556	
465.537	10.510	0.744	-0.200	0.560	1.134	9.977	0.384	-0.558	0.278
466.499	10.510	0.755			1.162	9.990	0.393		
467.499	10.530	0.762			1.141	10.007	0.393		
468.508	10.504	0.770			1.158	9.986	0.387		
469.504	10.549	0.761			1.170	9.995	0.383		
470.464	10.584	0.777			1.175	9.976	0.390		
471.453	10.603	0.772			1.181	9.981	0.383		
472.446	10.600	0.750			1.182	9.995	0.378		
476.502	10.494				1.150	9.956			
477.529	10.525	0.745			1.153	9.988	0.387		
478.477	10.503	0.747			1.154	9.959	0.380		
479.424	10.500	0.755			1.151	9.975	0.377		
487.530	10.478	0.789			1.107	9.960	0.402		
488.464	10.472	0.744			1.133	9.984	0.375		
489.458	10.464	0.746			1.127	9.971	0.379		
490.442	10.473	0.734			1.139	9.981	0.375		
493.434	10.549	0.760			1.138	9.973	0.369		
536.359	10.525	0.744	-0.195			9.984*	0.387	-0.554	
531.401	10.534					9.990*			
533.383	10.506					9.990*			
534.366	10.518					9.990*			
540.351	10.518					9.990			
595.257	10.598	0.763	-0.135	0.583	1.203	9.981	0.377	-0.549	0.274
596.254	10.576	0.753	-0.147	0.568	1.190	9.977	0.371	-0.554	0.275
597.254	10.549	0.748	-0.172	0.579	1.190	9.982	0.373	-0.547	0.282
601.254	10.473	0.743	-0.180	0.568	1.168	9.996	0.372	-0.540	0.278
603.235	10.502	0.742	-0.202	0.563	1.178	9.986	0.380	-0.564	0.272
604.251	10.525	0.755	-0.177	0.576	1.194	9.981	0.386	-0.552	0.277
625.233	10.511	0.750	-0.185	0.554	1.156	9.986	0.377	-0.537	0.273
627.218	10.458	0.748	-0.189	0.555	1.171	9.982	0.364	-0.537	0.281
630.235	10.484	0.745	-0.171	0.560	1.179	9.968	0.386	-0.544	0.273
631.232	10.520	0.762	-0.190	0.562	1.176	9.985	0.382	-0.549	0.271
633.239	10.543	0.786	-0.169	0.560	1.181	9.987	0.386	-0.535	0.276
634.215	10.538	0.766	-0.170	0.570	1.190	10.014	0.386	-0.532	0.286
638.209	10.493	0.740	-0.182	0.558	1.180	10.005	0.367	-0.534	0.263

		RA (1950)	Dec	Sp
CPD-58°2721	(Vr)	$10^h45^m58^s$	-58°52'45"	B+
LSS 1915	(C)	$10^h45^m27^s$	-58°56'51"	F2
HD93712	(K)	$10^h45^m56^s$	-58°26'04"	A0V

Accurate conventional photometry of CPD-58°2721 is complicated as it is surrounded by nebulosity and lies in a crowded star field in the region of the Eta Carina nebula. Observations in 'dark-moon' time indicated significant differences of the local 'sky' backgrounds for Vr and C due to the nebulosity, which could have given rise to errors of 0.01 mag if an incorrect 'sky' were used. Thus each star had its own associated 'sky' measurement, always taken from the same position.

4.2b CPD-58°2721B AND CPD-58°2721C.

A star lies south of CPD-58°2721 ($\Delta\alpha$=0.6" west $\Delta\delta$=11" south, Landolt 1986a), whilst another star 2" west can only be seen on SERC 1.2-m Schmidt SR and I photographic plates and so is probably cool. These stars shall be referred to as CPD-58°2721B and CPD-58°2721C respectively. Because of the problems associated with using a small diaphragm to try and exclude the 2 nearby stars, a large diaphragm (30") was chosen so as to always include them. However, Strömgren observations of CPD-58°2721B were made with a 9" diaphragm on 2 nights 5 days apart with the 1.0-m telescope in 1986 by Dr P.W.Hill. This was only possible with good seeing and in 'dark-moon' time. A 4th magnitude standard star was observed with

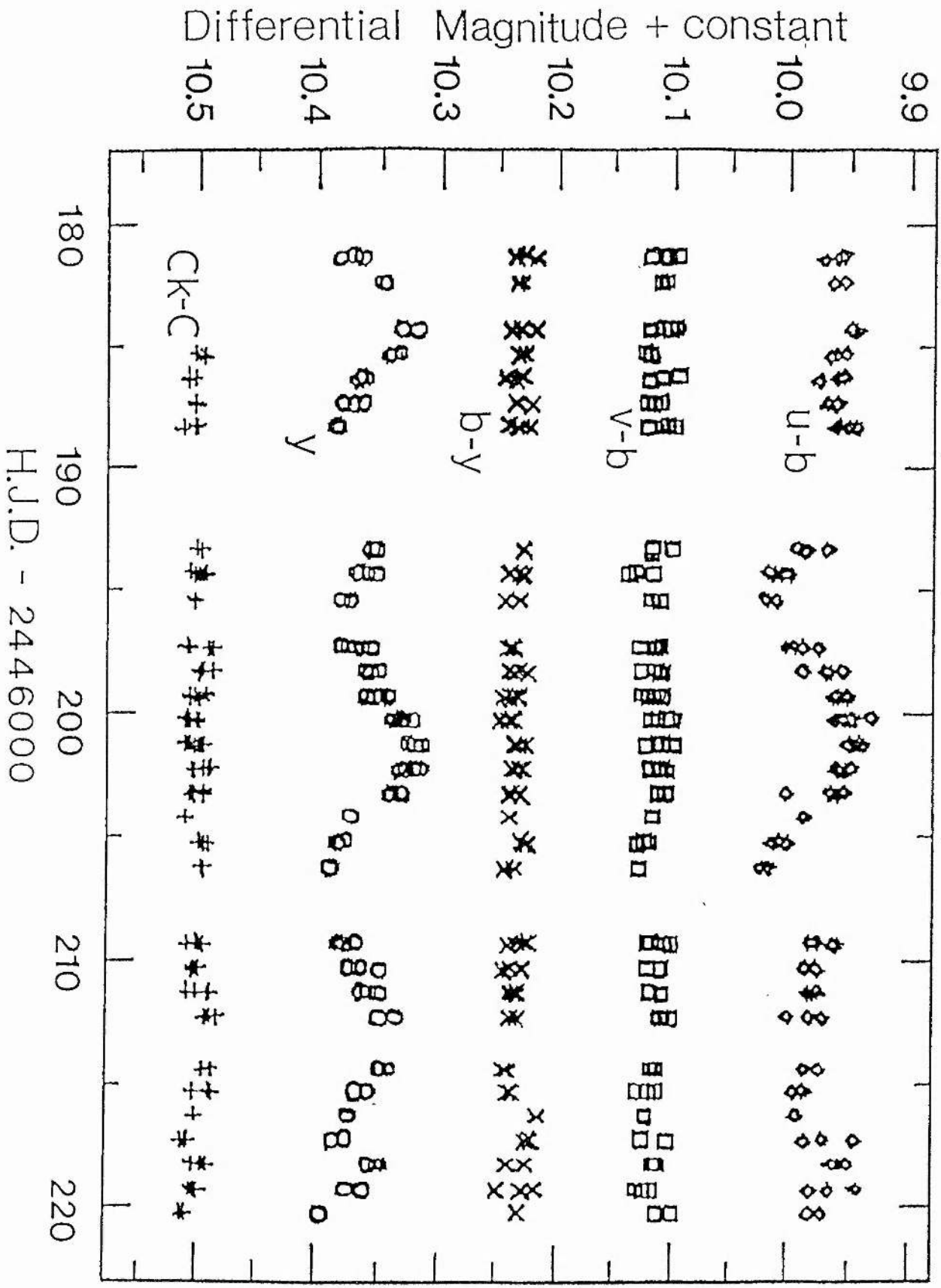

Figure 4.1 The 1985 uvby photometry. The plus signs show the Check-Comparison V observations.

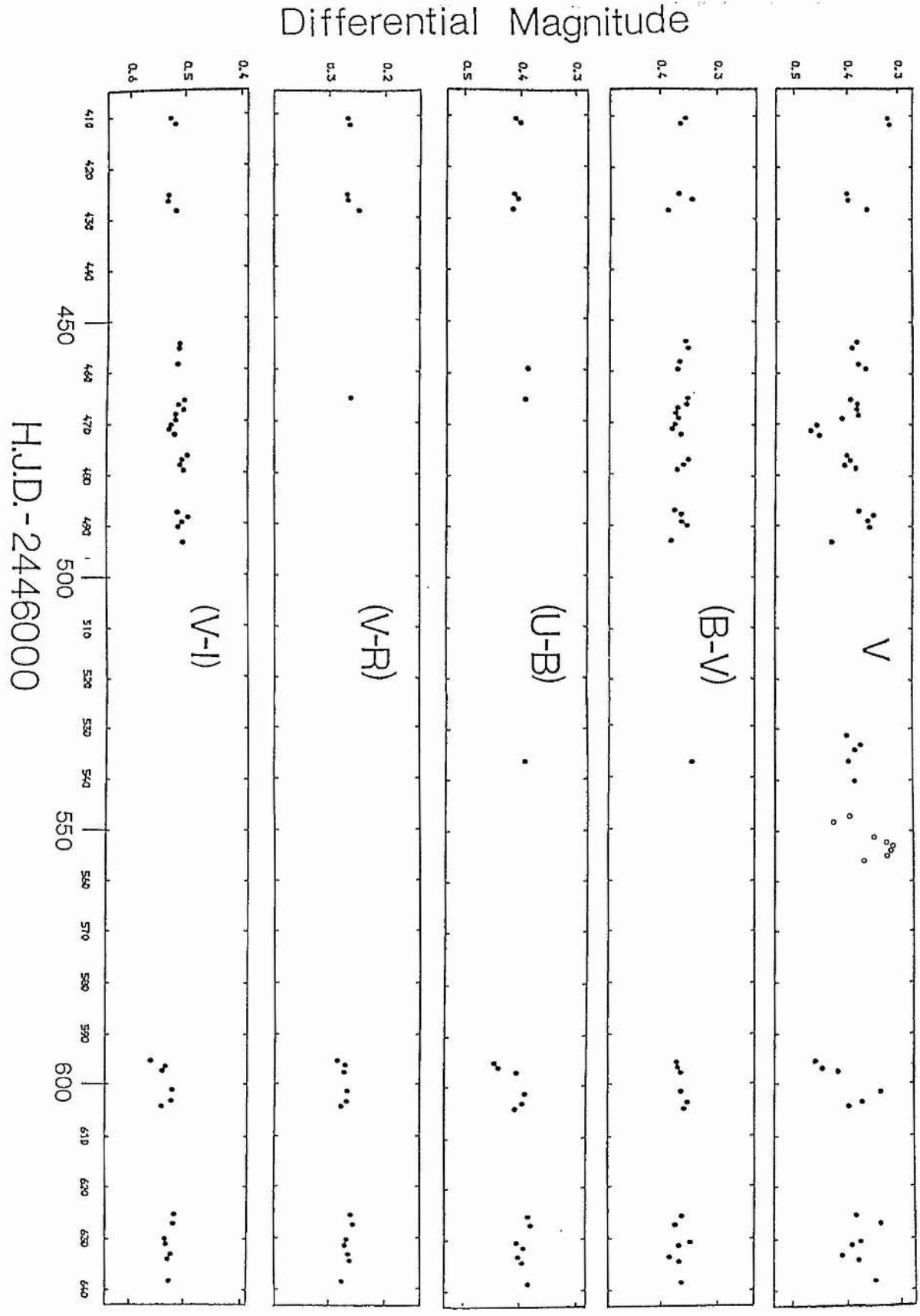

Figure 4.2 The 1985/86 UBVRI observations. The open circles represent V magnitudes from the 1986 Stromgren 'y' observations.

the 30" and 9" diaphragms before and after CPD-58°2721B to allow an estimate of the light loss from using the smaller aperture. These corrections amounted to several hundredths of a magnitude. The observations of CPD-58°2721B gave:

HJD-2446000	V	(b-y)	(v-b)	(u-b)
552.340	12.640	0.461	0.601	1.601
556.314	12.640	0.452	0.605	1.595

This is in good agreement with Landolt (1986a) who measured the magnitude and colour indices of CPD-58°2721B using broad-band photometry and found V=12.648.

Spectroscopic 2-D images of CPD-58°2721 and CPD-58°2721B obtained in 1984 at the AAT indicate that CPD-58°2721B is probably of spectral type F or later from the strength of its H and K lines (Sect. 5.1a). The Strömgren colours correspond to a somewhat metal-weak early-type G star. With mean magnitudes (from the 1986 Strömgren observations) of m_v=10.334 and m_v=12.640 for CPD-58°2721 and CPD-58°2721B respectively, CPD-58°2721B contributes on average, about 15 percent of the photons in V and so CPD-58°2721 appears $\sim$ 0.13 mag brighter.

Figure 4.3 The 1986 uvby observations.

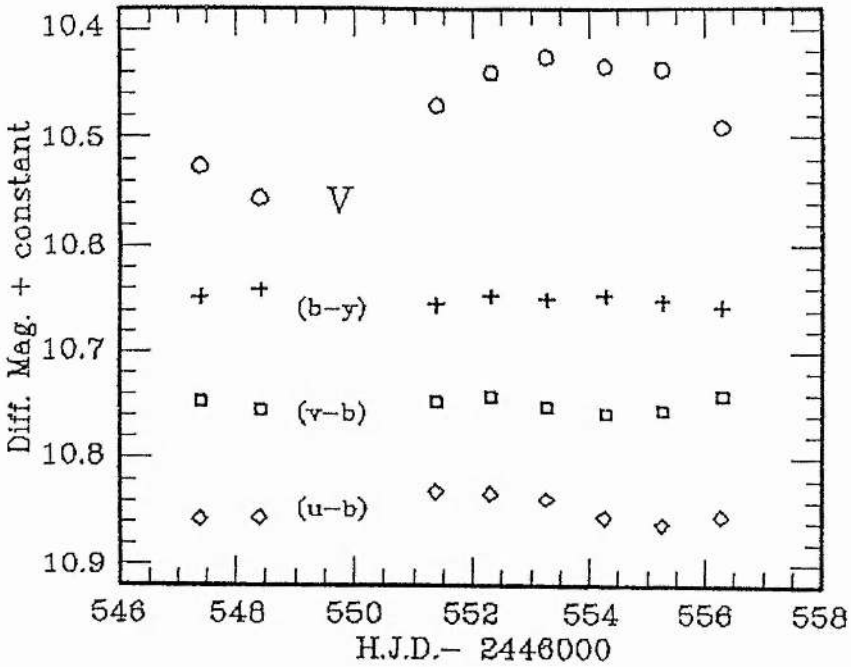

Figure 4.4 a) The Classical Power Spectrum of the differential 1985 V observations. Frequency is in cycles day^{-1}. b) Pre-whitened by 0.108 cycles day^{-1} (full line). Pre-whitened by 0.108 and 0.071 cycles day-1 (dotted line).

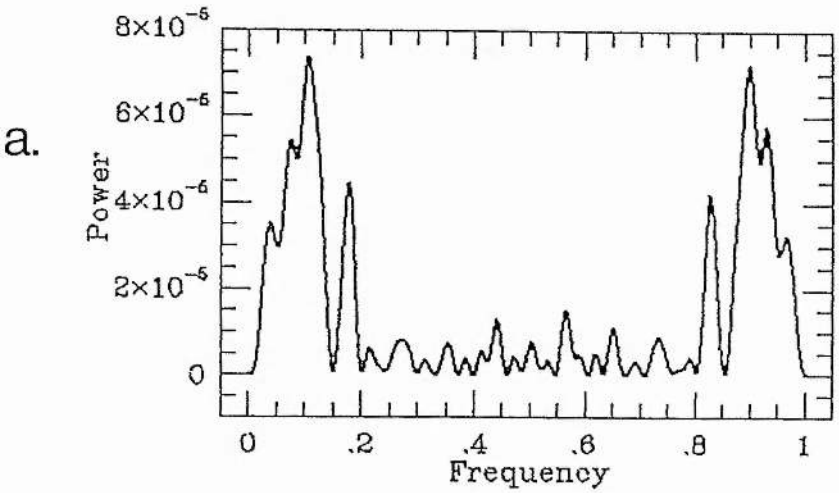

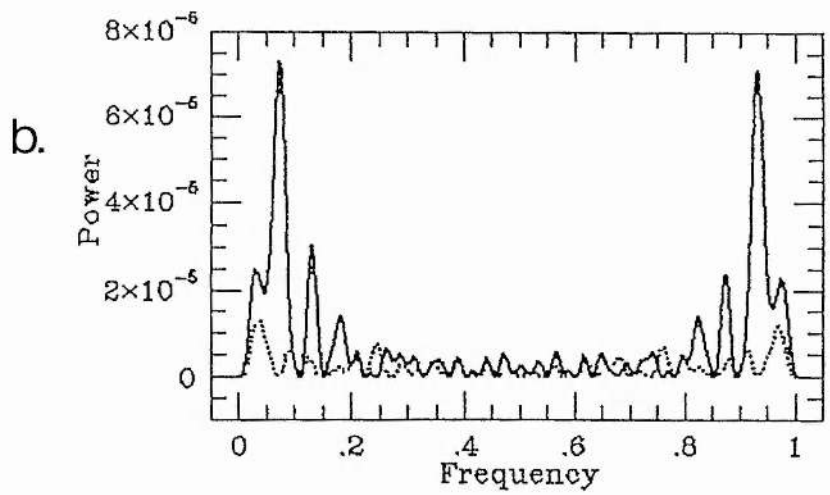

Table 4.3 Mean uvby photometry of the programme stars.

	<V>	<b-y>	<v-b>	<u-b>	<c_1>	<m_1>	n
CPD-58°2721 (Vr)	10.484	0.590	0.517	1.200	0.166	-0.073	110
	(023)	(007)	(010)	(024)	(026)	(016)	
LSS 1915 (C)	9.989	0.338	0.312	0.595	-0.029	-0.026	110
	(007)	(005)	(004)	(006)	(007)	(006)	
HD93712 (K)	8.961	0.010	0.160	1.192	0.872	0.150	104
	(008)	(004)	(004)	(006)	(009)	(006)	
CPD-58°2721B	12.640	0.457	0.603	1.598	0.392	0.147	2
	(006)	(003)	(004)	(010)	(009)		

Table 4.4 Mean UBVRI photometry of the programme stars.

	<V>	<B-V>	<U-B>	<V-R>	<V-I>
CPD-58°2721 (Vr)	10.511	0.756	-0.176	0.563	1.162
	(042)	(013)	(017)	(009)	(022)
n =	44	38	21	19	39
LSS 1915 (C)	9.981	0.382	-0.546	0.276	0.599
	(013)	(008)	(009)	(006)	(012)
n =	39	38	19	18	38
CPD-58°2721B*	12.648	0.661	0.092	0.400	0.769
	(006)	(004)	(000)	(022)	(018)

* Landolt 1986b (n=3)

Table 4.5 Fourier decomposition of the 1985 uvby light curve.

Mag. Colour	Variation (mag)	Freq.(cycles day^{-1}) f_1	f_2
u	0.15	0.109	0.071
v	0.11	0.108	0.071
b	0.09	0.108	0.072
V	0.08	0.107	0.071
(u-b)	0.07	0.106	0.066

4.2c MEAN PROPERTIES

The Strömgren observations given in Table 4.1 have been corrected for the effect of CPD-58°2721B by application of the formula;

$$m_A = -2.5\log(10^{-0.4m_{A+B}} - 10^{-0.4m_B})$$

where m_{A+B} and m_A are the observed and corrected magnitudes of CPD-58°2721 respectively and m_B is the mean magnitude of CPD-58°2721B determined in Sect. 4.2b. The UBVRI data in Table 4.2 has similarly been corrected for the effect of CPD-58°2721B using Landolt's (1986a) measurements. The data JD 2446531-40 were observed through a neutral density filter and have been corrected to V(C) = 9.990. Mean magnitudes and colours for CPD-58°2721, comparison, check and CPD-58°2721B are shown in Tables 4.3 & 4.4. The observations on JD 2446209 have not been included as there appears to be a zero-point shift for this night. Parentheses indicate standard deviation about the mean in millimagnitudes, and n is the number of observations. The differential light and colour curves for CPD-58°2721 are shown in Figs. 4.1-4.3. The differential light curve for the comparison stars (K-C) indicates a possible periodic variation of $\sim$0.01 mag over about 3 days. It is not clear which star may be responsible, but care has been taken to avoid consequent aliasing in the subsequent frequency analysis.

4.3 Frequency analysis

As may be seen from Figs. 4.1 & 4.2, the light curve of CPD-58°2721 cannot be represented by a single strictly-periodic variation. On the other hand it does not appear to be completely irregular. Two interpretations will be considered. In the first case the light curve may be quasi-periodic, meaning that the underlying variation is singly-periodic but that some process makes individual cycles vary in length. Secondly, the variation may be multiperiodic. Each alternative is examined in order to find a representation of the light curve of CPD-58°2721.

One way of examining a quasi-periodic variation is simply to measure the mean interval between maxima and/or minima in the light curve. Only the 1985 data are sufficiently dense for this to be carried out for CPD-58°2721, and even here the problem is complicated by the presence of short gaps. Identifying maxima as occurring on JD 2446184, 193, 201 and 213, and minima on JD 2446188, 196 and 206, a "characteristic period" of 9.4 ± 1.5 days is obtained. A precedent in the case of a hydrogen-deficient star was set by Fernie (1982) who found a "quasi-period" of 46 ± 5 days for RCrB.

Trimble (1972) was the first to point out that pulsations in high luminosity helium stars are extremely non-adiabatic. Non-linear calculations (Saio & Wheeler 1985) showed that light and radial velocity variations are not completely regular for low mass models. A Fourier-type frequency analysis may give a misleading result when applied to such a star. However, whilst a quasi-periodic variation represents a simple and adequate interpretation of the light curve, a search for strictly periodic variations has been made to see whether it is unique.

A frequency analysis using a least-squares Fourier method (Barning 1963) was made with the Fourier-analysis package PULSAR (Skillen 1985). The method involves measuring the frequency corresponding to the most significant feature in the power spectrum of the Vr-C observations by equating its peak with the centroid of a fitted Gaussian function. This frequency is then filtered from the data by regressing a sine-wave corresponding to this component on the data. If a second periodicity is present in the resulting pre-whitened data, it is removed by a simultaneous regression of both sinusoidal terms on the data. The process is repeated until there is no evidence of any remaining periodicities. The noise inherent in the power spectrum was adopted from the level of the strongest feature present in the power spectrum of the comparison star.

The power spectra of the 1985 differential u, v, b and V observations each displayed the strongest peak at ~ 0.108 cycles day^{-1} (f_1) (Fig. 4.4a). After pre-whitening to remove this component, the data showed the presence of a further periodic component at ~ 0.071 cycles day^{-1} (f_2) (Fig. 4.4b). The components at f_1 and f_2 were filtered by a simultaneous regression of two sine-waves on the data and the data examined for any remaining periodicities. Only the power spectrum of the V observations showed evidence of a remaining periodicity after multiple-frequency pre-whitening, with a peak at $f_3=0.035$ cycles day^{-1} five times greater than the adopted noise level. However, as $f_3 \gtrsim f_2/2$ it cannot be claimed to be an independent frequency. This is borne out by its non-detection in the u, v and b light curves. The (u-b) variations, indicative of temperature changes, showed periodicities of 0.106 cycles day^{-1} and 0.066 cycles day^{-1}. Table 4.5 summarises the results

Loumos & Deeming (1978) show that spurious peaks in the power spectrum are generally not significant provided the separation of the frequency components is $\gtrsim 1.5/T$, where T is the timespan in days of the observations, and consequently this is adopted as the resolution inherent in the power spectrum. The same criterion decides the lowest frequency for which useful information is available in the power spectrum, whilst the high-frequency limit is set by $1/2\,\Delta t$, where Δt is the mean sampling interval of the observations. In the present instance this gives a frequency resolution of ~ 0.038 cycles day^{-1}. As $f_1-f_2=0.037$ cycles day^{-1},

Figure 4.5 The differential 1985 V observations prewhitened by 0.108 cycles day^{-1} (top), 0.071 cycles day^{-1} (middle), 0.108 and 0.071 cycles day^{-1} (bottom).

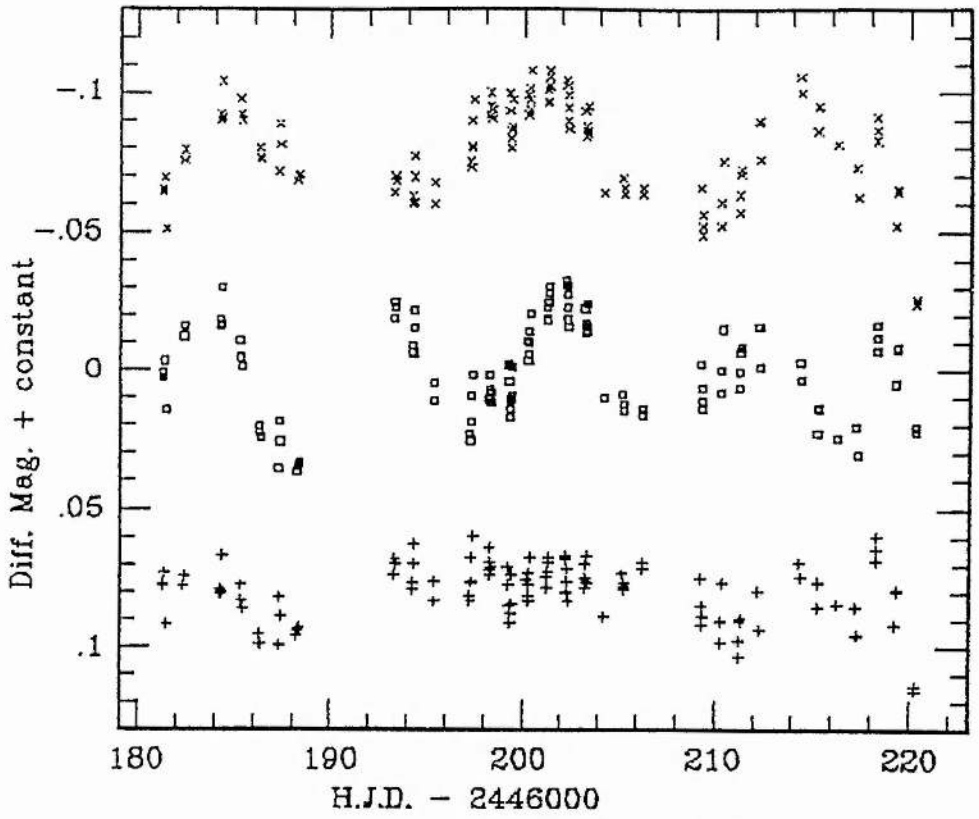

Figure 4.6 The fit to the differential 1985 V observations of the theoretical light-curve generated from two sine-waves with frequencies of 0.108 (f_1) and 0.071 (f_2) cycles day^{-1}.

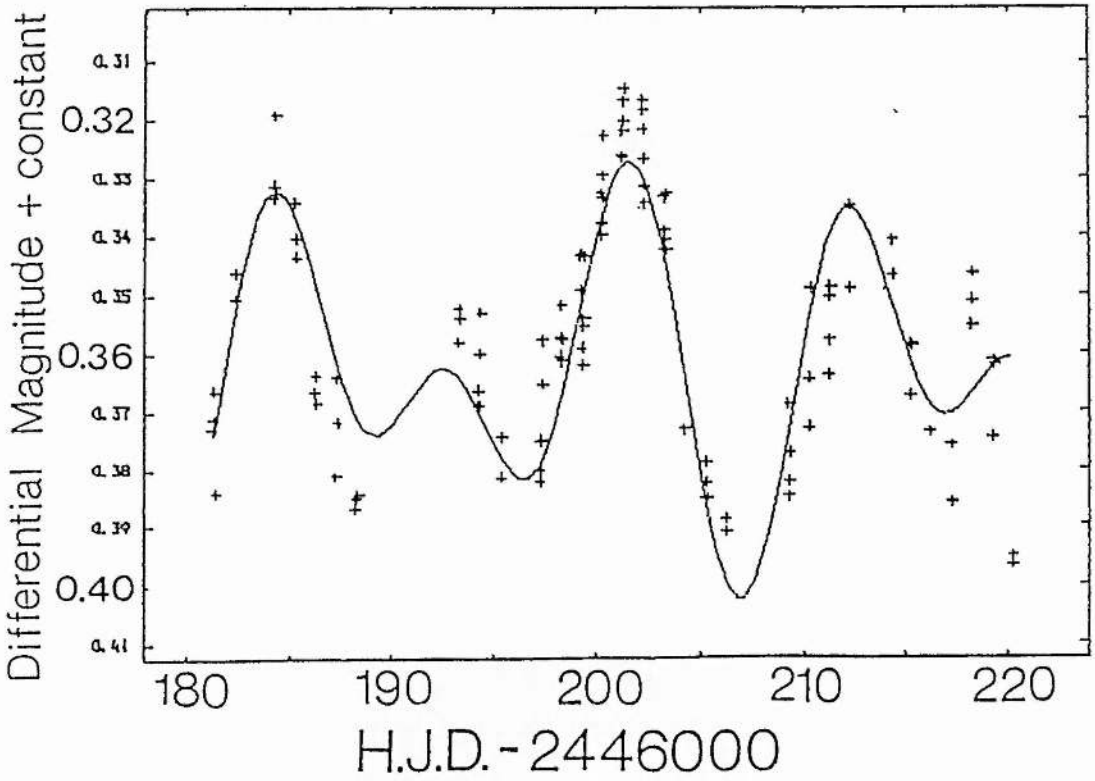

Figure 4.5 The differential 1985 V observations prewhitened by 0.108 cycles day^{-1} (top), 0.071 cycles day^{-1} (middle), 0.108 and 0.071 cycles day^{-1} (bottom).

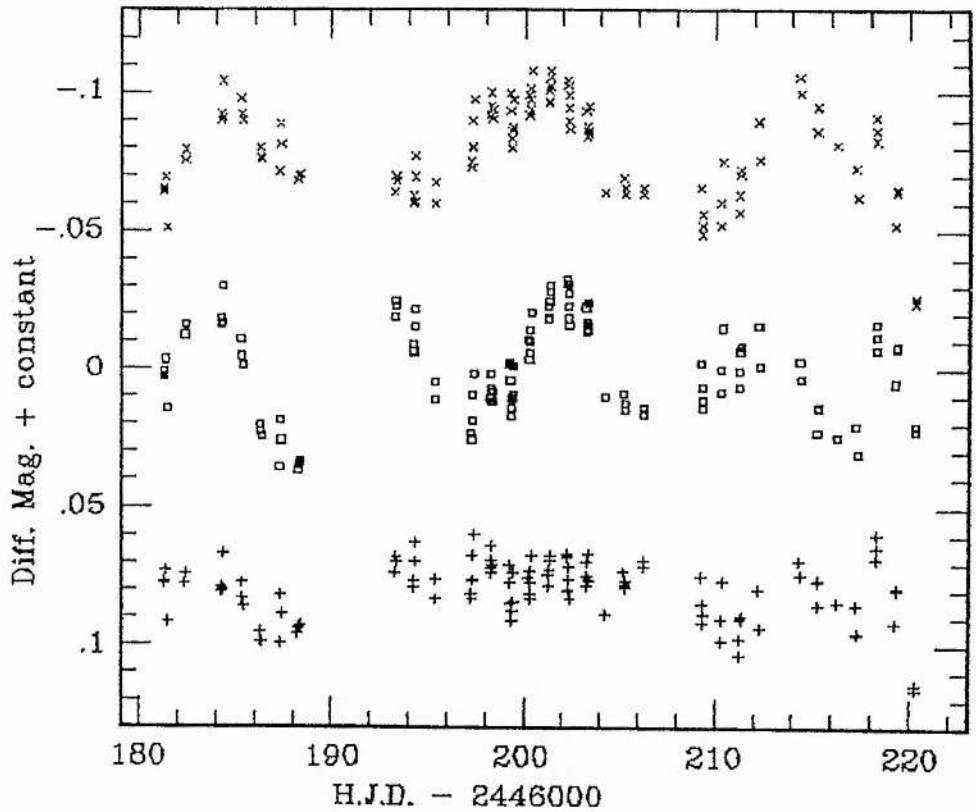

Figure 4.6 The fit to the differential 1985 V observations of the theoretical light-curve generated from two sine-waves with frequencies of 0.108 (f_1) and 0.071 (f_2) cycles day^{-1}.

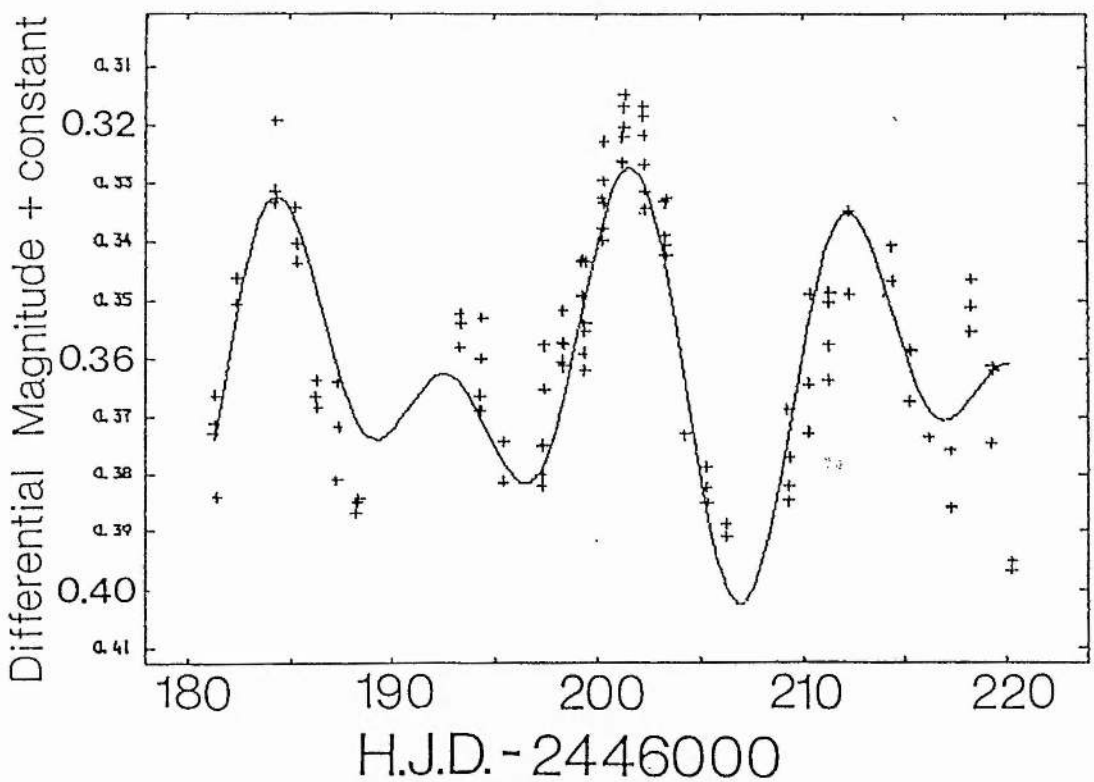

f_1 and f_2 are barely resolved. In an attempt to distinguish the presence of real peaks from those aliases which may be introduced into the power spectrum from regularities in the data sampling, tests were made on subsets of the data sample. The power spectra with the first third, and the last third of the data set omitted respectively, both showed a peak at $\sim$0.09 cycles day^{-1} ($=(f_1+f_2)/2$). Although the timespan, 228 days, of the Johnson V observations (which includes the V magnitudes from the 1986 Strömgren observations) is a considerable increase on the 1985 uvby data, observations were only made on 52 nights and are insufficient for a frequency analysis due to the paucity of the observations.

An independent search was made for possible periods using the string-length or phase-dispersion minimisation technique (Dworetsky 1983). This is an elaboration of the Lafler & Kinman (1965) method which involves the phase organisation of the data in the time domain to find the period that produces the least numerical scatter in the data. In this particular method the quantity minimized is the sum of the lengths of line segments joining successive points in phase space.

The interval 0 to 1 cycle day^{-1} was searched in steps of uniform frequency so that the maximum phase error for any pair of observations would always be 0.1 or less. The string-lengths were plotted against frequency and the minimum taken as the most likely period. In order to apply this technique to multiperiodic data, it is necessary to know a priori the most likely periods present and selectively pre-whiten the data before searching for periodic

content. Pre-whitening the u, v, b, V and (u-b) data sets to remove an f_1^{-1} day period produced in each case a minimum at $\sim$0.07 cycles day^{-1} and similarly, pre-whitening to remove an f_2^{-1} day period produced a minimum at $\sim$0.11 cycles day^{-1}, in good agreement with the results from the Fourier analysis.

Fig. 4.5 shows the light curve decomposed into its component parts according to the frequencies found above. The theoretical light curve generated from the addition of two sine-waves with periods of P_1=9.3 (0.108^{-1}) and P_2=14.1 (0.071^{-1}) days is seen to reproduce the general features of the observed light-curve (Fig. 4.6). It is therefore concluded that a quasi-periodic variation with a mean period of 9.4 days is responsible for the light curve of CPD-58°2721. Modulation by a second period of 14.1 days yields a good representation of the data, but the frequency resolution of the data set prevents a claim for the detection of a multiperiodic variation.

4.4 Origin of the variations

The results of the 1985 Strömgren photometry covering 40 days indicate light variations that have decreasing amplitude with increasing wavelength from 0.15 mag at u to 0.08 mag at V. Variations in colour are most pronounced with a 0.07 mag variation in (u-b), whilst smaller variations of $\sim$0.02 mag are present in (v-b) and (b-y). The 1986 Strömgren observations covering 10 days and the UBVRI observations obtained over 228 days showed larger variations of 0.11 mag and 0.18 mag in V respectively. This is in

good agreement with Landolt (1986a) who found a 0.15 mag variation in V from thirteen measures over a 3-year period (1978-81). As with the Strömgren observations, the light and colour variations present in the UBVRI observations appear to be in phase, with the amplitude largest in U and smallest in I. It might be argued that the variations identified in CPD-58°2721 could be due, at least in part, to variations of CPD-58°2721B. A one-magnitude variation of CPD-58°2721B in the visual region would produce a ~0.12 mag variation in V. However, this seems unlikely as the two observations of CPD-58°2721B made five days apart showed no evidence of photometric variability whereas in the same time interval CPD-58°2721 showed a 0.06 mag change in V. The close agreement in V between our observations and those of Landolt is further evidence that CPD-58°2721B is not variable over a longer timescale. Also the nature of the variations (largest amplitude in u) is that to be expected for a star with T_{eff}=14,000K which has a peak in its flux at ~2000A. If CPD-58°2721B is of spectral type F or later, as its H and K lines suggest, then its temperature corresponds to a peak in flux at ~5000A or longer, so that the amplitude of any variations would be expected to be greatest in V and smallest in u. No estimate of the effect of CPD-58°2721C has been possible. Again, its contribution should be greatest in V as the star appears to be cool.

The presence of Balmer emission in the spectrum of CPD-58°2721 has been interpreted as evidence that the primary is filling its Roche lobe and transferring mass towards the secondary (Sect. 5.2b). Adopting a primary mass of $1M_{\odot}$, the orbital

parameters given by Jeffery et al.(1987b) give a Roche radius $R_L \sim 25R_\odot$ for the primary and a secondary mass $\sim 2\text{-}3M_\odot$ for inclinations 90°-50°. Assuming that the secondary lies close to the main-sequence (Plavec 1986) we can estimate its minimum radius as $\sim 2R_\odot$. The absence of any trace of the secondary in the visible spectrum of CPD-58°2721 is taken as indicating that the secondary must be more than 10 times fainter than the primary. For such a system, eclipses would last about 4 days and be less than 0.1 magnitudes. Distortion of the Roche lobe-filling primary could give rise to ellipsoidal variations that would appear in the light curve as a periodic variation with half the binary period. However, there is no evidence of any periodicity present in the light curve which appears to be related to the binary period of 43.25 days estimated by Jeffery et al.(1987b), although this estimate is only provisional at best. To investigate the possibility that the 9.3 or 14.1 day periodicities found in the light-curve from the frequency analysis might arise from ellipsoidal distortions of the primary, least-squares fits were performed on the radial-velocity data set used by Jeffery et al.(1987b) for sine-waves with periods of 18.6 days and 28.2 days. The fits were very poor and no correlation between the radial velocity and the light curves could be found.

It therefore seems reasonable to attribute the variations in the light curve to some form of pulsational instability in the star. The simplest interpretation is that of radial pulsations where changes in the brightness arise from temperature and radius variations during the pulsations. From models of stellar

atmospheres for the EHe stars, Heber & Schönberner (1981) related Strömgren colours and effective temperature using a reddening-free index which they defined as:

$$[c_1] = c_1 - 0.1(b-y)$$

Fig. 4.7 shows $[c_1]$ plotted with the 1985 V observations for CPD-58°2721, which can be considered as showing the changes in temperature and brightness respectively during pulsation. To within observational error the flux and temperature variations appear to be in phase. Confirmation of T_{eff} changes during pulsation is shown by marked changes in the strengths of low-excitation metallic lines on a timescale of days, the changes in line strengths exhibiting a strong dependence on excitation potential (Sect. 5.2a). Hack (1960) observed a similar variation in the line strengths of Ups Sgr.

Although the binaries must have different evolutionary histories, their internal structure and hence their pulsational characteristics may be similar to those observed in the EHe stars. Effective temperatures and periods for nine extremely hydrogen-deficient stars are given in Table 4.6. The periods are consistent with models of radial pulsation in highly luminous helium stars (Wood 1976), and the apparent correlation between period and effective temperature is that to be expected for the case of radial pulsation. The hottest star listed in Table 4.6, BD-9°4395, has been proposed by Jeffery et al. (1985) to be undergoing non-radial pulsations. Whilst a confirmation of these results is desirable, it appears that parallels may be drawn between the photometric variability in KS Persei, Ups Sgr and

Figure 4.7 Plot showing the $[c_1]$ (with error bars) and V variations (consecutive nightly means joined) of the 1985 observations, indicative of temperature and luminosity variations respectively.

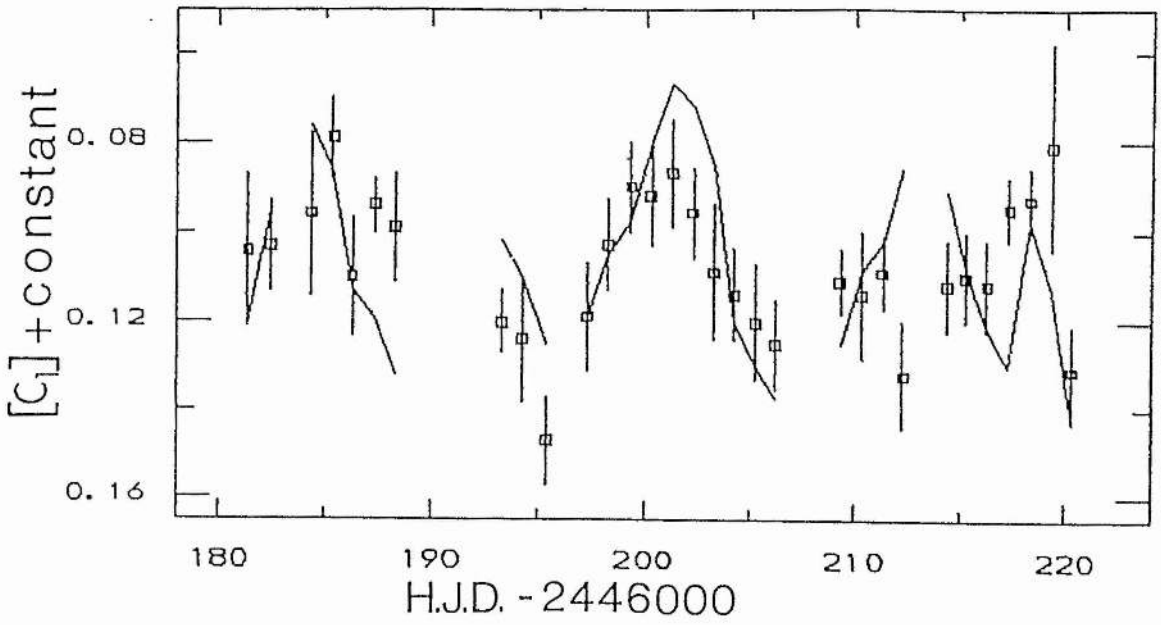

Table 4.6 Effective temperatures and pulsation periods for nine extremely hydrogen-deficient stars.

	T_{eff}(K)	Period(d)		Status
RY Sgr	7,100[1]	38		S
KS Persei	9,000[2]	30		B
BD+1°4381	9,500[2]	21		S
Ups Sgr	10,500[2]	20		B
BD-1°3438	10,900[2]	5-8		S
LSIV-1°2	11,900[2]	11		S
CPD-58°2721	14,000[3]	9	(P_1)	B
		14	(P_2^1)	
LSII+33°5	15,000[2]	3-4		S
BD-9°4395	23,000[2]	3.5		S
		11		

B=Binary, S=Single
References: 1.Schonberner (1975); 2.Drilling et al. (1984a); 3.Chapter 5.

CPD-58°2721 as EHdBs with EHe stars of similar temperature.

Figure 5.1 An unsharp, masked, deep H-alpha+[NII] plate of the Carina nebular complex (reproduced from Meaburn et al. 1984).

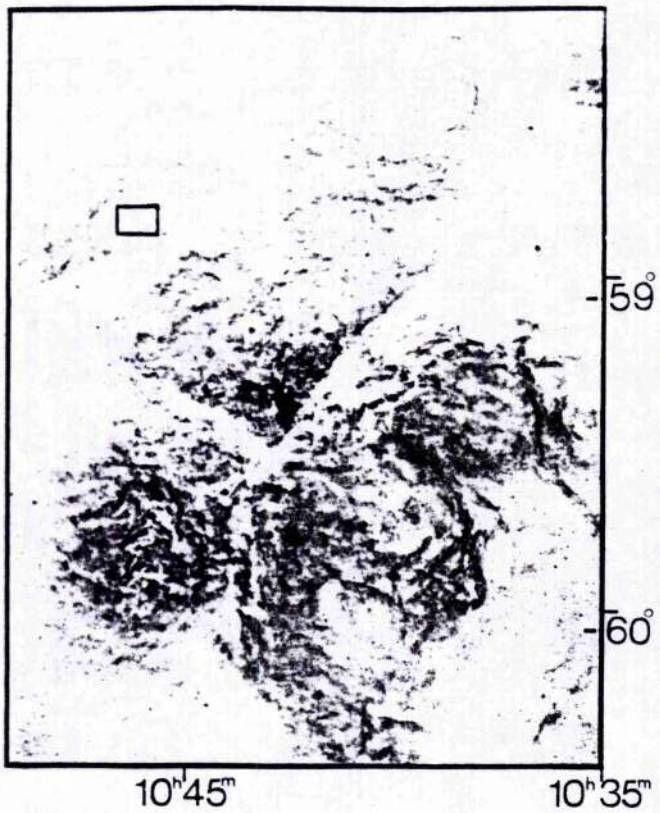

Figure 5.2 An enlargement from a deep H-alpha+[NII] plate of the Eta Carina nebula showing the region around CPD-58° 2721.

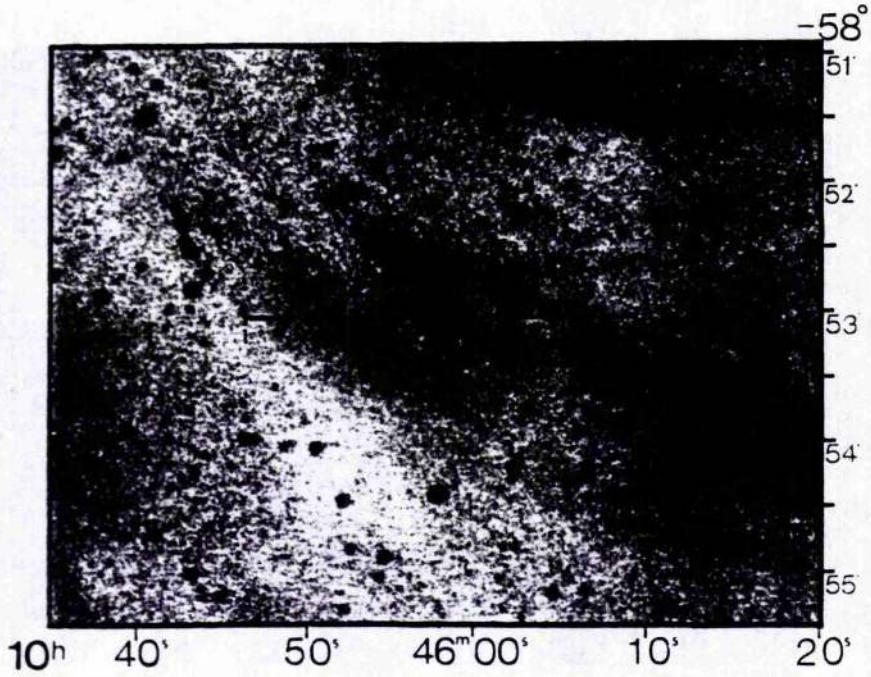

Figure 5.1 An unsharp, masked, deep H-alpha+[NII] plate of the Carina nebular complex (reproduced from Meaburn et al. 1984).

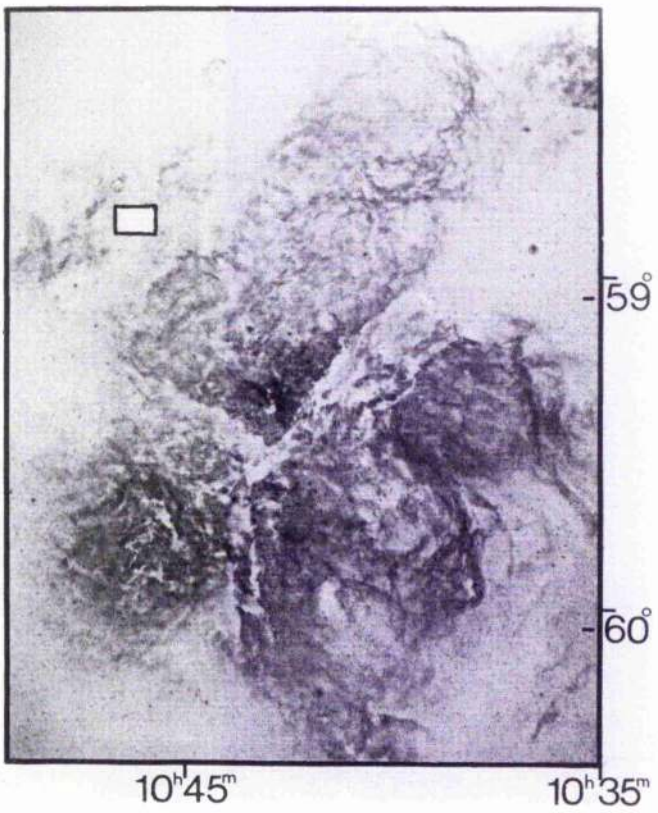

Figure 5.2 An enlargement from a deep H-alpha+[NII] plate of the Eta Carina nebula showing the region around CPD-58° 2721.

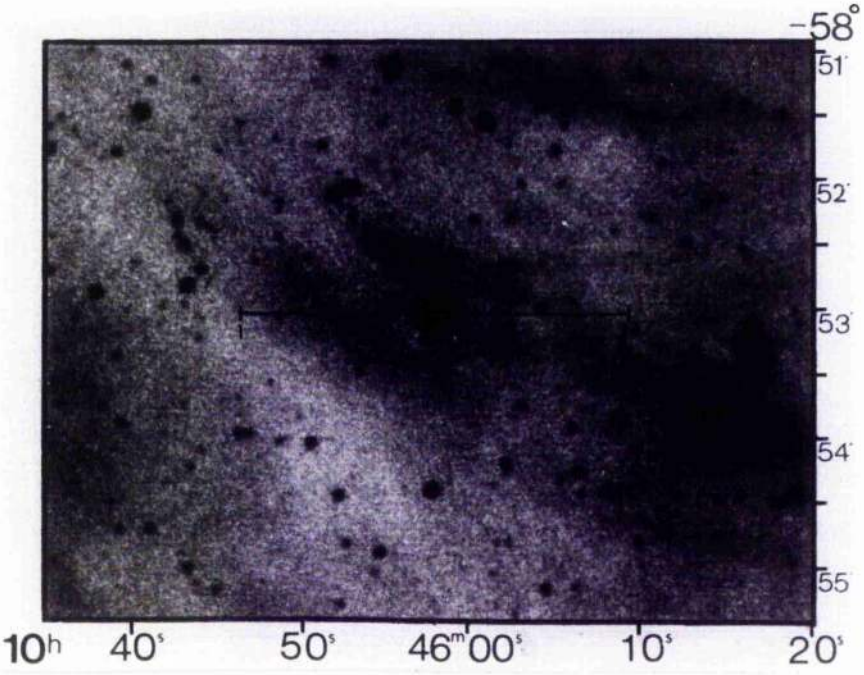

5. A Spectroscopic Investigation and Fine Analysis of CPD-58°2721

5.1 The Surrounding Nebula

5.1a DESCRIPTION

CPD-58°2721 is located on the outskirts of the Eta Carina nebula (NGC 3372), a vast region of ionised gas surrounded and crossed by dense neutral concentrations of dust, gas and molecules. It covers about 2 degrees on the sky which at a distance of 2.7 ± 0.4 kpc (Hutchmeier & Day 1975) corresponds to 94 pc. Fig. 5.1 is an unsharp, masked photograph of the Carina nebular complex reproduced from Meaburn et al. (1984), on which is indicated the region under investigation here. Fig. 5.2 is an enlargement from an Hα+[NII] plate showing the region around CPD-58°2721 (note the E-W direction is reversed from Fig. 5.1). Both plates were taken through a 100A interference filter centred on Hα+[NII] with the 1.2-m Schmidt telescope. Exposure times were 300 (Fig. 5.1) and 600 minutes. The positions of the slits across the star and nebula for the long and short-slit spectroscopy are indicated. CPD-58°2721 appears to be associated with a bright, roughly circular knot in the nebula with a diameter of $\sim$80", also visible on SERC 1.2-m Schmidt [SII], [OII], SR and J photographic plates, but not on B or [OIII] plates.

An important question to ask is whether the nebular emission arises from material surrounding the star, or whether it is a chance association of CPD-58°2721 and the Carina nebula along the line of sight? If the emission does arise from material in the vicinity of CPD-58°2721, what is the source of the excitation? It could be excited by a hot secondary, such as have been found in Ups Sgr and KS Persei from ultra-violet observations (Drilling & Schönberner 1982), or by the supergiant O and B stars in the Trumpler 16 association (Walborn 1973). It seems unlikely that either of the two stars close to CPD-58°2721 are the source of the excitation. CPD-58°2721B 11" south has strong, broad H and K lines in its spectrum (Fig. 5.3), suggesting a spectral-type F or later, whilst CPD-58°2721C 2" west can only be seen on SERC 1.2-m Schmidt SR and I plates and so is probably cool.

An estimate of the electron temperature T_e of the nebula can be made by studying the lines from ions which have energy-level structures that result in emission from two different upper levels with considerably different excitation energies. This can be applied to the ratio of the [NII] lines I(6548+6583A)/I(5755A), where I refers to the intensities of the lines corrected for extinction. The lines at 6548A and 6583A are well defined. However, [NII] 5755A lies at the edge of our spectral coverage; the signal-to-noise is correspondingly low and [NII] 5755A is not visible. Although a direct measure of T_e is not possible, the excitation state of the gas can be asserted from the nature of the emission lines present. Gaseous nebulae are generally classified

Figure 5.3 The CaII H and K lines of CPD-58°2721 and CPD-58°2721B. The spectrum of CPD-58°2721B has been smoothed to improve signal-to-noise. The H and K lines in CPD-58°2721 display a single interstellar component, and a stellar component which follows the radial-velocity curve of the binary.

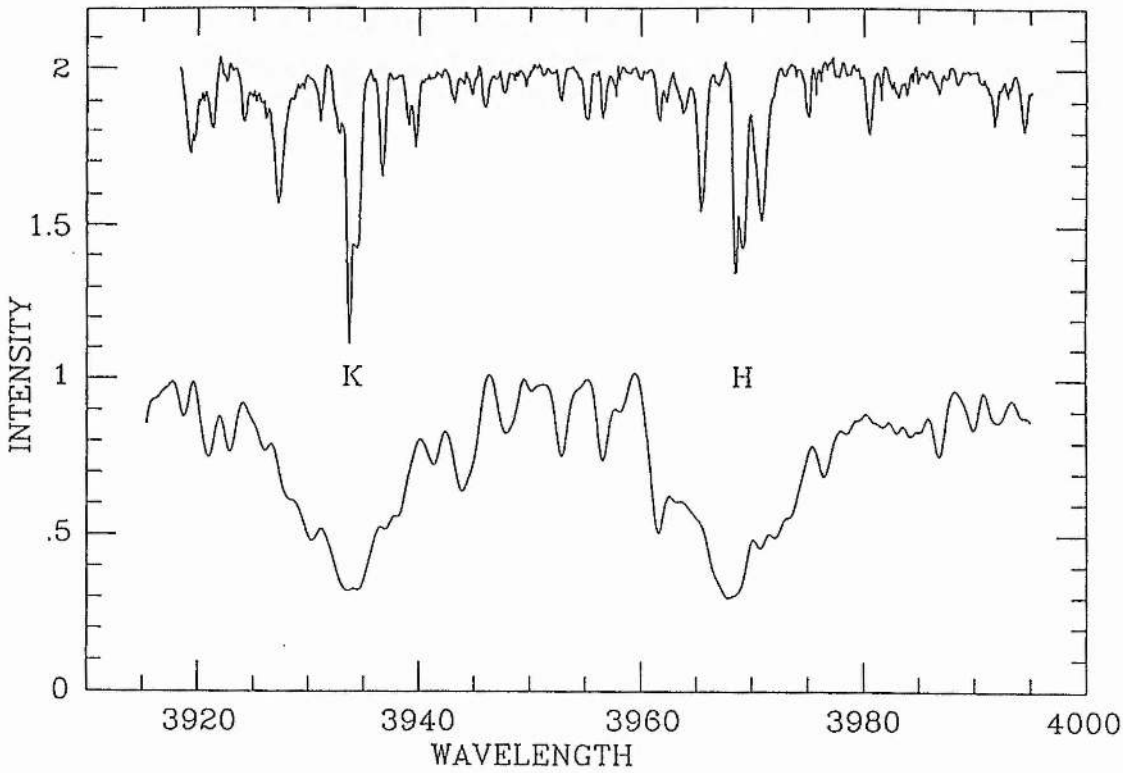

Figure 5.4 The [SII] 6716A and 6731A emission line profiles extracted from the short-slit spectroscopy.

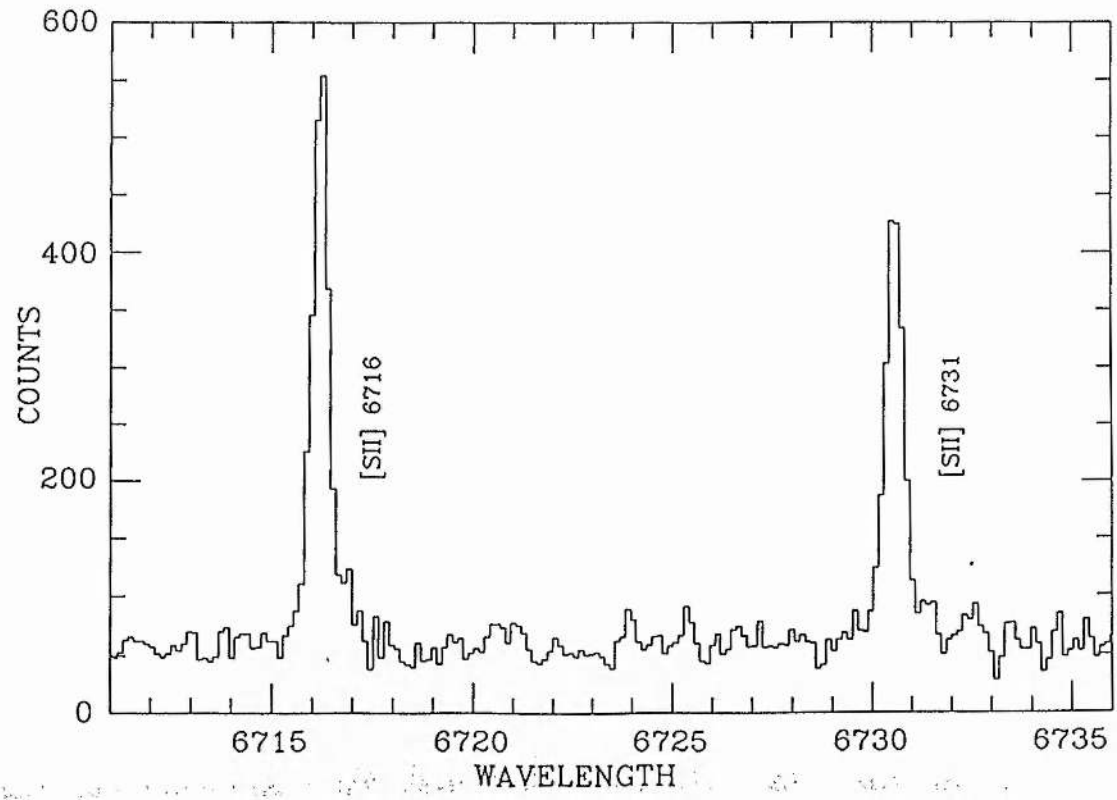

into the two main categories of HII (diffuse) regions or planetary nebulae. Nebular emission lines identified in the spectra are 3726 & 3729A [OII], 5876A [HeI], 6364A [OI], 6548 & 6583A [NII], Hα, and 6716 & 6731A [SII]. They are much more typical of a low-excitation HII region than a high-excitation planetary nebula. This is confirmed by the absence of features related to high-excitation lines such as [OIII] on SERC 1.2-m Schmidt photographic plates. $T_e=10^4$K is adopted after Faulkner & Aller (1965) who made optical determinations of $T_e \simeq 9{,}000$-$10{,}000$K at eight points over the Carina nebula. The line ratio I([NII]6548+6583A)/I(Hα), which is sensitive to changes in the excitation state of the gas, shows no significant variation along the slit length. The mean ratio from summing along the slit-length is 0.51 ± 0.12.

The electron density N_e may be estimated by measuring the effects of collisional de-excitation on two lines from the same ion with nearly the same excitation energy so that the relative populations of the two levels, and hence the ratio of the line intensities, is dependent upon the density. The most frequently used ratios are [OII] I(3729/3726A) and [SII] I(6717/6731A). The [SII] lines extracted from the short-slit spectroscopy are shown in Fig. 5.4, for which the measured intensity ratio is 1.22 ± 0.12. Although the lines are uncorrected for extinction and instrumental response, errors arising from these effects can be expected to be negligible. For $T_e=10^4$K we obtain $N_e=135\pm25\text{cm}^{-3}$ ($N_e=90\text{cm}^{-3}$ for $T_e=5\times10^3$K) (Osterbrock 1974a). The signal-to-noise of the [SII] 6716/6731A lines in the long-slit spectroscopy is insufficient to

determine whether there is any variation of N_e along the slit length.

As the radial velocities determined from Hα , [NII] and [SII] in the long-slit spectroscopy are similar, only the measurements from Hα are presented. The variation of the heliocentric radial velocity along the slit (aligned W-E) is shown in Fig. 5.5. The error on the individual velocities is estimated to be $\pm$2km s^{-1}. The radial-velocities show a shift towards more positive velocities to the east, with a mean of 11 ± 3km s^{-1}. Fig. 5.6 is the nebular spectrum 6540-6590A obtained from summing over all pixels along the slit. The emission line profiles show a small excess in the red wings which is not readily apparent in the spectra of the individual pixels. The [SII] lines from the short-slit spectroscopy in Fig. 5.4 appear to show the same phenomenon. It may represent unresolved splitting of the lines.

5.1b THE RELATION OF THE NEBULA TO CPD-58°2721

Dickel (1974) used the measurements of Graham (1970) to estimate that the foreground extinction for that part of the nebula in the direction of CPD-58°2721 is about 1.5 mag. The spectrum of CPD-58°2721 shows the 4430A interstellar extinction feature which is present in the spectra of heavily reddened stars. Schönberner et al. (1982) estimate $E_{B-V}=0.70\pm0.05$ for CPD-58°2721 from a study of its ultra-violet flux. Adopting the reddening law of Seaton (1979) leads to a visual extinction $A_V(=3.2E_{B-V})$ of 2.2 mag. As this is significantly larger than the foreground visual extinction,

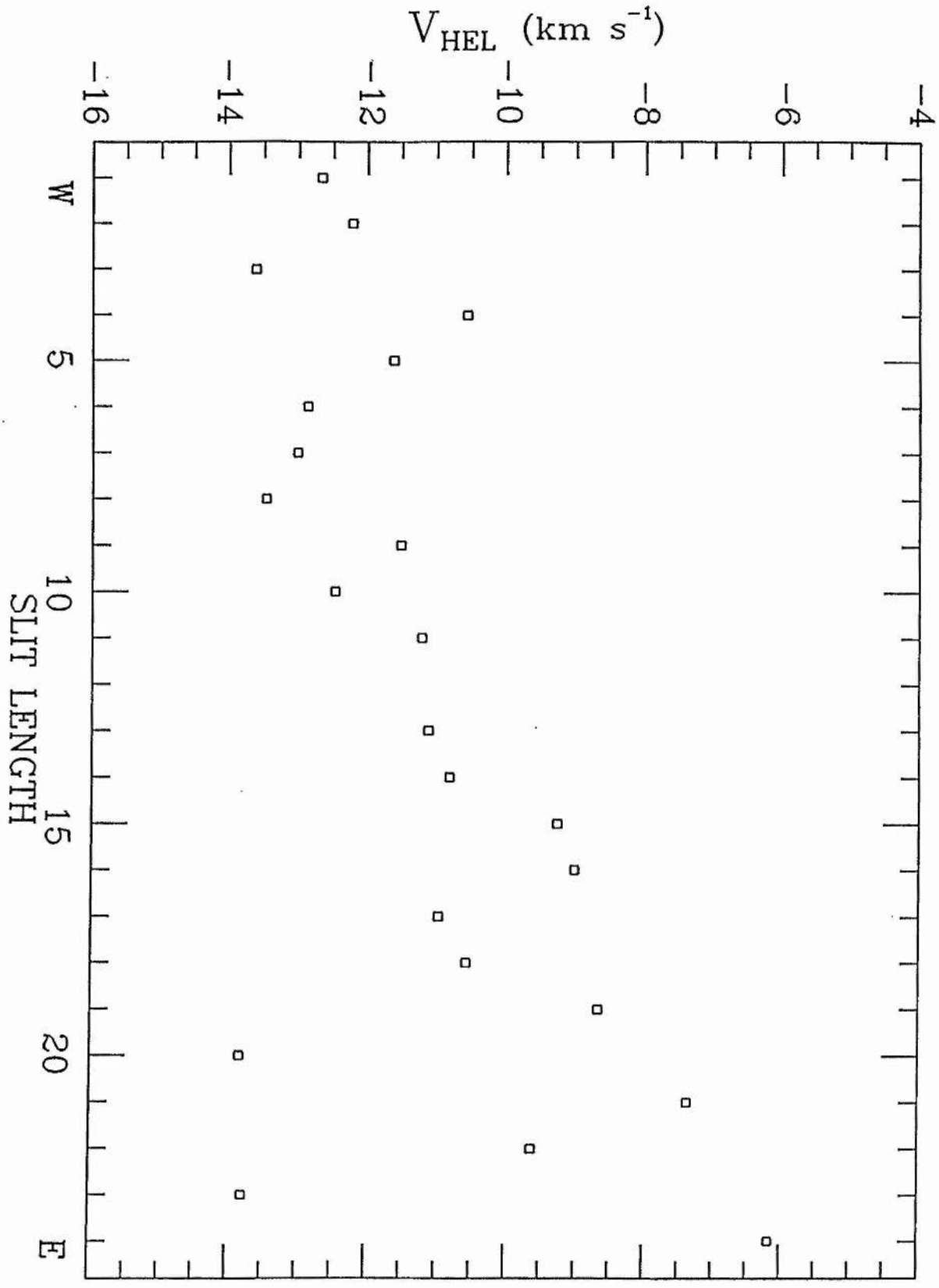

Figure 5.5 The variation of the heliocentric radial velocity V_{HEL} (km s^{-1}) determined from the Hα line as a function of position along the slit length.

it indicates that CPD-58°2721 lies in, or at a greater distance than, the Carina nebula. Using the Magnitude-Distance relation $M_V = -4.0$ for CPD-58°2721 at the distance of the Carina nebula. Certainly such a value would not be inconsistent with the M_V estimates of -3.2 ± 0.7 for KS Persei (Danziger et al. 1967) and -4.8 ± 1.0 for Ups Sgr (Rao and Venugopal 1985).

Dickel provides a contour map of the visual extinction across the nebula close to CPD-58°2721 after the contribution from the foreground extinction has been removed. The star lies well away from the direction where the nebular absorption is greatest. In the region of CPD-58°2721 any additional nebular extinction is probably small (< 1 mag). With an 0.7 mag excess over the estimate for the foreground extinction, the star could lie within or beyond the nebula. The interstellar CaII H and K line profiles appear single in CPD-58°2721 (Fig. 5.3). The star lies outside the region within which stars embedded in the Carina nebula display complex interstellar CaII line profiles (Walborn 1982, Walborn & Hesser 1982)

Meaburn et al. (1984) measured the radial velocities of [OIII] 5007A across the Carina nebula at low spatial resolution (3') and found large-scale velocity components over a range of 84km s^{-1}. A similar velocity range in Hα was found by Deharveng & Maucherat (1975). Within a region of diameter 3' (=2.4pc) inclusive of CPD-58°2721, Meaburn et al. found a single velocity component v_{HEL}=-8km s^{-1}, similar to the value observed here for the Hα line. Over a region ~10 times larger they find two velocity

components present, one continuously variable from $\sim$-30km s^{-1} to $\sim$-15km s^{-1}, and another constant at about -10km s^{-1}. It seems therefore, that the velocity of the ionised gas in the knot surrounding CPD-58°2721 is consistent with that of the ionised gas in the surrounding Carina nebula.

If CPD-58°2721 lies within the Carina nebula it is possible to estimate the size of the surrounding region expected to be ionised by the star. The energy source that produces the ionising radiation in a nebula is almost always ultra-violet radiation associated with a star with $T_{eff} \gtrsim 30{,}000$K. Although CPD-58°2721 appears to be too cool to ionise the surrounding region, it may be the case that a hot secondary provides the necessary ionising radiation. The hot secondaries detected in Ups Sgr and KS Persei have been variously estimated to be of spectral type B2-09.5 (see Chap. 3). If we consider the simplified case of a cloud of pure hydrogen of constant density surrounding the star, we can estimate the number of photons per second Q required to produce complete ionisation within the cloud out to a radius r. The presence of [OI] is taken as indicating that the knot is optically thick at Hα and radiation-bounded. Only those photons above the threshold frequency ν_o able to ionise hydrogen from the ground state need to be considered, and using the result that ionisation is complete within a radius r (often called the Strömgren sphere) and zero outside :

$$Q = \int_{\nu_0}^{\infty} L_\nu / h\nu = 4\pi r^3 N_H^2 \alpha_B / 3 \qquad \text{(Osterbrock 1974b).}$$

where L_ν is the luminosity of the star at a frequency ν, h represents Planck's constant and α_B is the recombination coefficient for hydrogen summed over all levels above the ground level. The physical meaning of this equation is that the total number of ionising photons emitted by the star per second just balances the total number of recombinations to the excited levels within the volume $4\pi r^3/3$. At the distance of the Carina nebula the angular radius of the knot corresponds to r=0.5pc. With $N_e=N_H=135 cm^{-3}$ and $T_e=10^4 K$ we obtain $Q=7x10^{46}$ photons s^{-1}. Model stellar atmospheres (Morton 1969, Hummer & Mihalas 1970) show that this would correspond to a B1-type main-sequence secondary, similar to those detected in Ups Sgr and KS Persei. That such a secondary is not detectable in the optical region is due to the dominance of the cooler primary at longer wavelengths.

In summary, the knot surrounding CPD-58°2721 has a nebular emission spectrum typical of an HII region, with $T_e=10^4 K$ and $N_e \approx 10^2 cm^{-3}$. The radial velocity of the ionised hydrogen in the knot is consistent with velocity measurements of the ionised gas in the surrounding Carina nebula. The heavy reddening of CPD-58°2721 indicates that the star lies within or at a greater distance than the Carina nebula. Whilst it has not been possible to confirm or discount a physical link between CPD-58°2721 and the surrounding nebula, the size of the knot at the distance of the Carina nebula would be consistent with ionisation by a hot secondary of a similar

Figure 5.6 The Hα and [NII] emission line profiles formed from summing the signal along the slit length (172.8 arcsec on the sky).

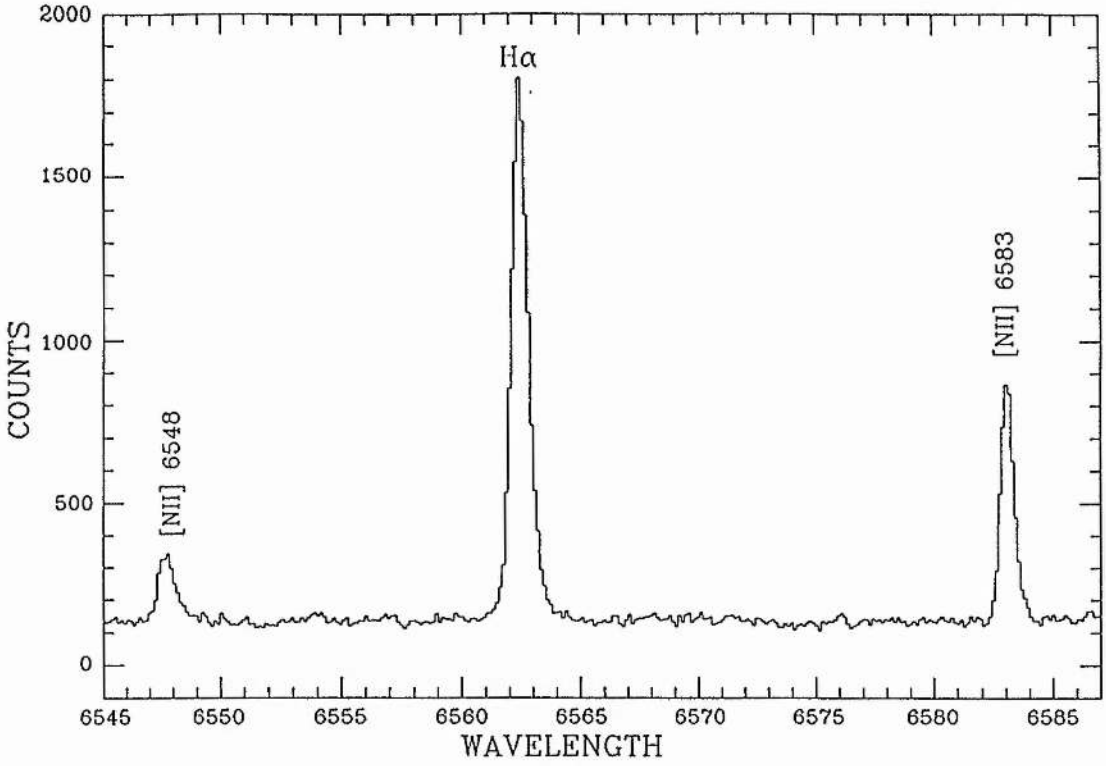

Figure 5.7 Comparison of the spectra of CPD-58°2721 (top) and the carbon-rich EHe star HD168476 in the wavelength region of CII 4267A (kindly supplied by Dr U.Heber).

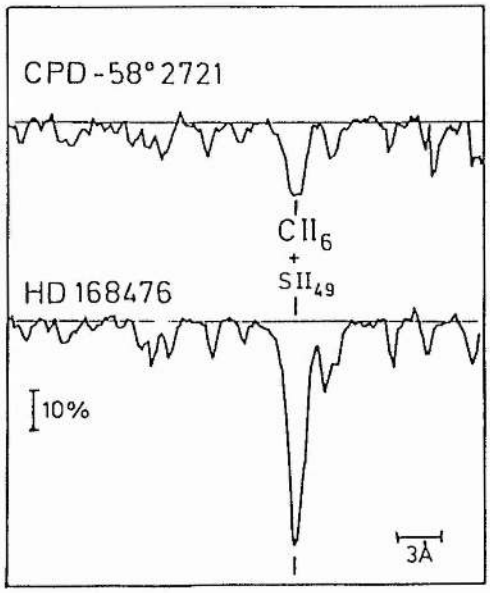

spectral type as have been detected in Ups Sgr and KS Persei. That the ultra-violet spectrum of CPD-58°2721 (Sect 5.3a) is due primarily to the visible star does not preclude the existence of a hot secondary.

5.2 The Spectrum Variability of CPD-58°2721

5.2a THE ABSORPTION SPECTRUM

The spectrum of CPD-58°2721 is very similar to those of the other EHdBs Ups Sgr, KS Persei and LSS 4300 (Hack 1960, Wallerstein et al. 1967, Schönberner & Drilling 1984). The hydrogen lines are far weaker than in 'normal' stars of similar temperature, whilst the lines of neutral helium and singly and doubly ionised metals are numerous and strong. Lines of nitrogen are strong but the only carbon line at 4267A is weak, in contrast to the carbon-strong spectra of the EHe stars. Fig. 5.7 compares the spectra of CPD-58°2721 and the EHe star HD168476 in the wavelength region of CII 4267A. Lines have been identified in the absorption spectrum of CPD-58°2721 from H, HeI, CII, NII, MgII, SiII & III, SII & III, CaII, TiII, CrII, MnII, FeII & III, NiII, and possibly AII and NeI. Oxygen lines are not present. All the lines show the same velocities and so must all arise in the same atmosphere. There is no trace of a secondary component.

Figure 5.8 Comparison of two CASPEC spectra of CPD-58°2721 taken on 1985 April 6th (top) and April 9th in the wavelength region of SiIII (multiplet 1).

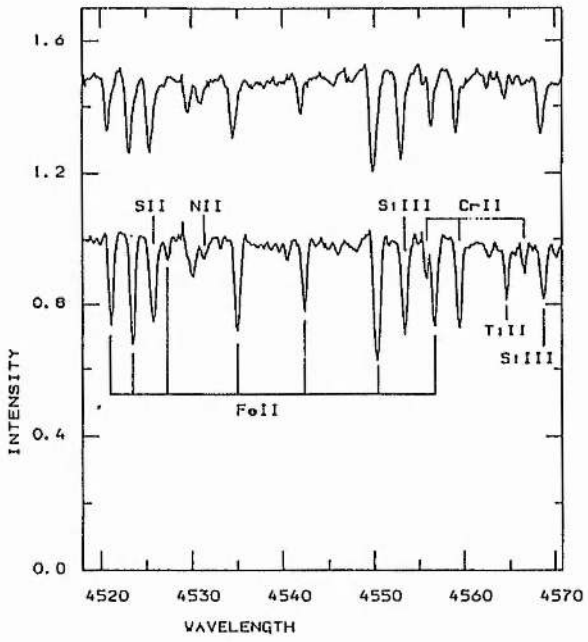

Figure 5.9 Changes in the residual intensities (R) of FeII lines (numbers given) between the two spectra of Figure 5.8, shown as a function of excitation potential. Line-strength changes in MgII and CrII are shown for comparison.

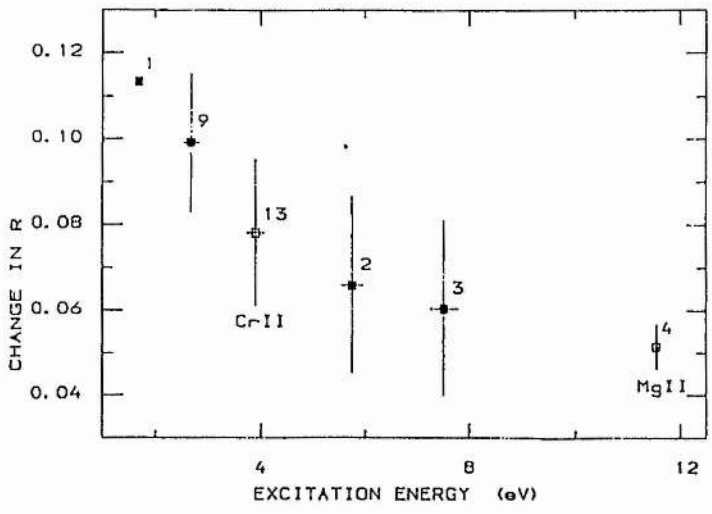

The two CASPEC spectra obtained on 1985 April 6th and 9th show marked changes in the strengths of low excitation metallic lines (Fig. 5.8). However, there is no general weakening of the lines, but a clear dependence on the excitation potential. Lines with low excitation potentials show the largest changes, while those with high excitation potentials change less. For elements with similar ionisation potentials, differential effects on lines for changes in temperature (or pressure) are essentially due to differences in excitation potentials. Thus we expect MgII and SiII to behave similarly and FeII and CrII to form a separate group. The behaviour of the FeII lines is shown in Fig. 5.9. Only those lines with a residual intensity R=0.6-0.8 on the 9th were used. This avoids the stronger saturated lines which are less sensitive to changes in the atmosphere, and the weaker lines which are more affected by noise. Note that the high excitation SiIII lines in Fig. 5.8 have almost identical equivalent widths in the two spectra. Hence it is concluded that these spectrum changes are probably related to the effective temperature changes deduced from the colour variations (Chap. 4), the weakened metallic lines on the 6th indicating a higher temperature prevailing than on the 9th.

As well as line-strength changes between the two spectra, line-profile changes are apparent. Some of the weakened lines on the 6th appear skewed, with a red excess in the line wings. The phenomenon of profile variations does not seem limited to any ion or group of ions, it does not even appear to affect all the lines of any one ion. This is unlike the line-strength changes which

exhibit a clear dependence on excitation potential. The changes in line profiles could be caused by slight mass motions which might be related to the stars photometric variability. Erratic or quasi-periodic changes in spectral line profiles occur frequently in supergiants (Rosendahl 1973a).

As lines of high excitation such as HeI, NII, and SiIII arise in the hotter parts of the atmosphere, lower than the line-forming regions of lower excitation such as H, FeII, TiII and CrII, velocity gradients have occasionally been found in the atmospheres of some supergiants (Inoue 1979). The heliocentric radial velocities for the lines of each ionic species given in Table 5.1 are shown in Fig. 5.10 (apart from that of CII 4267A which is poorly defined). Only the TiII, CrII and FeII lines are sufficiently numerous to allow detection of any small systematic differences between species. Fig. 5.11 suggests that there is a small ($\sim$ 3km s^{-1}) but significant difference in the velocity of the TiII lines and those of the CrII and FeII lines. For Ups Sgr, Bidelman (1950) concluded that any systematic differences in the radial velocities of the different elements are probably less than 3km s^{-1}.

Walker & Hill (1985) have reported the presence of radial-velocity changes in HD168476, although they failed to find any periodicities in the variations. Abt (1957) and Aydin (1979) report semi-regular radial-velocity changes in many supergiants with amplitudes of $\sim$5-10km s^{-1}, on a timescale as short as a hour. Jeffery et al. (1987b) have suggested that the

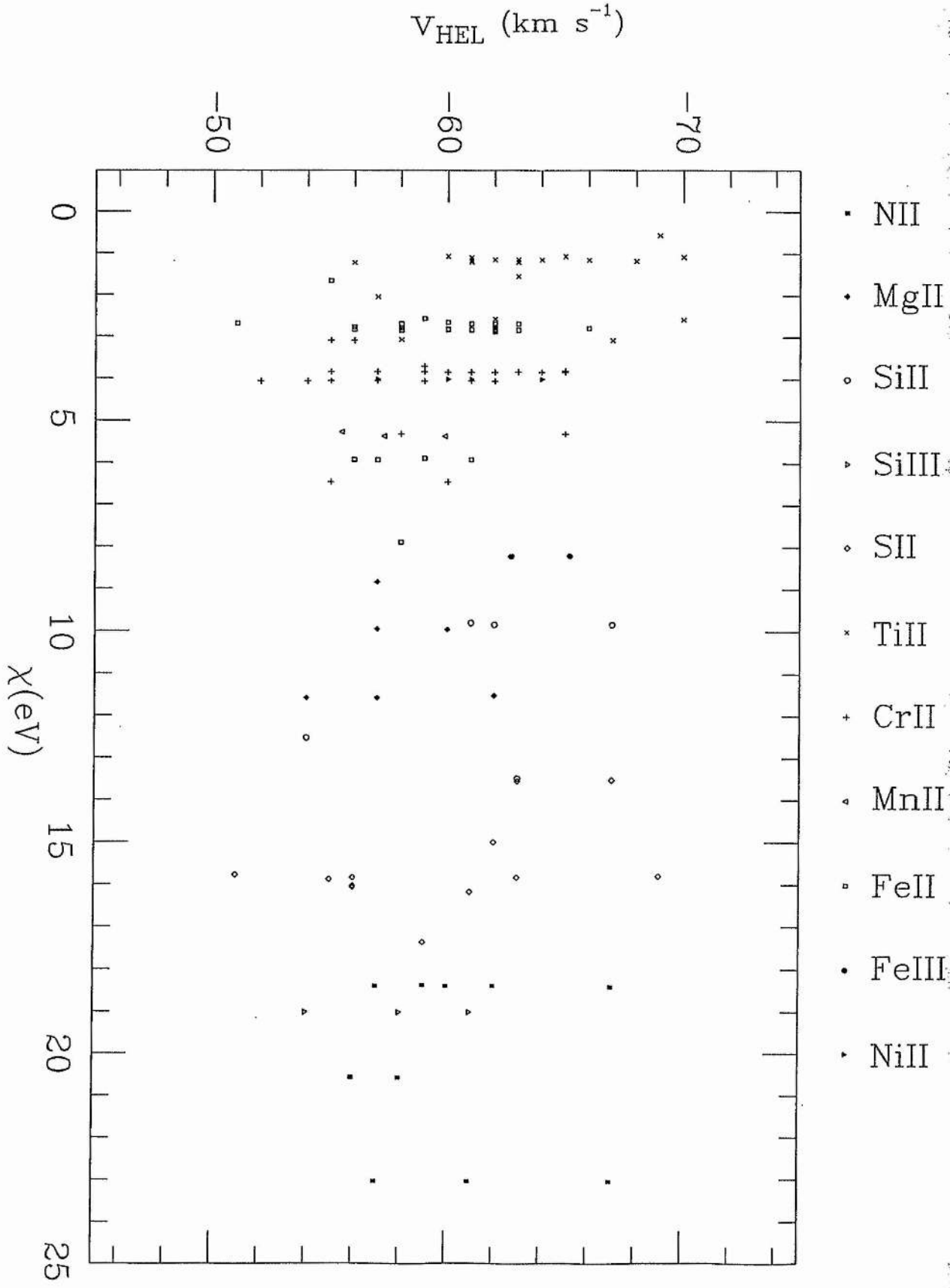

Figure 5.10 The heliocentric radial velocities of the lines used in the abundance analysis.

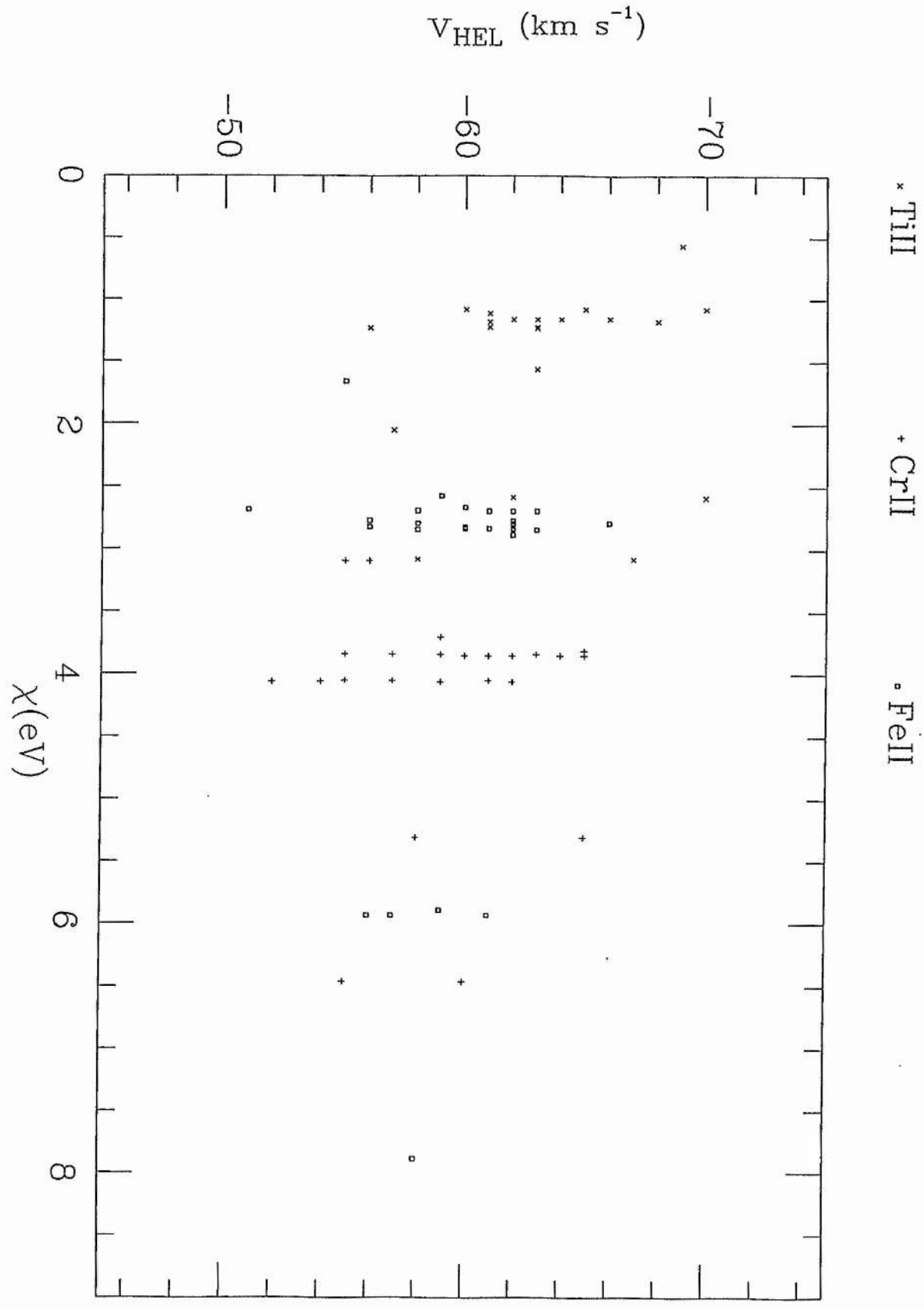

Figure 5.11 An expanded plot of Figure 5.10 showing only the TiII, CrII and FeII lines.

presence of small-amplitude radial-velocity variations in addition to that due to its binarity could help explain the large residuals obtained in their determination of a spectroscopic binary period for CPD-58°2721.

5.2b THE EMISSION SPECTRUM

Hα and Hβ appear in emission, and at some phases fill in the photospheric absorption line (Fig. 5.12). The emission is variable in strength and profile, and has a radial-velocity curve different from that of the photospheric lines. Three profiles of the Hα line are displayed in Fig. 5.13. They indicate variable large-scale velocity fields with relative velocities in excess of 100km s^{-1}. In 1982 February no photospheric absorption component is apparent whereas the 1984 April spectrum contains two peaks, suggestive of a photospheric absorption core similar to that found in shell stars (Underhill 1960). However, there is no evidence for a surrounding shell as has been found for Ups Sgr (Hack 1960; Sahade & Albano 1970), which unlike CPD-58°2721 displays a large infra-red excess (Drilling et al. 1984b). The emission appears stronger in 1985 March and again shows several components present. A weakened continuum during eclipse could produce an apparent strengthening of the emission. However, this seems unlikely as no evidence for eclipses has been detected photometrically (Chap. 4).

Figure 5.12 Hβ profiles from two CASPEC spectra taken on 1985 April 9th (top) and October 7th (kindly supplied by Dr U.Heber).

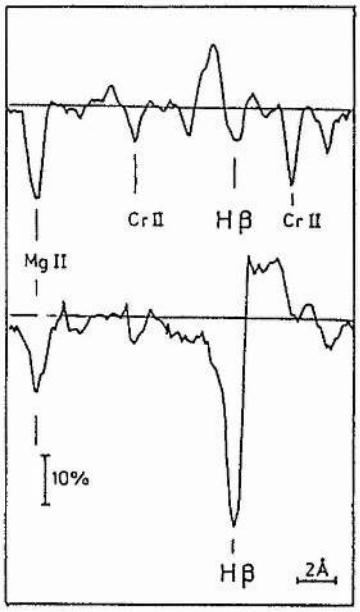

Figure 5.13 Changes in the Hα emission line profile, with dates shown. The rest wavelength is marked by an arrow in each line.

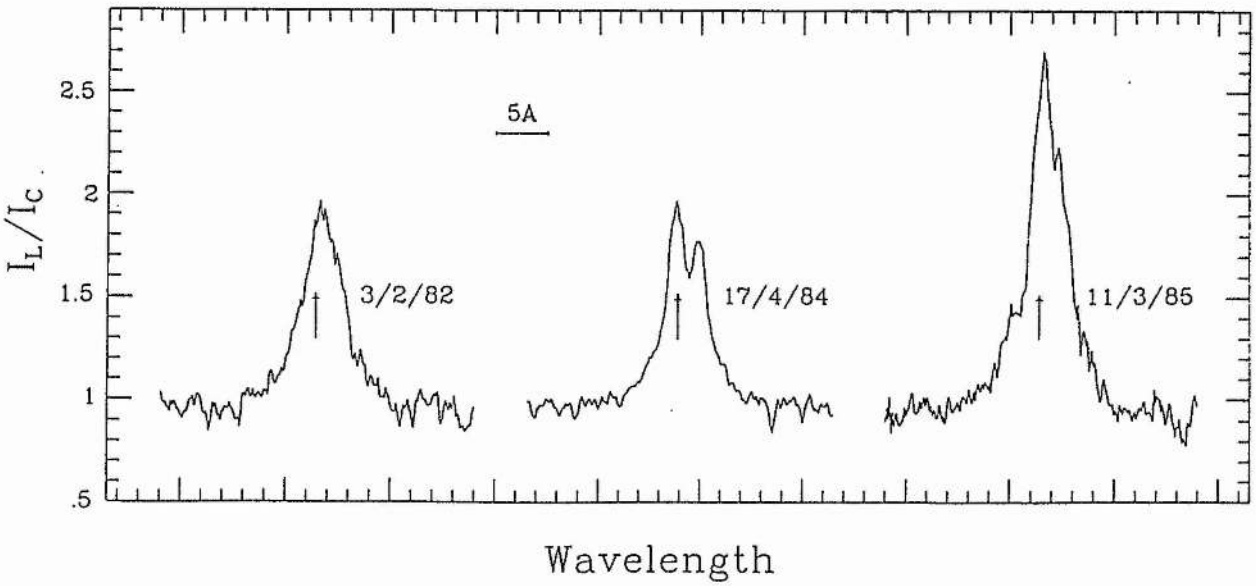

Figure 5.12 Hβ profiles from two CASPEC spectra taken on 1985 April 9th (top) and October 7th (kindly supplied by Dr U.Heber).

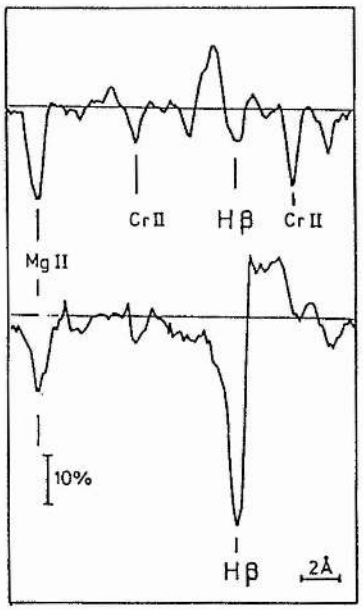

Figure 5.13 Changes in the Hα emission line profile, with dates shown. The rest wavelength is marked by an arrow in each line.

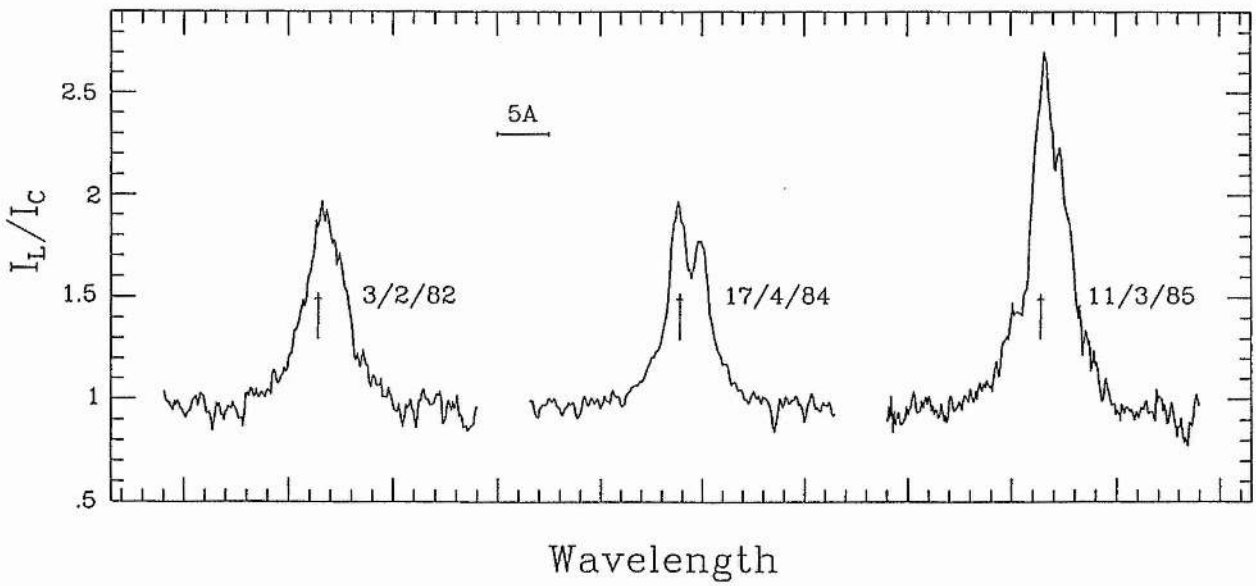

Strong and variable Hα emission has been found in KS Persei and Ups Sgr and has been interpreted as mass-transfer through the Lagrangian point (Hack 1960, Nariai 1967, 1972). The results presented here suggest that mass-transfer also occurs in CPD-58°2721. It is understandable why H emission is not present in the EHe stars if the emission observed in the EHdBs arises from mass-flow between the binary components. Rosendahl (1973b) finds that conspicuous emission in Hα is only expected for supergiants ($M_v < -6$) several magnitudes brighter than the EHe stars ($-2 > M_v > -6$, Drilling 1986).

5.3 Fine Analysis of CPD-58°2721

5.3a DETERMINATION OF ATMOSPHERIC PARAMETERS

In collaboration with Dr U.Heber of Kiel University, a fine-analysis of CPD-58°2721 was performed using a model atmosphere code developed at Kiel University by Dr D.Schönberner. A grid of constant flux continuum LTE model atmospheres covering the range $9{,}500K \leqslant T_{eff} \leqslant 15{,}000K$ and $0.5 \leqslant \log g \leqslant 2.0$ were generated with computers of the Technische Universität of West Berlin. The program has been described previously in detail by Hunger & Van Blerkom (1967), Wolf (1973), Schönberner (1973), and Schönberner & Wolf (1974). The atmosphere is assumed to be plane parallel, and in hydrostatic and radiative equilibrium. The models had a uniform chemical composition, with a helium abundance (number fraction) $n_{He}=0.99$. As neutral helium is the main source of opacity the

Figure 5.14 Observed flux distributions corrected for extinction of a) BD+1°4381 (T_{eff}=9,500K) b) LSIV-1°2 (T_{eff}=11,900K) c) CPD-58°2721 d) LSS 4300 (T_{eff}=14,400K).

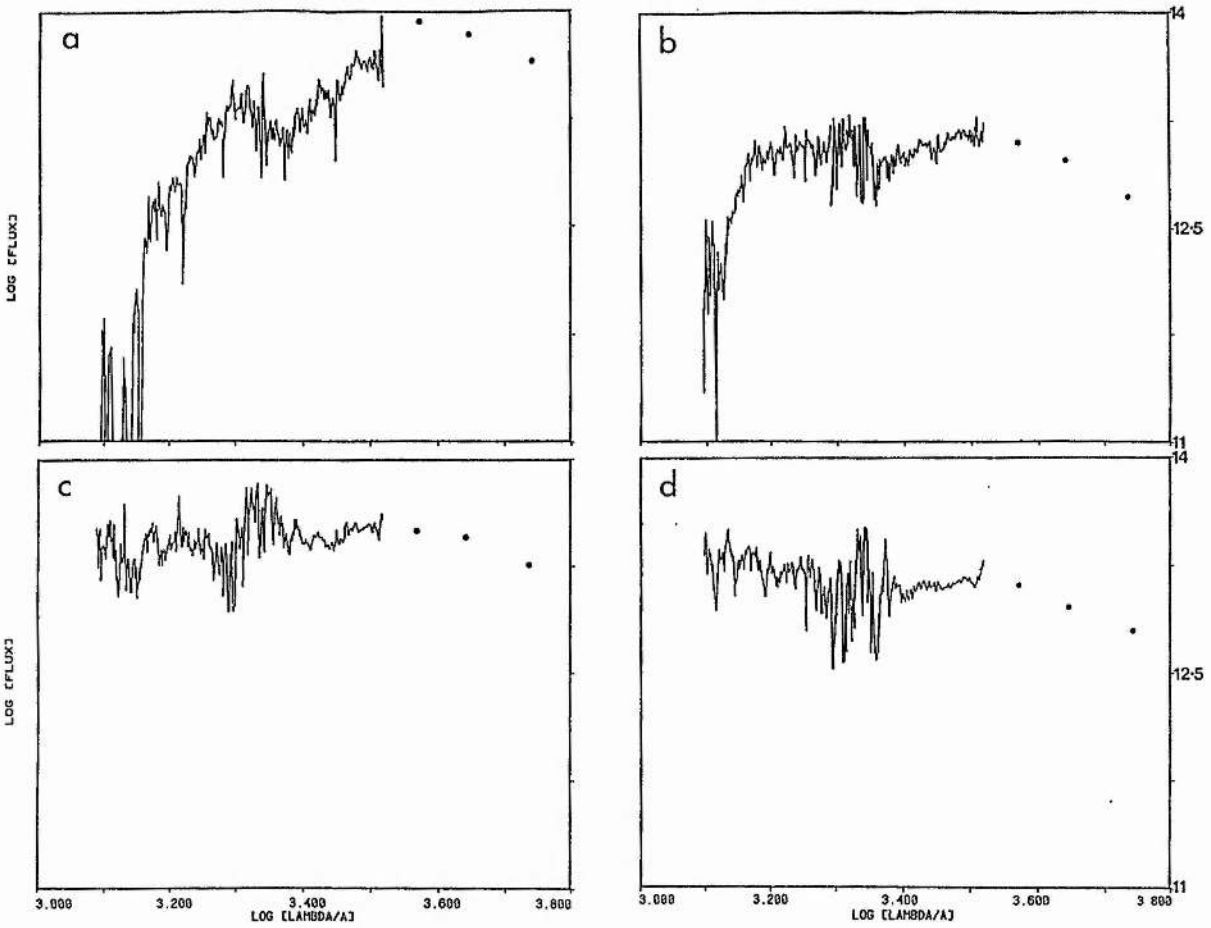

Figure 5.15 Model flux distributions for T_{eff}=9,500K log g=1.0 (bold line), T_{eff}=12,000K log g=0.5 (dash-dotted), T_{eff}=13,000K log g=1.5 (dotted), T_{eff}=14,000K log g=1.5 (thin line).

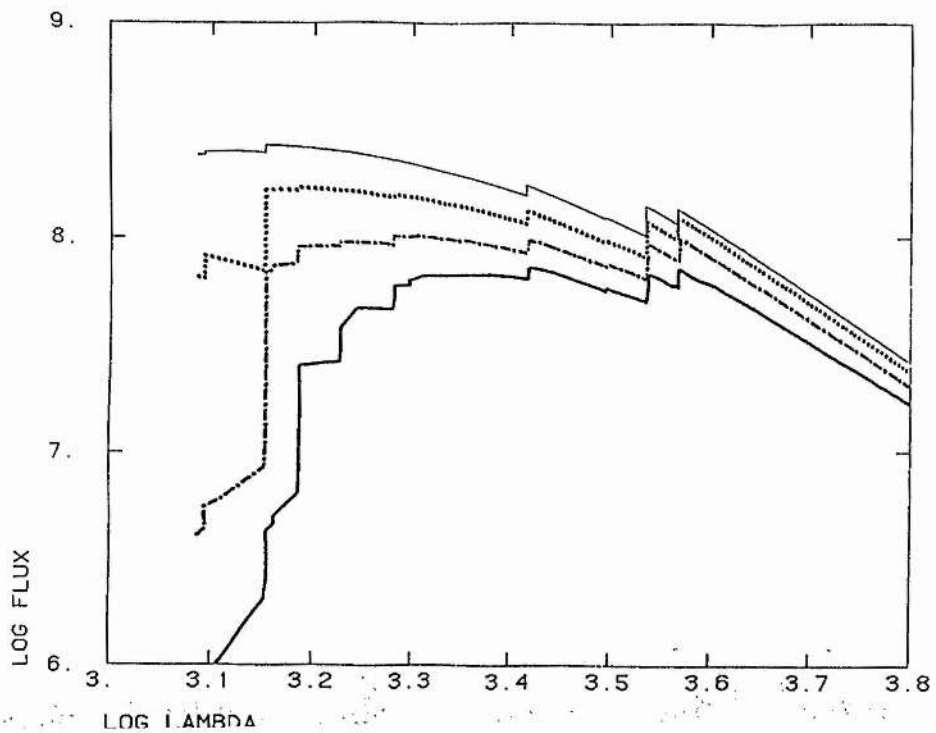

structure of the atmosphere is essentially determined by T_{eff}, g (gravity) and n_{He}. This is unlike the EHe stars in which carbon is much more abundant than in the EHdBs and can act as the main source of opacity because of the low opacity of neutral helium.

The ultra-violet spectrum of CPD-58°2721 (corrected for extinction) obtained with the IUE satellite using the SWP (1150-2000A) and LWR (1825-3300A) cameras is shown in Fig. 5.14 along with the UBV measurements (circles). A colour excess E_{B-V}=0.70 was adopted from Schönberner et al. (1982) who used the reversal of the 2200A feature as the criterion for zero reddening. The reddening law of Nandy et al. (1975) was used, normalised to R=3.2 (Seaton 1979). Also shown in Fig. 5.14 for comparison are the IUE observations and UBV measurements of the EHe stars BD+1°4381 (T_{eff}=9,500K) and LSIV-1°2 (T_{eff}=11,900K), and the EHdB LSS 4300 (T_{eff}=14,400K), each corrected for extinction using the recommendations of Drilling et al. (1984a) and Schönberner & Drilling (1984).

In the case of the single EHe stars the flux distribution of the star can give an accurate indication of T_{eff}. However, the binarity of CPD-58°2721 means that it may not be possible to use the flux distribution of the star to obtain an accurate temperature determination due to the presence of a secondary which may significantly alter the flux distribution. Schönberner et al. (1982) estimated T_{eff}=11,100K for CPD-58°2721 from ultra-violet and ground-based observations. It is obvious from a comparison of the observed flux distribution of CPD-58°2721 (Fig.5.14) with the

models, some of which are shown in Fig. 5.15, that if T_{eff}=11,100K then a flux excess is present in the SWP spectrum. KS Persei and Ups Sgr (T_{eff}=9,000K and 10,500K respectively) show far ultra-violet excesses due to the presence of a hot secondary (Drilling & Schönberner 1982), and have flux distributions like that of the hotter star LSS 4300. Schönberner & Drilling (1984) have suggested that LSS 4300 itself displays a small, far ultra-violet excess when compared to EHe stars of similar temperature. It has been possible to observe high-excitation lines directly from the hot secondaries in SWP spectra of Ups Sgr and KS Persei (Drilling & Schönberner 1982, Partharsarethy et al. 1986). This has not been possible for CPD-58^{o}2721 due to the poor signal-to-noise of its SWP spectrum.

It is necessary to include a microturbulence velocity v_t into the models to account for non-thermal broadening of spectral lines. A v_t of 10km s^{-1} was used, similar to that adopted in the analyses of Ups Sgr (Hack & Pasinetti 1963) and LSS 4300 (Schönberner & Drilling 1984). The Stark broadened HeI line profiles are sensitive to the electron density and can therefore be used to determine T_{eff} and the gravity. Similarly, the ionisation equilibrium of an element in successive stages of ionisation can supply another estimate of T_{eff} and gravity by requiring that the two ions give an agreement in abundance. The equivalent widths and profiles of 8 He lines, 5 SiII and 3 SiIII lines were computed for a range of T_{eff} and log g values. An agreement in T_{eff} and log g estimated from the HeI lines and that estimated from the SiII/SiIII ionisation ratio was found for T_{eff}=14,000K and log g=1.25. The

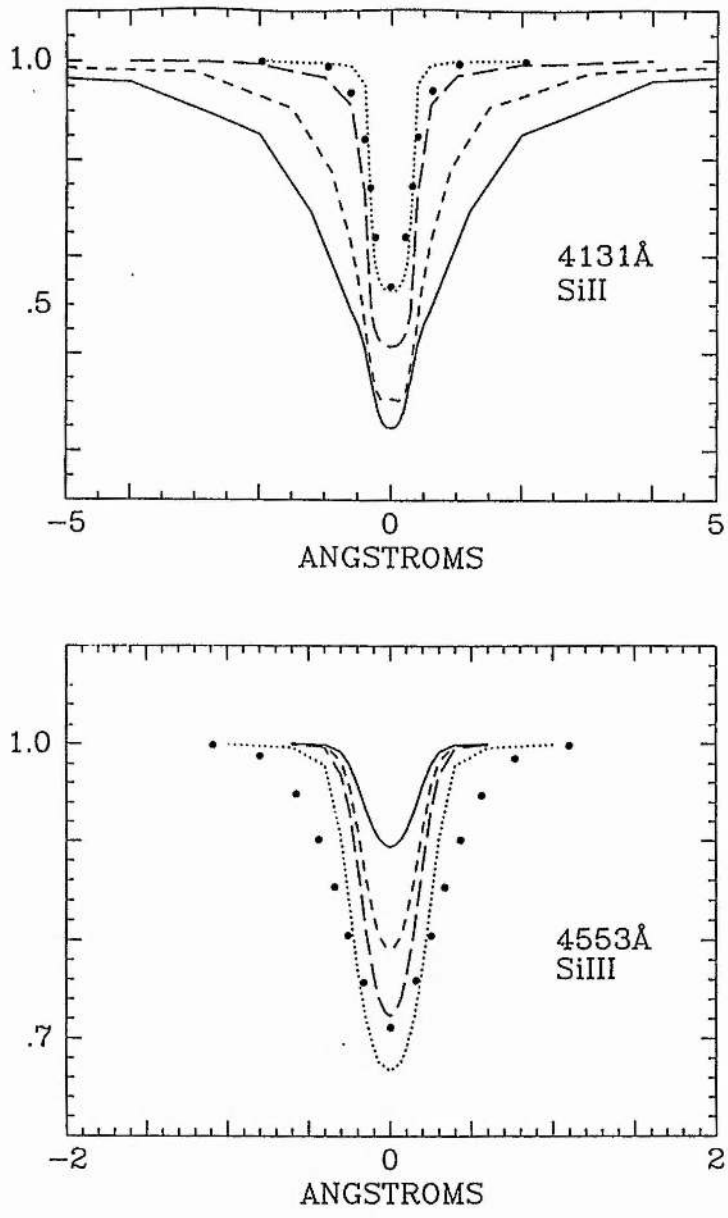

Figure 5.16 The behaviour of the computed 4131Å SiII and 4075 SiIII line profiles for various temperatures and gravities with an abundance $n_{Si}=1x10^{-4}$ and $v_t=10km\ s^{-1}$. The observed profiles are indicated by circles.

a) T_{eff}=11,000K log g=1.0 (solid line), T_{eff}=12,000K log g=1.0 (short-dashed), T_{eff}=13,000K log g=1.0 (long-dashed), T_{eff}=14,000 log g=1.25 (dotted).

b) T_{eff}=10,000K log g=1.0 (solid line), T_{eff}=11,000K log g=1.0 (short-dashed), T_{eff}=13,000K log g=1.0 (long-dashed), T_{eff}=14,000 log g=1.25 (dotted).

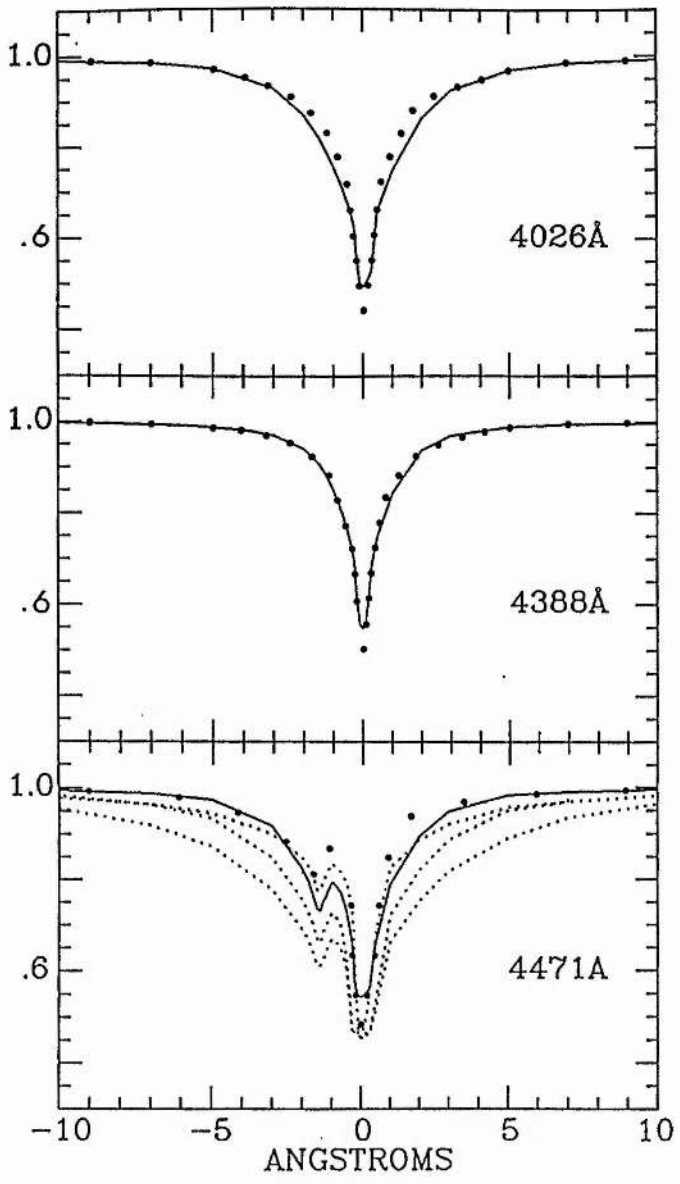

Figure 5.17 The computed (full line) and observed (circles) profiles of the HeI lines at 4026, 4388 and 4471Å for T_{eff}=14,000K and log g=1.25. The profiles (dotted) of the 4471Å line are also shown for (increasing depth) T_{eff}=10,000K and log g=1.0, T_{eff}=13,000K and log g=1.0, and T_{eff}=13,000K and log g=1.5.

errors from the fitting procedure are estimated to be $\Delta T_{eff} \approx \pm 500K$ and $\Delta \log g \approx \pm 0.25$. At this temperature there is no longer any evidence for an ultra-violet excess. Fig. 5.16 shows the behaviour of the SiII/III lines for various temperatures and gravities and an abundance of $n_S = 1 \times 10^{-4}$, somewhat smaller than that eventually adopted (2×10^{-4}). The fits at $T_{eff} = 14,000K$ and log g=1.25 would be improved with the larger abundance and inclusion of the instrumental broadening (0.25A FWHM). Fig. 5.17 shows the observed and computed profiles of the 4471A HeI line for several temperatures and gravities (the profile for $T_{eff} = 14,000K$, log g=1.5 has been omitted for clarity, but is almost identical to that for $T_{eff} = 13,000K$, log g=1.0), as well as those of the 4026A and 4388A lines in the adopted model. The importance of the silicon lines as a check on the model given by the HeI lines is demonstrated graphically in Fig. 5.17, which might otherwise have suggested $T_{eff} = 10,000K$ and log g=1.0. An additional check on the correctness of T_{eff} was by requiring that the abundances from all the lines be independent of their excitation potential. An idea of the effect on the determined atmospheric parameters caused by the omission of line-blanketing in the models is given by Heber (1983) who has estimated corrections of -300K in T_{eff} and -0.15 in log g for the EHe star HD168476, for which Walker & Schönberner (1981) determined $T_{eff} = 14,000K$ and log g=1.5.

With an estimate of T_{eff} and log g the microturbulence velocity was determined by requiring that the abundances from 10 NII and 12 SII lines show a minimum error in log n. The results shown in Fig. 5.18 indicate $v_t = 10 km\ s^{-1}$, in agreement with the

Figure 5.18 Determination of the microturbulence velocity v_t. The variance of the mean log n for 10 NII and 12 SII lines, plotted as a function of v_t (km s^{-1}).

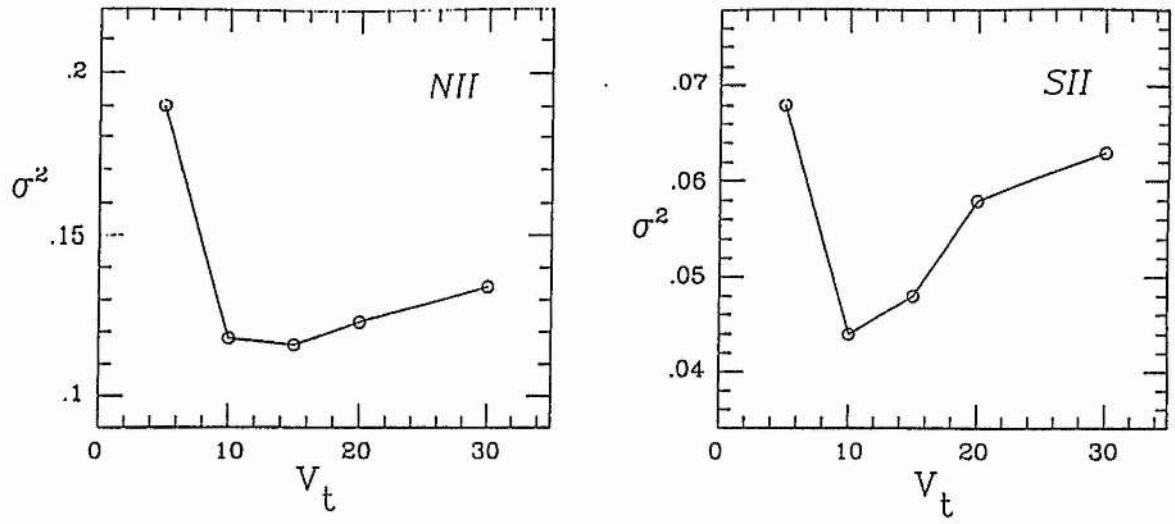

Figure 5.19 The effect of microturbulence (km s^{-1}) on the computed equivalent width of the 4643Å NII line.

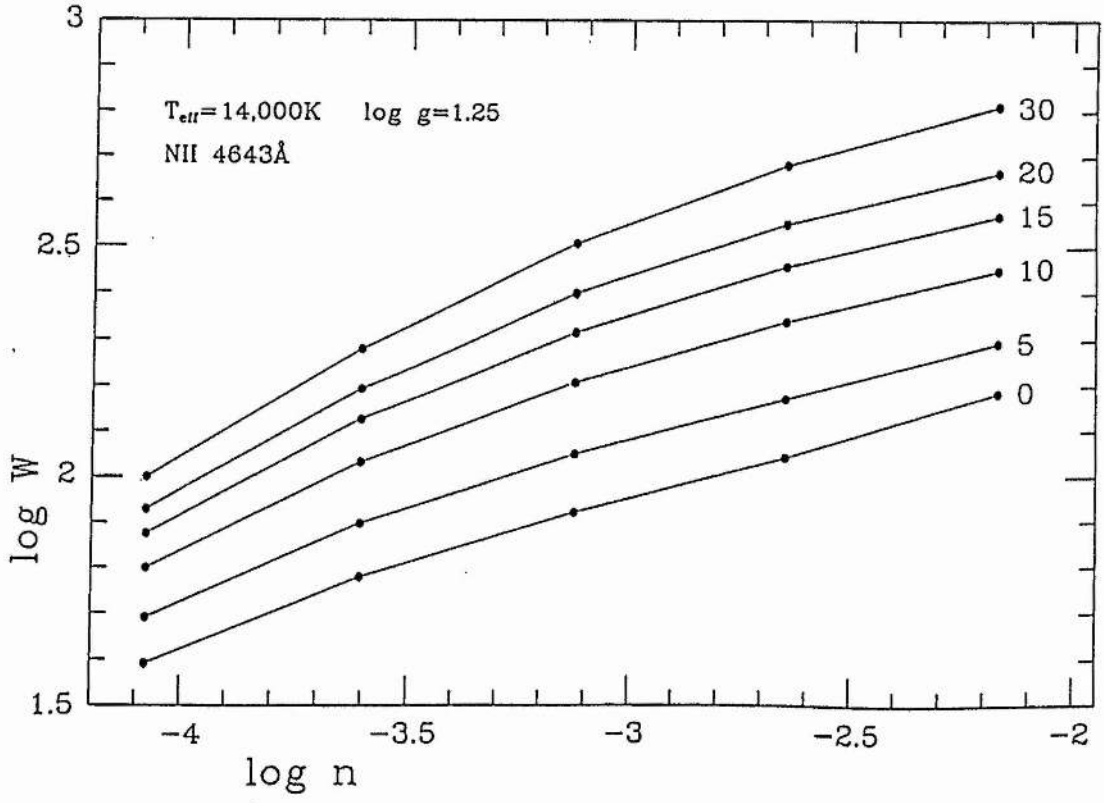

Figure 5.18 Determination of the microturbulence velocity v_t. The variance of the mean log n for 10 NII and 12 SII lines, plotted as a function of v_t (km s^{-1}).

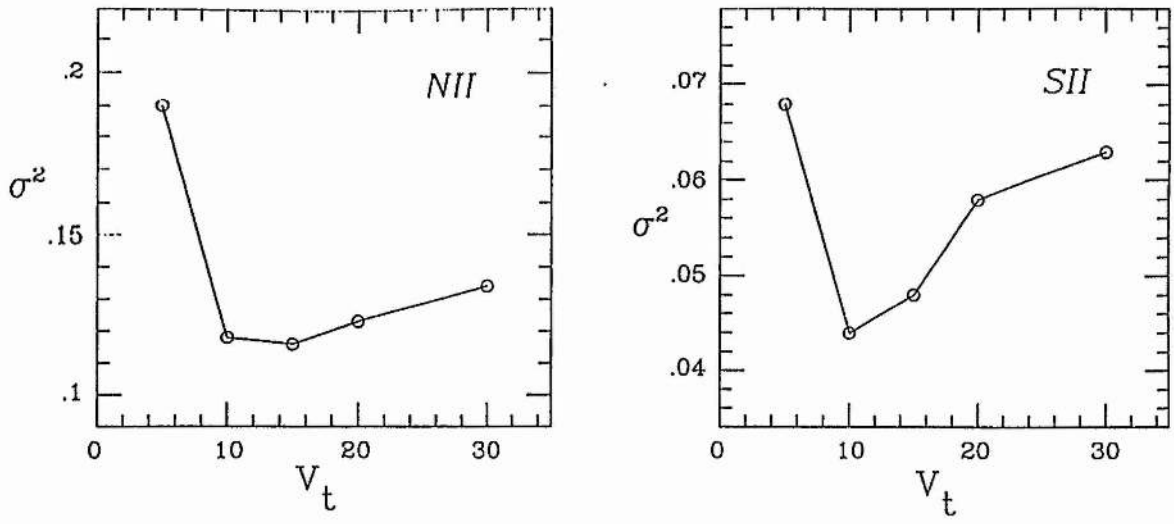

Figure 5.19 The effect of microturbulence (km s^{-1}) on the computed equivalent width of the 4643Å NII line.

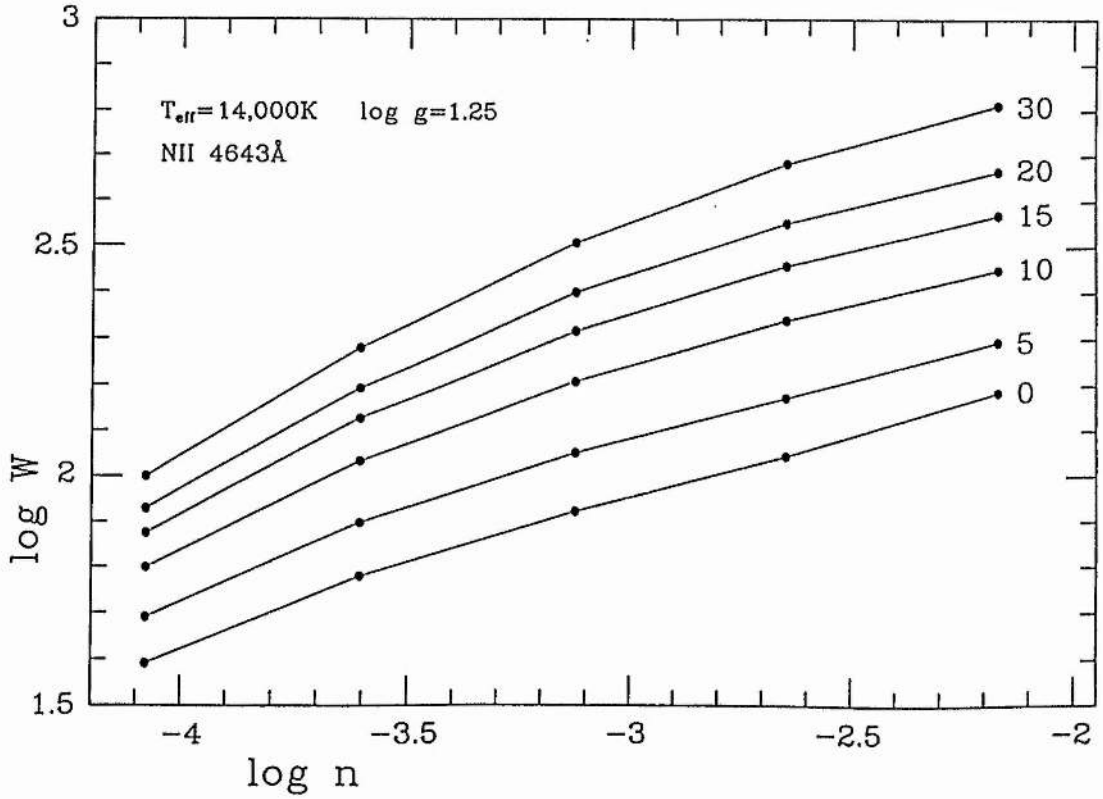

value adopted originally so that no correction to the T_{eff} and log g estimates from the v_t-dependent SiII/III equilibrium ratio was necessary. Fig. 5.19 demonstrates the effect of microturbulence on the computed equivalent width of the 4643A NII line.

5.3b ABUNDANCE DETERMINATIONS

The adopted model has T_{eff}=14,000K, log g=1.25 and n_{He}=0.99. Table 5.1 lists the multiplet number, laboratory wavelength, excitation energy, equivalent width, log gf and log n for each line used in the abundance analysis. The sources of the log gf values are indicated by initials in the column at far right. The errors given with the mean abundances are determined from the scatter between lines and do not take account of any systematic errors in f-values or uncertainties in T_{eff} and log g. Abundances were determined from individual curves of growth computed for each line except for TiII, CrII, and FeII for which, because of the greater number of lines involved, curves computed at 3900, 4200, 4500 and 4800A (Fig. 5.20) were used. That the curves are different in Fig. 5.20 is due to changes in opacity with wavelength. Fig. 5.21 is a theoretical curve of growth for all SII lines identified in the spectrum, although only 12 lines were judged to be sufficiently well-defined to be usable in the abundance determination. The NII and SII abundances were calculated first as these elements were used in the determination of the microturbulence velocity. The only carbon line present (Fig. 5.7) is the 4267A CII_6 line, which is blended but resolvable with SII_{49}.

Table 5.1 Lines used to derive element abundances.

mult no.	Line	eV	W(mA)	log gf	-logn	Source
HI					2.30	WSG
HeI					0.004	GJK
CII						
6	4267.14	17.96	138	0.96	4.26	WSG
NII						
5	4613.87	18.39	110	-0.59	2.89	DH
	4643.09	18.40	173	-0.37	2.55	DH
	4621.39	18.39	180	-0.47	2.40	DH
	4607.15	18.38	185	-0.47	2.36	DH
12	3995.00	18.42	243	0.30	2.79	DH
20	4803.27	20.58	62	-0.12	3.04	WSG
	4788.13	20.56	49	-0.37	2.99	WSG
38	4082.28	23.03	66	-0.34	2.17	GR
39	4041.32	23.04	67	0.85	3.19	WSG
	4044.75	23.03	37	-0.44	2.43	WSG
	n=10				$2.68^{+}_{-}0.34$	
MgII						
4	4481.20	8.83	540	0.98	3.29	WSM
10	4390.60	9.96	152	-0.50	3.80	WSM
	4384.65	9.95	146	-0.78	3.57	WSM
18	4739.59	11.52	129	-0.42	3.43	WSM
25	4851.10	11.58	161	-0.68	3.25	WSM
28	4193.44	11.58	94	-1.07	3.25	WSM
	n=6				$3.43^{+}_{-}0.22$	
SiII						
3	4130.90	9.80	369	0.60	3.74	SG
3.01	4075.45	9.84	118	-1.40	3.74	SG
	4076.78	9.84	77	-1.67	3.80	SG
7.06	4200.79	12.53	170	-0.42	3.49	SG
7.26	4198.13	13.49	76	-0.61	3.41	SG
	n=5				$3.64^{+}_{-}0.17$	
SiIII						
2	4552.65	19.02	250	0.29	3.42	WSM
	4567.85	19.02	124	0.07	4.20	WSM
	4574.80	19.02	109	-0.41	3.86	WSM
	n=3				$3.83^{+}_{-}0.39$	
SII						
9	4716.23	13.56	166	-0.52	4.17	WSM
	4656.74	13.53	150	-0.81	4.03	WSM
40	4524.68	15.00	223	0.12	4.00	WSM

43	4483.42	15.83	75	-0.43	4.13	WSM
	4432.41	15.80	43	-0.46	4.43	WSM
44	4162.70	15.88	157	0.78	4.64	WSM
	4153.10	15.83	151	0.62	4.55	WSM
45	3946.98	15.78	36	-0.84	4.14	WSM
46	4792.02	16.07	75	-0.12	4.33	WSM
49	4282.63	16.03	82	-0.10	4.41	WSM
59	4032.81	16.18	145	0.24	4.09	WSM
66	4259.18	17.37	94	0.52	4.32	WSM
	n=12				4.27 ± 0.21	
TiII						
11	4012.37	0.57	105	-1.61	4.77	DK
	4395.03	1.08	126	-0.47	5.58	W
	4450.49	1.08	47	-1.45	5.26	DK
20	4294.10	1.08	210	-1.05	4.21	RAS
31	4501.27	1.11	120	-0.75	5.37	DK
40	4417.72	1.16	35	-0.86	5.96	RAS
41	4290.22	1.16	71	-0.80	5.62	W
	4300.05	1.18	144	-0.47	5.38	W
	4307.90	1.16	75	-1.15	5.24	W
	4301.93	1.16	48	-1.16	5.48	DK
	4312.86	1.18	76	-1.16	5.22	DK
	4314.98	1.16	77	-1.13	5.24	DK
50	4563.76	1.22	74	-0.84	5.60	W
	4589.96	1.23	74	-1.73	4.71	RAS
51	4399.77	1.23	58	-1.32	5.21	DK
	4394.06	1.22	13	-1.59	5.66	DK
82	4571.97	1.56	118	-0.65	5.34	RAS
94	4350.83	2.05	17	-1.74	5.08	RAS
105	4163.64	2.58	83	-0.30	5.56	RAS
	4171.90	2.59	63	-0.56	5.46	RAS
114	4874.02	3.08	32	-1.01	5.18	RAS
115	4411.08	3.08	38	-1.32	4.77	RAS
	n=22				5.27 ± 0.39	
CrII						
18	4113.24	3.09	26	-3.11	4.23	KP
19	4051.97	3.09	47	-2.51	4.60	KP
26	4207.35	3.81	33	-2.68	4.21	KP
	4086.14	3.70	30	-2.61	4.32	KP
30	4824.13	3.85	320	-1.20	4.70	KP
	4848.24	3.85	117	-1.35	4.79	KP
	4864.32	3.84	99	-1.66	4.60	KP
	4876.48	3.84	113	-1.59	4.56	KP
	4812.35	3.85	51	-2.23	4.53	KP
	4836.22	3.84	57	-2.22	4.40	KP
31	4242.38	3.85	212	-1.70	3.82	KP
	4261.92	3.85	95	-1.93	4.39	KP
	4275.57	3.84	81	-2.12	4.32	KP
44	4558.66	4.06	196	-0.69	4.72	KP
	4588.22	4.06	181	-0.87	4.66	KP
	4618.83	4.06	130	-1.10	4.91	KP
	4634.11	4.05	115	-1.25	4.81	KP
	4555.02	4.05	64	-1.53	4.79	KP
	4592.09	4.06	87	-1.48	4.82	KP
	4616.64	4.05	79	-1.59	4.72	KP
162	4224.85	5.31	95	-1.70	4.15	KP

165	4098.44	5.31	54	-1.37	4.95	KP
192	4256.16	6.46	32	-1.44	4.56	KP
193	4070.90	6.46	54	-1.02	4.60	KP
	n=24				$4.55^{+}_{-}0.27$	
MnII						
5	4755.73	5.37	57	-1.51	4.64	KP
6	4326.76	5.37	41	-1.60	4.64	KP
	4345.6	5.37	20	-2.38	4.33	KP
	n=3				$4.54^{+}_{-}0.18$	
FeII						
3	3938.29	1.66	70	-3.89	3.31	GI
27	4273.32	2.69	102	-3.34	3.20	GI
	4303.17	2.69	176	-3.83	3.83	GI
	4351.76	2.69	190	-2.20	3.53	K
	4385.38	2.77	147	-2.47	3.66	FMWY
	4416.82	2.77	150	-2.34	3.78	FMWY
28	4122.64	2.57	111	-3.11	3.37	FMWY
	4178.85	2.57	230	-2.59	2.87	FMWY
	4296.57	2.69	140	-3.01	3.27	GI
29	3974.16	2.69	79	-3.51	3.26	GI
32	4314.29	2.66	68	-3.56	3.26	K
	4338.70	2.68	39	-4.20	2.91	K
37	4489.19	2.82	94	-2.92	3.62	FMWY
	4491.40	2.84	122	-2.56	3.77	FMWY
	4515.34	2.83	186	-2.48	3.32	FMWY
	4629.34	2.79	172	-2.37	3.63	FMWY
	4582.83	2.83	82	-3.08	3.57	FMWY
	4520.23	2.79	176	-2.60	3.31	FMWY
38	4508.28	2.84	187	-2.21	3.58	GI
	4522.63	2.83	219	-2.11	3.39	FMWY
	4541.52	2.84	134	-2.57	3.69	FMWY
	4576.33	2.83	117	-2.97	3.42	FMWY
	4583.83	2.79	243	-1.80	3.52	FMWY
	4620.51	2.82	75	-3.15	3.57	GI
43	4731.44	2.88	79	-3.36	3.26	GI
186	4625.91	5.93	60	-2.62	3.11	K
	4635.33	5.93	159	-1.65	3.34	K
187	4069.88	5.89	43	-3.08	2.89	K
	4111.90	5.93	51	-2.42	3.34	K
221	4449.66	7.89	40	-1.95	3.25	K
	n=30				$3.40^{+}_{-}0.26$	
FeIII						
4	4419.59	8.21	190	-2.33	3.89	KP
	4395.78	8.22	148	-2.71	3.88	KP
	n=2				3.89	
NiII						
1	4244.80	4.01	62	-2.67	4.64	KP
9	4362.15	4.01	83	-2.71	4.44	KP
11	4067.05	4.01	181	-1.86	4.51	KP
12	4015.50	4.01	113	-2.46	4.45	KP
	n=4				$4.51^{+}_{-}0.09$	

References

DH Dufton & Hibbert (1981) DK Danzmann & Kock (1980)
FMWY Fuhr, Martin, Wiese & Younger (1985) GI D.Gigas (1986, private communication) GJK Green, Johnson & Kolchin (1966)
GR Griem (1964) K Kurucz (1981) KP Kurucz & Peytremann (1975)
RAS Roberts, Andersen & Sørensen (1973) SG Schulz-Gulde (1969)
W Wobig (1962) WSG Wiese, Smith & Glennon (1969)
WSM Wiese, Smith & Miles (1966)

Figure 5.20 Theoretical curves of growth for FeII (top to bottom) at 3900, 4200, 4500 and 4800Å.

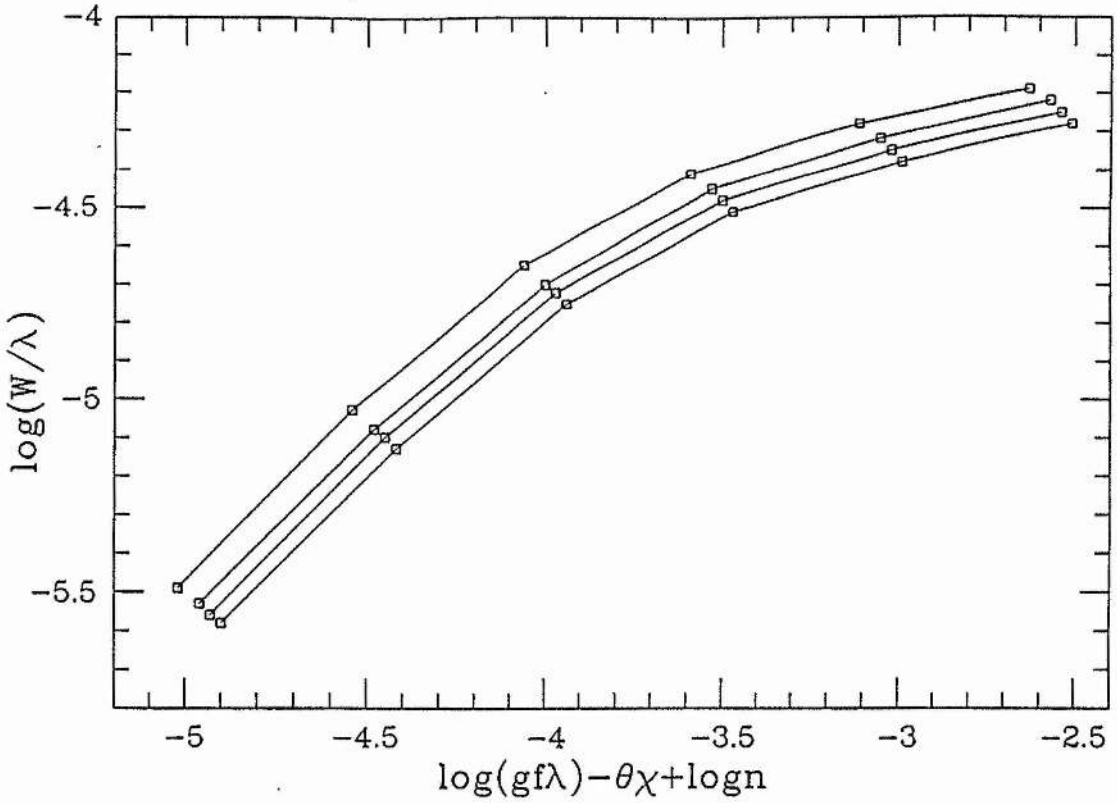

Figure 5.21 The theoretical curve of growth for all 34 SII lines identified in the spectrum with $n_S=8x10^{-5}$.

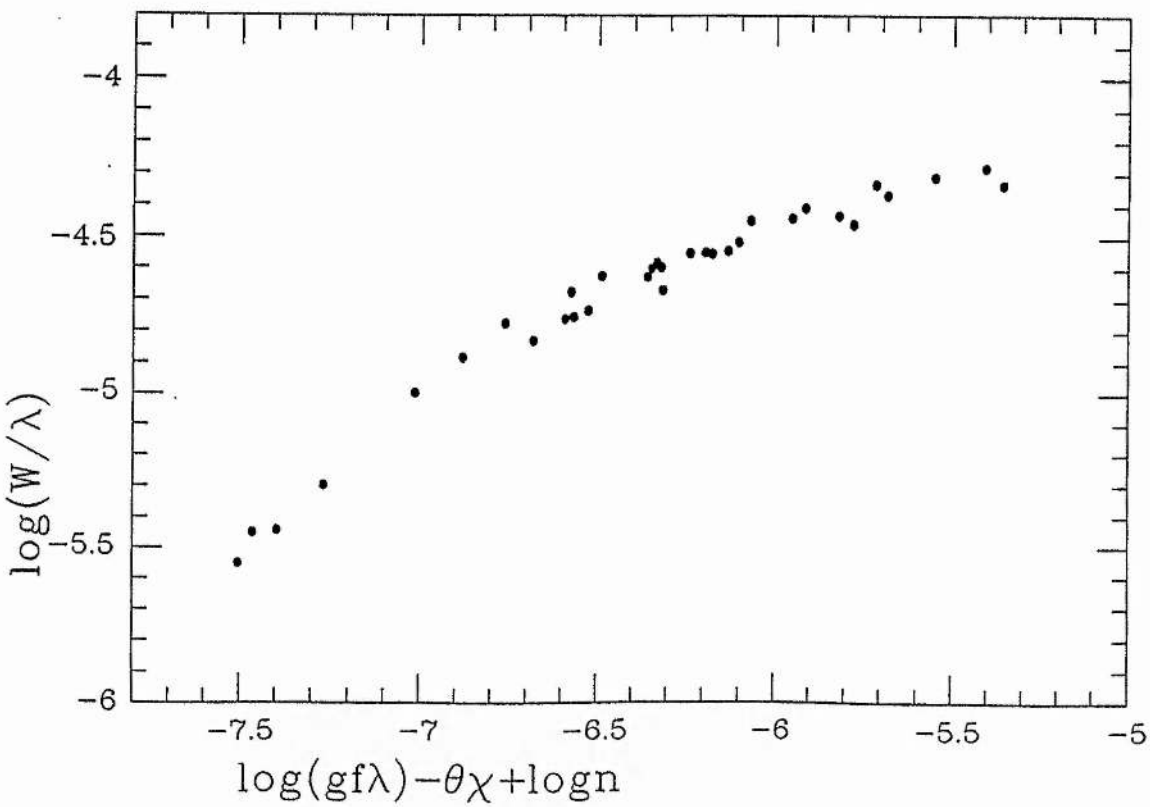

Figure 5.20 Theoretical curves of growth for FeII (top to bottom) at 3900, 4200, 4500 and 4800Å.

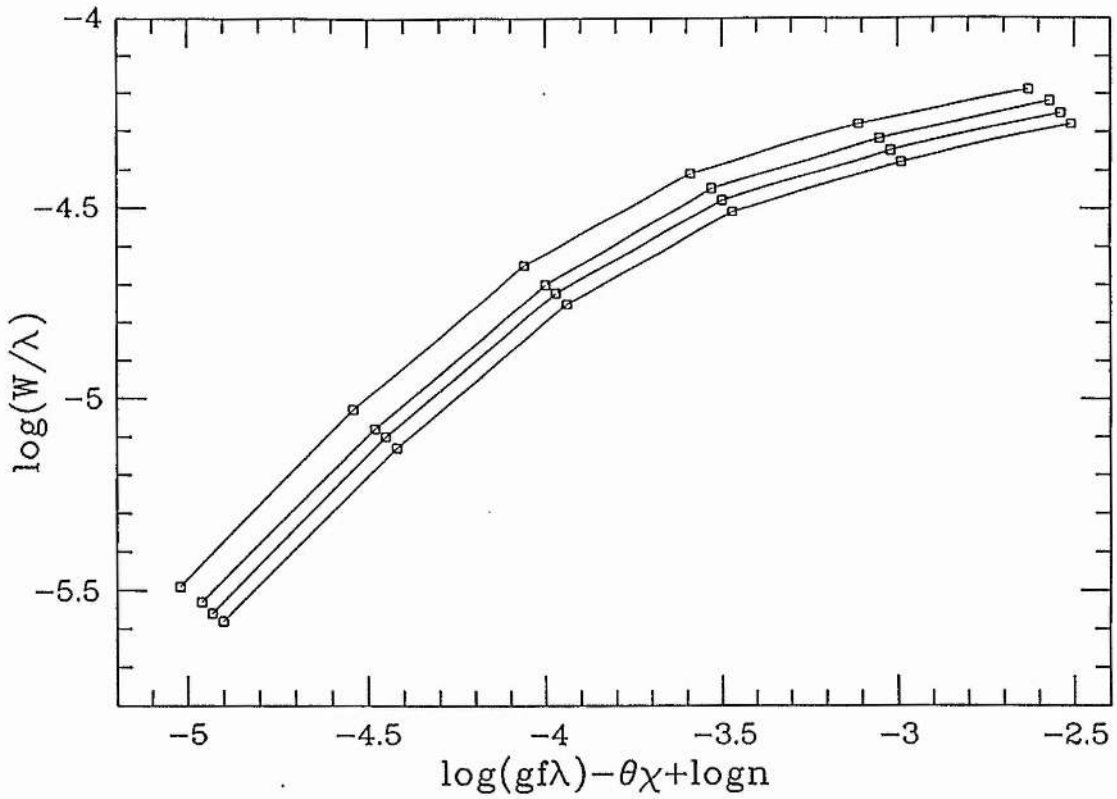

Figure 5.21 The theoretical curve of growth for all 34 SII lines identified in the spectrum with $n_S=8x10^{-5}$.

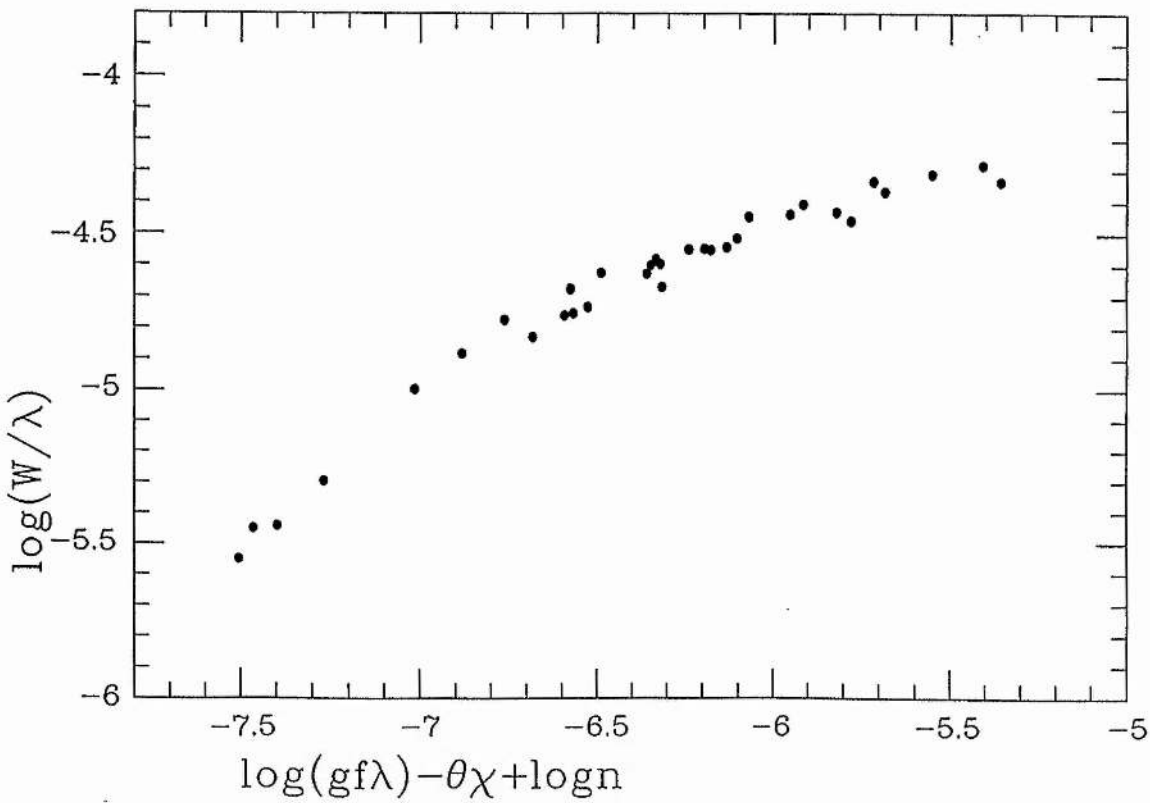

Knowing the sulphur abundance, the contribution to the equivalent width from the SII line was computed and subtracted, leading to an estimate for the carbon abundance of $n_C=5x10^{-5}$. A hydrogen abundance $n_H=5x10^{-3}$ was determined from the three lines Hγ, δ and ϵ. Fig. 5.22 shows the observed and computed profiles for Hδ with $n_H=5x10^{-4}$ and $5x10^{-3}$. As has been shown in Sect. 5.2b, the two Balmer lines of lowest excitation occur in emission. The other H lines are present only in absorption, although it may be the case that they are partly filled in by emission. The H abundance may therefore actually be higher than that estimated here.

The average elemental abundances listed in Table 5.2 have been normalised such that $\Sigma n_i \mu_i=12.15$ (where n_i is the number fraction and μ_i is the atomic weight number of element i) to allow comparison with stars of 'normal' composition. This is appropriate when the hydrogen is assumed to have been burnt to helium. The mass fractions are X=0.001, Y=0.973 and Z=0.026 (to which $Z_N=0.007$ is the largest single contributor). The abundances of CPD-58°2721 and HD168476 relative to the sun are shown in Fig. 5.23. Also shown relative to the sun are the abundances of LSS 4300 determined from a preliminary fine analysis of the star by Schönberner & Drilling (1984).

The observed abundances give important clues to the star's nuclear history and its likely progenitors and descendants. The most notable chemical distinction between the EHdBs and the EHe stars is the N/C ratio. The ratio $n_N:n_C=40$ calculated here for

Figure 5.22 Observed (circles) and computed profile of Hδ for $n_H = 5x10^{-4}$ (dashed line) and $5x10^{-3}$ (solid line).

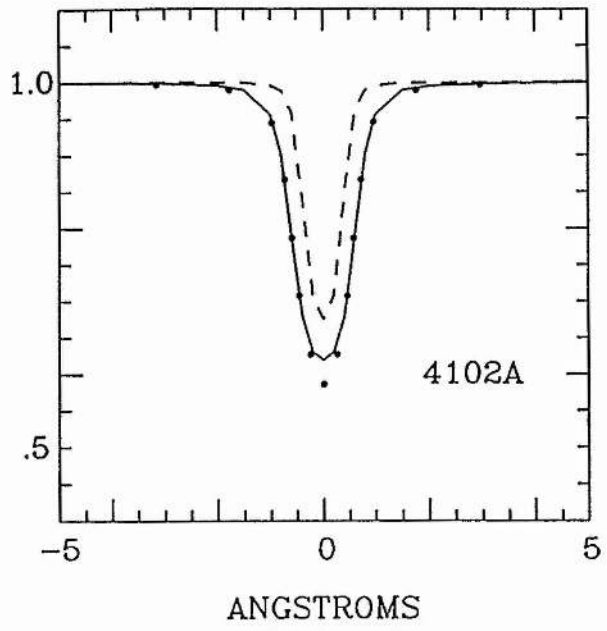

Table 5.2 Atmospheric parameters and normalised abundances for CPD-58°2721 and related objects.

	CPD-58°2721	LSS 4300[1]	HD168476[2]		
Teff(K)	14,000	14,400	14,000		
log g	1.25	1.4	1.5		
log L/M	4.7	4.6	4.5		
Abundances normalised to $\Sigma n_i \mu_i = 12.15$				B Stars[3]	Sun[4]
H	9.2	9.0	< 7.8	12.0	12.0
He	11.5	11.5	11.5	11.0	11.0
C	7.3	8.0	9.5	8.6	8.7
N	8.9	9.3	8.9	7.9	8.0
Mg	8.1	7.9	7.7	7.3	7.5
Si	7.8	7.8	7.7	7.5	7.5
S	7.3		7.0	7.2	7.2
Ti	6.3		5.7	4.5	4.9
Cr	7.0		6.2	5.5	5.6
Mn	7.0		6.2		5.5
Fe	8.1	7.5	7.5	7.6	7.5
Ni	7.0		6.5	5.1	6.2

References: 1.Schönberner & Drilling (1984) 2.Walker & Schönberner (1981) 3.Scholz (1972) 4.Holweger (1979).

CPD-58°2721 is higher than that observed in LSS 4300 and Ups Sgr ($n_N:n_C$ 20; Hack & Pasinetti 1963, Schönberner & Drilling 1984). The N/C ratio observed in the atmospheres of the EHdBs has been explained as the exposure of CNO-processed material at the surface of the star following mass-transfer (Schönberner & Drilling 1983). For the CNO-cycle in equilibrium, essentially all the CNO nuclei are converted to ^{14}N. The EHe stars also show the products of the CNO-cycle but with an admixture of the products of He-burning, about one percent of the helium having been converted to ^{12}C with the result that the $n_N:n_C$ ratio is roughly reversed to that observed in the EHdBs. The presence of the products of He-burning has been interpreted as direct evidence for mixing of the deep interior and the stellar surface (Paczynski 1971) which cannot have occurred in the EHdBs.

Hydrogen appears relatively abundant in CPD-58°2721 and LSS 4300 ($n_H > 10^{-3}$) when compared with that observed in the EHe stars ($n_H \ll 10^{-3}$) and the two cooler EHdBs Ups Sgr and KS Persei ($n_H \leqslant 10^{-4}$). Whereas the iron abundance in LSS 4300 and HD168476 is approximately solar, in CPD-58°2721 it appears overabundant by about 4 times. The iron group (Ti, Cr, Fe) as a whole is enriched (by an average of 0.4 dex), and the intermediate Z elements (Mg, Si, S) to a lesser extent (0.2 dex), against that observed in HD168476. However, as the differences are comparable with the individual errors for the mean abundance in each star, the results presented here should only be considered as suggestive of abundance differences.

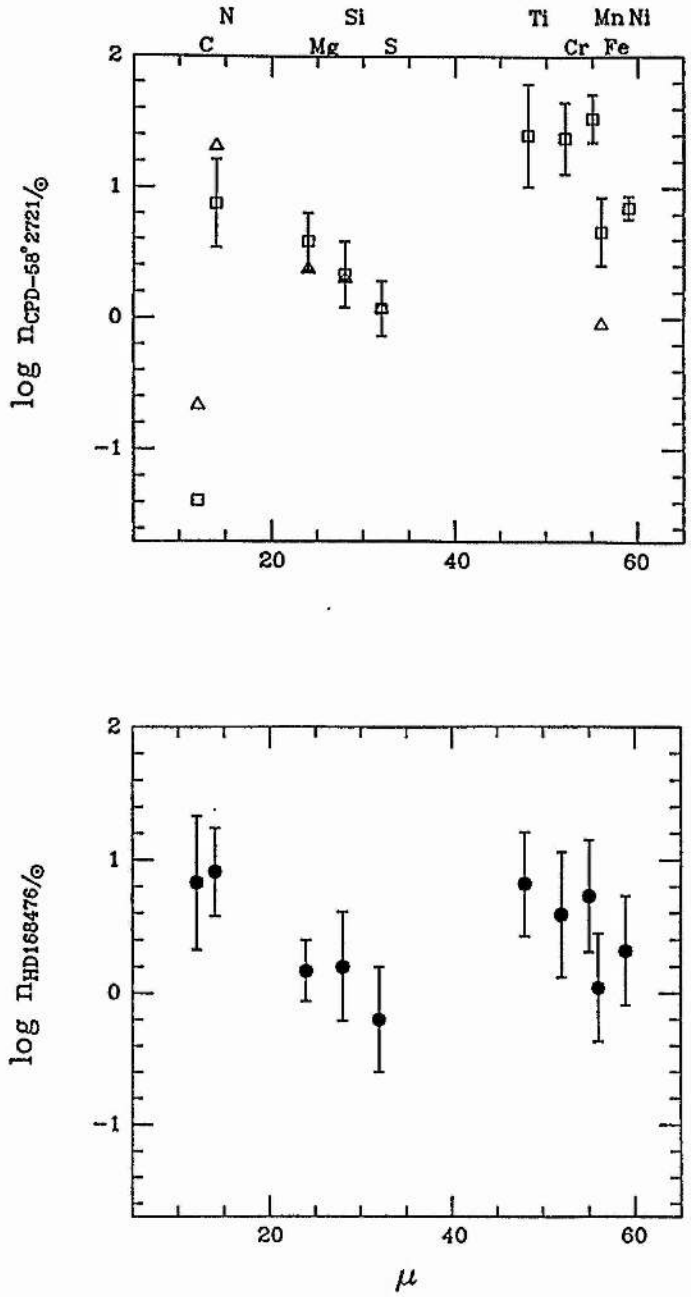

Figure 5.23 Abundances of CPD-58°2721 (top) and HD168476 shown relative to the sun. Uncertain values are shown without errorbars. The abundances of LSS 4300 relative to the sun are also shown and are indicated by open triangles.

Whereas the lighter elements can be affected by nuclear processing, the heavier elements presumably have maintained their primordial abundance and are essentially that of the interstellar medium out of which the star formed. The heavy metal content in CPD-58°2721 is consistent with the idea that it belongs to a young population of stars. This is supported by the observation that the EHdBs lie close to the plane of the galaxy and follow the galactic rotation (Drilling & Heber 1986, Jeffery et al. 1987a). The suggestion of a difference in the heavy metal content between CPD-58°2721 and LSS 4300, and in turn their greater abundance of hydrogen relative to that observed in Ups Sgr and KS Persei, suggests that the EHdBs do not form a homogeneous group with respect to their chemical composition. This would not be unexpected as the EHe stars show significant inhomogeneities in chemical composition and do not appear to belong to one single population (Heber 1983, 1986).

Knowing T_{eff} and log g allows the luminosity-mass ratio L/M to be determined. For CPD-58°2721 $\log L/M = T_{eff}^4/g = 4.7\pm0.3$ (solar units), whilst the corresponding estimate for LSS 4300 is 4.6. It was noted in Sect. 5.1b that CPD-58°2721 might be associated with the Eta Carina nebula at a distance of 2.7kpc, in which case $M_V = -4$. In order to calculate a luminosity it is necessary to know the bolometric correction. Adopting a correction of -1.0 ± 0.4 mag (Allen 1973), and using the relation $M_{bol} = 4.75-2.5\log L/L_\odot$, leads to $\log L/L_\odot = 3.9\pm0.2$. As the EHdBs are believed to have

masses in the range 0.5-2$M_{\odot}$ (Plavec 1986), the luminosity estimates from the L/M ratio would seem to be incompatible with a distance of 2.7kpc for the star. Even for the most favourable estimate d > 3kpc. The conclusion has to be drawn that CPD-58^{o}2721 is more distant than the Carina nebula, and that the the alignment of the star with a feature in the nebula is coincidental.

Summary of Work

A photometric study of the EHdBs and the EHe stars has detected four new variables (BD+1°4381, BD-1°3438, LSIV-1°2, CPD-58°2721), confirmed the suspected variability in a further two (LSII+33°5 and BD-9°4395), and shown that the variability of Ups Sgr is due to pulsation rather than to eclipses. The presence of colour changes in all but BD-9°4395 coincident with the luminosity variations, indicates that they are radial pulsators. The photometric variability of BD+1°4381 ($\sim$21 days) appears to represent a straightforward extension of radial pulsation in RCB stars to higher temperatures. The shorter timescale (5-8 days) of the variations in BD-1°3438 is consistent with radial pulsation of the star in its first overtone-mode. Variability in LSIV-1°2 appears to be due to a single period of $\sim$11 days. LSII+33°5 (T_{eff}=15,000K) falls in a temperature range previously devoid of confirmed variability in the EHe stars. Its irregular behaviour is like that of BD-1°3438, but on a shorter timescale of 3-4 days. So far, all the stars studied in detail in the range 9,500-15,000K have proved to be photometric variables. Similar to HD160641 the hotter star BD-9°4395 (T_{eff}=23,000K) does not show colour changes. The timescale of the variations, together with the absence of detectable colour changes, suggests that the variability of the star is due to non-radial pulsation. The change from radial to non-radial pulsation can be understood as an increase in surface gravity.

Three of four known EHdBs were observed. The observations of KS Persei suggest light and colour changes on a timescale of ~5 days, in addition to the ~30-day light variation previously reported. The light curve of CPD-58°2721 was subjected to a detailed frequency analysis. The presence of significant peaks in the Fourier transform of the light curve indicates that the light-curve is not completely irregular. A Fourier decomposition to elucidate strictly-periodic structure indicates that the general features of the light curve may be reconstructed from two sine-waves with periods of 9.3 and 14.1 days. The observations are insufficient, however, to allow a claim for multi-periodicity. Similar to the light curves of the other hydrogen-deficient stars it appears that it may be represented adequately by a quasi-periodic variation, with a mean period of 9.4 ± 1.5 days. No variation was found in the light curve which could be related to a binary period for the star which suggests that CPD-58°2721 is not an eclipsing binary.

The light variability of Ups Sgr had previously been ascribed to eclipses. The detailed photometric investigation of Ups Sgr presented here has failed to detect any evidence for eclipses but has revealed the presence of 20-day and 239-sec periodicities in the light curve. The large-amplitude (0.17 mag in V) quasi-periodic 20-day variation is clearly to be identified with radial pulsation of the supergiant primary in its fundamental mode. The origin of the coherent, small-amplitude (~0.02 mag) 239-sec pulsations is unclear.

Assuming Ups Sgr to comprise a $1M_{\odot}$ supergiant primary with T_{eff}=10,500K and a main-sequence companion, a grid of synthetic binary-star light curves were generated at wavelengths of 1600A and 5500A for various inclinations of the binary system to the line of sight. The small amplitude of any ellipsoidal light variations in the observed light curve implies a small inclination ($i \lesssim 30^{\circ}$), which from the mass function gives a secondary mass $\gtrsim 12M_{\odot}$. This is a mass-ratio much more extreme than previously thought. The models of the light curve indicate that a main-sequence secondary of $\backsim 11M_{\odot}$ and approximate spectral type B2 is consistent with the observed flux equivalency of the components at 1600A, and the concomitant non-detection of the secondary at optical wavelengths due to the dominance of the primary in the optical region.

The evolutionary history of Ups Sgr can be understood in terms of binary evolution involving two episodes of Roche-lobe overflow by the primary, which was originally the more massive component with a primordial mass in the range $\backsim 7\text{-}10M_{\odot}$. Ups Sgr is presently in a slow phase of mass-transfer in which the secondary is able to accrete all the mass lost by the primary, a consequence of the extreme mass-ratio. Depending on the effects of a future common-envelope phase(s), orbital shrinkage may bring the components sufficiently close to allow merging of the components in a Hubble time. However, Ups Sgr can not be regarded as a precursor of the RCB or EHe stars through a future merging of the binary components. Merging must produce a Type I supernova as the mass of the components would be above the Chandrasekhar limit. In the

absence of merging, a supernova event may still result if the secondary is sufficiently massive that it will be unable to avoid core collapse, otherwise Ups Sgr is destined to consist of a pair of degenerate dwarfs, each of $\sim 1 M_{\odot}$.

On photographic plates, CPD-58°2721 appears to be associated with a bright knot in the Eta Carina nebula. A spectroscopic study of the knot shows it to have a nebular emission spectrum typical of a low excitation HII region, with $T_e = 10^4$K and $N_e \simeq 10^2 cm^{-3}$. The radial velocity of the ionised hydrogen in the knot is consistent with the velocity of the ionised gas in the the surrounding Carina nebula. The heavy reddening of CPD-58°2721 indicates that the star lies within, or at a greater distance than, the Carina nebula. The size of the knot at the distance of the Carina nebula would be consistent with ionisation by a hot secondary of a similar spectral type as have been detected in Ups Sgr and KS Persei. That the ultra-violet spectrum of CPD-58°2721 is due primarily to the visible star does not preclude the existence of a hot secondary.

A fine abundance analysis of CPD-58°2721 was performed using a grid of constant flux continuum model atmospheres. The effective temperature and gravity were determined from the HeI line profiles and the ionisation equilibrium ratio of SiII/III. The model adopted has $T_{eff} = 14{,}000$K, $\log g = 1.25$ and $n_{He} = 0.99$. A microturbulence velocity of 10km s^{-1} was estimated using the NII and SII lines. The large $n_N : n_C = 40$ ratio can be understood as CNO-processed material revealed at the surface of the star following mass-transfer, and is somewhat higher than that found for

Ups Sgr and LSS 4300. The suggestion of a heavy-metal overabundance against that observed in LSS 4300, and the larger abundance of hydrogen in LSS 4300 and CPD-58°2721 to that estimated for Ups Sgr and KS Persei, suggests that the EHdBs are not homogeneous in their chemical composition.

Suggestions for future work

The unexpected detection of a 239-second period in the light curve of Ups Sgr presents a dilemma as the extremely short timescale of the luminosity variations appears inconsistent with variations of the supergiant primary or the main-sequence secondary. Further observations are needed to rule out the possibility, however unlikely, of an instrumental origin. As yet, it has not been possible to find any evidence for eclipses in the three EHdBs studied in detail. A search should be made for eclipses in LSS 4300, as their detection would allow determination of important system parameters. More accurately defined radial-velocity curves would help greatly in the search for eclipse-related variations. In this respect radial-velocity measurements are a matter of urgency for CPD-58°2721 and LSS 4300. If a sufficient number of contemporary radial-velocity measurements of Ups Sgr become available it may be possible to detect a changing mass-ratio from a change in the binary period over the last 60 years and so provide a useful check on evolutionary models.

The results of the photometric monitoring indicates the EHdBs and the EHe stars display similar photometric behaviour. The EHdBs are the result of an evolution involving mass-transfer whilst the EHe and RCB stars show no evidence of binarity and consequently must have a different evolutionary history. The fact that both groups have similar pulsational characteristics indicates that the overall structure of their outer layers, at least, must be comparable in spite of their different evolutionary status. It is important to continue and extend the observations in order to see whether the binaries behave as members of the EHe stars and to identify the existence and extent of a pulsational instability region. In the long term, evidence for period changes could indicate evolutionary effects. This demands sustained and continuous monitoring in order to determine the precise behaviour of these variables. Although a large amount of telescope time is required, the programme is well suited to small telescopes. It was regrettable that an additional 2 weeks awarded at the OSN in 1985 by the Panel for the Allocation of Telescope Time was later withdrawn by the SERC.

In the understanding of the evolutionary history of the EHdBs and the EHe stars an important clue comes from the precise knowledge of integral stellar parameters and the surface composition. Atmospheric parameters and abundances have so far only been determined for 5 EHe stars and 3 EHdBs. The sample needs to be increased greatly in order to investigate to what extent inhomogeneities exist between objects. The necessary high quality

spectroscopic data already exists to perform the analyses. It should then be possible to address the problem of the extreme hydrogen-deficiency itself.

References

Abbot, D.C., 1978. Astrophys.J., 225,893.

Abt, H.A., 1957. Astrophys.J., 126,547.

Aydin, C., 1979. Astrophys.Space Sci., 64,481.

Alexander, J.B., Andrews, P.J., Catchpole, R.M., Feast, M.W., Lloyd Evans, T., Menzies, J.W., Wisse.P.N.J. & Wisse, M., 1972. Mon.Not.R.astr.Soc., 158,305.

Allen, C.W., 1973. Astrophysical Quantities, 3rd edn, The Athlone Press, Londo

Barning, F.J.M., 1963. Bull.astr.Inst.Neth., 17,22.

Bidelman, W.P., 1950. Astrophys.J., 111,333.

Bell, S.A., 1987. Ph.D. thesis, University of St Andrews.

Boggess, A. et al., 1978a. Nature 275,372.

Boggess, A. et al., 1978b. Nature 275,377.

Bohlin, R.C. & Holm, A.V., 1980. NASA IUE Newsletter No.10,37.

Cameron, R.C., 1966. Georgetown Obs., Monogr. No.21.

Crawford, D.L. & Barnes, J.V., 1970. Astron.J., 75,978.

Danziger, I.J., Wallerstein, G. & Böhm-Vitense, E., 1967. Astrophys.J.,150,239.

Danzmann, K. & Kock, M., 1980. J.Phys.B., 13,2051.

De Greve, J.P. & De Loore, C., 1976. Astrophys.Space.Sci., 43,35.

de Jager, C., 1980. In: The Brightest Stars, eds McCormac.B.M., Reidel, Dordrecht, Holland.

Deharveng, L. & Maucherat, M., 1975. Astr.Astrophys., 41,27.

Delgado, A.J. & Thomas, H.-C., 1981. Astr.Astrophys., 96,142.

Dickel, H.R., 1974. Astr.Astrophys., 31,11.

Drilling, J.S., 1973. Astrophys.J., 179,L31.

Drilling, J.S., 1975. Astron.J., 80,128.

Drilling, J.S., 1978. Astrophys.J., 223,L29.

Drilling, J.S., 1979. Astrophys.J., 228,491.

Drilling, J.S., 1980. Astrophys.J., 242,L43.

Drilling, J.S. & Schönberner, D., 1982. Astr. Astrophys., 113, L22.

Drilling, J.S., Schönberner, D., Heber, U. & Lynas-Gray, A.E., 1984a. Astrophys. J., 278, 224.

Drilling, J.S., Landolt, A.U. & Schönberner, D., 1984b. Astrophys. J., 279, 748

Drilling, J.S., Heber, U. & Jeffery, C.S., 1985. IAUC No. 4086.

Drilling, J.S., 1986. In: IAU Coll. No. 87, Hydrogen-deficient stars and relate objects, eds Hunger, K., Rao, N.K. & Schönberner, D., Reidel, Dordrecht, Holland, p9.

Drilling, J.S. & Heber, U., 1986. In: IAU Coll. No. 87, Hydrogen-deficient stars and related objects, eds Hunger, K., Rao, N.K. & Schönberner, D., Reidel, Dordrecht, Holland, p67.

Drilling, J.S. & Hill, P.W., 1986. In: IAU Coll. No. 87, Hydrogen-deficient star and related objects, eds Hunger, K., Rao, N.K. & Schönberner, D., Reidel Dordrecht, Holland, p499.

Dufton, P.L. & Hibbert, A., 1981. Astr. Astrophys., 95, 24.

Duvignau, H., Freidlung, M. & Hack, M., 1979. Astr. Astrophys., 71, 310.

Dworetsky, M.M., 1983. Mon. Not. R. astr. Soc., 203, 917.

Eggen, O.J., Kron, G.E. & Greenstein, J.L., 1950. Publs. astr. Soc. Pacif., 62, 171

Faulkner, D.J. & Aller, L.H., 1965. Mon. Not. R. astr. Soc., 130, 393.

Feast, M.W., 1979. IAU Coll. No. 46, p246, eds Bateson, F.M., Smak, J. & Urch, I.H. University of Waikoto, Hamilton, New Zealand.

Feast, M.W., 1986. In: IAU Coll. No. 87, Hydrogen-deficient stars and related objects, eds Hunger, K., Rao, N.K. & Schönberner, D., Reidel, Dordrecht, Holland, p151.

Fernie, J.D., 1982. Publs. astr. Soc. Pacif., 94, 172.

Florentin-Neilsen, R., 1983. Inst. Astrophys. Oslo, Report No. 59, 141.

Fuhr, J.R., Martin, G.A., Wiese, W.L., Younger, S.M. 1985. In: Atomic data for controlled fusion research, Vol. IV, ed Wiese, W.L.

Gaposchkin, S., 1945. Astron.J., 51,109.

Graham, J.A., 1970. Astron.J., 75,703.

Green, L.C., Johnson, N.C. & Kolchin, E.K., 1966. Astrophys.J., 144,369.

Greenstein, J.L., 1950. Astrophys.J., 111,20.

Greim, H.R., 1964. Phys.Rev., 165,258.

Grønbech, B., Olsen, E.H. & Strömgren, B., 1976. Astr.Astrophys., 26,155.

Hack, M., 1960. Mem.Soc.Astron.Ital., 31,43.

Hack, M. & Pasinetti, L., 1963. Contr.Oss.Astro.Milano-Merate, Nuova ser. No. 215.

Hack, M., Flora, U. & Satin, P., 1980. In: Close Binary Stars: Observations and Interpretation, eds Plavec, M.J., Popper, D.M. & Ulrich, R.K., Reidel Dordrecht, Holland, p67.p271.

Heard, J.F., 1962. Publs.David Dunlap Obs., 11, No.9.

Hamann, W.-R., Schönberner, D. & Heber, U., 1982. Astr.Astrophys., 116,273.

Heber, U., 1983. Astr.Astrophys., 118,39.

Heber, U., 1986. In: IAU Coll.No.87, Hydrogen-deficient stars and related objects, eds Hunger, K., Rao, N.K. & Schönberner, D., Reidel, Dordrecht, Holland, p33.

Heber, U. & Schönberner, D., 1981. Astr.Astrophys., 102,73.

Heber, U., Hunger, K., Jonas, G. & Kudritzki, R.P., 1984. Astr.Astrophys., 130,119.

Heber, U., Jonas, G. & Drilling, J.S., 1986. In: IAU Coll.No.87, Hydrogen-deficient stars and related objects, eds Hunger, K., Rao, N.K. & Schönberner, D., Reidel, Dordrecht, Holland, p67.

Hill.G., 1979. Publs.Dom.Astrophys.Obs., 15,297.

Hill, P.W., 1986. In: IAU Coll.No.87, Hydrogen-deficient stars and related objects, eds Hunger, K., Rao, N.K. & Schönberner, D., Reidel, Dordrecht, Holland, p489.

Holweger,H., 1979. In: Liege International Astrophys.Symp., p117.

Hummer,D.G. & Mihalas,D., 1970. Mon.Not.R.astr.Soc., 147,339.

Hunger,K., 1975. In: Problems in Stellar Atmospheres and Envelopes, eds Baschek,B, Kegel,W.H. & Traving,G., Springer-Verlag, Berlin, Heidelberg New York, p57.

Hunger,K., 1986. In: IAU Coll.No.87, Hydrogen-deficient stars and related objects, eds Hunger,K., Rao,N.K. & Schönberner,D., Reidel, Dordrecht, Holland, p261.

Hunger,K. & Van Blerkom,D., 1967. Z.Astrophys., 66,185.

Hutchmeier,W.K. & Day,G.A., 1975. Astr.Astrophys., 41,153.

Iben,I. & Tutukov,A.V., 1985. Astrophys.J.Suppl., 58,661.

Iben,I. & Tutukov,A.V., 1987. Astrophys.J., 313,727.

Inoue,M.N., 1979. Publs.astr.Soc.Japan, 31,11.

Jeffery,C.S. & Malaney,R.A., 1985. Mon.Not.R.astr.Soc., 213,61P.

Jeffery,C.S., Skillen,I., Hill,P.W., Kilkenny,D., Malaney,R.A. & Morrison,K., 1985. Mon.Not.R.astr.Soc., 217,710.

Jeffery,C.S., Hill,P.W. & Morrison,K. 1986. In: IAU Coll.No.87, Hydrogen-deficient stars and related objects, eds Hunger,K., Rao,N.K. Schönberner,D., Reidel, Dordrecht, Holland, p95.

Jeffery,C.S., Drilling,J.S. & Heber,U., 1987a. Mon.Not.R.astr.Soc., 226,317.

Jeffery,C.S., Drilling,J.S. & Hill,P.W., 1987b. Mon.Not.R.astr.Soc, 225,1005.

Kaufmann,J.P. & Schönberner,D., 1977. Astr.Astrophys., 57,169.

Kippenhahn,R. & Meyer-Hofmeister,E., 1977. Astr.Astrophys., 54,539.

Kurtz,D.W., 1985. In: Seismology of the Sun and Distant stars, eds Gough,D.O. Reidel, Dordrecht, p147.

Kurucz,R.L., 1981. Smithsonian Astrophys.Obs.Spec.Rep. 390.

Kurucz,R.L. & Peytremann,E., 1975. Smithsonian Astrophys.Obs.Spec.Rep. 362.

Lafler,J. & Kinman,T.D., 1965. Astrophys.J.Suppl., 11,216.

Osterbrook, D.E., 1974. In: Astrophysics of Gaseous Nebulae, eds Burbridge.G. Burbridge,M., W.H.Freeman & Company, San Francisco, p21.

Paczynski,B., 1971. Acta.Astr., 21,1.

Parthasarathy,M., Cornachin,M. & Hack,M., 1986. Astr.Astrophys., 166,237.

Plavec,M.J. 1971. In: IAU Symp.No.51, Extended Atmospheres and Circumstellar Matter in Close Binaries Systems, eds Batten,A.H., Reidel Dordrecht, Holland, p216.

Plavec,M.J., 1979. Inf.Bull.var.Stars No.1598.

Plavec,M.J., 1986. In: IAU Coll.No.87, Hydrogen-deficient stars and related objects, eds Hunger,K., Rao,N.K. & Schönberner,D., Reidel, Dordrecht, Holland, p231.

Rao,N.K. & Venugopal,V.R., 1985. J.Astrophys.Astr., 6,101.

Roberts,J.R., Andersen,T. & Sørensen,G., 1973. Astrophys.J., 181,567.

Robinson,E.L., 1979. In: IAU Coll.No.53, White dwarfs and variable degenerate stars, eds Van Horn,H.M. & Weidemann,V., University of Rochester, N.Y., U.S.A., p343.

Robinson,E.L., Shafter,A.W., Hill,J.A., Wood,M.A. & Mattei,J.A., 1987. Astrophys.J., 313,772.

Robinson,R.D., 1985. In: The RGO Spectrograph (2nd edition), Anglo-Australian Observatory.

Rosendahl,J.D., 1973a. Astrophys.J., 182,523.

Rosendahl,J.D., 1973b. Astrophys.J., 186,909.

Sahade,J. & Albano,J., 1970. Astrophys.J., 162,905.

SAAO Facilities Manual (3rd edition), 1982. South African Astronomical Observatory.

Saio,H., Wheeler,J.C. & Cox,J.P., 1984. Astrophys.J., 218,318.

Saio,H. & Wheeler,J.C., 1985. Astrophys.J., 295,38.

Saio,H., 1986. In: IAU Coll.No.87, Hydrogen-deficient stars and related objects, eds Hunger,K., Rao,N.K. & Schönberner,D., Reidel, Dordrecht,

Landolt, A.U., 1986a. In: IAU Coll.No.87, Hydrogen-deficient stars and related objects, eds Hunger, K., Rao, N.K. & Schönberner, D., Reidel, Dordrecht, Holland, p51.

Landolt, A.U., 1986b. IAUC No.4133.

Loumos, G. & Deeming, T.J., 1978. Astrophys. Space Sci., 56, 285.

Lynas-Gray, A.E., Walker, H.J., Hill, P.W., Kaufmann, J.P., 1981. Astr. Astrophys. Suppl. Ser., 44, 349.

Lynas-Gray, A.E., Kilkenny, D., Skillen, I. & Jeffery, C.S., 1987. Mon. Not. R. astr. Soc., 227, 1073.

MacConnell, D.J., Frye, R.L. & Bidelman, W.P., 1972. Publs. astr. Soc. Pacif., 84, 388.

Malcolm, G.J. & Bell, S.A., 1986a. Mon. Not. astr. Soc. South Africa, 45, 19.

Malcolm, G.J. & Bell, S.A., 1986b. Mon. Not. R. astr. Soc., 222, 543.

Meaburn, J., Lopez, J.A. & Keir, D., 1984. Mon. Not. R. astr. Soc., 211, 267.

Menzies, J.W., Banfield, R.M. & Laing, J.D., 1980. S.A.A.O. Circ., 1, 149.

Meyer-Hofmeister, E., 1982. In: Astronomy and Astrophysics Subvol.2b, eds Schaifers, K. & Voigt, H.H., Springer-Verlag Berlin, Heidelberg, New York, p188.

Morton, D.C., 1969. Astrophys. J., 158, 629.

Nandy, K., Thomson, G.I., Jamar, C., Monfils, A. & Wilson, R., 1975. Astr. Astrophys., 44, 195.

Nariai, K., 1967. Publs. astr. Soc. Japan, 19, 564.

Nariai, K., 1972. Publs. astr. Soc. Japan, 24, 495.

Nather, R.E., 1978. Publs. astr. Soc. Pacif., 90, 477.

Nicolet, B., 1978. Astr. Astrophys. Suppl. Ser., 34, 1.

Osawa, K., Nishimura, S. & Nariai, K., 1963. Publs. astr. Soc. Pacif., 15, 313.

Osmer, P.S. & Peterson, D.M., 1974. Astrophys. J., 187, 117.

Osterbrook, D.E., 1974a. In: Astrophysics of Gaseous Nebulae, eds Burbridge, G. & Burbridge, M., W.H. Freeman & Company, San Francisco, p112.

Holland, p425.

Schinckel, A.E., Philips, M.M. & Hill, P.W., 1982. In: A Guide to Wavelength Identifications for the CuAr Lamp of the RGO Spectrograph, Anglo-Australian Observatory.

Scholz, M., 1972. In: Vistas in Astronomy, Vol.14, Pergamon Press, Oxford, New York.

Schönberner, D., 1973. Astr. Astrophys., 28,433.

Schönberner, D., 1975. Astr. Astrophys., 44,383.

Schönberner, D., 1977. Astr. Astrophys., 57,437.

Schönberner, D., 1978. Mitt. Astr. Ges., 43,266.

Schonberner, D., 1979. Astr. Astrophys., 79,108.

Schönberner, D., Drilling, J.S., Lynas-Gray, A.E. & Heber, U. , 1982. In: Advances in Ultraviolet Astronomy: Four years of IUE Research. NASA CP-2738, p593.

Schönberner, D. & Drilling, J., 1983. Astrophys. J., 268,225.

Schönberner, D. & Drilling, J., 1984. Astrophys. J., 276,229.

Schönberner, D. & Wolf, R.E.A., 1974. Astr. Astrophys., 37,87.

Schulz-Gulde, E., 1969. J. Quant. Spectroscop. Radiat. Transfer, 9,13.

Schwarzchild, M. & Harm, R., 1967. Astrophys. J., 150,961.

Seaton, M.J., 1979. Mon. Not. R. astr. Soc., 187,73P.

Seydel, F.L., 1929. Pub. Amer. Astron. Soc., 6,278.

Skillen, W.J., 1985. Ph.D. thesis, University of St Andrews.

Trimble, V., 1972. Mon. Not. R. astr. Soc., 156,411.

Tutukov, A.V. & Yungelson, L.R. 1979. In: IAU Sym. No.83, 1979. Mass loss and evolution of O-type stars, eds Conti, P.S. and de Loore, C.W.H., Reidel, Holland, p1.

Underhill, A.B., 1960. In: Stars and Stellar Systems Vol.VI, ed Greenstein, University of Chicago Press, p415.

Walborn, N.R., 1973. Astrophys.J., 179,517.

Walborn, N.R., 1982. Astrophys.J.Suppl., 48,145.

Walborn, N.R. & Hesser, J.E., 1982. Astrophys.J., 199,535.

Walker, H.J. & Hill, P.W., 1985. Astr.Astrophys.Suppl.Ser., 61,303.

Walker, H.J. & Kilkenny, D., 1980. Mon.Not.R.astr.Soc., 190,299.

Walker, H.J. & Schönberner, D., 1981. Astr.Astrophys., 97, 291.

Wallerstein, G., Greene, T.F. & Tomley, L.J., 1967. Astrophys. J., 150,245.

Warner, B., 1967. Mon.Not.R.astr.Soc., 137,119.

Webbink, R.F., 1984. Astrophys.J., 277,355.

Wiese, W.L., Smith, M.W. & Glennon, B.M., 1966. Atomic Transistion Probabilites, NBS, Washington.

Wiese, W.L., Smith, M.W. & Miles, B.M., 1969. Atomic Transistion Probabilites, NBS, Washington.

Wilson, R.E., 1914. Lick Obs. Bull., 8, No.267,132.

Wilson, I.R.G. & Dopita, M.A., 1985. Astr.Astrophys., 149,295.

Wolf, R.E.A., 1973. Astr.Astrophys., 26,127.

Wobig, K.H., 1962. Z.Astrophys., 55,100.

Wood, P.R., 1976. Mon.Not.R.astr.Soc., 174,531.

Yungelson, L.R., 1982. In: Ejection and accretion of matter in binary systems, eds Tremko, J., Slovak Academy of Sciences, Bratislava, p11.